

**Real-time monitoring of the gas phase chemistry of key
atmospheric VOCs using atmospheric simulation
chambers to evaluate their SOA forming potential**

by

K. Timo Carr

A thesis submitted to the University of Leicester

for the degree of

DOCTOR OF PHILOSOPHY

Chemistry Department

University of Leicester

November 2012

Abstract

The oxidation of a range of Volatile Organic Compounds (VOCs) has been studied, from small alkenes (e.g. ethene C₂) to larger sesquiterpene species (e.g. β-caryophyllene C₁₅). The gas-phase reactions of these VOCs, largely emitted from biogenic sources, can form oxidation products with high mass and low volatility to contribute to aerosol formation, namely for monoterpene and sesquiterpene species. These organic aerosols formed from chemical reactions in the atmosphere are secondary organic aerosols (SOA). Aerosols can have a profound impact on both climate and health issues at regional and global scales. Processes that govern these gas-to-particle phase reactions are still not fully understood. This thesis presents detailed gas-phase composition data from the various VOCs examined, and tries to highlight important gas-phase species involved in the processes for SOA formation in the atmosphere.

The gas-phase composition was measured in real-time utilising the University of Leicester Chemical Ionisation Reaction-Time of Flight-Mass Spectrometer (CIR-ToF-MS). Experiments were conducted under two different environments, “dark” ozonolysis experiments were studied at the EUropean PHOtoREactor (EUPHORE) atmospheric simulation chamber (Valencia, Spain) whilst “light” photooxidation experiments were conducted at the Manchester Aerosol Chamber (MAC) facility (Manchester, UK). The ozonolysis experiments focused around small alkene species (ethene, isobutene, and trans-2-butene), isoprene and monoterpenes (myrcene, α-pinene and limonene) in the absence of NO_x and investigated with and without radical scavengers in order to suppress side reactions. Under dry conditions the primary oxidation products for smaller alkene ozonolysis averaged yields for formaldehyde (HCHO) as 1.56 ± 0.09 , 1.21 ± 0.03 and 0.15 ± 0.01 for ethene, isobutene and trans-2-butene respectively. Other major gas phase product yields were recorded. Under wet conditions HCHO yields increased dramatically for ethene ozonolysis, to 3.09 ± 0.12 and 1.94 ± 0.31 for isobutene, but no substantial difference was observed for trans-2-butene with an average yield of 0.19 ± 0.04 . Observations on gas-phase composition

varied little based on the latter and model comparisons were made using the Master Chemical Mechanism (MCMv3.1). Photolysis experiments were conducted for isoprene, monoterpenes (limonene, α -pinene and myrcene) and a sesquiterpene, β -caryophyllene. This led to a direct comparison of composition and yields were obtained for certain oxygenated VOCs (oVOCs). The major gas phase products of isoprene ozonolysis, methacrolein (MACR) recorded average yields of 0.24 ± 0.16 and methyl-vinyl ketone (MVK) at 0.15 ± 0.01 for dry conditions, whilst yields of 0.36 ± 0.04 and 0.17 ± 0.02 were observed for wet conditions respectively. Similar yields were observed for photolysis conditions. The highest average yields in the gas phase for all monoterpene species were the primary aldehyde species formed (e.g. pinonaldehyde for α -pinene), ranging averaged yields from 0.115 to 0.583 for ozonolysis reactions and 0.119 to 0.270 under photolysis conditions. Where applicable, SOA yields were determined using a Differential Mobility Particle Sizer (DMPS) and composition of the particle phase made off-line using Liquid chromatography-ion trap mass spectrometry (LC-MSⁿ). A unique method of organic seed formation was also constructed for photolysis experiments for isoprene and limonene using β -caryophyllene as a precursor for the organic seed. Finally mesocosm experiments of direct emissions from tree species *Ficus cyathistipula*, *Ficus benjamina* and *Caryota millis* (to simulate tropical Asian conditions) and *Betula Pendula* (to encompass European environments). The tropical monoterpene producing species formed SOA, whereas the European isoprene dominant species did not. Implications of this are further discussed along with the difference observed in gas-phase composition and yields of oxidation products produced from all experiments. An Am²⁴¹ source and a newly developed hollow cathode source was utilised in both campaigns so instrumental sensitivity, in particular for lower mass species is also discussed.

Evidence from the experiments shows that SOA formation is only observed from monoterpene and sesquiterpene compounds. Here isoprene did not form any substantial SOA and we argue it can inhibit SOA formation. Important gas phase species for SOA contribution were those of C₁₀ or higher, in particular the primary aldehyde oxidation products of monoterpenes that were observed in both gas and particulate phase.

To Mum, Dad, brother and the rest of the family

With Love

Acknowledgements

I would firstly like to thank my supervisor, Professor Paul Monks for his help during this process, but more importantly for the opportunity to join his research group and for the time and unforgettable experience obtained from field campaigns, both domestic and abroad. Thanks also go out to everyone part of the Atmospheric Group, past and present, for all the help over the years, especially to Dr Iain White, whom in his small time here has been a massive help, and Dr Robert Blake, for his sense of humour that has made working in his company a delight. Huge special thanks are to be given to the hero Dr Kevin Wyche for his help and role as a secondary supervisor throughout my time here. We shared many sleepless nights in the labs whilst on field campaigns, but at least we managed to taste the delights of Valor ice cream and chocolates “as big as a man’s head”.

To all the other people who have helped out and I have had the privileged to meet whilst on field campaigns, those from University of Birmingham, (Dr Marie Camredon, Dr William Bloss) University of York (Dr Jacqueline Hamilton), University of Leeds (Dr Andrew Rickard), University of Manchester (Prof Gordon McFiggans, Dr Rami Alfarra) and everyone at the EUPHORE facility.

Finally I would like to thank my wonderful family for all your love and support during this time (yes Dad, money is included in support). To you, my remarkable parents I cannot thank you enough, not only during this, but for my whole life, you have always been there and I will forever be indebted to you both. Mum and Dad, I could not ask for a better upbringing. And to you, brother Denny who has fathered beautiful daughters since my time here (now who has the harder job?) and your loving wife Emma. To all you other family members scattered around the planet, thank you, especially my second mother Silva Peters in Germany and my amazing Swedish cousins, Lina and Bjorn.

Table of Contents

Contents

CHAPTER 1. Introduction	1
1.1 The atmosphere	2
1.2 Tropospheric Chemistry	3
1.2.1 Hydroxyl (OH) radical and ozone (O ₃)	4
1.2.2 The nitrate radical (NO ₃)	8
1.2.3 Sources of Tropospheric VOCs	10
1.3 Atmospheric aerosols.....	11
1.4 Ozonolysis of alkenes	16
1.5 OH-initiated reactions	18
1.6 Simulation Chamber.....	19
1.7 The Master Chemical Mechanism (MCM)	20
1.8 Thesis Motivation.....	21
1.9 Thesis Overview	23
CHAPTER 2. Instrumentation and Experimental	26
2.1 CIR-ToF-MS	27
2.1.1 Calibration.....	36
2.1.2 Errors for CIR-ToF-MS.....	45
2.2 Simulation Chambers	48
2.2.1 EUPHORE Aerosol Simulation Chamber.....	48
2.2.2 Manchester Aerosol Chamber (MAC)	50
2.3 Other instrumentation	52
2.3.1 Scanning Mobility and Differential Mobility Particle Sizers	52
2.3.2 Fourier Transform Infrared Spectroscopy (FTIR)	56
2.3.3 GCxGC/TOF/MS.....	59
2.3.4 HPLC and LC-MS	59
2.3.5 TOF-AMS	60
2.3.6 Hygroscopicity Tandem Differential Mobility Analyser (HTDMA).....	61
2.3.7 CO Monitor (EUPHORE).....	61
2.3.8 O ₃ Analyser	62
2.3.9 NO _x analyser	63

2.4	Experimental Approach.....	64
2.4.1	EUPHORE experimental methodology.....	64
2.4.2	ACES experimental methodology.....	65
2.5	Yields of stable organic species and SOA.....	66
CHAPTER 3. Ozonolysis of simple alkenes and oxidation of isoprene		68
3.1	Ethene ozonolysis.....	69
3.1.1	Detection of HCHO and formic acid.....	73
3.1.2	Yields of stable organic products from ethene.....	76
3.1.3	MCM model comparison of ethene.....	81
3.2	Isobutene ozonolysis.....	83
3.2.1	Yields of stable organic products from isobutene.....	88
3.2.2	MCM model comparison of isobutene.....	90
3.3	Trans-2-butene ozonolysis.....	92
3.3.1	Yields of stable organic products from trans-2-butene.....	96
3.3.2	MCM model comparison of trans-2-butene.....	99
3.4	Isoprene oxidation.....	100
3.4.1	Yields of stable organic products from isoprene.....	109
3.4.2	MCM model comparison of isoprene.....	113
3.4.3	Carbon balance measurements of isoprene ozonolysis.....	114
3.4.4	SOA formation from isoprene.....	116
3.5	Discussion.....	119
CHAPTER 4. Ozonolysis and photolysis of monoterpenes.....		121
4.1	Monoterpenes in the atmosphere.....	122
4.2	Myrcene oxidation.....	122
4.2.1	Ozonolysis of myrcene.....	123
4.2.2	Photooxidation of myrcene.....	128
4.2.3	Yields of stable organic species (myrcene).....	131
4.2.4	SOA formation (myrcene).....	136
4.3	α -pinene oxidation (photooxidation and ozonolysis).....	137
4.3.1	Yields of stable organic species of α -pinene.....	144
4.3.2	Comparison to atmospheric model of α -pinene.....	150
4.3.3	SOA formation for α -pinene.....	152
4.4	limonene oxidation.....	156

4.4.1	Limonene ozonolysis	157
4.4.2	Yields of stable organic species from limonene	164
4.4.3	Comparison to atmospheric model of limonene	172
4.4.4	SOA formation for limonene	174
4.5	Discussion.....	180
CHAPTER 5. Sesquiterpene (β -caryophyllene) photooxidation		183
5.1	β -caryophyllene in the atmosphere.....	183
5.2	β -caryophyllene photolysis	184
5.2.1	Gas phase composition from β -caryophyllene oxidation.....	188
5.2.2	Yields of stable organic species from β -caryophyllene.....	192
5.3	SOA formation from β -caryophyllene oxidation.....	199
5.4	Discussion.....	203
CHAPTER 6. Mesocosm Experiment.....		205
6.1	Experimental methodology.....	205
6.2	Experimental set-up.....	206
6.3	Results (BVOC emissions and gas phase products)	208
6.4	SOA formation.....	211
6.6	Discussion.....	212
CHAPTER 7. Conclusion		216
Future Work		221
References.....		224

List of Figures

Chapter 1

- Figure 1.** Diagrammatic representation of the atmosphere showing the changes of temperature and pressure with rising altitudes taken from Finlayson-Pitts and Pitts (2000).....3
- Figure 2.** OH-initiated oxidation of methane and CO in the troposphere adapted from Wayne (2000).....7
- Figure 3.** Current scientific knowledge on radiative forcing contributions of various sources, including aerosols, as presented in the IPCC Fourth Assessment Report: Climate Change 200712
- Figure 4.** The reaction scheme for initial ozonolysis reaction with alkenes. After initial 1,3 dipolar ozone addition to the C double bond, a carbonyl compound is formed with a carbonyl oxide (the Criegee Intermediate CI) which can then go on to react or rearrange further to produce further carbonyls, aldehydes, esters and hydroperoxides.....17
- Figure 5.** Overview of an OH radical addition to a carbon-carbon double bond of an alkene adapted from Calvert 200218

Chapter 2

- Figure 6.** Schematic of the CIR-TOF-MS to indicate crucial instrumentation sections taken from Wyche et al 2008.....29
- Figure 7.** A schematic of the drift cell to indicate principle components. The ion source encompasses both the ^{241}Am and HCD source. The x mm represents a length of 16.07 mm for the radioactive source and 19.53 mm for the lengthened HCD source.....35
- Figure 8.** Sensitivity values obtained from both the ^{241}Am source (dark blue) and HCD (light blue) for compounds in a 1 ppm gas-standard cylinder. All

compounds show an increase in sensitivity except for the small alkene trans-2-butene.....	36
Figure 9. Set-up procedure used for a standard bag calibration run made at RAFT facility at the University of Leicester.....	38
Figure 10. Injections of 200 ppb calibrate of cyclohexanone into three separate tedlar bags to test the injection method employed during bag calibrations runs.....	39
Figure 11. Set-up for direct sampling of the gas standards. A N ₂ gas cylinder (BOC special gases, purity 99%) and the 1ppm gas standard cylinder were connected to MFCs. Flow were adjusted to establish dynamic dilution.....	40
Figure 12. A typical multiple cylinder calibration run using the ~1ppm gas standard. The dotted gaps represent a 10 minute equilibrium time between adjustments of flow rates between N ₂ and the gas standard.....	41
Figure 13. The evolution of m/z ion channel 59 following three additions of acetone into the EUPHORE aerosol chamber. The data is represented in 1 min minute time frames. Clear increasing at times of injection are observed where injections of 50.3 mg (111 ppb), 47.4 mg (98 ppb) and 47.37 mg (98 ppb) were made.....	44
Figure 14. The evolution of m/z ion channel 59 following three additions of acetone into the EUPHORE aerosol chamber. The data is represented in 1 min minute time frames. Clear increasing at times of injection are observed where injections of 50.3 mg (111 ppb), 47.4 mg (98 ppb) and 47.37 mg (98 ppb) were made.....	45
Figure 15. Example calibration curve for m/z ion 137 of α-pinene.....	46

Figure 16.	Comparisons of both differing compounds, and different calibration methods to evaluate the impact of changing concentrations and the impact this has on precision. Isorpene permeation tubes (orange triangles), HCHO perm tubes (blue squares, purple diamonds), limonene bag calibrations (green lines) average of errors from different gas standard cylinder calibration runs (blue diamonds, green triangles, red squares).....	47
Figure 17.	The EUPHORE CHAMBER facility. The outer housing makes it possible for both daytime and nighttime chemistry to be observed. For the ozonolysis experiments, conditions followed that of nightitme chemistry.....	49
Figure 18.	The Aerosol chamber at Manchester. The outer housing with the Leicester CIR-TOF-MS connected to the inlet (left) and inside the chamber with 18m ³ teflon bag and the arc xenon lamp with the bank of halogen lights (right).....	51
Figure 19.	The Differential Mobility Analyzer. Charged polydisperse aerosol enter the DMA. The negatively charged central rod attracts the positively charged aerosols whilst repelling the negatively charged aerosols towards the DMA walls. Neutral aerosols are unaffected and exit with excess air. A narrow selection of positively charged aerosols exit as the monodisperse gas. Diagram is based on the TSI 3080 model adapted from the TSI website.....	54
Figure 20.	A flow schematic of the CPC (left) and the “optics” section of the CPC (right). Diagrams taken from the TSI website.....	56
Figure 21.	Schematic of the interferogram of the FTIR.....	57
Figure 22.	The chamber set-up of EUPHORE, with special emphasis on the FTIR and CIR-TOF-MS. Not all instrumentation has been included. The dotted lines represent the instruments below situated below the chamber. Solid lines show instrumentation in the chamber.....	58

Chapter 3

Figure 23. Top panel shows the time evolution of ethene ozonolysis with CO (black) scavenger. The CO addition (black dashes) are followed by measurement of CO by the FTIR. O₃ (blue) addition is measured from ozone monitor (see chapter 2) following addition into the chamber (blue dashes). Final addition of ethene (green dashes) shows reaction start time (t₀). Ethene then follows degradation as the reaction proceeds. All data plots have been dilution corrected. Middle panel shows a comparison of the time evolution of HCHO from ethene ozonolysis recorded from three instruments, CIR-ToF-MS (diamonds), FTIR (triangles) and HCHO monitor (solid line). Both FTIR and CIR-ToF-MS data has been averaged over a 5 minute period, whereas the HCHO monitor achieves data acquisition approximately every 20 seconds. Bottom panel. Comparison of FTIR (triangles) and CIR-ToF-MS (diamonds) for the detection of formic acid.....71

Figure 24. the proposed ozone reaction with ethene. Stable organic species are displayed in boxes. Here two oxidation products are expected from ethene ozonolysis, HCHO and formic acid. HCHO is expected to be produced in more quantities as its production is formed directly after ozone addition to the double bond. The brackets evolve the reaction pathway with the decomposition and isomerisation steps of the Criegee intermediate to produce formic acid.....72

Figure 25. The yields obtained from ethene ozonolysis experiments in the presence of CO scavenger under similar initial reagents for “dry” and “wet” chamber conditions on 09/05/08. The data has been dilution corrected and the change in ethene was taken from the FTIR recording.....74

Figure 26. A comparison of the formic acid detection for “wet” conditions of an ethene ozonolysis experiment from both FTIR (triangles) and CIR-ToF-MS (diamonds) recordings. The formic acid is still close to the detection limit of the

CIR-TOF-MS which is evident from the scatter of data points, each data point representing an average of 5 min data from an acquisition of 1 minute data intervals.....76

Figure 27. The yield calculation based on values that have not been corrected for dilution loss. Results obtained are from an excess CO scavenged experiment on 09/05/08. The resulting curvature of data points indicate a problem with final yield calculation due to dilution loss of the gaseous species.....77

Figure 28. The dilution corrected yields obtained from an excess CO experiment. The CIR-TOF-MS yield (red diamonds) and the FTIR (triangles) show consistent yields established, 1.16 and 1.20 respectively.....78

Figure 29. Comparison of the MCM model (output) compared to measured experimental data (markers or thick lines) for the ethene CO experiment run on 09/05/08 under dry (left) and wet (right) conditions. The model shows good correlation with the reagents ethene (green) and ozone (blue) and the CO scavenger (black). The resulting oxidation product formaldehyde (red) also shows good correlation to the model, whereas formic acid (yellow) is largely overestimated by the CIR-ToF-MS (diamonds) and marginally by the FTIR (triangles).....82

Figure 30. The model output (solid thin lines) compared to experimental measured data (markers or thick solid lines). This experiment utilised cyclohexane (black) as an OH scavenger.....83

Figure 31. a to c are displayed to show the time evolution of an isobutene ozonolysis reaction conducted on 02/05/08 with the presence of a cyclohexane scavenger. Figure xa demonstrate major reagents ozone (blue) and isobutene (green) from FTIR (triangles) and CIR-ToF-MS (diamonds) along with the high levels of cyclohexane (black). Figure b highlights the difference of compounds of formic acid (yellow) and HCHO (red) from the instrumentation available and finally the observed mass channels showing growth greater than 3σ of

background noise. These include acetic acid (pink), propionic acid (brown), methanol (orange), acetone (grey), cyclohexanone (light blue) and acetaldehyde (light pink). Experimental data from this day was chosen as it highlights the CIR-ToF-MS capability of detecting a range of masses during an experimental run.....86

Figure 32. The differing detected maximum concentration values determined from FTIR (light grey) and CIR-ToF-MS (grey). In all circumstances has the CIR-ToF-MS given a higher concentration level compared to FTIR measurements. These were compared to calculated maximum theoretical concentrations (dark grey).....87

Figure 33. the ozonolysis of isobutene. The formation of formic acid follows that from the Cl_2 intermediate as seen in ethene ozonolysis. The two additional methyl groups enables the formation of acetone, which can further lead to the formation of acetic acid.....87

Figure 34. MCM model comparisons to experimentally determined data. Trace profiles are as; (Top) Cyclohexane (black), Isobutene (green) and ozone (blue); (Middle) Formic acid (yellow) and HCHO (red); (Bottom) Cyclohexanone (pink), acetone (grey) and acetic acid (light blue).....91

Figure 35. The initial conditions and time traces for the trans-2-butene (green) experiment during a CO (black) scavenged experiment on 15/05/08. The intercomparison between FTIR (triangles), CIR-TOF-MS (diamonds) and monitors (solid lines) detections of trans-2-butene show good correlation, with similar results for major oxidation products acetaldehyde (pink) and HCHO (red).....94

Figure 36. A reaction scheme of trans-2-butene ozonolysis adapted from the MCM mechanism. O_3 attacks the double bond, and owing to the structure of butane species, acetaldehyde and a corresponding criegee intermediate is formed. Acetaldehyde reacts with OH to produce similar radical species similar to those

before and hence promote formation of stable species such as formaldehyde and acetic acid.....	95
Figure 37. A comparison of the 1 ppm gas standard cylinder with a ²⁴¹ Am ion source run under dry and humid (80% RH) conditions. The overall trend seems to show a decrease in sensitivity with increase in RH.....	96
Figure 38. A comparison of yields of acetaldehyde from both FTIR (triangles) and CIR-TOF-MS (diamonds) during a CO scavenged experiment of trans-2-butene + O ₃ on 15/05/08. The results show good intercomparison between both instruments.....	97
Figure 39. MCM model comparison of the initial reagent conditions, trans-2-butene (green), CO (black) and ozone (blue) above, with a comparison of the two dominant oxidation species formaldehyde (red) and acetaldehyde (gold) below. The model output reflect the experimentally data observed for the exception of ozone decay which it under predicted in the model.....	100
Figure 40. A simplified oxidation mechanism scheme of the initial Isoprene ozonolysis reaction. All stable oxidation products compounds have been highlighted within a box.....	104
Figure 41. A simplified reaction mechanism of OH addition to isoprene showing the formation of primary stable organic species adapted from the MCM mechanism.....	106
Figure 42. A subtraction of the gas-phase composition from initial conditions (red) from a time 2 hours after reaction start to highlight the differences in gas-phase composition and oxidation products.....	107
Figure 43. Temporal profiles from Exp 1 (Straight Isoprene + Ozone system). The data has been taken from 10 minutes before injection of the precursor to the time when flushing commences. A steady loss of O ₃ (black) is observed during the experiment. The injection of Isoprene (TOF green diamonds, FTIR green	

triangles) is pragmatic along with the reaction degradation, followed by the formation of the three most dominant gas-phase oxidation products, HCHO (red), MACR (blue) and MVK (yellow) from the CIR-TOF-MS data.....	108
Figure 44. Injection analysis of isoprene for EUPHORE chamber experiments. The CIR-ToF-MS measurements (grey) are very realistic, in all circumstances just below the potential calculated concentration (dark grey). The FTIR reading (light grey) underestimates this value by a greater fraction and so the isoprene data is more reliable with the CIR-ToF-MS data.....	109
Figure 45. The MCM model comparison of isoprene ozonolysis experiments from a “straight” ozone reaction (left) and a CO scavenged (right).....	113
Figure 46. Time profiles for the carbon balance accounted for in the gas-phase of chamber experiments comparable to ozonolysis and photolysis experiments performed at EUPHORE and MAC respectively.....	116
Figure 47. An isoprene (green) photooxidation experiment conducted in the presence of an organic seed produced from β -caryophyllene (purple) photolysis.....	118

Chapter 4

Figure 48. Chemical structure of myrcene.....	122
Figure 49. Difference in gas composition of myrcene ozonolysis experiments.....	124
Figure 50. Time evolution profile of the straight myrcene ozonolysis experiment.....	126
Figure 51. Observed mass channels of myrcene ozonolysis that have been identified from the proposed reaction mechanism of myrcene.....	126
Figure 52. The proposed mechanism of Myrcene ozonolysis based on current knowledge and mechanisms adapted from isoprene reactions.....	129

-
- Figure 53.** Time profiles of myrcene photolysis reactions. Top shows the degradation of myrcene (green) with some of the major oxidation products, HCHO (red), m/z ion 111 (orange) and m/z 139 (red). Middle panel describes the chamber conditions with NO (light blue) NO₂ (dark blue), O₃ (blue) and NO_x (black) with the bottom panel showing SOA mass formation.....130
- Figure 54.** Difference in gas composition of myrcene ozonolysis experiments.....138
- Figure 55.** Time evolution of the α -pinene system. Diamond shapes is TOF data, squares is HPLC and triangles is FTIR, Red is HCHO, Black with red line borders (ozone), Green diamonds (ToF), Pink triangle (FTIR) α -pinene, Green is pinonaldehyde (HPLC), blue pinonaldehyde (TOF).....139
- Figure 56.** Time profiles of oxidation products, α -pinene oxide (yellow), acetic acid (green), acetone (black), formic acid (purple), 4-oxo (orange). FTIR measurements (triangles) have been included in CIR-ToF-MS (diamonds).....140
- Figure 57.** Time profiles of detected mass channels corresponding to the directly produced stable species following the peroxy radical reactions with HO₂ and RO₂ as presented in the reaction mechanism.....141
- Figure 58.** The MCM mechanism route for the ozonolysis of α -pinene, simplified to identify the stable products detected and show their reaction pathways.....143
- Figure 59.** Model comparison (lines) to experimentally determined data by CIR-ToF-MS (diamonds) for reagents α -pinene (green), ozone (black) and oVOCs HCHO (red), pinonaldehyde (blue) and pinonic acid (white) for a O₃ + VOC reaction in dark conditions.....151
- Figure 60.** Gas-phase composition of limonene (red) at start of the reaction and the differing composition of the gas-phase after 2 hrs of reaction time (blue). The difference in spectra helps in easily identifying the potential oxidation products, and the fragments from the mass spectra.....159

-
- Figure 61.** The time profiles of limonene (green), ozone (black) and two of the major oxidation products observed during limonene ozonolysis, HCHO (red) and limaldehyde (blue). The injection period of limonene addition (dotted red lines) is closely followed by the reaction start time with ozone addition (black lines). Almost immediate formation of HCHO is detected with fill of ozone into the chamber and after a period of 20 min the primary aldehyde is observed.....160
- Figure 62.** Calculated concentrations based on 100% of mass successfully injected into the chamber (black) and the measured concentration levels observed for both analytical instruments FTIR (light grey) and CIR-TOF-MS (dark grey). Observations conclude an overestimation as high as 116.79% for FTIR measurements and a maximum underestimation of 21.59% for CIR-TOF-MS readings.....161
- Figure 63.** Time evolution of detected observed m/z ions from the CIR-TOF-MS during the limonene + O₃ system, of those higher in mass than limonene.....161
- Figure 64.** Proposed mechanism of limonene degradation adapted from the newly developed MCM mechanism to evaluate the initial stable oxidation products formed (in boxes). Organics encompass lower mass species HCHO, acetic acid, formic acid, acetone and methanol.....163
- Figure 65.** Comparison of experimentally determined gas-phase data (triangles FTIR, diamonds CIR-ToF-MS) to MCM outputs (lines) for a O₃ + limonene reaction depicting the degradation of limonene (green) and ozone (black) accompanied by the formation of limonaldehyde (blue) and HCHO (red).....174
- Figure 66.** SOA mass analysis of limonene for low ppb concentrations, showing nucleation events and growth of aerosol.....179

Chapter 5

Figure 67.	Degradation pathway of initial OH addition to the internal carbon-carbon double bond. The dotted lines represent several intermediate radical species formed throughout the reaction pathway.....	185
Figure 68.	Chemical reaction mechanism to represent the addition of OH to the external double bond and ozone addition to the internal double bond. Following oxidation similar products are expected to be formed to those with OH addition to the internal double bond. Represented here are the expected primary oxidation products.....	187
Figure 69.	the gas phase composition of the chamber at lights on (red) and 1.5 hour after reaction time (blue) to highlight the difference in mass spectra obtained to clearly evaluate the mass channels representative of the reacted precursor and resulting oxidation products. Obvious higher mass channels of interest are visible, those at m/z ion channels 253, 237, 219, 209 and 207. Experimental results were taken from 3 rd July 2008.....	189
Figure 70.	Initial gas chamber conditions (top panel) from the initial β -caryophyllene nucleation experiment to form an organic seed for isoprene on 3 rd July 2008 for ozone (blue), NO (light blue), NO ₂ (dark blue) and NO _x (black).....	190
Figure 71.	Acetic acid time profiles obtained from “straight” β -caryophyllene nucleation experiments. Differing profiles made yield determination difficult to assess for specific experiments. 250 ppb b experiment (red), 250 ppb experiment original (blue).....	197
Figure 72.	Acetic acid time profiles during phase 1 of the seeded isoprene experiments. Compared to the nucleation experiments in figure 68, the shape of evolution of acetic acid are consistent among all three experiments conducted on 30 th June (green), 3 rd July (red) and 4 th July (blue).....	198

Figure 73. DMPS data for the SOA mass (black) and SOA number concentration (grey) for photolysis of β -caryophyllene for the initial stage of a seeded experiment isoprene experiment on 3rd July 2008.....199

Chapter 6

Figure 74. Fig tree species time evolution of the major oxidation product of isoprene (red) from both the plant chamber and reaction chamber. Included here is the formation of the major oxidation products MVK and MACR (blue). The increase in of monoterpene detection (black) after lights on is due to the injection of 15 ppb of limonene into the reaction chamber following lights off to ensure capable detection of monoterpenes with the hollow cathode source.....209

Figure 75. Time evolution of dominant BVOCs of silver birch during a nucleation experiment. The monoterpene emission concentration are larger than that of isoprene, the opposite observation compared to the tropical fig species in figure 71.....209

Figure 76. SOA mass formation for two different tree species. The top panel displays the SOA mass (black) and number concentrations (grey) for a birch tree experiment conducted on 6th July 2009. The bottom panel displays the SOA data for a fig tree experiment conducted on 23rd June 2009.....213

List of Tables

Chapter 2

Table 1.	Analytical instruments used during experimental runs at EUPHORE	50
Table 2.	Analytical instruments used during experimental runs at MAC	52

Chapter 3

Table 3.	Initial experimental conditions of ethene ozonolysis during TRAPOZ.....	70
Table 4.	Detection of m/z ion channels during ethene experiments.....	78
Table 5.	HCHO yields from ethene ozonolysis under various conditions compared to past literature data.....	79
Table 6.	HCOOH yields from ethene ozonolysis under various conditions compared to past literature data of HCOOH yield.....	80
Table 7.	Initial experimental conditions of isobutene ozonolysis during TRAPOZ.....	84
Table 8.	Detection of m/z ion channels during isobutene experiments.....	89
Table 9.	Initial experimental conditions of trans-2-butene ozonolysis during TRAPOZ.....	93
Table 10.	Detection of m/z ion channels during trans-2-butene experiments.....	98
Table 11.	Acetaldehyde yields from trans-2-butene ozonolysis under various conditions compared to past literature data.....	99
Table 12.	HCHO yields from trans-2-butene ozonolysis under various conditions compared to past literature data.....	99
Table 13.	Initial experimental conditions of isoprene ozonolysis during TRAPOZ.....	105

Table 14.	Initial experimental conditions of isoprene photooxidation during ACES 2.....	105
Table 15.	Detection of m/z ion channels during isoprene photolysis experiments.....	110
Table 16.	Detection of m/z ion channels during isoprene ozonolysis experiments.....	111
Table 17.	MVK and MACR minimum yields from isoprene oxidation (photooxidation and ozonolysis) under various conditions compared to past literature data.....	112
Chapter 4		
Table 18.	Initial experimental conditions of myrcene ozonolysis during TRAPOZ.....	123
Table 19.	Initial experimental conditions of myrcene ozonolysis during TRAPOZ 2.....	123
Table 20.	Initial experimental conditions for myrcene photooxidation during ACES 2.....	124
Table 21.	Detection of m/z ion channels during myrcene experiments (TRAPOZ campaign).....	131-132
Table 22.	Detection of m/z ion channels during myrcene photooxidation experiments (ACES 2).....	132-133
Table 23.	Detection of m/z ion channels during myrcene ozonolysis experiments (TRAPOZ).....	134
Table 24.	Aerosol yields of myrcene experiments.....	136
Table 25.	Initial experimental conditions for α -pinene ozonolysis during TRAPOZ.....	138
Table 26.	Initial experimental conditions α -pinene ozonolysis during TRAPOZ 2.....	139
Table 27.	Initial experimental conditions for α -pinene photooxidation during ACES 2.....	139
Table 28.	Detection of m/z ion channels during α -pinene ozonolysis experiments (TRAPOZ).....	144-145

Table 29.	Detection of m/z ion channels during α -pinene photooxidation experiments (ACES).....	145-146
Table 30.	Detection of m/z ion channels during α -pinene ozonolysis experiments (TRAPOZ 2).....	147
Table 31.	Relative abundances for fragmentation of large oxidation products detected in the α -pinene system.....	148
Table 32.	Aerosol yields of α -pinene experiments.....	152
Table 33.	Detected structures in particle phase from off-line analysis of filter samples of α -pinene. Major product is given at the top, followed by secondary and tertiary products, with the addition of identified structures.....	153-154
Table 34.	Initial experimental conditions of limonene ozonolysis during TRAPOZ.....	157
Table 35.	Initial experimental conditions of limonene ozonolysis during TRAPOZ 2.....	158
Table 36.	Initial experimental conditions of limonene photooxidation during ACES and ACES 2.....	158
Table 37.	Detection of m/z ion channels during limonene ozonolysis experiments (TRAPOZ) with proposed structures.....	166-167
Table 38.	Detection of m/z ion channels during limonene photolysis experiments in ACES (nucleation experiments.....	168-170
Table 39.	Detection of m/z ion channels during limonene ozonolysis experiments (TRAPOZ 2).....	170-171
Table 40.	Aerosol yields of limonene experiments.....	175
Table 41.	Detected structures in particle phase from off-line analysis of filter samples from limonene. Major product is given at the top, followed by secondary and tertiary products, with the addition of identified structures.....	177-178
Chapter 5		
Table 42.	Initial experimental conditions of β -caryophyllene nucleation experiments during ACES.....	188

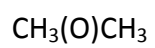
Table 43.	Initial experimental conditions of β -caryophyllene seeded experiments during ACES 2.....	189
Table 44.	Detection of m/z ion channels during β -caryophyllene nucleation experiments.....	192-193
Table 45.	Detection of m/z ion channels during β -caryophyllene seeded experiment.....	193-194
Table 46.	Aerosol yield of β -caryophyllene seeded experiments during 2008.....	200
Table 47.	Detected structures in particle phase from off-line analysis of filter samples β -caryophyllene. Major product is given at the top, followed by secondary and tertiary products, with the addition of identified structures.....	200-202

Chapter 6

Table 48.	Conditions measured during the mesocosm experiments.....	207
Table 49.	The yields of observed gas-phase oxidation products based on the amount BVOC reacted and oxidation product formed.....	211

List of Abbreviations

BVOC	Biogenic Volatile Organic Compound
CI	Criegee Intermediate
CIR-ToF-MS	Chemical Ionisation Reaction Time of Flight Mass Spectrometry
EUPHORE	European PHOtoREactor Facility
FTIR	Fourier Transform Infra Red spectroscopy
HPLC	High Performance Liquid Chromatography
MAC	Manchester Aerosol Chamber
MCM	Master Chemical Mechanism
SOA	Secondary Organic Aerosol
RH	Relative Humidity
VOC	Volatile Organic Compound
oVOC	oxygenated Volatile Organic Compound
Small Compounds:	
HCHO	Formaldehyde
CH ₃ OH	Methanol
CH ₃ CHO	Acetaldehyde



Acetone



Formic acid



Acetic acid

CHAPTER 1. Introduction

The study of the atmosphere and processes within provides a challenge as the area is wide ranging and consists of a complex set of multi-phase interactions. Important aspects of the atmosphere include the study of impacts from global issues ranging from increases in greenhouse gases (and the connection between these and global warming), to regional concerns such as air quality. In addition other aspects, such as the scientific understanding of aerosols in the atmosphere and what role they play in the atmosphere in terms of radiative budget on a global scale is of great importance to fully understand the impact aerosols can have on climate. Processes that govern the formation of Secondary organic aerosols (SOAs) in the atmosphere are still not fully understood despite progress over past few years (Hallquist et al., 2009), and accordingly the work here focuses on further understanding these processes through the formation of SOAs using simulation chambers (see Chapter 2). SOAs are formed following oxidative processes of Volatile Organic Compounds (VOCs), hereafter also called precursors, including a combination of chemical and physical processes like gas-to-particle phase conversion (such as nucleation), or condensation of gaseous compounds upon pre-existing aerosol particles (see section 1.3). Chamber studies (see section 2.2) provide the means of simplifying a complex system (such as the Earth's atmosphere) by being able to isolate compounds and their reaction pathways believed to form SOAs in the atmosphere. Not only is the isolation of compounds to be studied an important and vital factor, but the environmental conditions can also be controlled. This work attempts to identify which compounds give rise to SOAs and more specifically in which environments (e.g., OH or O₃ see section 1.2) aerosol formation is dominant and so provide a greater insight into SOAs in the atmosphere as results from chamber studies can be applied to the atmosphere.

1.1 The atmosphere

The atmosphere of the Earth plays a major role in maintaining life on earth, providing a barrier to the ultraviolet (UV) radiation from the sun. The bulk of the atmosphere consists of nitrogen and oxygen. It is the trace species that are important to several atmospheric processes (Atkinson, 2000). 90% of the total atmospheric mass is located in the troposphere. This is the lowest region of the atmosphere up to 10 km in height to the tropopause, the height of which itself is dependent upon latitude and season. Owing to the position of the troposphere most of the trace species found within this region are emitted from the ground. The bulk composition of the troposphere is 78% N₂, 21% O₂, 1% Ar and 0.036% CO₂ (Atkinson, 2000). Trace gases, although small by many fractions play an important role in atmosphere such as aerosol formation. The work in this thesis is based upon the chemistry that occurs within the troposphere. The atmosphere itself can be divided into regions based on the vertical temperature profile. Each of these has its unique physical and chemical characteristic, with a gradual decrease with height. Figure 1 helps to illustrate the different characteristic sections of the atmosphere.

The work presented here is focused around the tropospheric region of the atmosphere, where the bulk of the atmosphere is retained. Accordingly sources of VOCs and the chemical reaction pathways undertaken in this region will be briefly examined discussed here.

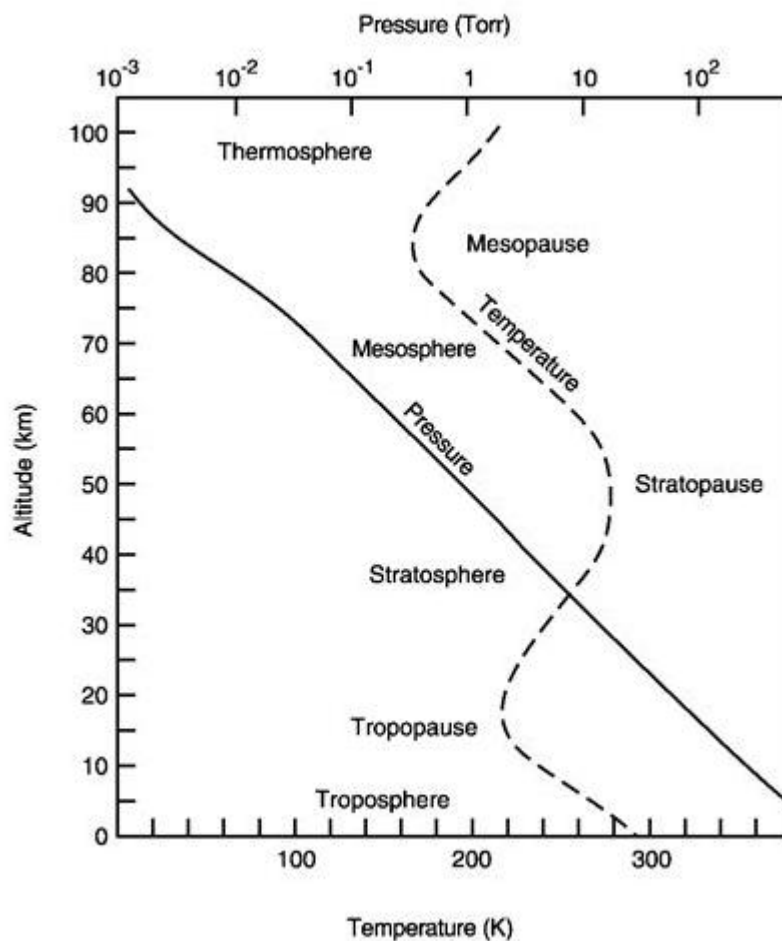


Figure 1 Diagrammatic representation of the atmosphere showing the changes of temperature and pressure with rising altitudes (taken from Finlayson-Pitts and Pitts (2000))

1.2 Tropospheric Chemistry

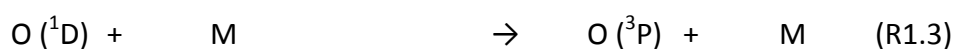
A large number of species are emitted into the atmosphere including volatile organic compounds (VOCs) from biogenic and anthropogenic sources. Particulate matter (PM), O_3 , CO, NO and NO_2 have profound environmental and health impacts (Pöschl, 2005, Harrison et al., 2000, Chameides et., 1999, Akimoto., 2003, Koch., 2007). The chemistry of these species is of particular interest, especially the oxidation processes of atmospheric oxidants. The formation and reactions of these will be discussed next.

The chemistry of the atmosphere is initiated by the process of photochemistry that is driven by the solar spectrum from the sun. The resulting photochemistry reactions (see section 1.2.1 and 1.2.2) form several radical species that have a considerable affect on the resulting composition of the atmosphere by producing highly reactive atoms (or radicals) from photolabile molecules. The high reactivity of these radical species is confirmed by the low concentration detected in the atmosphere on scales as low as parts per trillion (ppt). In the atmosphere, deposition and photochemical processes govern the removal of VOCs by timescales varying from months to minutes (Atkinson & Arey, 2003). Photochemical reactions are dominated by those with the hydroxyl radical (OH) during sunlight hours, but also include reactions driven by peroxy radicals (HO_x and RO_x , where R is an organic substituent), halogen radicals (XO_x , where X are halogens such as Cl, Br, I etc) reactions with ozone (O_3), and during the night with nitrate radicals (NO_3). These reactions are covered in detail in the following sections. The result of photochemistry in the atmosphere is the formation of oxygenated VOCs (oVOCs) which under similar processes result in the removal of these highly oxidised species (such as acids and peroxides) through pathways including continued oxidation to form CO_2 , uptake by atmospheric aerosols and dry deposition (direct loss at the Earth's surfaces) or wet deposition (uptake into rain droplets). However the importance for each of these processes is still not well understood.

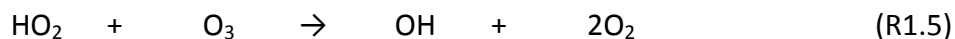
1.2.1 Hydroxyl (OH) radical and ozone (O_3)

The hydroxyl radical is one of the most important species in the atmosphere when considering its low concentrations (2.6×10^6 molecules cm^{-3}), and its role in the atmosphere as a “cleaning mechanism” in the troposphere owing to its high reactivity with a wide-range of organic compounds. For example 90% of isoprene is removed by the OH radical. Primary sources of OH radicals are photooxidation of ozone initiated by UV light in the presence of water. Low levels of ozone are important in the troposphere because photooxidation of O_3 at wavelengths > 290 nm forms the excited oxygen, $\text{O}(^1\text{D})$ atoms (R1.1), which then go on to react with water vapour to produce

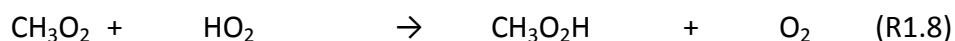
OH radicals (R1.2). O (¹D) can also be quenched via collision with molecular oxygen or nitrogen (R1.3), to form ground state O (³P) which can then reform O₃ (R1.4) or are deactivated to ground state oxygen:



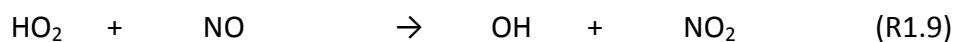
The chemical pathway to OH radical production in the troposphere is heavily reliant upon the fraction of O (¹D) atoms formed and the presence of water in high concentrations. It has been found that 10% of atomic oxygen is excited so that this can form the O(¹D) in the marine boundary layer which then generates OH (Wayne., 1993). The reaction step involved are humidity dependent and as a result environments with high humidity (RH > 50%), such as above forests can produce OH radicals from this reaction as its primary source. OH can also be formed from other processes (e.g. photooxidation of oxygenated volatile organic compounds (oVOCs)) involving products of oxidation, and so can be deemed as secondary sources of OH. Compounds involved in the formation of secondary OH include HONO, HCHO, H₂O₂ and acetone as photooxidation of these species lead to the release of OH. The fate of OH in unpolluted areas (low NO_x) can create peroxy radicals (HO₂ and CH₃O₂) from the reaction with methane or CO. From here HO₂, which has only a lifetime of a few minutes, can react with ozone leading to more ozone destruction (R1.5) and reforming of the HO₂ with the reaction of O₃ with OH (R1.6):



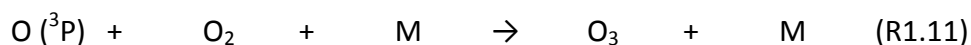
Alternatively HO_2 can form peroxides acting as a chain termination reaction by either combining HO_2 (R1.7) or reacting with organic peroxy radicals (R1.8) to form organic hydroperoxides and oxygen:



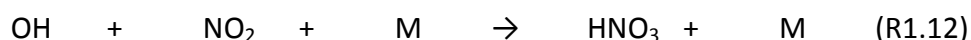
In addition, CH_3O_2 can also oxidise NO to NO_2 . In polluted areas where high levels of NO_x are common the formation of the peroxides contend with the oxidation of NO to NO_2 . NO can be oxidised with HO_2 as a source of OH and NO_2 (R1.9)



The formation of NO_2 is significant as this can be a further source of ozone from photooxidation of NO_2 (R.10). Ozone, another important species in the troposphere with regard to degradation of VOCs, is then formed through collisionally stabilised $\text{O} (^3\text{P})$ reactions with oxygen (R1.11):



The net photochemical formation or loss of O_3 in the troposphere depends on NO concentration, and the rate is determined by the reaction of HO_2 radical with NO . Other results of OH radicals may be the formation of nitric acid (R1.12), which is dependent on the NO_2 :



This is a significant way of losing NO_x and HO_x in the troposphere. Other productions of HO_x can be from ozonolysis of alkenes dependent upon the structure of the alkenes. A summary of all the reactions mentioned is given in figure 1.2, which summarises the OH -initiated oxidation of methane and CO . Ozone is formed from NO_2 following photooxidation, steps that were previously highlighted (R1.10 and R1.11).

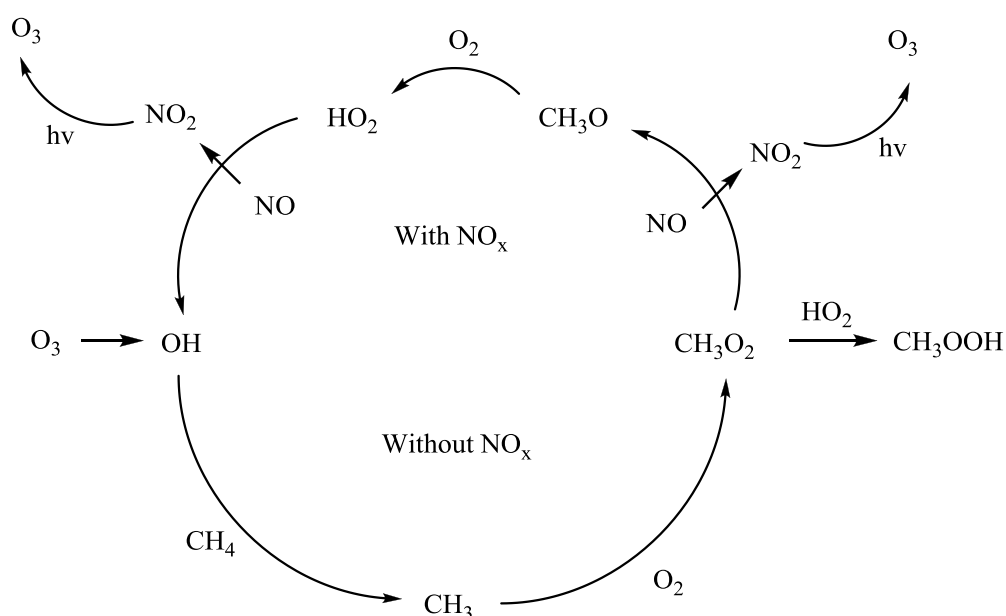


Figure 2. The oxidation of methane adapted from Wayne et al 2000. OH is reformed from the oxidation of NO to NO_2 in the presence of NO_x . Reactions involved in the absence of NO_x are given in the bottom half of the diagram.

1.2.2 The nitrate radical (NO₃)

Another important radical species is that of the nitrate radical (NO₃) which is formed by NO and NO₂ reactions with O₃ (R1.13 and R1.14):



The nitrate radical are formed continuously in the presence of NO_x and O₃ but are rapidly photolysed during the day with a lifetime of ~5 s. As a result there are low daytime concentrations of NO₃, making it more important with respect to night time chemistry. It has been known that NO₃ has high reactivity with VOCs such as unsaturated hydrocarbons species like isoprene. The three main reaction species therefore can be linked, as any factors that influence OH concentrations, and the amount of NO to NO₂ conversion will impact of the net formation of O₃. NO₂ can also react with NO₃ to form dinitrogen pentoxide (R1.15) an important loss of NO_x by deposition or uptake by aerosols:

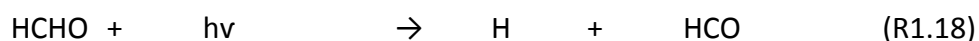


The N₂O₅ can then react with water vapour to form HNO₃ (R1.16), thereby a loss process of N₂O₅ and ultimately NO₃.



HNO₃ has contributed towards atmospheric acidification of particles (Wayne, 1993). The heterogeneous reactions of N₂O₅ and NO₃ contribute to formation of aerosol nitrate (Zhang et al., 1994, Tang et al., 2004, Sullivan et al., 2007) as well as influences on aging of organic aerosols in the atmosphere (Tang et al., 2010).

A secondary source of OH and NO radicals is the photolysis of HONO (R1.17). Other secondary sources include that of the photooxidation of formaldehyde (HCHO) that is produced from oxidation of methane (Figure 1.2) a major trace gas emission in the atmosphere (R1.18).



HONO formation is due to both heterogeneous and homogeneous processes involving NO_x, although these mechanistic are not fully understood (Indarto, 2012). HONO has also been observed to form at night, leading to morning pulses of OH levels after sunrise (Atkinson, 2000). The photolysis of HCHO leads to two radical fragments (H and HCO), both of which can re-enter the HO_x chain via the reactions of these radical species (R1.19 and R1.20)



OH formation can then be explained as previously shown in reaction schemes R1.5 and R1.9. It is believed that industrialisation has changed the oxidative capacity in the

troposphere, which is the total atmospheric burden of the three oxidants, OH, O₃ and H₂O₂, although some have used this term to present the mean total global OH (Thompson, 1992). Thereby an increase in NO_x, and considering secondary OH production shown above, has increased the reaction processes involving VOCs. Moreover, OH initiated oxidation reactions produce a wide range of products, which can influence aspects such as radiative forcing, air quality (from the formation of ground level ozone and SOA) and acid rain.

1.2.3 Sources of Tropospheric VOCs

Tropospheric VOCs have numerous sources including both biogenic and anthropogenic origins. Natural sources include biomass burning, vegetation and agriculture (Piccot 1992), whereas anthropogenic contributions are from man-made sources including industry and automobile emissions. The thesis focuses upon the impact from naturally occurring VOCs so-called biogenic volatile organic compounds (BVOCs). These often consist of hydrocarbons along with partially oxidised VOCs such as alcohols, acids, ketones and aldehydes released in smaller quantities. BVOCs are a family of highly reactive species in the atmosphere and so play an important and significant role in atmospheric chemistry. It was Went (1950) whom first suggested the importance of BVOCs in the atmosphere, which was further strengthened by Chameides (1988) and Trainer (1987). The most abundant BVOCs consist of isoprene (hemiterpene), C₅ species, compounds classified as monoterpenes, C₁₀ species, and sesquiterpenes, C₁₅ species, which compose of, by definition, multiple isoprene units (Lathiere, 2005). A range of monoterpenes and sesquiterpenes are emitted into the atmosphere, and so a selected few compounds within each family are studied here. Due to the high reactivity and volatility they all exhibit in the gaseous atmosphere, and as a result of double bonds functionalities, this can lead to the formation of a vast scope of gas phase oxidation products that will be discussed in the following chapters. Owing to this fast reactivity of VOCs, reactions will occur within the troposphere and are

potential sources for tropospheric aerosols. Estimated emissions of VOCs studied are given in each corresponding chapter, but briefly biogenic emissions account for up to 90% of all VOCs (Guenther et al, 1995). Due to this large accountability of VOCs the potential formation of SOA from these biogenic species are of particular interest and importance. Also included is an examination of ozonolysis reactions of lower mass VOC such as ethene, which can also be of significant interest as ethene emission rates are estimated to be about 15 Tg yr^{-1} (Leather 2012).

1.3 Atmospheric aerosols

Aerosols are described as relatively stable suspension of solid or liquid particles in a gas (Finlayson-Pitts and Pitts 2000) and can be classed into two categories, primary and secondary. Primary particles are directly emitted into the atmosphere from sources such as volcanic eruptions, combustion of fossils fuels, mineral dust, sea salt, industry, traffic-related suspensions from roads, biomass burning and soil (Seinfeld et al 1998, Buseck et al 1999). Primary particles usually consist of coarse particles (diameter $> 10^{-6}$ m). Secondary particles are formed through chemical and physical processes in the atmosphere, such as gas-to-particle conversion (nucleation) and condensation of gaseous compounds on pre-existing aerosol particles.

These consist of finer particles (diameter $< 10^{-6}$). Atmospheric aerosols have been the focus of extensive investigations due to their impacts in climate change through direct and indirect radiative forcing (Charlson., 1992; Tsigaridis., 2007) although this characteristic is not fully understood and current scientific knowledge regarding aerosols and climatic influences are outlined by the IPCC (Intergovernmental Panel on Climate Change) given in Figure 3.

Radiative Forcing Components

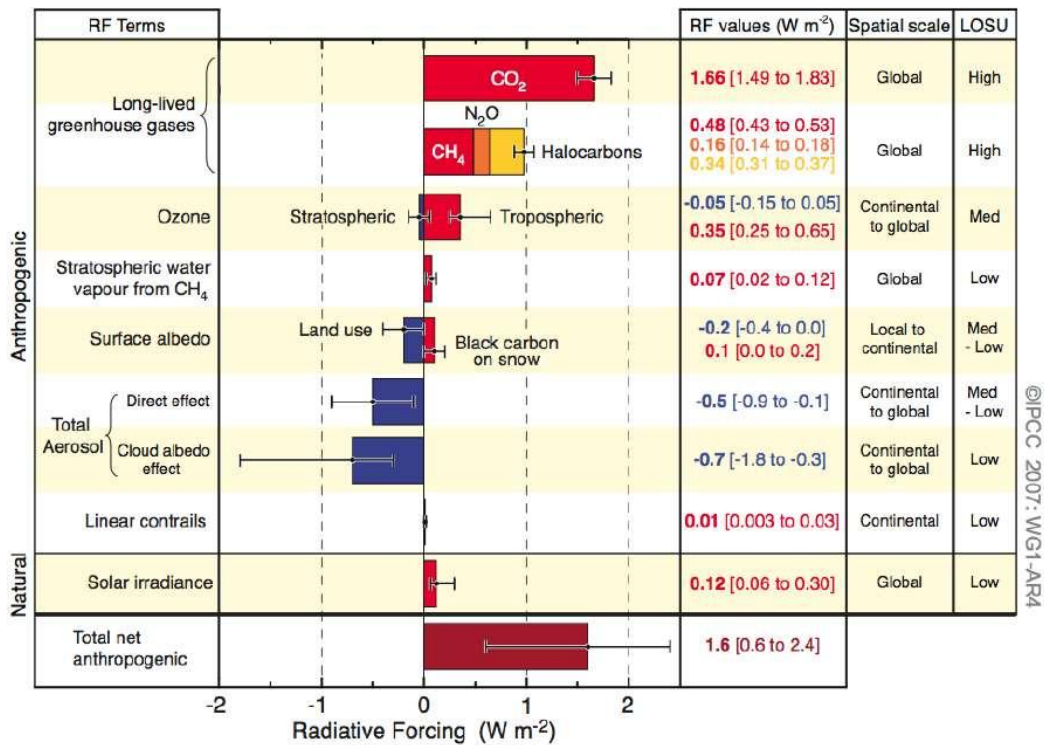


Figure 3 Current scientific knowledge on radiative forcing contributions of various sources, including aerosols, as presented in the IPCC Fourth Assessment Report: Climate Change 2007

Compounds relating to the influences upon health on a local, regional and global scale are not yet been fully established (Alfarra., 2006). Chemical and physical transformations of airbourne particles are diverse, changing aspects of the particles such as composition, particle size and structure (Pöschl., 2007). Aerosols residing in the troposphere also contribute to smog and increase such influences on lung difficulties, particularly in large urban areas. Other properties include the ability to act as cloud condensation nuclei (CCN) in which water droplets can condense onto the particles to form cloud droplets (Sun et al 2006, Lohmann et al 2005), although the ability to act as CCN in dependent on properties such as size and chemical composition (Novakov et al 1993). The main sink of aerosol particles in the atmosphere reside in wet deposition for particles in accumulation mode (0.1 – 1 μm), which involves precipitation of cloud particles that reach the Earth’s surface. Other sink include dry deposition, the process of airbourne particle removal through means such as diffusion,

convective transport and adhesion to the Earth's surface. These also play an important role in regional and local health effects and air quality (Monks, 2009).

Atmospheric composition of inorganic aerosols are largely made up from sulphate (SO_4^{2-}) and nitrate (NO_3^-) constituents, which are formed in the atmosphere following the oxidation of gaseous SO_2 and NO_x . For both these constituents, there is a gas phase and multiphase route to the formation of sulphuric and nitric acid. The gas phase reactions involve the previously discussed OH radical, whilst the multiphase reactions entail a number of different oxidation agents (such as H_2O_2 and O_3) following the uptake of SO_2 and N_2O_5 in the liquid phase (the latter a result of hydrolysis previously mentioned). Owing to the low saturation vapour pressure of sulphuric acid it prefers to reside in the particle phase, whereas higher saturation vapour pressures for nitric acid make the partitioning of this compound into the particle reliant upon humidity, temperature and the presence of NH_3 (to form NH_4NO_3). Both constituents in the particle phase can be neutralised by ammonia, and as sulphuric acid is always neutralised before nitric acid, the latter tends to reside in the gas phase where ammonia concentrations are low. Nitric acid can also be neutralised by other components found in mineral dust (Pérez, 2008). Here, the interest lies within organic aerosols (OA) formed as a result of natural emissions, as the contribution of OAs can range from 30-70% of total aerosol mass (Zhang, 2007), although the formation, composition and processes involved are not fully understood. Similar to primary and secondary particles, OAs also have primary aerosol (POA) and secondary aerosol (SOA) sources dependent upon direct emission into the atmosphere, or from chemical reactions. Primary particles are directly emitted into the atmosphere as liquids or solids from sources including biomass burning, volcanic eruption, soil, sea salt, mineral dust, incomplete combustion of fossil fuels and related wind-driven debris from roads or biological material such as pollen (Pöschl 2005). It is fundamentally important to differentiate between POA and SOA as POAs can be controlled, whereas SOAs, following a multitude of chemical reaction pathways in the atmosphere are difficult to monitor. Establishing this difference between POA and SOA can be complicated owing to POA that evaporates and reacts in the gas phase of the atmosphere leading to further aerosols (Donahue et al., 2006), giving SOA characteristics similar to POA in the

atmosphere through aging. SOA are formed from chemical reactions of VOCs released in the atmosphere. VOCs emissions into the atmosphere are estimated to be 10 times larger from biogenic sources compared to anthropogenic sources (Heald et al., 2008; Tsigaridis, 2007). VOCs formed from oxidative mechanisms in the atmosphere are believed to contribute to aerosol formation through such processes as nucleation or gas-to-particle phase partitioning. New particles are formed via the process of nucleation of non or low volatile gas-phase compounds emitted from both biogenic or anthropogenic sources. Nucleation can occur by several different methods, i) binary nucleation, ii) ternary nucleation and iii) ion-induced nucleation. An example of binary nucleation is the nucleation of sulphuric acid and water, which occurs when the saturation vapour pressure (of a sulphuric acid-water mixture) exceeds the vapour pressure of sulphuric acid. However particle formation rates have been shown to be greater than the calculated binary nucleation rates (Holmes 2006) indicating that further formation mechanisms must exist. One process that enhances rates is ternary nucleation. Ammonia has been shown to enhance sulphuric acid nucleation rates by decreasing the vapour pressure of sulphuric acid (Weber et al., 1998). Finally, ion-induced nucleation is the process where the ionic charge in particles increases the formation of larger particles due to the effect of electrostatic forces in enhancing the stability of charge clusters and promoting higher growth rates. However current measurement methods restrict the potential for full understanding of nucleation processes as current instruments are only able to detect particles as small as 3 nm. A potential lag time of up to 4 hours between nucleation and detection can be observed due to the time needed for the particle to grow to these detectable levels (Holmes 2006). An important mechanism of particle growth is known as agglomeration or coalescence. Essentially this is where a large particle moves through a field of smaller particles, with this larger particle “sweeping up” the smaller ones, and increasing its size. Gas-to-particle phase partitioning of organic compounds is dependent upon the liquid-phase vapour pressure at ambient temperatures, the surface area of particles per volume of air and the chemical nature of the absorbing particles. Gas-to-particle partitioning is best described by Pankow (1994) where equation (1) has been used to parameterize this chemical process.

$$K_{p,i} = \frac{F_i/TSP}{A_i}$$

Where the partition constant for a compound i [$K_{p,i}$ ($\text{m}^3 \mu\text{g}^{-1}$)] is controlled by the concentration of total particulate matter [TSP ($\mu\text{g m}^{-3}$)] and the particle associated concentration [F_i (ng m^{-3})] and the gaseous concentration [A_i (ng m^{-3})] of compound i . Pankow then derives an equation for the partition constant that uses adsorptive and absorptive contributions to $K_{p,i}$ by theoretical predictions

$$K_{p,i} = \frac{1}{p_{L,i}^0} \left[\frac{N_s a_{tsp} T e^{(Q_L - Q_v) / RT}}{1600} + \frac{f_{om} 760 RT}{MW_{om} \zeta_i 10^6} \right]$$

The two terms in brackets representing adsorption to solid particle surfaces (first term) and the absorption into a liquid organic matter phase (second term). Where R is the gas constant ($8.314 \text{ J mol}^{-1} \text{ K}^{-1}$), T is the temperature (K), $p_{L,i}^0$ is the vapour pressure of the compound i as a liquid, N_s is the surface concentration of sorption sites for adsorbing surface, TSP is total concentration of suspended particulate matter, a_{tsp} is the specific area of suspended particles, Q_L is the enthalpy of desorption from adsorbing surface, Q_v is the enthalpy of vaporisation of the pure liquid, f_{om} is the weight fraction of TSP that is the absorbing om phase, om is the organic material, MW_{om} is the mean molecular weight of the absorbing organic material and ζ_i is the activity coefficient of the compound i in the om phase on the mole fraction scale.

Essentially gas to particle partitioning is an equilibrium of partitions that are based on vapour pressure, aerosol concentration and activity coefficients. Approximations can be made where compounds with a liquid phase vapour pressure of less than 10^{-6} Pa reside purely in the particle phase (which are known as non volatile compounds) and those with a vapour pressure greater than 1 Pa exist only in the gas phase (Wayne, 1993). The intermediate group are classed as semi volatile organic compounds (SVOCs)

which are present in either particle or gas form (Donahue et al., 2006). Primary sources of these VOCs include both anthropogenic and biogenic, with atmospheric alkenes and their ozonolysis mechanisms having received renewed interest in recent years, owing to their importance in atmospheric phenomena such as secondary organic aerosol (SOA) and their role as a source of radical species, which is particularly significant during night time chemistry (Gutbrod et al, 1997). Important for growth of aerosols are the hygroscopic properties of particles (i.e. a measure of water uptake). These can be altered through oxidative processes and so are important for not only aerosol growth, but growth of individual particles following oxidative processes. If organic compounds push this property beyond thresholds the particles can take up water (Hegg, 2008).

1.4 Ozonolysis of alkenes

Ozonolysis reactions of simple alkenes are discussed in Chapter 3, and so ozone addition to alkenes is briefly described here. Ozonolysis methodology is also applied to reaction mechanisms with isoprene and monoterpenes elucidated in Chapter 3 and 4. Ozone reaction with the double bonds of alkenes in the troposphere can be part of day and night time chemistry. Although it is believed that daytime chemistry is dominated by OH chemistry high levels of ozone can still present a significant source of oxidation initiation. Alkene-ozonolysis in the gas phase is best described by the mechanism outlined by Criegee using knowledge of the liquid-phase reaction system (Criegee., 1975). A summary of the reaction scheme is given in Figure 4. An unstable and energy rich primary ozonide is formed following the electrophilic addition of O_3 to the alkene double bond to yield a primary ozonide, or 1,2,3 trioxolane (1). This primary ozonide then rapidly decomposes in a highly exothermic step into a carbonyl oxide and a carbonyl compound via cleavage of a C-C bond and an O-O bond (2). It is this decomposition of Criegee Intermediates (CI) that produce OH as a by-product

(Pfeiffer., 2001). The excited carbonyl oxide or CI can undergo bimolecular reaction, or eject an $O(^3P)$ to yield a carbonyl compound (3). Reaction with water (4) can lead on to produce an aldehyde or a carboxylic acid via an excited α -hydroxy hydroperoxide intermediate (4a). The stabilised Criegees that do not react in bimolecular reactions decompose and rearrange to form an acid (5) or an ester (6) (Olzmann 1997; Kroll 2001) dependent on the substituent present and the stereochemistry of the Criegee intermediate that governs the reaction pathways. In the ozonolysis of simple alkenes $O(^3P)$ atoms are not formed in significant amounts (Wegener 2007) but this is not the case for larger biogenic species. Owing to ozonolysis reactions occurring at night it can play a role as a nighttime source for OH radicals. In addition to ozone reactions for a range of VOCs from simple alkenes to monoterpenes, photooxidation reactions for certain species were also conducted and so the reaction of the OH radical on alkene functional group species will also be discussed. Works regarding humidity affects have also been studied for ozonolysis reactions, as reaction steps shown (Figure 4) indicate specific oVOCs are formed from stabilised CI through H_2O dominant channels that could be important contributors towards SOA formation.

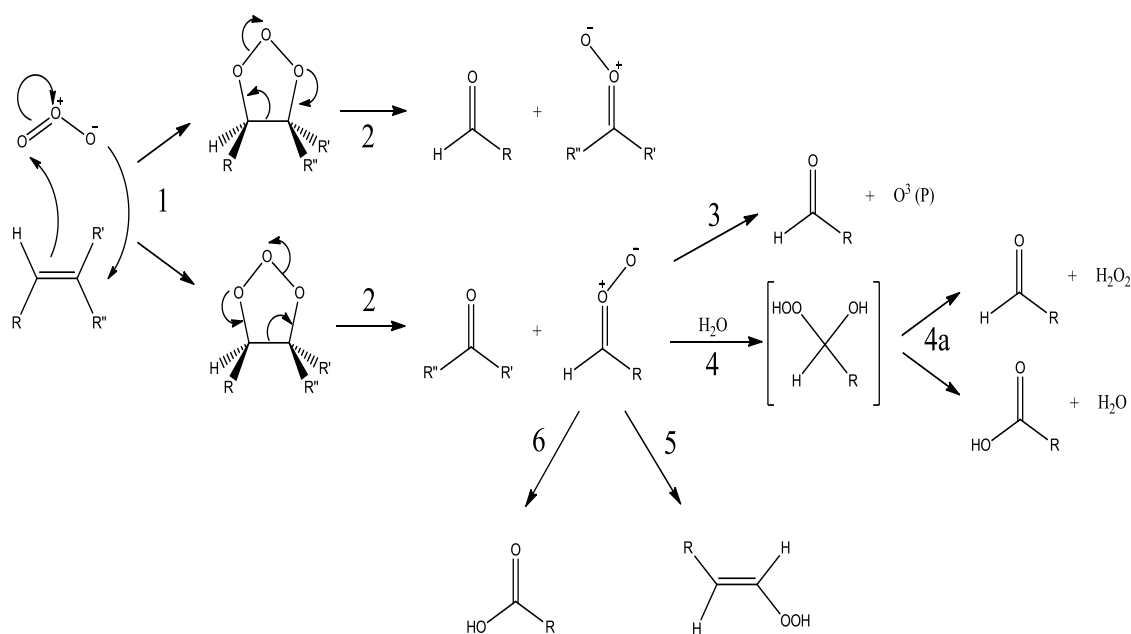


Figure 4. The reaction scheme for initial ozonolysis reaction with alkenes. After initial 1,3 dipolar ozone addition to the C double bond, a carbonyl compound is formed with a carbonyl oxide (the Criegee Intermediate CI) which can then go on to react or rearrange further to produce carbonyls, aldehydes, esters and hydroperoxides.

1.5 OH-initiated reactions

OH addition to an alkene species like the ozone reaction occurs at the carbon double bond. Figure 5 shows an overview of OH addition to a carbon-carbon double bond in an alkene species. The OH radical seeks out the electron-rich area of the double bond formed from the occupied p-orbitals, and attaches itself to one of the carbons. The carbon to which the addition of the OH radical is favoured is governed by the carbon attached to the larger number of alkyl groups. The C-OH bond formed involves the unpaired electron on the OH radical and an electron from the double bond, resultantly the remaining electron that was involved in the π -bond becomes localised on the neighbouring carbon. The resulting intermediate (A_i and A_{ii}) can then undergo addition of O_2 in an oxygen rich environment to produce the radical species (X_i and X_{ii}). In a NO_x environment, reaction with NO can then occur to form nitrate species. These reaction steps are also a source of NO_2 with O abstraction, and a HO_2 or RO_2 source depending on the compound involved in the decomposition stage via bond cleavage.

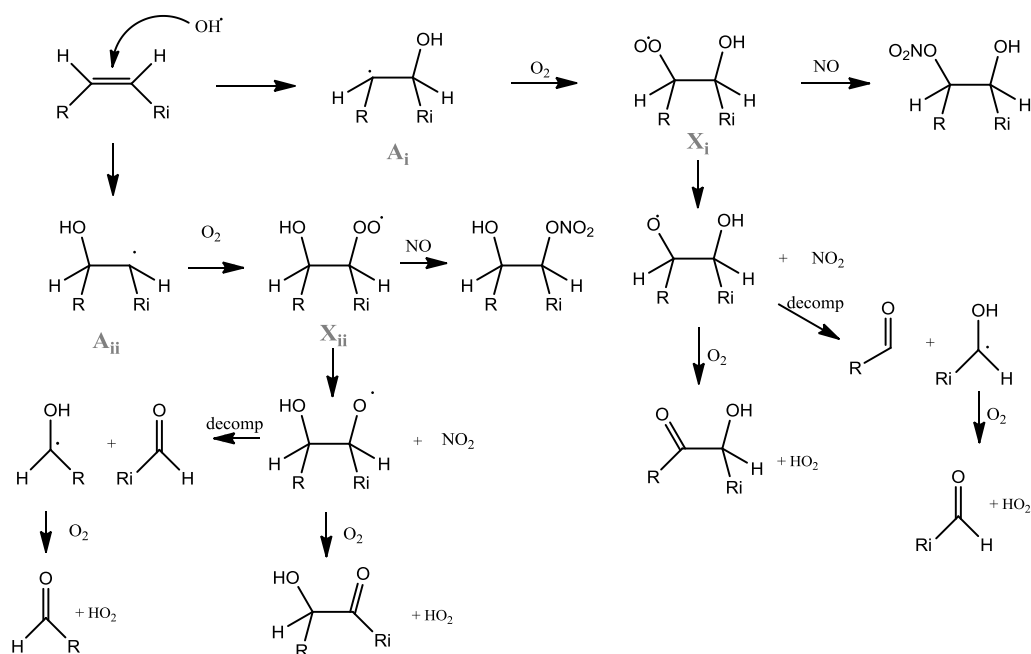


Figure 5. Overview of an OH radical addition to a carbon-carbon double bond of an alkene adapted from Calvert (2000).

A further reaction mechanism must also be considered, H-atom abstraction which is dominant in alkane reactions with OH. It is believed that these reaction mechanisms become important with increasing temperatures and so will be discussed further, as oxidation products formed via this reaction pathway could be observed from photooxidation reactions that have the potential to produce unsaturated aldehydes and ketones which could be potential contributors to aerosol formation owing to the low volatility that they exhibit. This reaction step is seen as unimportant for smaller sized alkenes in which most of the past work has been focused upon reaction rates as large oxidation products are not observed during the oxidation process. For example the extent of H abstraction for ethene was <2.5% of the reaction contribution (Howard 1976; Bartels et al., 1982), this value increasing with molecule size and so this reaction step could be deemed important for the production of oxidation products that display characteristics of those that play a role in SOA formation.

1.6 Simulation Chambers

The study of reactions of simple alkenes, isoprene and monoterpenes under atmospherically relevant conditions under both “dark” ozonolysis and photooxidation experiments were conducted at two different chamber sites. This will be addressed in more detail in Chapter 2. Chamber studies have played an increasing role in understanding gas-phase atmospheric processes, and are becoming increasingly utilised to explore the chemistry behind aerosol formation and evolution from gas-phase processes. Difficulties within this area in science are due to both current restrictions on sensitivities of instrumentation available for field and laboratory studies, alongside the chemistry involved within these processes. Chamber facilities come into their own as they have the ability to essentially simplify a complex system, (i.e. the atmosphere) by focusing investigations on experimentally “constrained” conditions. Resultantly, specific investigations into targeted tropospheric processes can be made. These include SOA forming potential of individual VOCs dominant in the

troposphere, along with the monitoring of changes in the atmosphere in response to these “controlled” oxidative processes (e.g. changes in reaction rates of VOCs and OVOCs with differing relative humidity). Evaluation of these experiments are crucial in order to better understand tropospheric processes, of which are the contributing factors towards SOA formation in the atmosphere. Other advantages of using chamber facilities is the ability to study reactions and processes close to atmospheric relevant concentrations and timescales (between several hours to days). In this study, work is presented on an hour timescale for a variety of different VOCs and focused around the gas-phase speciation detected with the University of Leicester Chemical Ionisation Reaction-Time of Flight-Mass Spectrometer (CIR-ToF-MS). This instrument essentially is able to measure a range of VOCs and oxygenated oVOCs in real-time at sensitivities approaching sub parts per billion (ppb) range. Details of this instrument are given in Chapter 2. From the observed gas-phase composition and evolution, we are also able to compare experimentally determined results to that of current atmospheric models in order to evaluate the present accuracies of models, and thereby current scientific understanding. The model used for comparison purposes was that of the Master Chemical Mechanism (MCM)

1.7 The Master Chemical Mechanism (MCM)

The model process exploited a numerical simulation through a zero dimension box model approach. The degradation of VOCs ethene, isobutene, trans-2-butene, isoprene, α -pinene and limonene are all evaluated in the Master Chemical Mechanism version 3.1 (MCM) which describes the degradation of a total 142 non-methane VOCs. The protocols used for describing the MCM and the series of subsections used for initiation reactions, the degradation chemistry of first generation products and further degradation of these products for aromatic VOCs are given in detail by Jenkin et al., (2003). The reaction protocols described were extracted from the website <http://mcm.leeds.ac.uk/MCMv3.1/> for the isoprene and α -pinene system, with the

subsets of each reaction accounting for evolution for a total number of 201 organic species in the isoprene mechanism, and a total number of 321 species for the α -pinene system. A newly updated version of the MCM (version 3.12) has the degradation pathway for limonene oxidation (extracted from the website <http://mcm.leeds.ac.uk/MCM/>). Mechanisms for reactions of simplified ozonolysis were also run on the model for comparative purposes. This mechanism accounts for a total 539 organic species. The MCM utilises photolysis rates, $j(\text{photolysis})$, calculated from parameterisations as a function of solar zenith angle. These are derived from a two stream isotropic scattering model for clear sky conditions, unless measured photolysis rates are available. Owing to the “dark” experiment conditions used, $j(\text{photolysis})$ rates can be ignored for modelling purposes. However, it is important to take into account wall loss when considering chamber studies and initial HONO concentrations. An auxiliary mechanism for wall loss has been set up for the EUPHORE chamber facility that accounts for the loss of organic species to the chamber walls.

1.8 Thesis Motivation

As previously mentioned, there is still a gap in the scientific knowledge between gas-phase reactions in the atmosphere and the formation of particulate species due to the complexity of chemistry and microphysics involved. Therefore the principle aims of this study are:

- Identify and quantify the gas-phase composition from the oxidation of various VOCs present in the atmosphere under varying conditions and
- Bridge the gap between aerosol and gas-phase compounds by identifying species present in both phases.
- To understand potential influences on SOA formation, experiments were conducted under differing conditions to evaluate the atmospheric implications from these varying environments

In order to present accurate data, the instrumentation capabilities of the CIR-ToF-MS were also tested under a variety of conditions, with the potential use of a differing ion source with the potential advantages of this outlined.

These objectives were achieved through experiments conducted at atmospheric simulation chambers, the Manchester Aerosol Chamber (MAC), at the University of Manchester, UK as part of the APPRAISE (Aerosol Properties, PRocesses And InfluenceS on the Earth's climate) project, and the European PHOtoREactor (EUPHORE), in Valencia, Spain, as part of the NERC funded TRPAOZ (Total Radical Production and degradation Products from Alkene OZonolysis) project.

The TRAPOZ project was a 2 month intensive programme conducted in two separate one month slots during August 2008 (TRAPOZ 1) and May 2009 (TRAPOZ 2). The purpose of the project was to directly observe the total radical production and degradation products of selected alkenes during ozonolysis experiments. The production of these radicals is of interest as it could influence the radical budget in rural and urban environments, thereby affecting the oxidative capacity of the atmosphere, the ability to remove of greenhouse gases and pollutants.

The ACES project was part of a larger consortium involved with the APPRAISE scheme, also NERC funded. The APPRAISE work was based on further understanding atmospheric aerosols in order to improve models climate change on regional scales. By establishing influences of aerosols on clouds (indirect affect on climate change), the Earth's radiation budget (absorption and scattering of radiation) and their contribution to feedback processes between land, climate and the biosphere, advances to climate models are expected, providing less uncertainty in climate change models. In order to achieve these goals, a project was funded a total of 5.6 million from NERC and 4 work packages (WP) were created within the APPRAISE project. These consisted of WP1: Chamber studies of biogenic VOC emissions and SOA formation, WP2: Field Measurements, WP3: Development of SOA formation mechanisms and WP4: Scaling-up activities relating local scale measurements to regional and global scales. Work produced in this thesis is part of WP1, where separate 3 month campaigns were conducted at the Manchester Aerosol Chamber during November 2007 (ACES 1), June-

July 2008 (ACES 2) and June-July 2009 (ACES 3). Specific to the work package, the aims of ACES was to, i) quantify BVOC emissions from native and commercial tropical forest plant species; ii) characterise gaseous oxidation products from key BVOCs and compare emissions to mechanisms developed in WP3; iii) Characterisation of SOA formed from BVOCs in a range of photochemical and seed aerosol conditions; iv) comparison of SOA formation processes from single BVOC experiments to a number of BVOCs in a mesocosm experiment; and v) use synthetic mixtures of precursor compounds to replicate emissions observed during mesocosm experiments to further validate model predictions.

1.9 Thesis Overview

The thesis is presented in 6 further chapters, and within each chapter, a brief introduction to the VOC studied and their atmospheric relevance is included, except for the experimental chapter. The following work is subdivided into 6 chapters:

Chapter 2 describes both the experimental approach and instrumentation utilised in the investigation. This includes a brief description of the two chamber facilities utilised, the MAC and EUPHORE with a brief description of all instrumentation used with emphasis on the CIR-ToF-MS. The differing experimental approaches on both sites is described to highlight the difference between the “dark” ozonolysis experiments run at EUPHORE and photooxidation experiments run at MAC.

Chapter 3 explores ozonolysis of simple alkenes. Here the focus is on detection of gas-phase species from a fairly simple system (e.g. ethene). Due to on-site instrumentations, comparisons could be made to evaluate the performance of the CIR-ToF-MS to identify and quantify oxidation species from single parent VOCs. The abilities of gas-phase detection of the CIR-ToF-MS were also tested under higher

humidity environments in order to determine the influence of wet conditions on its performance. It is known that potential back reactions from protonated compounds and water under high humidity conditions has been attributed to reduction in sensitivity for certain species. A brief examination on the potential use of a new ion source on the CIR-ToF-MS is also explored. Previous studies using this instrument have been exclusively conducted with a ^{241}Am source and the wide applications of this technique have been presented, with a new ion source adapted from hollow cathode discharge. The scale of partitioning of VOCs and their oxidation products into the aerosol phase are largely influenced by atmospheric conditions such as NO_x concentrations, humidity and the presence of pre-existing seed particles. Here exploration of isoprene oxidation is used to investigate the influences of such factors into potential SOA formation, and how controlled changes in the oxidative environment can alter the magnitude of SOA and important oVOC production.

In Chapter 4, the investigations of several monoterpenes are explored with emphasis based on comparisons of the gas-phase composition from both ozonolysis and photooxidation experiments being compared. The influences of SOA yield from differing environmental conditions are also explored in order to build-up a better picture of gas-phase and aerosol connections for the species myrcene, limonene and α -pinene.

Chapter 5 presents atmospheric investigations of sesquiterpene oxidation. A new novel approach to forming an organic seed from β -caryophyllene was also explored and results presented for potential future chamber atmospherically relevant experiments, given the fast reaction rate of this species. The gas-phase composition of the degradation pathway is presented under photooxidation conditions.

Chapter 6 examines the potential aerosol formation from fig and birch tree species in a mesocosm experiment. Dependent on the tree species, either dominant emitters of isoprene or monoterpenes were investigated at relatively low atmospheric concentrations. The gas-phase composition was probed, and with the identification from individual oxidative systems, specific characteristics of oVOCs were elucidated. High levels of isoprene from tree emissions resulted in no SOA formation, differing to higher levels of monoterpene concentrations where compared to isoprene resulted in SOA formation. The potential for isoprene suppression of SOA in certain environmental conditions is explored.

Finally, Chapter 7 summarises the scientific findings of these investigations with attempts to highlight future work to be carried out to ascertain further approaches to research to aid in achieving greater understanding in aerosol formation and their influences on climate.

CHAPTER 2. Instrumentation and Experimental

This chapter describes the instrumentation involved in the current work. Both aerosol simulation chambers are briefly described within this chapter, with special attention made on the operations of the University of Leicester Chemical Reaction Ionisation-Time of Flight-Mass Spectrometer (CIR-ToF-MS). Chapters 3 to 6 describe results from several atmospheric chamber experiments conducted to better understand the chemistry and secondary organic aerosol forming potential of several atmospherically relevant VOCs. In order to observe the dynamic interplay between different atmospheric oxidation precursors and their volatile and semi-volatile VOC products, measurements of gas phase species are required in real-time. In the studies presented, this was achieved by using the (CIR-ToF-MS) developed and built at the University of Leicester.

Several methods currently exist for the measurement of VOCs and OVOCs. Gas chromatography (GC) (Isidorov et al., 2003; Xu 2003) usually coupled to a mass spectrometer (GC-MS), Fourier Transform Infra red (FTIR), differential optical absorption spectroscopy (DOAS) and Proton Transfer Reaction-Mass Spectrometer (PTR-MS)(Hewitt et al., 2003; Steeghs et al., 2004). This chapter is subdivided into three sections: Section A describes in detail the operating system of CIR-ToF-MS and calibration work conducted. Section B presents a description of the two chamber facilities, European PHOtoREactor (EUPHORE) and Manchester Aerosol Chamber (MAC) with inclusions of on-site instruments important in these studies. Section C finally describes the methodology approach for the two major differing experiments conducted, “dark” ozonolysis and “light” photooxidation.

2.1 CIR-ToF-MS

CIR-ToF-MS works on the same principles as PTR-MS where proton transfer is achieved from the reagent gas to sample gas along a fixed reaction vessel, the drift tube (Blake et al., 2004). If excess proton donors are available, the concentration of the targeted acceptor molecules in the sample can be calculated by using the measured ratio of donor to acceptor ion signals. The PTR-MS studies come into their own as on-line measurements can be conducted in real-time. Common PTR-MS are equipped with a quadrupole mass spectrometer which hinders examination of a complex system as m/z ion channels have to be preselected for analysis. In doing so, sensitivities for the selected channels are increased, but they do suffer from not monitoring the entire spectra. In comparison ToF-MS system allows almost instantaneous acquirement of an entire mass spectrum. This is vital for analysis of unknown systems coupled to the characteristically standard higher resolution of a ToF-MS over the quadrupole counterpart makes this technique ideal for low concentration analysis of gas-phase organic atmospheric species. As such, a sensitivity trade-off between selected channels over measuring larger spectra can be seen. Work within the thesis is based on measurements of known and unknown gaseous environments. The recorded mass spectras were then analysed to compare unknown emissions (e.g. mesocosm, Chapter 6) to known VOCs studied at specified concentrations (e.g. nucleation experiments, Chapter 4).

CIR-ToF-MS was operated under conditions that promote ionisation based upon the same principals as Proton Transfer Reaction-Mass Spectrometry (PTR-MS). It was Lindinger et al (1998) who achieved the initial application of proton-transfer to online mass spectrometry, using water vapour as chemical ionisation reagent, producing hydronium to undergo proton transfer. The basis of PTR-MS is governed by proton transfer from hydronium (if water is used as the reagent gas) to analytes in the sample gas (R) in the drift cell to give an ionised molecule RH^+ . (R2.1). It is this protonated molecule that is detected and measured in PTR-MS.



PTR ionisation is particularly useful in the detection of VOCs as only molecules with proton affinities higher than that of a H₂O (691 kJ/mol) can accept a proton from H₃O⁺. A limitation of this functionality would thereby be that compounds of lower proton affinities cannot be seen, but with this is the benefit of a cleaner mass spectrum as the ionisation technique excludes major air components such as N₂, O₂ and CO₂, thus eliminating strong background signals. The mechanism of ionisation used in our instrument is considered a fairly soft technique as it reduces ion fragmentation within the drift cell (Blake et al, 2004). The CIR-ToF-MS is able to detect VOCs in the gas phase in concentrations at the parts per billion level and has good mass resolution, particularly for lower mass compounds ($m/\delta m = 1000$)(Blake et al 2004). Its ability to detect all mass channels within 30 microseconds makes this instrument ideal for recording atmospheric change in real time. CIR-ToF-MS has so been named as this encompasses a more generic term to PTR because additional chemical ionisation reagents such as NO⁺ and O₂⁺ can be used instead of H₃O⁺ (Wyche et al., 2008).

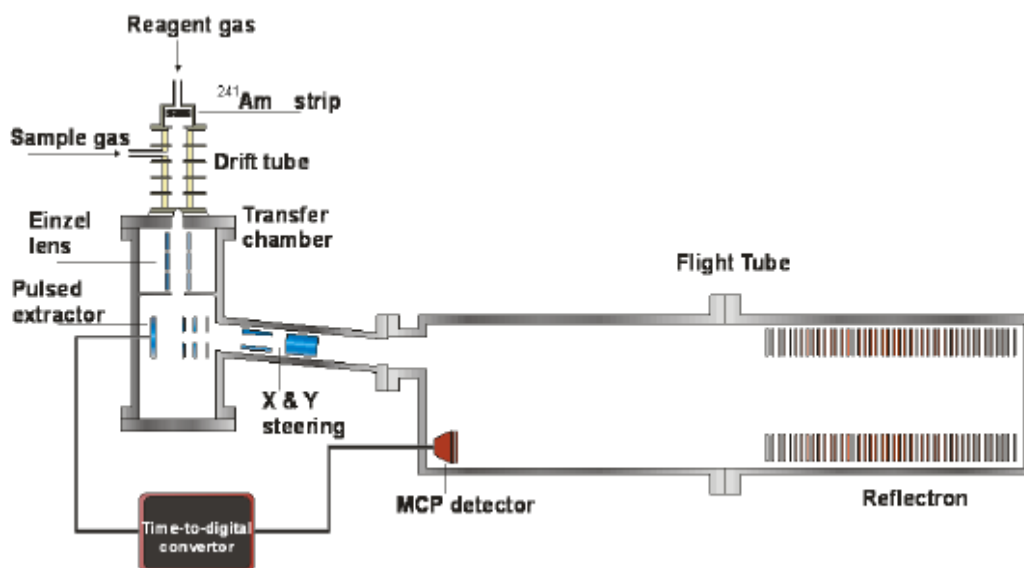


Figure 6. Schematic of the CIR-TOF-MS to indicate crucial instrumentation sections taken from Wyche et al., (2008)

Figure 6 displays a schematic of CIR-ToF-MS displaying the principal components of CIR-ToF-MS instrument; the ion source (^{241}Am strip), an ion-transfer region, the drift tube, a reflectron time-of-flight mass spectrometer and a detector consisting of a micro channel plate (MCP). The design of the ion drift tube within the CIR-ToF MS instrument is similar to that described by Hanson et al., (2003) who produced a system capable of operating at a pressure of ~ 10 Torr, resulting in an increased sensitivity owing to increased ion yield. Differences in pressures of the CIR-ToF-MS were maintained from a mechanical pump for the drift tube region and turbomolecular pumps for the remainder of the instrument, the transfer chamber and the flight tube. The ultimate operating pressure highlights a restraint on the performance of the instrument, as higher pressures will give higher yields but will also lower the mean free pathway. Therefore suitable intermediate pressures are required. The optimum size of the aperture between the drift tube and the CIR-ToF-MS was $200\ \mu\text{m}$ which limits the pressure within the drift tube to 8 mbar. Furthermore, the pressure of the flight tube should not exceed 10^{-6} mbar to operate the MCP used for detection of ions. This results in a differential region of pressure in both regions, whilst trying to keep the CIR-

ToF-MS (flight chamber) as low as possible. Normally pressures were run at 4×10^{-4} mbar in this region.

The ion source is a radioactive strip Americium-241 attached to the inner wall of a stainless steel cylinder. This isotope decays emitting both γ -rays and α -particles, the latter is of interest in the context of this work. Advantages of using ^{241}Am as the ionisation source are that it produces large amounts of α -particles in the region of 10^7 ions s^{-1} . Furthermore with a half-life of 432.2 years it can serve as a base for a stable source of α -particles compared to other potential sources such as Polonium (Po^{210}). The radioactive strip of ^{241}Am is contained within a steel cylinder at the top of the drift tube which enables the produced α -particles to interact with the gas within the drift tube components. Previous work on the same instrumentation by Blake et al., (2004) has shown that the ion source used within the CIR-ToF-MS has been measured to produce 3×10^9 ions s^{-1} (or an ion current of ~ 500 pA) which is similar to that obtained from the work done by Hanson et al., (2003). Purified nitrogen gas is used to carry the water vapour into the drift tube via a bubbler system. Nitrogen gas purity $> 99.99\%$ (BOC gases UK) is streamed through a bubbler. The bubbler is a small (10 cm^3) glass cylinder half filled with distilled water stoppered with a rubber bung with two holes allowing access to and from the cylinder of a constant flow of nitrogen, resulting in a stream of water vapour leaving the bubbler. The flow enters the drift tube where the α -particles are used to ionise the water vapour as it passes through the drift tube, to provide the H_3O^+ ions, which in turn then undergo proton transfer with the sample gas. The ion source and drift tube are held together by four nylon rods to a flange on top of the transfer stage, and have been coupled through two stainless steel plates. The first plate is in contact with the ion source and is used as an exit point for the ions. As such it operates under the same potential as the ion source. For the second plate, an electric field matching or exceeding that used in the drift tube is used, this change in potential being important as it not only prevents α particles from entering the drift tube, thus eliminating the formation of ions within it, but also converts higher water clusters into $\text{H}_3\text{O}^+\cdot\text{H}_2\text{O}$ and H_3O^+ before coming into contact with the sample gas (Hanson 2003).

The sample gas consists of the gas-phase composition extracted from the aerosol chamber and is drawn into the drift tube through the second inlet, and as such, bypasses the radioactive strip and reacts with the H_3O^+ ions to undergo proton transfer reactions. Both the water vapour and the sample gas enter the drift tube at the top and exit at the bottom through the potential gradient that is formed by the gradual increase in current on the plates going down the drift tube. The mean free pathway (λ) in the drift tube of a molecule can be represented by equation 1.1

$$\lambda = \frac{RT}{\sqrt{2} \pi d^2 N_A P} \quad (1.1)$$

Where T is temperature, d is the diameter of the molecule, P is pressure, whilst R and N_A represent the gas constant and number of molecules respectively.

The ion source itself is held at a high positive potential of $\sim 2.5\text{-}3$ kV relative to the ground (Blake 2004). The design of the drift tube is 10 cm in length and is constructed of circular stainless steel guide plates that are separated by 6.3 mm in height, static dissipative (SD) polytetrafluoroethylene (PTFE) cylinders. PTFE cylinders were used as a means to minimise sample loss through wall sticking. Viton o-rings are placed in between these cylinders to seal the SD Teflon and guide plates and fittings (Lindinger, Blake, Hanson, 2003). The pressures applied within the drift cell during the experiment (~ 6 mbar) means that a low-level radiation source can be employed as there will be sufficient ionization through the α -particles, and as very few radicals are formed, means that it is able to provide fairly clean background conditions.

A useful parameter to define when describing the ionisation condition of the drift tube is the E/N , where E is the electric field cm^{-1} across the drift tube and N is the gas number density (cm^{-3}). Controlling this defines the voltage gradient which draws positive ions formed from the ionised water down the drift tube, where proton-transfer takes place as the sample gas mixes with the ions. To achieve this within the drift tube, for each plate a potential difference is applied between them by separating the interface plate and the orifice plate electrically by a 0.05cm thick Teflon disk (sealed with o-rings). Hanson et al., (2003) operate this potential difference to be the

same as that of the drift tube, but to minimise cluster formation this field is increased in this investigation. The control of a ramped voltage region near the end of the drift tube is known as a collision induced dissociation chamber (CID). As this is a unique and important aspect of the CIR-ToF-MS, it will be discussed here in more detail.

In an electric field the mobility (μ) in $\text{cm}^2 \text{V}^{-1} \text{s}^{-1}$ of an ion can be used to determine its terminal velocity by the relationship in equation 1.2

$$v_d = \mu E \quad (1.2)$$

where E is the electric field (applied across the source), v_d is the drift velocity (of electrons responding to the electric field) and μ is the electron mobility. The reduced mobility (μ_0) (equation 1.3) has been reported as (de Gouw 2007)

$$\mu_0 = \left(\frac{N}{N_0} \right) \cdot \mu \quad (1.3)$$

Where N is the number density of gas in the drift cell, and N_0 is the gas number density at standard pressure (1 atm) and temperature (273.15 K). Substituting equation 1.2 and 1.3 gives a drift velocity in equation 1.4:

$$v_d = \mu_0 N_0 \left(\frac{E}{N} \right) \quad (1.4)$$

Controlling the E/N can be used as a determination of the ion fragmentation and water clustering. E/N values are represented in Townsends (Td), where one Td is 10^{-17}V cm^2 . Essentially this controls the level of clustering occurring in the drift tube, low E/N values (<120 Td) promote formation of water clusters from water molecule addition to hydronium ions which can further influence the rate of proton transfer to the analyte species. Under high E/N conditions (>200 Td), water clustering reduces with the penalty of increased fragmentation of the analyte species due to the high energy collisions. Thereby a compromise must be established. Here an E/N value of 120 Td gives the lowest fragmentation of ions, whilst also maintaining a manageable amount of water clustering. The optimum settings for the instrument were studied previously by Wyche et., (2007) and Wyche et al., (2008) during chamber

photooxidation experiments. The cluster binding energy of the monohydrate water cluster was estimated to be 1.37 eV, and so a larger energy environment will cause H₂O molecules to be dislodged and eradicate clusters.

From the drift tube the gas then exits via a 200- μ m critical orifice in stainless steel plate and proceeds to a short differentially pumped chamber. The ions are then focused into a narrow beam by a series of Einzel lenses. As the ions enter the region, or grid, within a pulsed extractor, the potential is rapidly changed, in effect pulsing the ions at regular intervals into the flight tube through a system of spatial focusing electrodes and steering plates, initiating the flight time sequence. A reflectron then reflects the ions back towards a MCP detector. It is this time measurement that forms the basis of time-of-flight. An ion's mass-to-charge ratio (m/z) is determined by this time measurement. A known strength electric field is used to accelerate ions (Wolff 1953). Separation of ions is attained by the m/z ratio of a particle, as heavier particles will reach slower speeds. CIR-ToF-MS employs a reflectron, which can alter the direction of ion flight (Mamyrin 1973) by using a constant electrostatic field to reflect ions toward the detector (MCP). The reflectron is equipped with an ion mirror that reverses the direction of the ions entering it. By reversing the direction flight of the ions the spread of flight times of ions with the same m/z caused by difference in kinetic energy is reduced. An advantage of using a reflectron is that a longer flight path is achieved, and as such greater resolution can be achieved. The signals arriving at the anode of the MCP detector are then preamplified through a built in discriminator which produces an emitter-coupled logic (ECL) pulse whenever a predetermined threshold is overcome, or exceeded. A time-to-digital converter (TDC) then produces the histograms of the mass spectrum on the computer. It is also used to regulate pulses of the pulse extractor which is essential to obtain regular scans and forms the onset of ions into the flight chamber. 1 sec scans were taken in this study and averaged spectra over a period of 1 minute to give the final mass spectrums using the GRAMS/AI program of the instrument. This program was a control and acquisition program developed by KORE for use with the CIR-ToF-MS. A detailed description of this program can be found in work presented by Blake 2005, p. 69. According to Blake et al., (2004), for a mass range of 0-300 Da, roughly 10^4 scans s^{-1} is achievable, making

the instrument realistic at measuring real-time changes and thus monitoring the chemistry of systems of atmospheric importance.

Recent developments of the CIR-ToF-MS have seen the use of a new ion source, the hollow cathode discharge (HCD) source, which was implemented on two intensive campaigns during studies described within this work. This progression was based on the work done by Hanson et al., (2009). Essentially the fundamentals of PTR-MS remain the same where H_3O^+ ions are required for proton transfer with a trace gas or analyte. The hollow cathode source produces an ion beam (via cathodic sputtering in a glow discharge) that breaks down H_2O and in a second step these fragments recombine to form protonated water ions (H_3O^+). Good pulse repetition of the source enables a long life-time and can even increase the number of hydronium ions. Similar to Hanson et al., (2009) the high ion production rate compared to the ^{241}Am source of the discharge source leads to improved sensitivity which can be attributed to the number of hydronium ions formed, providing H_3O^+ ions reported with a purity of > 99.5 % (Lindinger et al., 1998). The HCD achieves this by generating dense plasmas through promotion of oscillations of hot electrons inside the cathode which can enhance ionization. Similar to the ^{241}Am source, H_3O^+ ions are produced with small amounts of contaminant species (Hansel et al., 1995). An improved ion count was observed with initial assembly of the new ion source. However to achieve optimisation of these ion counts, differing from the ^{241}Am set-up, an improved set up was obtained with inlet flow of the sample gas through the top of the drift cell whilst with the vapour sample entering the drift cell from the side. This was the reverse of optimised conditions for the ^{241}Am source in order to prevent flow of trace gases onto the ion source. Figure 7 displays a schematic of the drift cell used for the ^{241}Am source. The sample gas and vapour flows are exchanged for the HCD source, as this was found to produce the highest numbers of ions, and so increase sensitivity. The input flows of the drift cell for the HCD source are reversed for increased ion counts to optimise sensitivity of analytes.

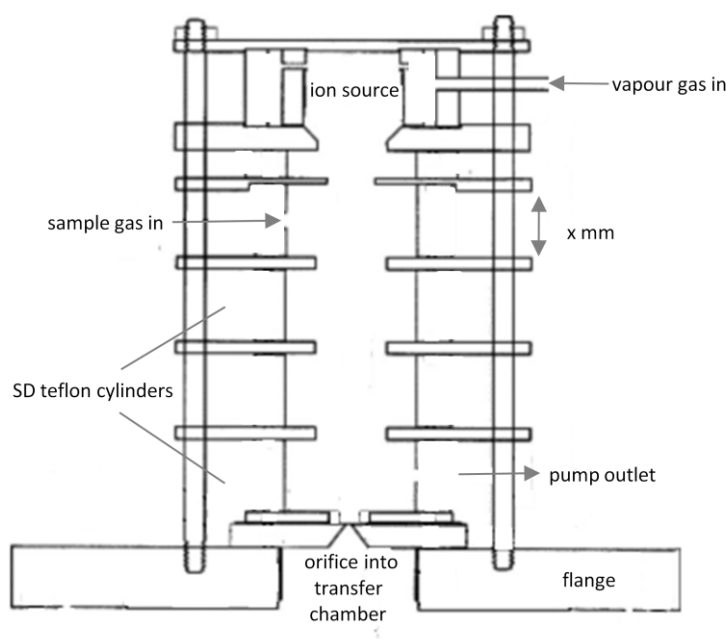


Figure 7. A schematic of the drift cell to indicate principle components. The ion source encompasses both the ^{241}Am and HCD source. The x mm represents a length of 16.07 mm for the radioactive source and 19.53 mm for the lengthened HCD source.

A maximum average number of 17600 raw ion counts were achieved (during set-up of the second TRAPOZ campaign), compared to total number of 5800 raw ion count for the ^{241}Am system (during initial set up of the first TRAPOZ campaign). Despite this improvement, a larger contamination of NO^+ was observed (from a low of 30 counts for ^{241}Am , to a count in excess of 1000 for HCD source). This contaminant could influence the maximum possible sensitivity of the HCD regardless of the higher ion counts obtained. Overall the sensitivity of organic compounds were increased, but not for other species. Figure 8 exemplifies the differing sensitivity values obtained from calibrations run of the same standard gas cylinder (calibrations are discussed later). For the exception of the small alkene trans-2-butene all other compounds exhibit higher sensitivities. The increase in ions produced therefore has a positive effect on the sensitivity on a majority of organic species expected in atmospheric oxidation processes. Data was analysed using Grams AI software (KORE) and IGOR Pro software.

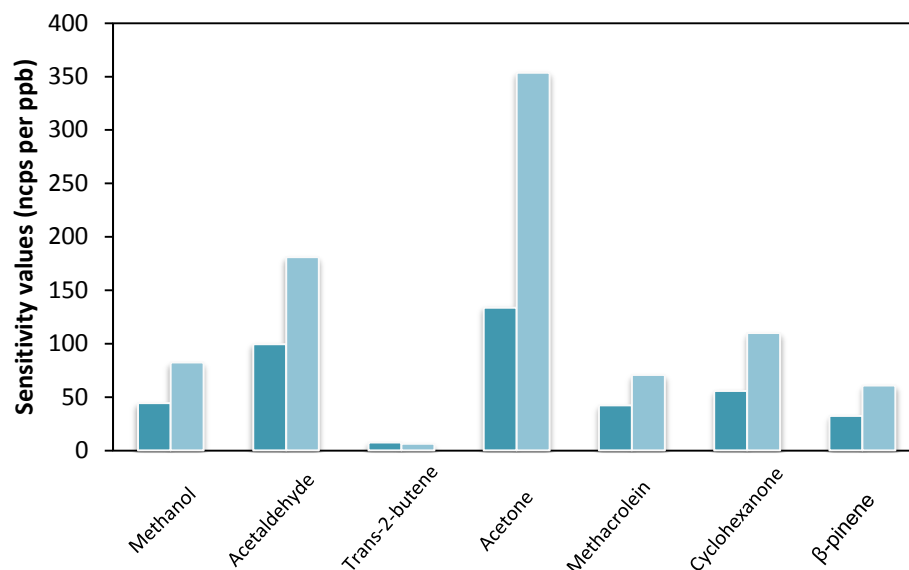


Figure 8. Sensitivity values obtained from both the ^{241}Am source (dark blue) and HCD (light blue) for compounds in a 1 ppm gas-standard cylinder. All compounds show an increase in sensitivity except for the small alkene trans-2-butene.

2.1.1 Calibration

Calibrations for the CIR-TOF-MS were conducted in the following ways; (i) bag calibrations, made off-site at the RAFT facility at the University of Leicester, chamber calibrations in which increasing known concentrations of specified compounds were injected into the chamber, (ii) direct sampling of a 1 ppm gas standard, made both on site at the chamber facilities, and off site in the RAFT laboratory (iii) sampling of gas standards, both on-site and off-site (iv) chamber calibrations

- (i) **Bag Calibrations;** Figure 9 illustrates the procedure of a standard bag calibration run. A Tedlar bag was filled for 2.5 minutes with nitrogen gas of >99% purity (Grade 6 Nitrogen, BOC UK) at a flow to fill a 5L volume of a 10L bag (A). A liquid calibrate (see appendix for chemicals used) solution in hexane to a known concentration was made as a calibration standard. A typical solution was made using a 10 ml addition of reagent

grade hexane (Sigma Aldrich) using a 10 ml Hamilton syringe (accuracy within 1%) into a 50 ml beaker. The VOC was then injected (volume of 1ul) into the beaker using a Hamilton Syringe (accuracy within 1%). The calibrate was then injected into a 10 L Teflon bag using another 10ul Hamilton syringe (cleaned 5 times with hexane for each calibration run). The bag was then filled further with nitrogen for 2.5 minutes to fill to the capacity of 10 L volume. A nitrogen fill was conducted after the injection procedure (C) to “remove” any possible sticking of the calibrate on the septum of the tedlar bag. Finally the bag was connected to inlet line of the CIR-TOF-MS where a flow of 80 mL min⁻¹ made it possible for a 30 minute run to be achieved (similar to the drift cell conditions set during campaigns). The typical bag calibration run was 15 minutes. Because new bags could not be used for each calibration run, bags were designated according to concentration levels injected into the bag, the whether or not they were used in the presence of “humid” runs. Humid runs were conducted by filling the bag up with humidified air up to 80 % relative humidity (RH) utilising the KIN-TEC system. The standard cylinder had a bag designated for use only for the “high” undiluted concentrations so not to contaminate the “low” concentration runs. An injection of 1 µl of calibrate usually was around 200 ppb. To increase the concentration for multiple calibration runs, a further addition of 1 µl (eg 200 ppb) would be made into the second bag. The cleaning process of the bags was to fill it with N₂ and evacuate the air from the bag using a mechanical pump. This procedure was then repeated 5 times, and left filled with N₂ overnight and evacuated the next day in preparation for the next calibration run.

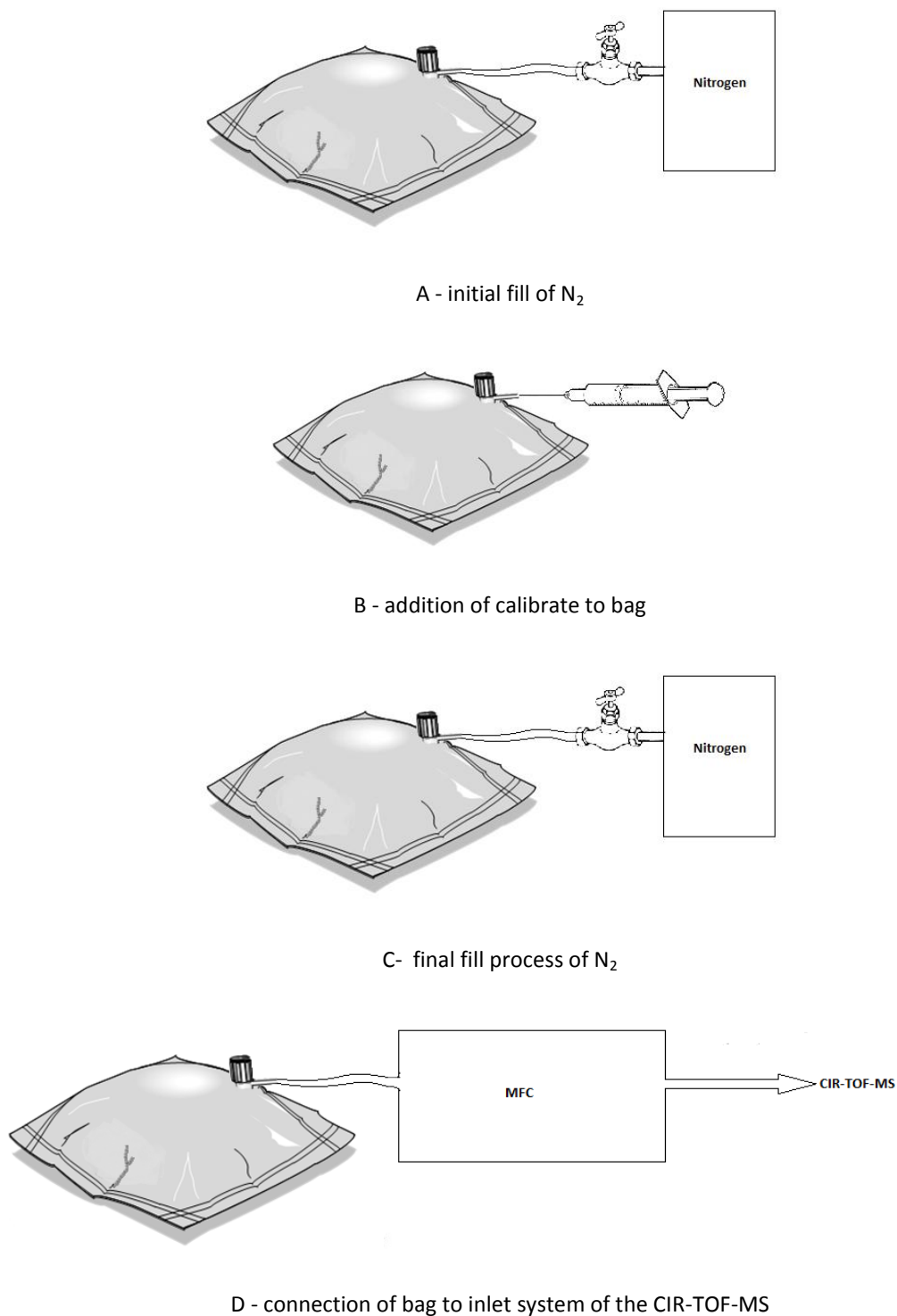


Figure 9. Set-up procedure used for a standard bag calibration run made at RAFT facility at the University of Leicester.

To test the injection accuracy, a run of the same calibrate solution (200 ppb solution of cyclohexanone) was injected into 3 separate bags (each 1 μ l). The results of the calibration run are shown in figure 10, where the

variability of the injection technique gave a final error less than 1%. The values are based on the m/z ion 81. The attained sensitivity calibration (ncps per ppb) values varied from 97.69 (bag 1), 97.48 (bag 2) and 96.18 (bag 3) given an average sensitivity of 97.12 ± 0.81 (assuming a 200 ppb concentration for each injection). Therefore it can be assumed that the variations due to injection error will be minimal.

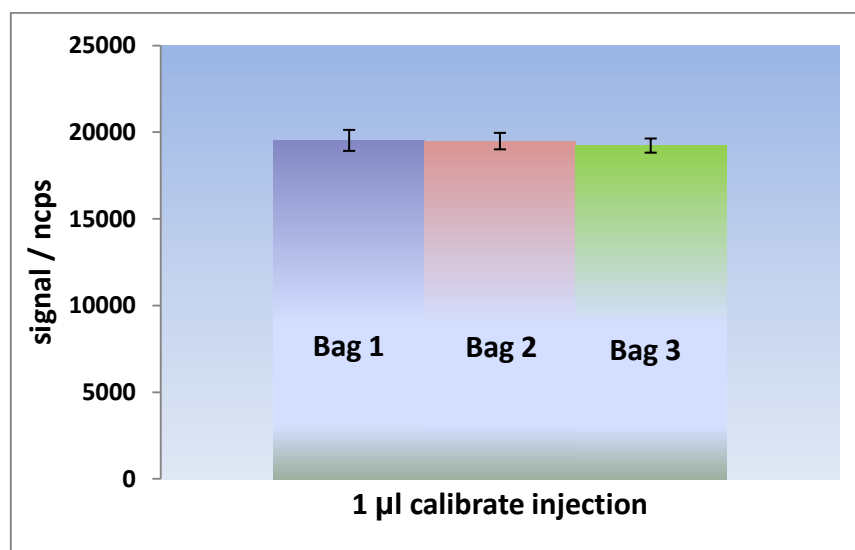


Figure 10 Injections of 200 ppb calibrate of cyclohexanone into three separate tedlar bags to test the injection method employed during bag calibrations runs.

- (ii) **Direct sampling of gas standard cylinder;** a 1 ppm gas standard (BOC Special Gases, UK) was used to calibrate for the compounds methanol, acetaldehyde, trans-2-butene, acetone, methacrolein, cyclohexanone and β -pinene, the accurate concentrations given in appendix A2. Figure 11 shows the set up of a dynamic dilution where the flow of the cylinder and nitrogen flow could be adjusted accurately using mass flow controllers (MFC) Millipore, Tylan 260 Series. The flows were adjusted by a MFC control unit (ASM Europe, serial no. 4.284014/11).

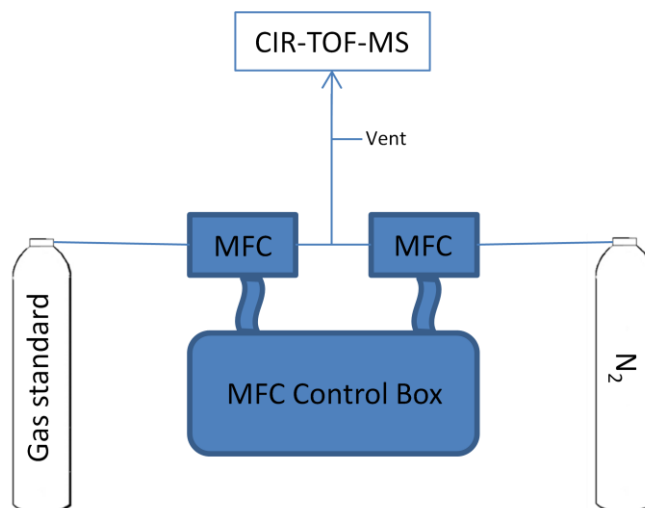


Figure 11. Set-up for direct sampling of the gas standards. A N₂ gas cylinder (BOC special gases, purity 99%) and the 1ppm gas standard cylinder were connected to MFCs. Flow were adjusted to establish dynamic dilution.

Utilising dilution, multiple point calibration runs were possible. The conditions for typical multiple point calibration run are as follows; an initial N₂ run was made for background purposes, by setting the flow of N₂ to 500 mL min⁻¹ and flow of cylinder to 0 ml /min for a total run of 15 min. An increase in cylinder flow to 100 ml/ min to an N₂ flow of 500 mL min⁻¹ gave an average concentration of 175 ppb (average concentration over all compounds) for a further 15 min run. All “standard” calibrations runs were made in 15 min run blocks, with an equilibrium time of 10 min between each run. For data processing, the first 3 min of data were discarded to ensure equilibrium of the flow was attained. The concentrations were systematically increased by raising the flow of the cylinder by 100 mL min⁻¹, whilst the N₂ flow was reduced by 100 mL min⁻¹ until a pure cylinder flow was obtained (i.e. at a flow rate of 0 mL min⁻¹ (N₂) and 500 mL min⁻¹ (cylinder)) Figure 12 shows a typical multiple point calibration run.

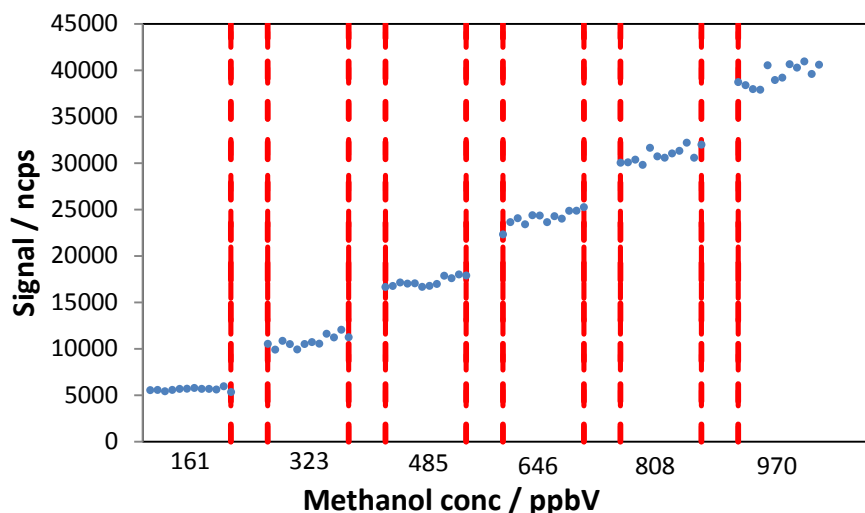


Figure 12. A typical multiple cylinder calibration run using the ~1ppm gas standard. The dotted gaps represent a 10 minute equilibrium time between adjustments of flow rates between N₂ and the gas standard.

- (iii) **Sampling of gas standards;** Gas standards were produced using certified permeation tubes (Eco-Scientific, UK). The permeation tubes emit a stable flow of analyte vapour from a central tubular device that has walls made from a permeable membrane and are able to produce accurate gas concentrations whilst operating under controlled temperatures. The rate of emission is based on the rate of weight loss that is measured over certain time period. The permeation tubes bought were certified off-site at Kin-Tec and were made to be within 2% of the stated emission rate. The permeation tubes were placed inside a glass oven, housed in a controlled heating block ($\pm 0.1^{\circ}\text{C}$). By setting the temperature of the certified tubes as specified, and obtaining a controlled flow of inert gas (N₂) over the tube, an accurate concentration mixture of the analyte can be obtained at trace levels. The flow of inert gas was controlled using a 491M humidification unit (KIN-TEC Laboratories, UK). An additional base module downstream (housing its own permeation oven) enabled multiple calibration runs to be made using two different temperature settings. A typical calibration run would be conducted as follows: The “warm-up” procedure was

conducted using the start up procedure within the KIN-TEC operated system manual. The initial flow rates were set at 4 mL min⁻¹ and reduced step wise down to 0.5 mL min⁻¹ (a higher flow rate giving a less concentrated concentration mixture). Thereby, the lower limit of the instrument was governed by the flow rate set on the dilution flow, which must always be greater than the sample inlet flow of the CIR-ToF-MS instrument. The N₂ carrier gas has a small flow (0.1 L min⁻¹) which passed through the permeation ovens to gather the analyte before rejoining a larger dilution flow. The concentration (C_j) were calculated using equation (1.5)

$$C_j = \frac{(E \times K_o)}{(F_D \times 1000)} \quad (1.5)$$

Where E is the emission rate (ng min⁻¹), K_o is a compound specific constant which converts emission rate to nL min⁻¹ from ng min⁻¹ (calculated from 22.4/MW) and F_D is the flow rate of the total dilution gas (L min⁻¹). Further downstream from the two permeation ovens was the 491 M-HG standard humidification module used to examine “humid” calibrations by adding water vapour to the dilution flow without making contact with the component mixture and water. A gas standard, if bubbled through water, will change in concentration due to components of the analyte’s interaction with water. This module allows the saturation of a dilution gas with the addition of water vapour to the final span of the gas mixture without contacting the analyte with the liquid water. The concentration of water vapour is determined by the ratio of partial pressure to the total gas pressure. For the humid samples, as relative humidity is temperature dependent, and differing temperatures were in operation, the mixture flow inside the module unit transported into ambient laboratory temperatures before sampling correction factors had to be taken into account. To minimise this effect,

the sample lines from the module unit output to the CIR-ToF-MS were heated to try and maintain constant temperatures. The correction factor (CF) was determined using equation (1.6)

$$RH = RH_S \times \left(\frac{P_S}{P_D} \right) \quad (1.6)$$

Where RH_S is the relative humidity inside the humidification module and P_S is the vapour pressure at the sensor temperature and P_D is the vapour pressure at the delivery temperature. Using sensors to monitor the difference in temperatures (in the KIN-TEK unit and ambient lab environment) the correction factor (CF) was determined and used to correct the RH at the sensor given in equation (1.7).

$$RH = RH_S \times CF \quad (1.7)$$

In order to make sure the calibration was run at the correct RH, the RH was set to the calculated RH_S determined from the correction factor. High RH values could not be experimentally obtained owing to this correction factor. This was due to the upper limit of RH_S being in the region of 85-90%, so cooler conditions were required to achieve a saturated mixture. Over the course of a calibration run, a gradual decline in temperature was observed, with the addition of occasional “spikes”. As such, data was only considered accurate when the RH was maintained within $\pm 5\%$ of the target RH. All data outside this parameter was discarded and not included in calibration calculations. Figure 13 provides an example permeation tube calibration run.

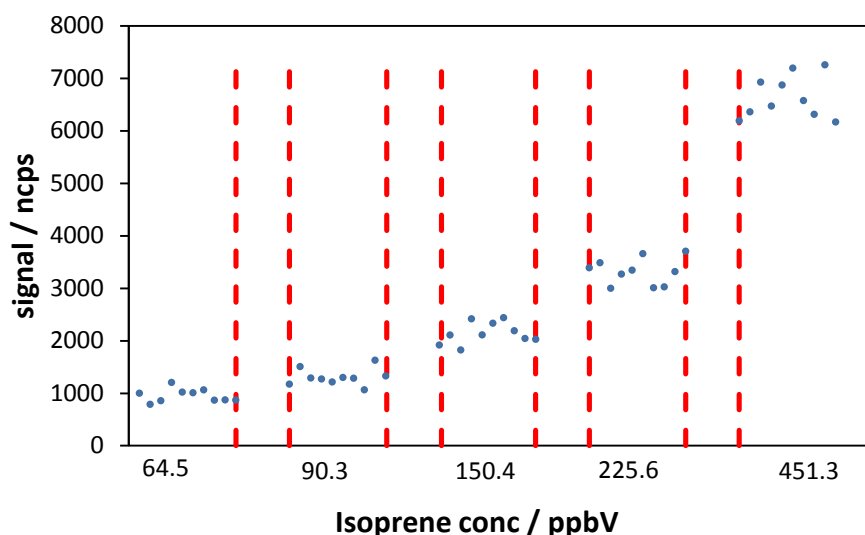


Figure 13 Calibration run from an isoprene permeation tube. The gaps of the dotted lines represent a 15 minute equilibrium period between altering of flow rates.

- (iv) **chamber calibration**; a known concentration of specified VOCs and oVOCs were injected in increasing amounts into the aerosol simulation chamber using procedures similar to the injection of VOCs during experimental runs (see section 2.4). Figure 14 shows a calibration run of the chamber on the afternoon on 26/05/09 with regards to acetone. During this calibration run the compounds acetic acid, acetone, formaldehyde, acetaldehyde, nopinone, cis-2-butene and myrcene were injected into the chamber. Having knowledge of possible fragmentation of larger compounds was key in these calibration runs as compounds were selected that would not interfere with m/z signals of smaller compounds due to fragmentation or dehydration. The observed downwards slopes during the time after injection can be explained by dilution loss in the chamber and potential loss to wall sticking itself, in addition to removal of sample from the chamber from differing instrumentation. As only an initial injection was made, there was no replenishment of sample within the chamber. Potential leaking of the chamber was not established during the campaign.

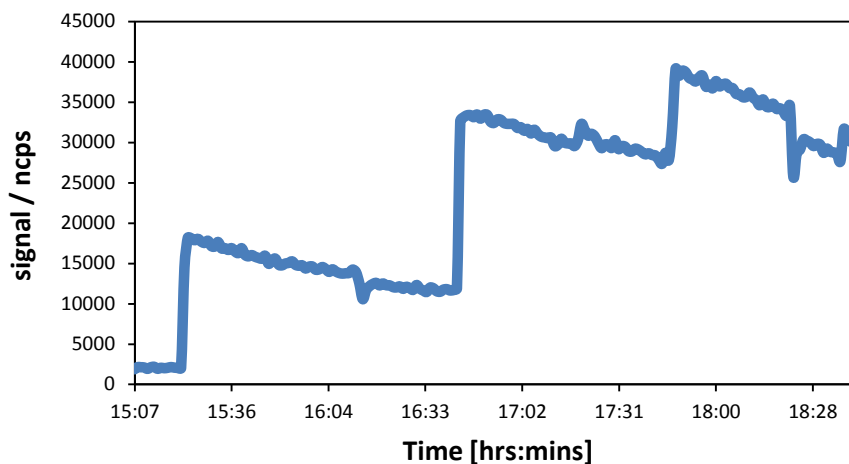


Figure 14 The evolution of m/z ion channel 59 following three additions of acetone into the EUPHORE aerosol chamber. The data is represented in 1 min time frames. Clear increments are observed where injections of 50.3 mg (111 ppb), 47.4 mg (98 ppb) and 47.4 mg (98 ppb) were made.

2.1.2 Errors for CIR-ToF-MS

Data analysis from the CIR-ToF-MS involves three main stages: first, a spectrum obtained are mass calibrated (converting from the time to the mass domain) and summed (peak areas are integrated for each mass channel). Spectra are then background subtracted and each signal normalised to the hydronium base peak and hydronium monohydrate cluster (m/z 19 + 37 = 1,000,000 normalised ion counts). To calculate mixing ratios, each signal (as normalised counts per second or ncps) is then divided by a calibration factor (f_c) unique for each analyte of interest (in units ncps ppb⁻¹).

The calibration factor is calculated from an external standard (methods previously outlined). A gas mixture of known concentration is analysed under identical conditions to that of the sample mixture (including integration period, humidity etc.). f_c is obtained through the same process described above; background subtracting, normalising spectra and dividing the integrated signal by the known concentration.

This is valid provided the standard (and sample) concentration is within the linear range of the instrument (which can be obtained by constructing a calibration curve as depicted in Figure 15) from an α -pinene calibration run. The slope gives f_c whilst the intercept conveys the background signal.

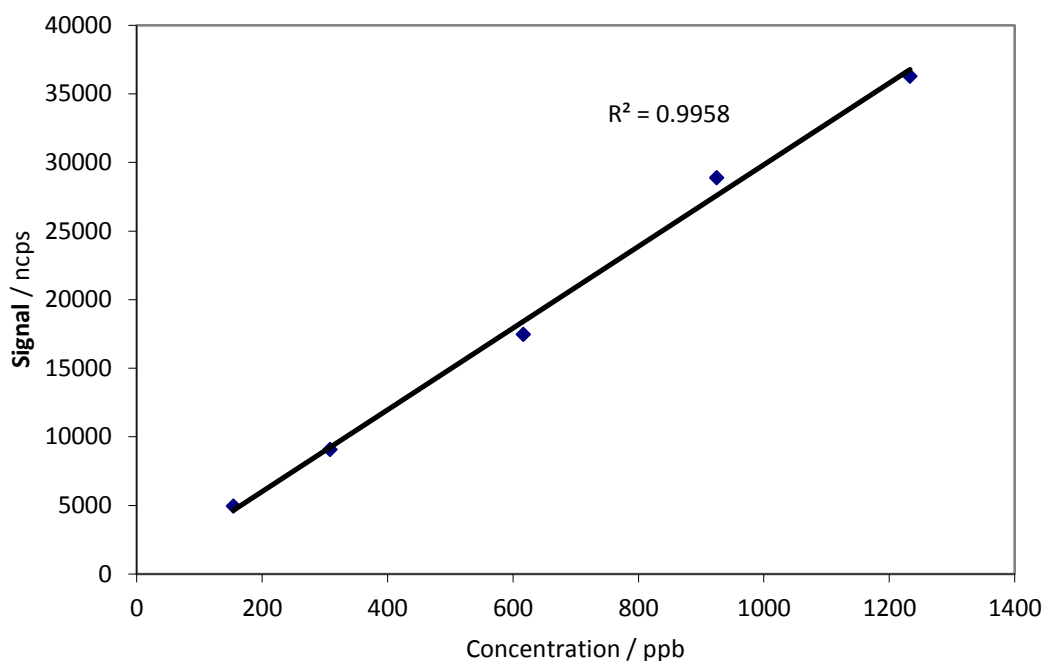


Figure 15. Example calibration curve for m/z ion 137 of α -pinene taken from the bag calibration method.

In this case, the uncertainty of the calculated compound mixing ratio is dealt with by calculating two estimates of the error in concentration quantification, the accuracy and the precision. Accuracy encompasses systematic errors of the standard calibrations. These involve overall uncertainties in gravimetric dilution of compounds suspended in gas cylinders, the volumetric dilution of pure liquid compounds inside tedlar bags and emission rates from certified permeation tubes to include all three calibration methods. Precision of the instrument is a measure of the ability to reproduce given measurement, here the repeatability of the mass spectrometer taking into account fluctuations on the system parameters (e.g. temperature and pressure). The precision can be characterized as the relative standard deviation (RSD) of given

measurements presented as a percentage. Differing calibration methods produced similar results as shown in Figure 16. From the various compounds all demonstrate non-linear behaviour, where lowering concentrations are accompanied by an increase in RSD. This can be associated with the signal-to-noise aspects of the instrument, essentially as concentration falls; instrumentation noise becomes more influential on the measured signal. At a certain threshold, the measured signal will become indistinguishable from that of background “noise”, and the detection limit can be deemed to have been exceeded. The precision of the instrument was therefore deemed to be a minimum sensitivity of 20 ncps. The detection limit can be improved by averaging measured signals as more signals summed together will improve detection levels greater than that of the background noise. Resulting, the majority of the data averaging here is based on 5 and 10 minute data sets from 1 minute time scale recordings, which themselves are averages of 1 sec scans.

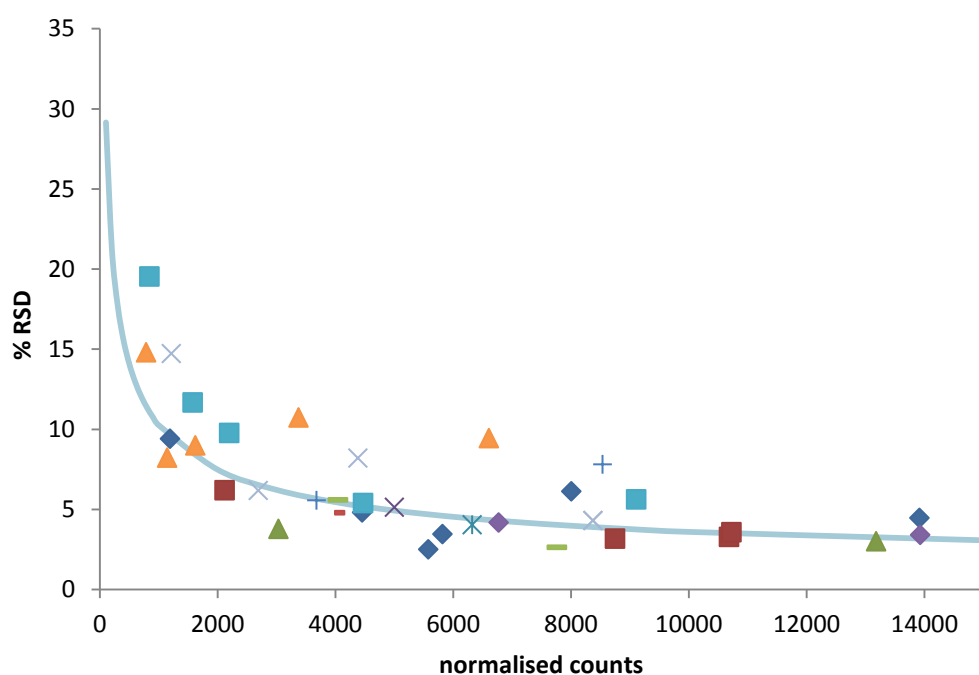


Figure 16. Comparisons of both differing compounds, and different calibration methods to evaluate the impact of changing concentrations and the impact this has on precision. Isoprene permeation tubes (orange triangles), HCHO perm tubes (blue squares, purple diamonds), and limonene bag calibrations (green lines) average of errors from different gas standard cylinder calibration runs (blue diamonds, green triangles, red squares)

Error bars are calculated with this precision, whilst considering systematic errors. Gas standard cylinders were certified given a nominal % uncertainty. The % uncertainty of the emission rate can be calculated based upon uncertainties in permeation rate, oven temperature fluctuations and flow rates through the base modules of the KIN-TEK unit. Bag standards comprise of uncertainties following dilution based upon imprecision of both primary (measuring fixed volume of hexane in the calibrate liquid) and secondary (measuring fixed volume of stock solution and the volume of the bag) dilutions. Based upon this, the resultant error bars from the inaccuracy of the standard preparation are symmetric and can be quoted as a %. Both accuracy and precision errors were taken into account for the formulation of error bars. For all tables in the following chapters, a limit of detection was set at 3 times the base level of observed noise. This was annotated as below detection limit (bdl). This varied slightly from experiment to experiment but all yields given as bdl (below detection limit) signify that any observed data falls within this limit of detection and so evaluated as non significant.

2.2 Simulation Chambers

Two simulation chambers were utilised for the work presented here. Night time ozonolysis experiments were performed at the EUPHORE simulation chamber and photooxidation (OH initiated) experiments at the newly constructed aerosol chamber in Manchester.

2.2.1 EUPHORE Aerosol Simulation Chamber

The “dark” ozonolysis experiments were conducted at the CEAM EUropean PHOtoREactor (EUPHORE) facility. A more detailed description of the EHPHORE facility

can be found in Becker et al., (1996) and so will only be briefly discussed here. A picture of the EUPHORE facility is given in Figure 17. Advantages of using the EUPHORE simulation chambers is the ability to simulate both daytime and night time chemistry, owing to a mechanical housing system that can be deployed. Each chamber consists of a half-spherical Teflon bag, made from fluorine-ethene-propene (FPE) with a thickness of 0.13 mm, which holds a gas volume of approximately 200 m³. Operating pressures were between 100-200 Pa to stabilise it against wind distortion, and heating was controlled by the refrigeration system. To insure sufficient mixing of the reactants (mixing time < 1.5 minutes) the chamber has two inbuilt “mixing fans” that can produce a throughput of 8000 m³ h⁻¹. The floor of the chamber provides access for both the introduction of reactants and the introduction of sampling lines for a comprehensive suite of analytical instruments, an overview of the instruments given in Table 1.

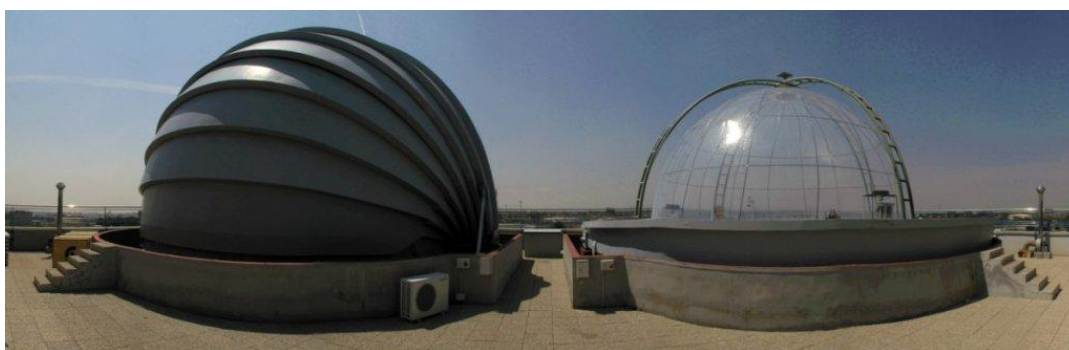


Figure 17. The EUPHORE CHAMBER facility. The outer housing makes it possible for both daytime and nighttime chemistry to be observed. For the ozonolysis experiments, conditions followed that of nighttime chemistry (left)

During chamber experiments, small losses of VOCs and OVOCs are possible due to loss of air through leaks. To compensate for this loss, clean air is added into the chamber. This evidently would indicate a small loss of products through dilution, and this dilution rate was measured using an inert tracer, SF₆.

Table 1. Analytical instruments used during experimental runs at EUPHORE

Instrument	Measured Parameter	Detection limit
Dew-Point Hygrometer	H ₂ O	few ppm
UV photometric ozone analyser (ML9810) / FTIR	O ₃	1 ppb
IR absorption CO analyser (TE48C)	CO	5 ppb
Photolytic chemiluminescence (CLD770)	NO/NO ₂	0.2 ppb ^a
CIR-TOF MS / FTIR	VOC, OVOCs	sub ppb 1x10 ⁶ molec cm ⁻³ / 0.1
LIF / PERCA	OH/HO ₂	ppt
HCHO Monitor (AL4001)	HCHO	1 ppb
HPLC	Hydroperoxides	~1 ppb
FTIR	SF ₆	
SMPS (TSI 3082/3022)	Aerosol volume and size	
ESI-MS / LC-MS ^b	SOA	

a for NO

b off line analysis conducted at the University of York

2.2.2 Manchester Aerosol Chamber (MAC)

The Manchester Aerosol Chamber (MAC) at the University of Manchester is newly constructed and as such a paper describing and characterising the chamber will be given in future work by McFiggans et al., (2012). Only a brief description of the chamber facility is given here. The chamber is smaller than that of the EUPHORE site, approximating the maximum volume at 18 m³. The Teflon bag is also made from FEP and is housed within a square wooden hut with its inner walls coated with reflective “space blankets” to ensure even illumination of the chamber and that irradiation is maintained in the chamber. The lighting source to replicate solar radiation (the actinic spectrum over 290-800 nm) is provided by a 6 kW Xenon arc lamp accompanied by three rows of halogen lamps. These have been characterised to give a maximum total actinic flux over 460-500 nm as given in Hamilton et al., (2011). A picture of the ACES chamber facility with the irradiation source is given in figure 18. A cooling system is in place from an air conditioning system between the lights and the bag to remove

unwanted heat effects. HEPA filters (Donaldson Filtration Ltd, UK) were used to purify the air before humidification (ultrapure deionised water, Purelab Ultra System, Elga) and introduction into the bag. These filters used Purafil (Purafil Inc, USA) and charcoal. This process was found to be capable of removing O₃, NO₂ and VOCs, but still had some difficulty with NO levels. Unique to the Aerosol Chamber is the mounting of the bag on three aluminium fixed frames, the top and bottom frame able to move freely to the fixed middle frame allowing collapsing and expansion of the bag. This allowed filling and evacuation of air in the bag. Similar to the EUPHORE facility, the Manchester Aerosol also has a suite of instruments on site, an overview given in Table 2.



Figure 18. The Aerosol chamber at Manchester. The outer housing with the Leicester CIR-TOF-MS connected to the inlet (left) and inside the chamber with 18m³ teflon bag and the arc xenon lamp with the bank of halogen lights (right)

Table 2. Analytical instruments used during experimental runs at MAC

Instrument	Measured Parameter	Detection limit
<i>GAS PHASE MEASUREMENTS</i>		
Chemiluminescence detector (TSI 42i)	NO/NO ₂	
UV photometric gas analyser (Model 49C)	O ₃	
CIR-TOF MS	VOC, OVOCs	sub ppb
<i>AEROSOL MEASUREMENTS</i>		
CPC (TSI 3786)	SOA particle number concentration (water-based)	< 2.5 nm
DMPS (DMA*/TSI 3025A)	SOA particle size and number	3.4 – 34 nm
DMPS (DMA*/TSI 3010)	Aerosol volume and size	20 – 500 nm
TOF AMS / GCxGC-TOF-MS / LC-MS ^b	SOA composition	
HTDMA	SOA water uptake	

*based on the Vienna design (see Williams et al., 1999)

^b off line analysis done at the University of York

2.3 Other instrumentation

A brief overview of the other instrumentation in operation during the experimental run is given here. Filter samples collected during the chamber experiments were collected for off-line analysis and the techniques employed will also be briefly mentioned. The chemical characterisation of the aerosol was made by GCxGC/TOF/MS and LC-MS at the University of York.

2.3.1 Scanning Mobility and Differential Mobility Particle Sizers

Both facilities were equipped to measure aerosol formation in the chamber. The EUPHORE facility was equipped with a Scanning Mobility Particle Sizer (SMPS) system, and the Manchester Aerosol Chamber was equipped with a Differential Mobility Particle Sizer (DMPS). Both essentially operate in the same way and provide both

particle numbers and mass concentration data. This is achieved by a combination of a Differential Mobility Analyser (DMA) with a Condensation Particle Counter (CPC). The EUPHORE chamber utilised a TSI model 3081 CPC and a model 3022 DMA, whereas the Manchester facility operated two CPC systems (TSI model 3052A and TSI model 3010). These were coupled to two Vienna design DMAs (Williams 1999), one standard DMA for monitoring of particles between 20-500 nm and one ultrafine DMA for particles of sizes between 3.4-34 nm. Further an ultrafine water-based CPC TSI model 3786 was also available for measurements of water-based components. Following is a brief description of the components of the SMPS/DMPS system.

The DMA produces monodisperse aerosols by passing a polydisperse sample through a neutraliser. Here the polydisperse aerosols pass a radioactive bipolar charger, giving the particles a single negative, positive or zero charge. These charged particles then enter the DMA and are separated according to their electrical mobility, where a charged “inner element” provides repulsion to the negatively charged particles and are driven towards the outer walls. The neutral particles exit along with the excess air and the positively charged particles are attracted towards the charged “central rod” where particles within a narrow range of electrical mobility are able to pass through the open slit and the DMA exit. Figure 19 represents a diagram of the principles behind a DMA.

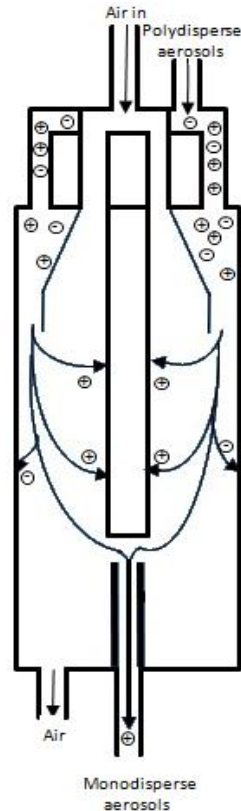


Figure 19. The Differential Mobility Analyzer. Charged polydisperse aerosols enter the DMA. The negatively charged central rod attracts the positively charged aerosols whilst repelling the negatively charged aerosols towards the DMA walls. Neutral aerosols are unaffected and exit with excess air. A narrow selection of positively charged aerosols exit as the monodisperse gas. Diagram is based on the TSI 3080 model adapted from the TSI website. (http://www.tsi.com/uploadedFiles/Product_Information/Literature/Spec_Sheets/3080.pdf)

The CPC exploits condensation techniques to enlarge sub micrometer particles to sizes that are within detection ranges. As such the operation of the CPC strongly relies on the condensation of vapour onto the particles. These operations of the CPC are discussed in more detail by Keady et al., (1986) and will only be briefly mentioned here. The reactions rely on heterogeneous condensation, in which a certain level of super saturation is reached in the system to allow vapour to condense on the aerosol particles. Super saturation can also reach levels at which homonucleation occurs, where vapour molecules cluster together based on van der Waals forces to form

nucleation sites. The supersaturation (S) can be measured as a saturation ratio by equation (1.8).

$$S = \frac{P}{P_s} \quad (1.8)$$

Where P is the actual vapour partial-pressure and P_s is the saturation vapour pressure for a given temperature. The dependency on vapour to condense onto particles at certain saturation ratios is given as the Kelvin diameter, which looks at the minimum particle size that can act as condensation nuclei:

$$S = \frac{P}{P_s} = \exp^{\frac{(4\gamma m)}{pRTd}} \quad (1.9)$$

Where γ is the surface tension, m is the molecular weight and p is the density of the condensing species. R is the gas constant (8.314 J/mol K), T is absolute temperature (K) and d is the Kelvin diameter, in which the critical equilibrium is defined where neither condensation nor evaporation occurs. In essence, the smaller the droplets, the easier for the vapour to escape the liquid particles, and larger particles will grow until the vapour is depleted, causing the saturation ratio to fall until equilibrium is reached with regards to the particle droplet. No particles will grow if the saturation ratio is below the critical saturation ratio.

These particles are enlarged in a heated saturator where alcohol vapour condenses onto the particles. These particles are then detected via a laser beam. The passing droplets scatter light, where the pulses are collected by a photodetector and converted into electrical pulses. These pulses are then counted and the rate is a measure of particle concentration.

The CPC consists of three major components, the sensor, the microprocessor, and the flow system. The flow rate is maintained by an oil-free rotary pump with eight carbon vanes and can operate at a low flow rate (0.3 L min⁻¹) and a high flow rate (1.5 L min⁻¹). The microprocessor uses an analog-to-digital (A/D) converter that measures

photodetector voltages, temperatures and flowrates. It is the photodetector detection that formulates the counters of the particle numbers at the sensor. The aerosol samples from the DMA enter the saturation tube. Here water is drawn up from the liquid reservoir through the “tilted” wick which is evaporated and saturates the aerosol stream. This vapour then cools in the vertical condenser and becomes supersaturated and condensation can begin to form larger droplets. The stream then enters the sensor, where the main beam from the laser diode can be disrupted by the aerosol samples, and a difference is taken from this and a reference photodiode to give the intensity of the incident beam, as so the particle number. A schematic of the sensor is given in figure 20

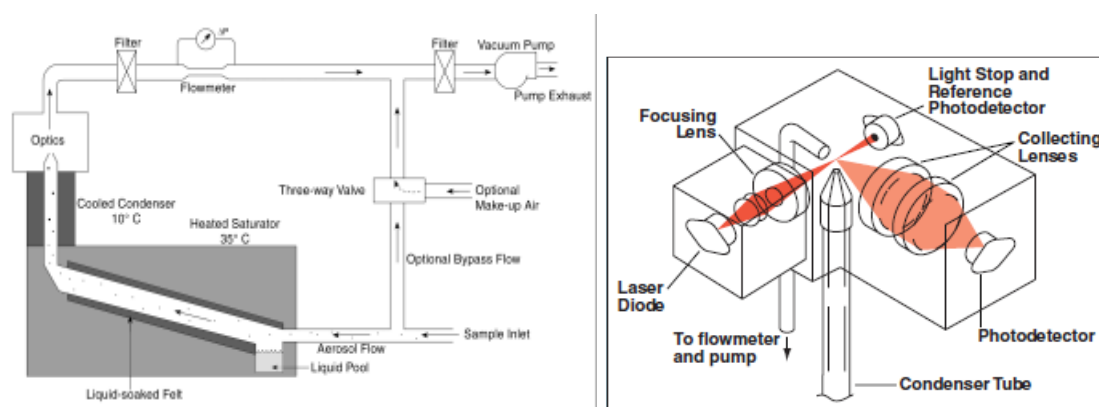


Figure 20 A flow schematic of the CPC (left) and the “optics” section of the CPC (right). Diagrams taken from the TSI website.

2.3.2 Fourier Transform Infrared Spectroscopy (FTIR)

The FTIR was used to measure VOCs, SF₆, O₃ and OVOCs during the ozonolysis experiments run at the EUPHORE facility. The FTIR essentially measures the ability of a sample to absorb light at a given wavelength. Infrared radiation is passed through the sample which is absorbed depending on the type of bond and element present. This is characteristic of the frequency of vibrations of bonds within a compound giving it a unique “fingerprint” spectrum. Key to the FTIR is the interferometer, a schematic of

the technique is given in figure 21. Light is collimated from a polychromatic source and directed towards a beam splitter. The beam is split approximately 50% towards the moving mirror and the fixed mirror. The mirrors reflect this light back to the beam splitter, where 50% of the original light enters the chamber. The moving mirror enables the different wavelengths to enter the chamber and the resulting differences in light intensity and the optical pathways constructs an interferogram measured by the detector. Following Fourier transform, an IR spectrum is obtained.

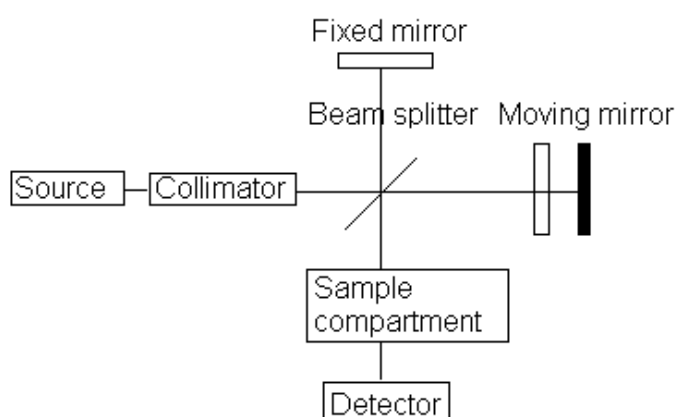


Figure 21 Schematic of the interferogram of the FTIR

Figure 22 shows the set-up of the FTIR at the EUPHORE facility. Specifically at EUPHORE, the distance between the FTIR sensors is approximately 9 m in length. White mirrors, which make up the long path optical path system across the chamber stand at a height of 0.5m. The FTIR at EUPHORE recorded data at a time resolution of 5 minutes with a spectral resolution of 0.5 cm^{-1} from a long path absorption system (653.6 m). The infrared spectra covered the range of $400 - 4000 \text{ cm}^{-1}$.

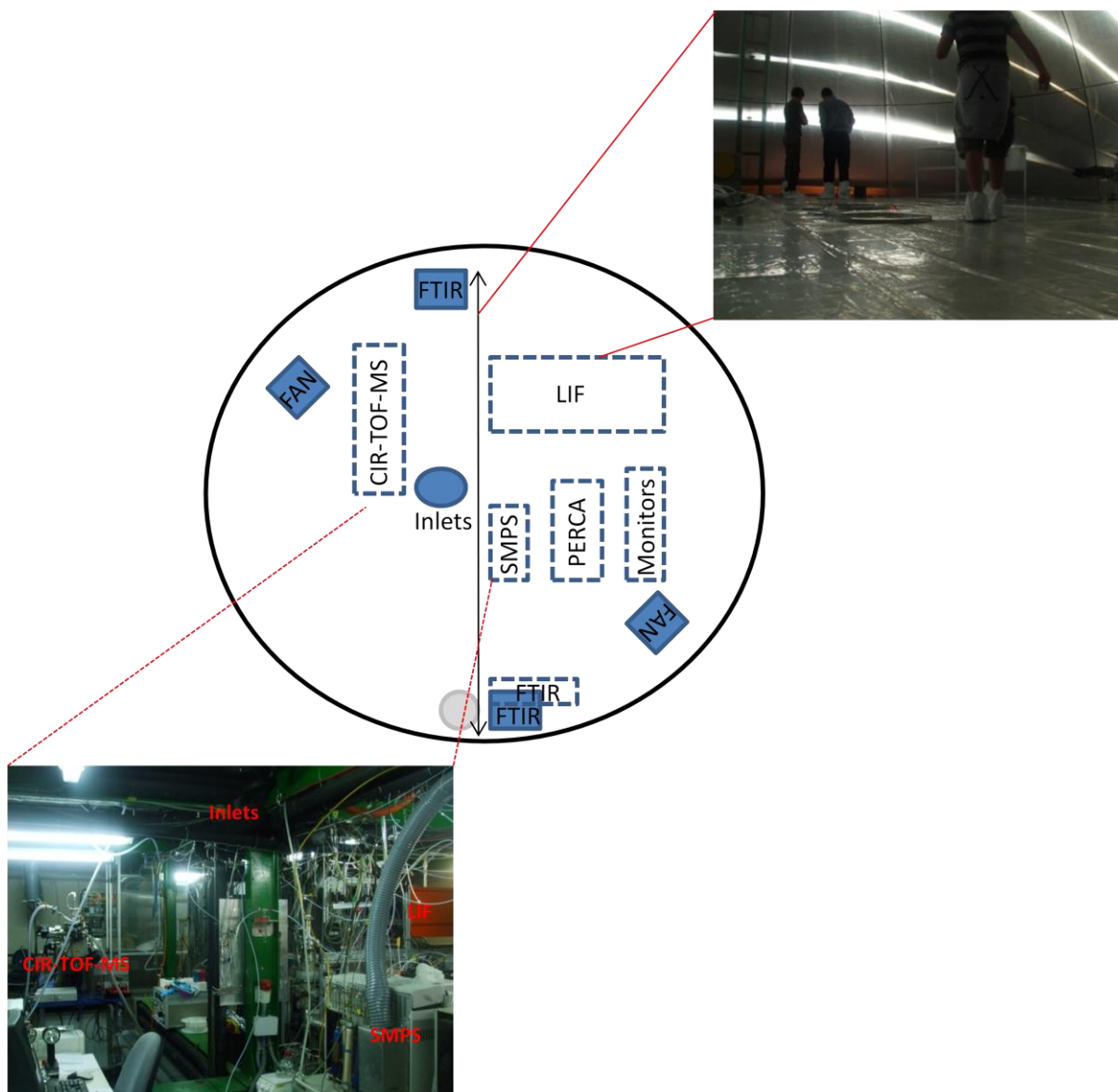


Figure 22 The chamber set-up of EUPHORE, with special emphasis on the FTIR and CIR-TOF-MS. Not all instrumentation has been included. The dotted lines represent the instruments situated below the chamber. Solid lines show instrumentation in the chamber.

Discrepancies were observed in the chamber studies between the FTIR and CIR-TOF-MS. For certain species, example isoprene, the CIR-TOF-MS record no less than 7% of the maximum amount possible for injection. Some loss is expected due to wall loss of the chamber, and depending on the species and their viscosity some experiments were difficult to analyse (eg methylchavicol). Looking at the table of results, a variation of results were obtained, sometimes better for the FTIR and to conclude, careful

consideration had to be taken into account regarding the validity of some of the observed results during the TRAPOZ campaign. Figure A1 (see Appendix) shows the recalculations of injections of the TRAPOZ 1 campaign, where comparisons between, theoretical (based on 100% of compounds successfully injected into the chamber) and the FTIR and CIR-TOF-MS recorded data levels

2.3.3 GCxGC/TOF/MS

The Gas Chromatography was used to provide detail regarding the chemical make-up of the semi-volatile fraction of the SOA. The TOF-MS resembles the theory discussed of the CIR-TOF-MS (see section 2.1) where compounds are separated based on molecular weight and the formation of a mass spectra used to identify specific compounds based on time separation. Further to this is the GC component of the instrument. In essence this is a separating technique. A mobile phase of the sample is created from injection of a gaseous sample into a column with a flow of an inert gas (eg helium) known as a carrier gas. The column itself is covered with the stationary phase made of a microscopic layer liquid or polymer. The interaction between this mobile phase and the stationary phase separates different components from the gaseous sample. Here a thermal desorption is coupled to the GC x GC/TOF/MS. In the thermal desorption, the sample is injected into an autosampler (MPS2) holding a glass vial. Following desorption of the filter, small quantities of sample were injected into a column (TDU/CIS4, Gerstel, Germany). Following separation the sample then enters a Pegasus III reflectron TOF-mass spectrometer resulting in mass spectra. A more detailed description of the technique employed can be found in Hamilton et al., (2007)

2.3.4 HPLC and LC-MS

Both Liquid chromatography-ion trap mass spectrometry (LC-MSⁿ) and high performance liquid chromatography (HPLC) make use of liquid chromatography (LC).

LC comes into its own over GC with analysis of the most polar fractions of SOA (eg carboxylic acids). The separation technique is similar to gas chromatography with the exception that the mobile phase is liquid and is forced through a column utilising small packing particles usually at high pressures.

HPLC was utilised at EUPHORE to conduct on-line analyse of organic hydroperoxides and some stable species in the gas phase of the chamber. The principle of HPLC is as follows; a sample is injected in a liquid mobile phase. As the solution moves through the column, chemical interactions with the stationary phase slow the solution. The retention time of an analyte is dependent upon the strength of interaction with the stationary phase, the flow rate of the mobile phase the composition of the solvent used as the mobile phase.

LC-MSⁿ was used to as an off-line technique to analyse aerosol samples obtained from filters collected during experimental runs. A detailed description of this instrument is given in Hamilton et al., (2008). Briefly, samples were injected via an autosampler (Agilent 1100 series) into a column with 5- μ m particle size (Aligent, 4.6 mm x 150 mm). The samples were then investigated in both positive and negative ionisation modes using an HCT Plus ion trap mass spectrometer (Brunker Daltonics GmbH, Bremen, Germany).

2.3.5 TOF-AMS

A Time-of-flight Aerosol Mass Spectrometer (TOF-AMS) was used to measure the composition of the secondary organic aerosol. It works similar to the TOF techniques previously described, and the composition determined from the mass spectra produced from the AMS. A detailed operating description of the TOF-AMS (Aerodyne Research Inc., USA) can be found in Drewnick et al., (2005)

2.3.6 Hygroscopicity Tandem Differential Mobility Analyser (HTDMA)

A Hygroscopicity Tandem Differential Mobility Analyser (HTDMA) is used to measure size resolved aerosol hygroscopic properties. The change in aerosol distribution to change in relative humidity will be dependent upon the size and chemical composition of the particles. The HTDMA system also employs a DMA component (BMI, Haywood, CA, USA) described previously, using a Strontium-90 source. Briefly, the HTDMA was used to measure on-line size resolved water uptake at 90% RH, and dried aerosol samples to <10% RH using a Nafion drier (Perma Pure, MD-110-12, NJ, USA). The selected monodisperse samples are then humidified to 90% using a Gore-Tex system (more details described by Cubison et al., (2006)). The samples are passed through a resistance coil for 15 seconds before measurements of size distribution of the humid sample are made utilising a DMPS technique, DMA (BMI) and CPC (TSI, 3782). The humidity is measured using a dew point hygrometer (EdgeTech, Dewmaster, MA, USA) and Peltier units (Supercool, AA-040-12-22, Sweden) were used to control the temperature.

2.3.7 CO Monitor (EUPHORE)

As part of the ozonolysis experiments, carbon monoxide (CO) was used as a second scavenger species in addition to cyclohexane. CO was measured using a narrow IR radiation that absorbs IR at a wavelength of 4.6 μm . This was achieved using a Gas Filter Correlation (GFC) CO analyser. Here sample is drawn into an absorption cell. This cell is radiated with the narrow IR radiation by use of a filter that blocks out most of the wavelength. Two measurements of CO absorption are attained by the use of a rotating copper wheel that holds N_2 and CO in separate compartments. As this wheel rotates, the N_2 compartment is IR transparent and so absorption is due to the CO in the sample cell. As the wheel rotates to the CO compartment, the gas filter absorbs all the IR radiation, in effect scrubbing radiation that can be attributed to CO in the

sample cell. CO absorption from this cycle can lead to the concentration of CO using the Beer Lambert law in equation (2.0):

$$T = \frac{I}{I_0} = 10^{-\sigma cl} = 10^{-\epsilon lc} \quad (2.0)$$

Where T is transmission, I is intensity of transmitted light, I_0 is intensity of incident light, ϵ is absorption coefficient, l is path length, σ is the absorption cross section and c is the concentration.

2.3.8 O₃ Analyser

At the MAC facility, the ozone was measured using a UV photometric gas analyser, model 49C (Thermo Scientific, MA, USA) and by an FTIR and O₃ analyser at the EUPHORE site. O₃ absorbs UV light at 254 nm, an absorption characteristic that is followed by only few molecules in the troposphere. Two absorption cells are irradiated with a mercury lamp emitting light intensity at 254 nm and the absorption is measured by photodiodes of opposite sides of the cells to the mercury lamp. Samples are drawn into the cells from the chamber via a Teflon tube, consisting of an O₃ scrubbed and unscrubbed analyte sample regulated by a pair of alternating valves. Using the Beer Lambert law, the light intensity of the two cells, O₃ scrubbed analyte (I_0) and unscrubbed analyte (I), the concentration of O₃ can then be calculated following rearrangement of the Beer Lambert law in equation (2.0) to give equation (2.1):

$$[O_3] = \frac{1}{\sigma l} \ln\left(\frac{I_0}{I}\right) \quad (2.1)$$

Under humid conditions, interference due to condensation of sample air onto the absorption cells have been reported (Meyer (1991), Kleindienst (1993)).

2.3.9 NO_x analyser

In ACES, the NO and NO₂ mixing ratios were measured using chemiluminescence. Chemiluminescence is the emission of light as a result of a chemical reaction via an excited intermediate;



Where A and B are the reagents and I* is an excited intermediate. The NO_x analyser utilises the reaction of NO and O₃ to form excited NO₂* (R2.3) that emits light as it reverts to a lower energy state (Clyne 1964) (R2.4).



The excited NO₂ intermediate can also undergo quenching (R2.5). A chemiluminescence detector Model 42i (Thermo Scientific, MA, USA) was in operation at the Manchester Chamber, whilst a photomultiplier tube (PMT) was used at the EUPHORE site. Here NO₂ is measured by conversion of NO₂ into NO (R2.6):



The difference between measurements of total NO_x (NO and NO_2) and NO using the chemiluminescence technique then gives the NO_2 concentration. Although the experiments in the latter were aimed at “ NO_x free” conditions, it should be highlighted that NO_x analysers were used to confirm the absence of NO and NO_2 during chamber studies. NO_x however was present during studies conducted at the ACES facility. The experimental approaches for each chamber are discussed next.

2.4 Experimental Approach

Both experiments used a similar experimental approach; the conditions of each experiment (eg VOC, NO_x and O_3 concentrations) were set at the start of the run. The reaction start times were established as either “lights on” for the photooxidation experiments, or the addition of VOC or O_3 (whichever species was added last) during the ozonolysis experiments. Described is a more detailed experimental approach for each chamber. The initial experimental conditions can be obtained in Chapters 3 to 5.

2.4.1 EUPHORE experimental methodology

All ozonolysis experiments were conducted under “dark” conditions (closed chamber housing; $j(\text{NO}_2) < 2 \times 10^{-6} \text{ s}^{-1}$) close to atmospheric pressures and ambient temperatures, and in NO_x -free conditions. The majority of experiments were run in a low humidity environment ($\sim 0.33\%$ RH), for the exception of a few “wet” experiments that were approximating 20% RH. Four types of experiments were performed, a

“straight” ozone reaction (VOC/O₃), the addition of OH scavengers (VOC/O₃/CO and VOC/O₃/Cyclohexane) and a “wet” scavenged reaction (Cyclohexane). To ensure that OH was successfully scavenged, concentrations were used to ensure > 95% of OH was removed by the scavenger and not from reactions with the VOC. The general procedure of the experiment was to introduce SF₆ (an inert dilution tracer), the scavenger and ozone (at a rate of 20 ppb min⁻¹). In many of the scavenged reactions ozone was injected into the chamber before the reaction was initiated by the addition of a known VOC concentration. Excess ozone concentrations were used over that of VOC precursor to minimise impurity effects. In some experiments, the order of injection changed, with addition of VOC made ahead of ozone. A summary of the experiments are outline in Table 1. The cleaning process involves the evacuation of the chamber followed by fill and flush periods using O₃ between morning and afternoon runs, complemented by an overnight fill of O₃ to clean impurities between days.

2.4.2 ACES experimental methodology

All photooxidation experiments were conducted in the presence of NO_x, under both “high” and “low” VOC conditions with the initial VOC:NO_x ratio approximating 2:1. “High” concentrations were at 250 ppb and “low” concentrations were given at 50 ppb. The parent VOC was introduced into the chamber via an injection system utilising a flow of filtered nitrogen into a “heated” glass bulb to ensure non-sticking of the VOC onto the walls. O₃ was produced and controlled via a high capacity O₃ generator and the NO_x levels were introduced using a cylinder containing 10% NO₂ in nitrogen via a charge line. Once the initial conditions were set, the air conditioning unit was switched on followed by the turning on of the lights to represent the reaction start time (Time = 0). A cleaning process between experiment runs was controlled by a computerised system. Here a flush/fill period of 12 min where a 3 m³ min⁻¹ flow of clean air is filled and evacuated from the bag. Addition of ozone was optional and each clean period

consisted of a cycle of 5 to 6 flush/fill periods. Further cleaning overnight with filling of the bag with air consisting of ppm levels of O₃ assured multiple experiments to be completed following the clean cycling period.

2.5 Yields of stable organic species and SOA

Yields of stable organic gaseous species were calculated using sensitivity values for specific compounds following calibration techniques previously discussed. Once concentrations were achieved, yields were determined by plotting the amount of oVOCs formed against the volume of precursor VOC reacted. For major oxidation products (high concentrations produced), this line obtained was usually straight, and the yield was then obtained from the slope. The determination of some stable organic species yields were complicated due to dilution and other sinks (eg OH produced in radical free experiments). This produced non linear plots and so “initial” yields were determined from the start of the reaction (where a plot of oVOC formed versus VOC consumed gave a straight line). SOA yield were calculated using similar principles which is given in equation (2.3)

$$Y = \frac{\Delta M_o}{\Delta ROG} \quad (2.3)$$

Where ΔM_o is the organic aerosol mass concentration ($\mu\text{g m}^{-3}$) produced for a certain amount of reacted organic gas, ΔROG ($\mu\text{g m}^{-3}$) (Baltensperger 2005; Paulsen 2005).

The following chapters will discuss the results obtained from chamber simulations of compounds with greater emphasis based upon the gas phase speciation of the chamber environment, with further analysis given for aerosol formation utilising other instrumentation described here to obtain SOA potential of the VOCs examined.

Furthermore, the observed results will be compared to theoretical results of the MCM (where possible) to evaluate current understanding of the gas phase chemistry following degradation of VOCs.

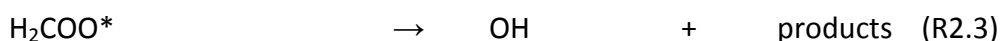
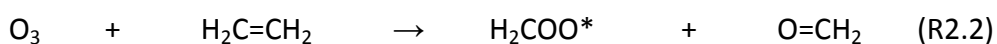
CHAPTER 3. Ozonolysis of simple alkenes and isoprene oxidation

This Chapter investigates the ozonolysis of the simple alkene species ethene, isobutene, trans-2-butene and cis-2-butene. Simple alkenes provide the simplest reaction model to be studied, and as such are the easiest to compare to atmospheric models (in this case the MCM), and validate instrumentation deployed during experimental campaigns. The results described here were obtained during the TRAPOZ project (see Chapter 2); with the aim of studying radical production from these alkene + O₃ reactions. A detailed description of the radical production results for ethene and ozone are available from Alam et al. 2010. Here, the emphasis is on the detection of stable species from oxidation of VOCs and their corresponding oVOCs for the purposes of evaluating the ability of CIR-ToF-MS to measure various gas species. Additionally we assess current atmospheric models for the production of stable organic species by comparing the experimentally observed data to that of the MCM model (see Chapter 2). The detection of HCHO and the influence of humid conditions on other low mass species such as formic acid are discussed with a short instrumental comparison between FTIR and CIR-ToF-MS to evaluate the effectiveness of the measurement technique and ability of the CIR-ToF-MS to accurately detect low level compounds.

The structurally more complex compound isoprene (C₅H₈) is also investigated here. Isoprene was studied at both chamber facilities (described in Chapter 2), and so a comparison of O₃-initiated and OH-initiated oxidation can be established, looking at the difference in production of stable species to identify and evaluate reaction routes previously established.

3.1 Ethene ozonolysis

The reaction of ozone with alkenes has been of interest for some years, it is known to form OH through decomposition from an initial Criegee intermediate (Donahue et al., 1998, Gutbrod et al., 1996, Olzmann et al., 1997). Ethene reacts with O₃ to form the Criegee biradical and formaldehyde (HCHO) (R2.2). The Criegee species then decomposes to form OH and other products (R2.3)



In the case of ethene, detection of HCHO would prove useful as an indicator for any OH produced as it is formed along with the Criegee intermediate. The CIR-ToF-MS was deployed during several ‘scavenged’ ethene experiments. Here CO and cyclohexane was used to react with OH preferentially to the VOC examined. This technique is used to isolate the ozone reaction with minimal influences from OH reactions on the precursor VOC. Table 3 gives an overview of the experimental conditions employed for ethene ozonolysis experiments conducted. Figure 23 shows the time evolution of three important reagents of a “dry” ethene and CO scavenged experiment conducted in May 2008. CO injection was preceded by addition of ozone into the chamber before the reaction start with the injection of ethene. The ethene was injected by two consecutive 50 µL injections at 08:21 and 08:23. Ethene’s proton affinity 680.5 kJ mol⁻¹; Hunter et al., (1998) renders it insensitive towards detection using the CIR-ToF-MS (water’s proton affinity is 691 kJ/mol) and so ethene data is provided from FTIR observations. Following the addition of ethene, the two oxidation products formaldehyde (HCHO) and formic acid (HCOOH) are observed to grow over the course of the experiment with the degradation of ethene and the reactant species O₃.

Table 3: Initial experimental conditions of ethene ozonolysis during TRAPOZ

Exp Date	VOC	Type	Initial Mixing ratios				RH / % ^b	Duration / min	Temp/ K ^b
			[VOC] ₀ / ppbV	[Ozone] ₀ / ppb ^a	[CO] ₀ / ppm	[Cyclohexane] ₀ / ppm			
09/05/08 (am)	Ethene	2	493.8	485	628.74		0.4	120	291.7
09/05/08 (pm)	Ethene	2,4	502.8	447.7	6582.12		19.7	85	295.2
12/05/08	Ethene	3	490.5	497.9		18.71	0.2	208	296.2

1, Straight Ozone/alkene, 2 with added CO, 3 with added cyclohexane, 4 with added H₂O, a measurements based on the ozone analyser, b values given as an average values measured over the duration of the experiment c, based on CIR-TOF-MS measurement, d based on FTIR measurement

Ethene is the simplest alkene in terms of both its structure and in the interpretation of experimental results following oxidation. Adapting the proposed alkene + O₃ chemistry previously described (see Chapter 1), a reaction mechanism can be formulated (Figure 24).

Following ozone addition, the ozonide rapidly decomposes to form formaldehyde and the excited biradical Criegee intermediate which undergoes further decomposition to form the peroxyradical and radical species. The production of radical species was the focal point of the work reported by Alam et al (2010) based on the studies conducted as part of the TRAPOZ campaign. Here, we simply note that two oxygenated species, HCHO and HCOOH are formed. The acid is formed from bimolecular reactions as suggested by Calvert et al (2000) with the addition of water to the collisionally stabilised Criegee radical.

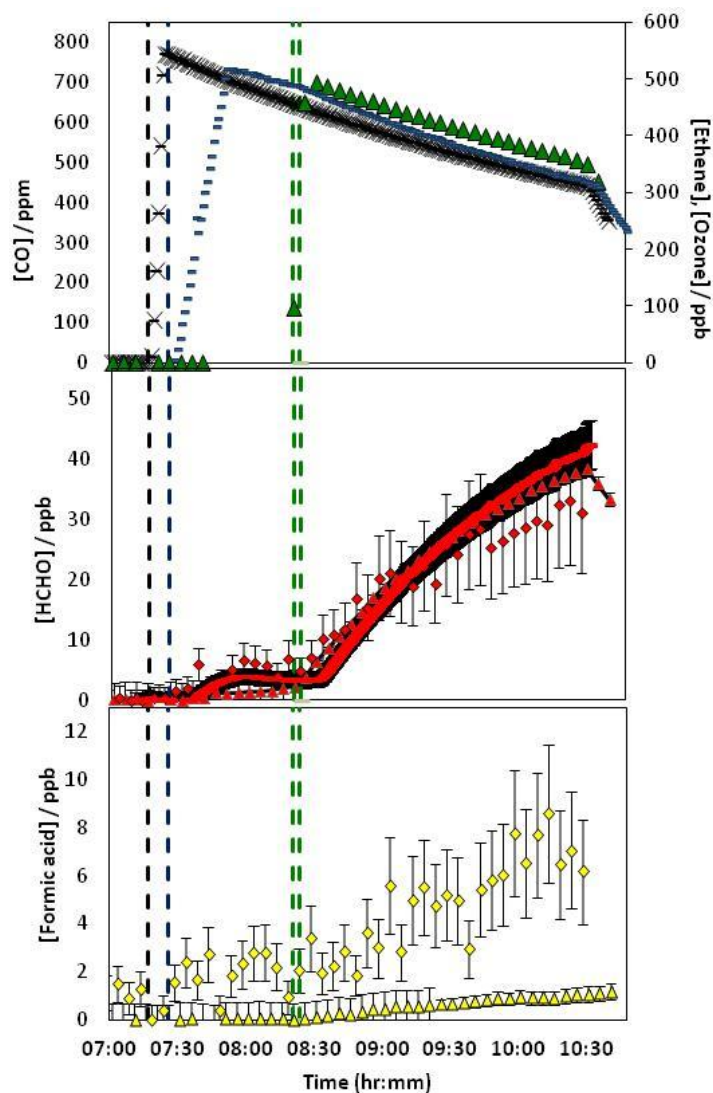


Figure 23 Top panel shows the time evolution of ethane (green) ozonolysis with CO (black) scavenger. The CO addition (black dashes) is followed by measurement of CO by FTIR. O₃ (blue) addition is measured spectroscopically (see Chapter 2) following addition into the chamber (blue dashes). Final addition of ethene (green dashes) shows reaction start time (t_0). Ethene then follows degradation as the reaction proceeds. All data plots have been dilution corrected. Middle panel shows a comparison of the time evolution of HCHO from ethene ozonolysis recorded from three instruments, CIR-ToF-MS (diamonds), FTIR (triangles) and HCHO monitor (solid line). Both FTIR and CIR-ToF-MS data has been averaged over a 5 minute period, whereas the HCHO monitor acquires data approximately every 20 seconds. The bottom panel displays comparison of FTIR (triangles) and CIR-ToF-MS (diamonds) for the detection of (HCOOH).

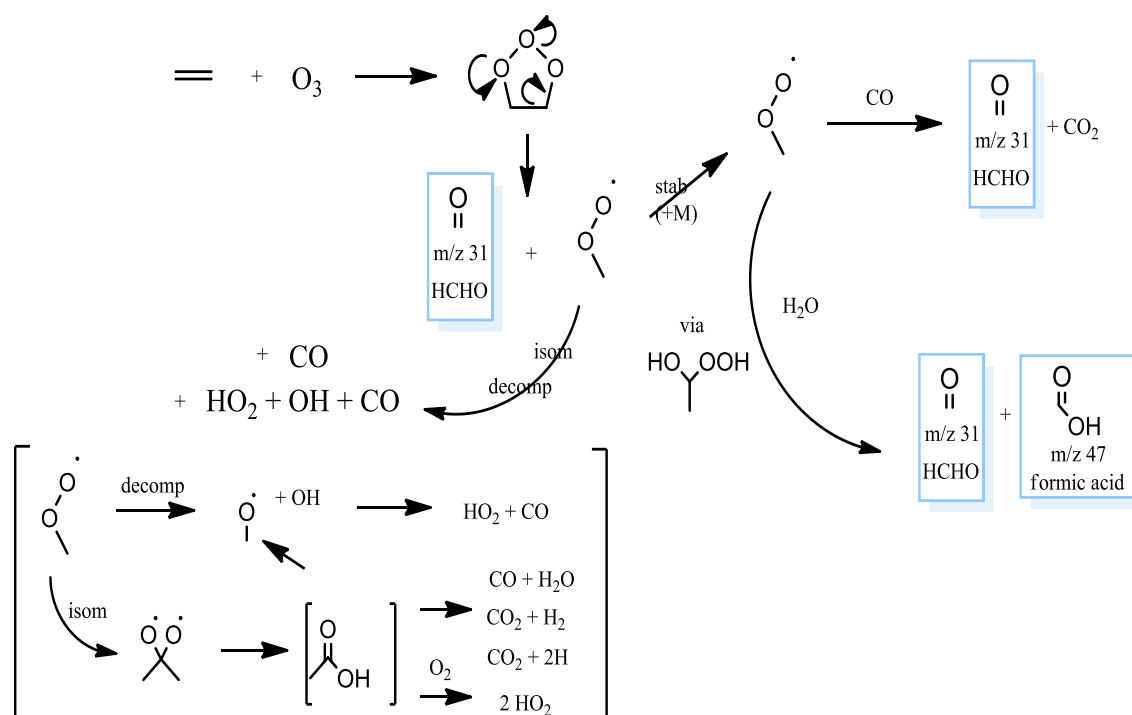


Figure 24 The proposed ozone reaction with ethene. Stable organic species are displayed in boxes. Here two oxidation products are expected from ethene ozonolysis, HCHO and HCOOH. HCHO is expected to be produced in higher quantities as its production is formed directly after ozone addition to the double bond. The brackets evolve the reaction pathway with the decomposition and isomerisation steps of the Criegee intermediate to produce HCOOH.

HCOOH has been proposed to form from the addition of H_2O to the dioxirane intermediate that is produced following isomerisation of the Criegee biradical (Orzechowska 2005). HCHO detection by CIR-ToF-MS compares well with the observations by both the FTIR and HCHO monitor (see Figure 28). This is used as a basis for instrument comparison in order to evaluate the accuracy of the instruments. As expected with a more humid system, the H_2O channel of the peroxy radical becomes more plausible and more formic acid will be expected. This is observed during the CO scavenged experiment (using FTIR measurements) as seen in Figure 23. However, concentrations of formic acid of several ppb appeared to approach the limit of detection of the CIR-TOF-MS for this compound. The detection of both these compounds is discussed in the following section.

3.1.1 Detection of HCHO and formic acid

HCHO and formic acid both have important relevance in atmospheric processes. HCHO is an important atmospheric compound owing to its capacity to influence tropospheric ozone formation. It influences the cycling of HO_x radicals and produces radicals that are used in the formation of O₃. Formic acid, and indeed other organic acids are known to be present in all environments (Volkamer 2007). These acids influence the acidity in cloud precipitation and so can alter reactions within clouds that are dependent on pH processes, potentially including OH chemistry. Further influences from low mass acids can play a part in total indirect radiative forcing as salt products produced from these acids via dissolution exhibit low critical supersaturations that bring forth activation of cloud droplets acting as cloud condensation nuclei (Yu., 2000).

The detection of HCHO has often been associated with complications in PTR-MS systems, particularly the variation of detection with humidity (Warneke et al., 2011). The close proton affinity of HCHO compared to water (712.9 kJ/mol and 691 kJ/mol respectively) means the back reaction of HCHO and H₃O⁺ is important to consider. The proton transfer of hydronium to an analyte (in this case formaldehyde) in the sample gas follows reaction (R2.4):



Where the proton transfer results in protonated HCHO along with the release of a water molecule. However if a large excess of water molecules is present, the back reaction of proton transfer is possible (R2.5)



The rate coefficients of these reaction rates have been determined as $1.4 \times 10^{-9} \text{ cm}^3 \text{ s}^{-1} \text{ molecule}^{-1}$ for R2.4 and $3 \times 10^{-11} \text{ cm}^3 \text{ s}^{-1} \text{ molecule}^{-1}$ for R2.5 (Hansel et al., 1997). Resultantly, in the presence of water molecules the sensitivity is expected to decrease. To evaluate the effectiveness of the CIR-ToF-MS in detecting ambient HCHO, a comparison was made with measurement taken by the FTIR spectrometer at the EUPHORE chamber facility (see Chapter 2). The sensitivity from dry to wet conditions during calibration runs was reduced from 11 ncps ppb⁻¹ to 2 ncps ppb⁻¹ highlighting the reduced sensitivity of HCHO under the two environmental regimes. Figure 25 shows the yields obtained for both “dry” and “wet” conditions of HCHO yield during a CO scavenged experiment for both applied sensitivity values.

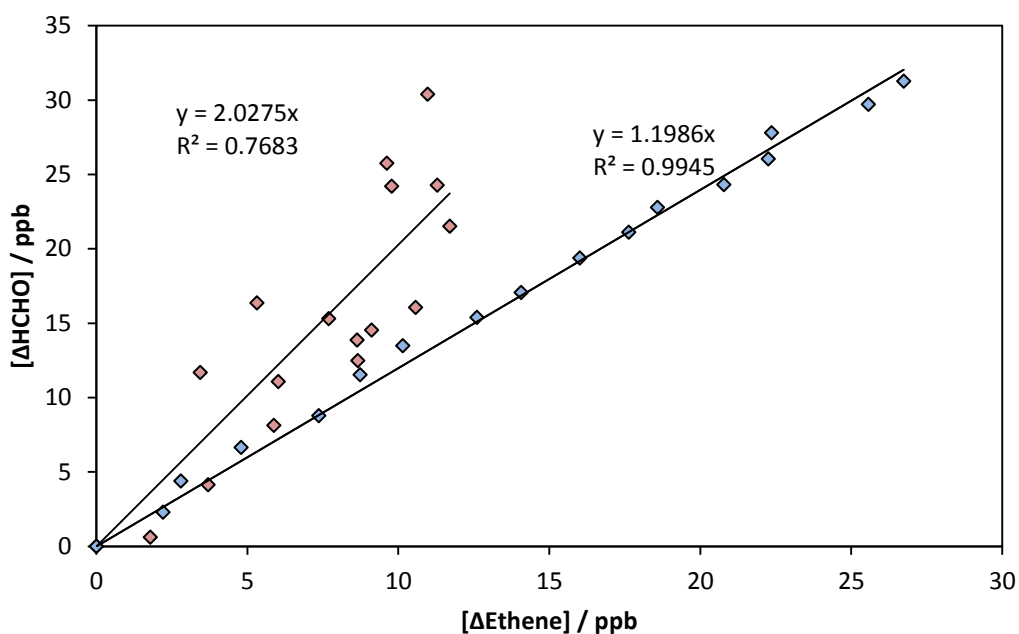


Figure 25 The yields obtained from ethene ozonolysis experiments in the presence of CO scavenger under similar initial reagents for “dry” (blue) and “wet” (red) chamber conditions on 09/05/08. The graph displays the loss of ethene and the responding increase of HCHO from a single experimental run. The data has been dilution corrected and ethene measurements were made by FTIR spectrometer.

The yields in Figure 25 were calculated taking into account chamber dilution as described in section 3.1.2. A difference of 40 % was observed between wet and dry

conditions. The scatter in data points of the wet conditions compared to the dry conditions indicates the lower sensitivity value, but this percentage error indicates the CIR-ToF-MS capability of detection of HCHO for low detection for a concentration of a few ppb.

Formic acid also has a proton affinity close to that of water (742 kJ/mol), making it very difficult to detect at low concentrations. During the “dry” experiments, the FTIR detected only a few ppb of formic acid (≤ 1 ppb). The complications of the CIR-ToF-MS sensitivity due to the low concentrations are apparent when comparing the evolution traces from both the FTIR and CIR-ToF-MS (Figure 26). However, during the “wet” experiments, more formic acid is expected due to the reaction pathways described in Figure 24. Here the CIR-ToF-MS measurements track the growth of formic acid based upon measurements taken by FTIR, but are still close to the detection limit as can be seen from the scatter of data in Figure 26. Owing to this, there will be a slight difference in yield calculated from both instruments. Figure 26 shows the difference in average concentration between the measurement techniques and thus calculated yield (described in section 3.1.2) of an ethene + O₃ experiment for the detection of formic acid. As such the yield of compounds at low concentrations which are close to the CIR-ToF-MS detection limit (i.e., compounds close to the proton affinity of water (691 kJ mol⁻¹) has been established based on FTIR measurements.

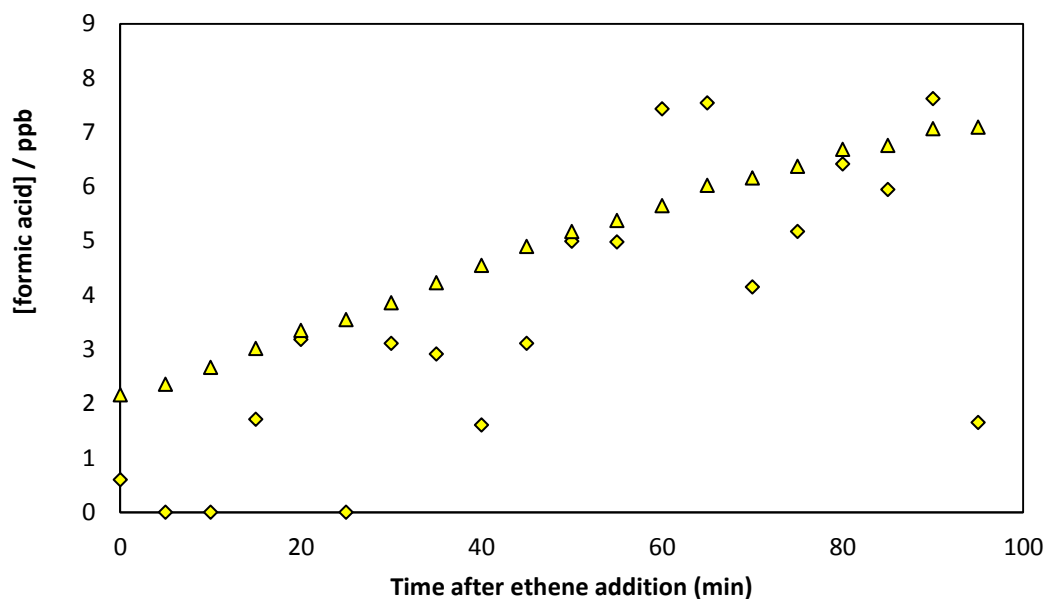


Figure 26. A comparison of formic acid detection for “wet” conditions during an ethene ozonolysis experiment from both FTIR (triangles) and CIR-ToF-MS (diamonds) measurements. The formic acid is still close to the detection limit of the CIR-TOF-MS which is evident from the scatter of data points, each data point represents an average of 5 min data from an acquisition of 1 minute data intervals.

3.1.2 Yields of stable organic products from ethene

The concentration of stable products decreased during the experiments due to dilution loss of gaseous species in the chamber. Dilution accounted for a total loss of 80 % during the ethene ozonolysis experiments. As such, the yield could be evaluated using the equation described in Chapter 2. Figure 27 displays the yield calculation for HCHO with a non-corrected dilution system.

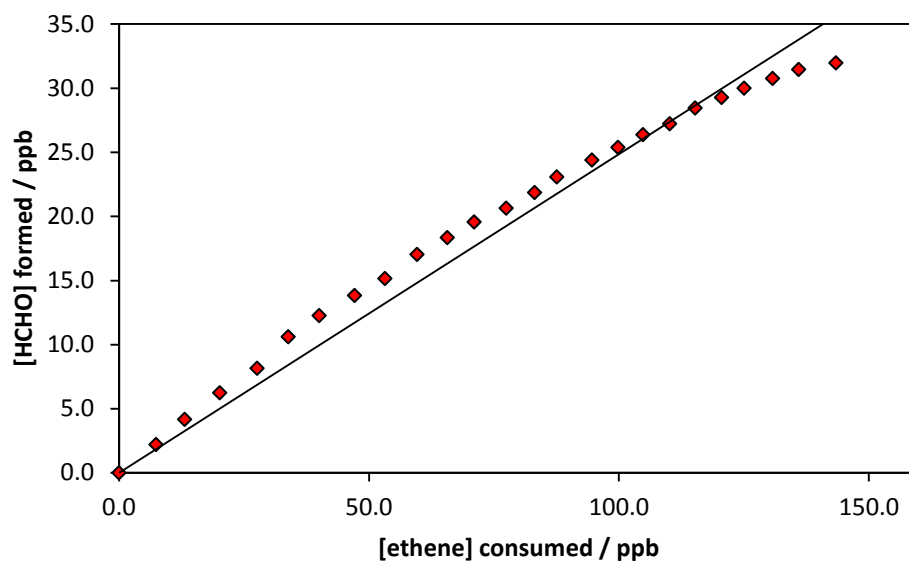


Figure 27. HCHO formation based on values that have not been corrected for dilution loss. Results obtained are from an excess CO scavenged experiment on 09/05/08. The resulting curvature of data points indicates a problem with final yield calculation due to dilution loss of the gaseous species.

To account for these losses, SF_6 was used as a tracer of chamber dilution. The corrected dilution yield is given in Figure 28 with a comparison of yield between the FTIR and CIR-ToF-MS measurements.

All other yield calculations were conducted in a similar fashion. The two stable organic products HCHO and formic acid were studied under 4 key experimental conditions. Table 4 presents the observed m/z ion channels and the yields obtained from ethene ozonolysis experiments. The yields were calculated using the best available data from all instrumentation employed at the EUPHORE site as specified. The yield given is representative of product formed against ethene reacted. Here also an average yield of both instrumentation was given as the FTIR and CIR-ToF-MS values showed a consistent yield to one another.

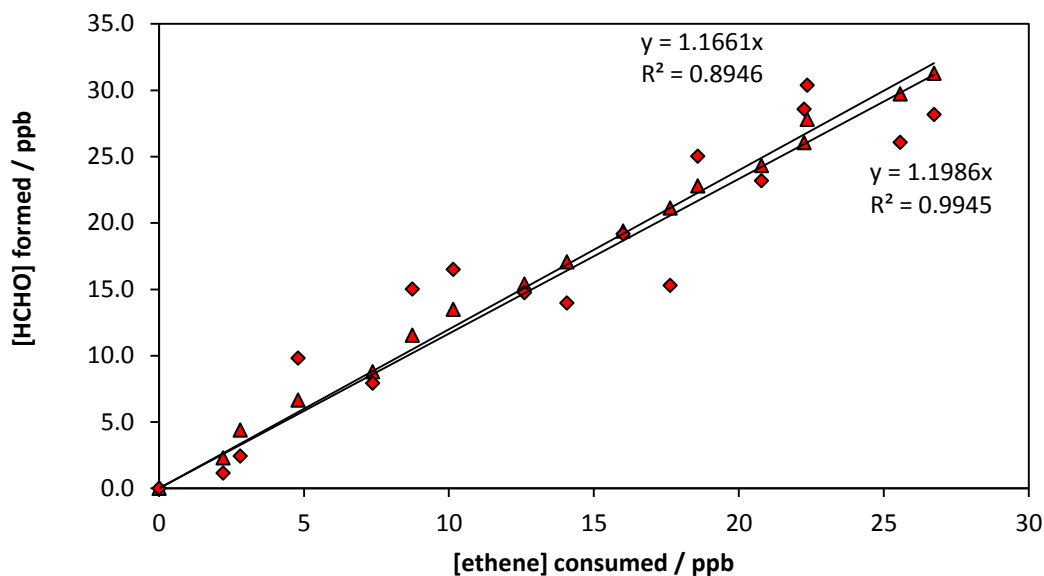


Figure 28. The dilution corrected yields obtained from an excess CO experiment. The CIR-TOF-MS yield (red diamonds) and the FTIR (triangles) show consistent yields established, 1.16 and 1.20 respectively.

Table 4. Detection of m/z ion channels during ethene experiments and their corresponding product yields

Compound	Identification / Product Yield
Signals Detected from CIR-TOF-MS	
<i>ethene + O₃ + CO (09/05/08, am)</i>	
47, 31	47 – HCOOH / bdl 31 – HCHO / 1.13 ± 0.06^a
<i>ethene + O₃ + CO (H₂O) (09/05/08, pm)</i>	
47, 31	47 – HCOOH / 0.56 ± 0.03^a 31 – HCHO / 3.09 ± 0.12^b
<i>ethene + O₃ + CHEX (12/05/08)</i>	
99, 85 ^{e(99)} , 47, 43 ^{e(99)} , 31	47 – HCOOH / 0.21 ± 0.02^c 31 – HCHO / 1.98 ± 0.05^d

Product yields are given as product relative to ethene converted

a = average yield value obtained from CIR-TOF-MS and FTIR

b = yield obtained from FTIR measurements

c = yield resulting from CIR-ToF-MS measurements

d = HCHO monitor determined yields

e(x) = fragment of indicated number (x)

bdl = below detection limit, (this and following tables represent signals below 3σ of background noise levels)

(H₂O) represents wet experimental conditions, RH > 50%

An average yield of 1.56 for dry conditions (in the presence of either CO or cyclohexane scavengers) and as high as 3.08 for humid conditions were achieved for HCHO. These yields exceed the values obtained in previous work (Table 5). Wolff et al., (1997) found yields ranging from 0.21 to 0.29. However this low yield is also in contrast to other work, Wegener (2007) found HCHO yields of 1.00 ± 0.08 for dry conditions and 0.88 ± 0.08 for wet conditions, whilst Grosjean et al., (1996), and Grosjean and Grosjean (1996) have shown similar high yields of 1.060 ± 0.071 and 0.992 ± 0.061 under 55% RH conditions with cyclohexane as a scavenger with Neeb et al., (1998) also confirming high yields in the range of 0.92, with yields of 0.618 found by Horie and Moortgat (1991). Based upon this range of data it appears that the HCHO yields are fairly consistent, although a large overestimation is found within wet experimental conditions. The high yield obtained can be explained by the low sensitivity of HCHO under humid conditions as previously stated and so FTIR measurements were used as these have also been shown to compare well (in dry conditions) with other CIR-ToF-MS measurements in order to gain the most accurate yield measurements.

Conditions	Yield (this study)	Past studies	
O ₃	-	0.21 – 0.29 0.92 0.618	Wolff et al 1997 Neeb et al 1998 Horie and Moortgat 1991
O ₃ (H ₂ O)	-	1.00 ± 0.08	Wegener et al 2007
O ₃ + CO	1.13 ± 0.06	1.00 ± 0.08	Wegener et al 2007
O ₃ + CO (H ₂ O)	3.09 ± 0.12	0.88 ± 0.08	Wegener et al 2007
O ₃ + CHEX	1.98 ± 0.05		
O ₃ + CHEX (H ₂ O)	-	1.060 ± 0.071 0.992 ± 0.061	Grosjean et al 1996 Grosjean and Grosjean 1996

(H₂O) is representative of conditions involving RH at levels greater than 50%

Under wet conditions, the formic acid yield for the CO scavenged experiments increased from below detection levels to 0.56. The increase in formic acid yield is not unexpected as shown from the “wet” reaction pathway which the biradical Criegee intermediate takes to form formic acid. Past work reported for the formic acid yield

under varied conditions from ethene ozonolysis are shown in table 6 and differ substantially. Under wet conditions ranging from 20% to 65% relative humidity, yields of 0.42 Neeb et al., (1997) and 0.33 Orzechowska and Paulson (2005) were determined respectively. Within dry conditions however, yields as high as 0.36 Orzechowska and Paulson (2005), 0.25 to 0.38 Su et al (1980) were established along with yields as low as 0.06 Herron and Huie (1977), 0.04 Thomas et al., (1993), and 0.01 by Neeb et al., (1997). However recent work by Leather (2012) using Chemical Ionisation Mass Spectrometry, focused specifically on determining the effect of humidity on formic acid yield and observed increasing yields of 0.07 to 0.41 for an RH ranging from <1% to 30%. These observations were in contrast to work conducted by Wolff et al., (1997) who also studied ethene ozonolysis with CO scavengers. However this work does produce evidence towards an increase in yield of formic acid under wet conditions.

Conditions	Yield (this study)	Past studies	
O ₃	-	0.36 0.06 0.28 – 0.35 0.01 0.07	Orzechowska and Paulson 2005 Herron and Huie 1977 Su et al 1980 Neeb et al 1997 Leather et al 2011
O ₃ (H ₂ O)	-	0.42 0.33 0.18 ^a 0.36 ^b 0.40 ^c 0.41 ^d	Neeb et al 1997 Orzechowska and Paulson 2005 Leather et al 2011 Leather et al 2011 Leather et al 2011 Leather et al 2011
O ₃ + CO	Bdl		
O ₃ + CO (H ₂ O)	0.56 ± 0.03		
O ₃ + CHEX	0.21 ± 0.02		
O ₃ + CHEX (H ₂ O)	-		

^aRH % = 11, ^bRH % = 21, ^cRH % = 27, ^dRH % = 30

This was established from calibration runs of formic acid under similar wet conditions to present a new sensitivity value that would take into account potential loss of sensitivity due to an excess of H₂O molecules in the drift tube (reaction cell) of the CIR-ToF-MS. With wet calibration methods achieved, a more reliable sensitivity value was obtained to be applied to the data collected from the chamber experiments.

3.1.3 Atmospheric model comparison of ethene

The ethene + O₃ system has been evaluated using the MCM, focusing on comparing the predicted degradation rates to the experimentally observed data, and the formation of the two main oxidation products. By choosing the initial conditions of the experiment, model prediction is able to be compared to experimentally determined data. The results of ethene ozonolysis show extremely good correlation matching the VOC degradation measured in the chamber using several different types of instrumentation (CIR-ToF-MS, FTIR and HCHO monitors) as shown in Figure 29 and 30 (all model comparison plots to experimental data will all have a grey background from here on). The comparison of experimental data to modelled data indicates that the degradation of ethene under the chosen experimental conditions is well understood as predictions of the model are in good agreement with the observed data. The formation of HCHO is also well modelled against the CIR-ToF-MS dataset which also correlates well with other instrumentation as previously shown. The formation of formic acid however seems to be overestimated based upon the predictions of the model. The model assumes formic acid formation only through the H₂O channel, and so under dry conditions no formation is expected. The overestimation in formic acid could be accounted for by out-gassing from the chamber walls as formic acid is released from the chamber walls creating an “outside of experimental controlled” source, and so can contribute to higher than expected levels of formic acid. The MAC is still currently undergoing tests to fully characterise the chamber.

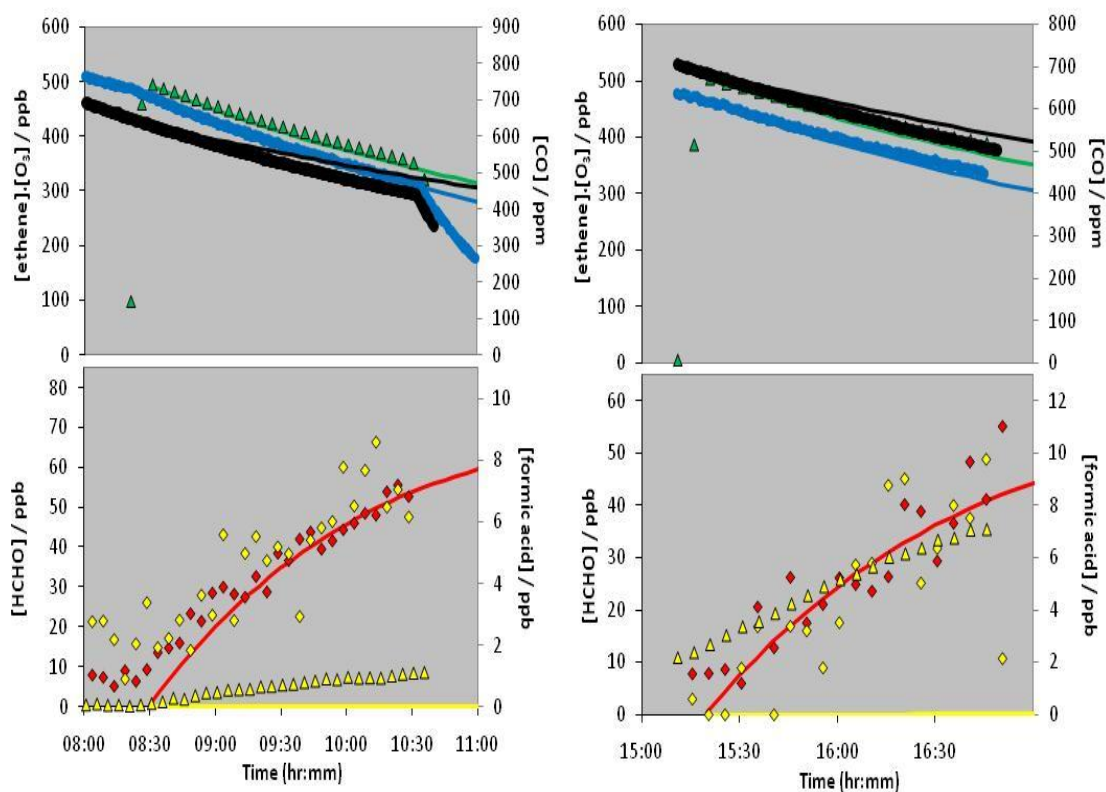


Figure 29. Comparison of the MCM model (output) compared to measured experimental data (markers or thick lines) for the ethene CO experiment run on 09/05/08 under dry (left) and wet (right) conditions. The model shows good correlation with the reagents ethene (green) and ozone (blue) and the CO scavenger (black). The resulting oxidation product formaldehyde (red) also shows good correlation to the model, whereas formic acid (yellow) is largely overestimated by the CIR-ToF-MS (diamonds) and marginally by the FTIR (triangles).

These models were run with no change to branching ratios of reaction pathways. This is in contrast to work by Alam et al., (2011) where branching ratios were changed to optimise the model for radical yields experimentally determined. However, because of the good fit of degradation the precursor, and trend in formation of the oxidation products between modelled and experimentally determined results, it can be concluded that the model predicts both accurately.

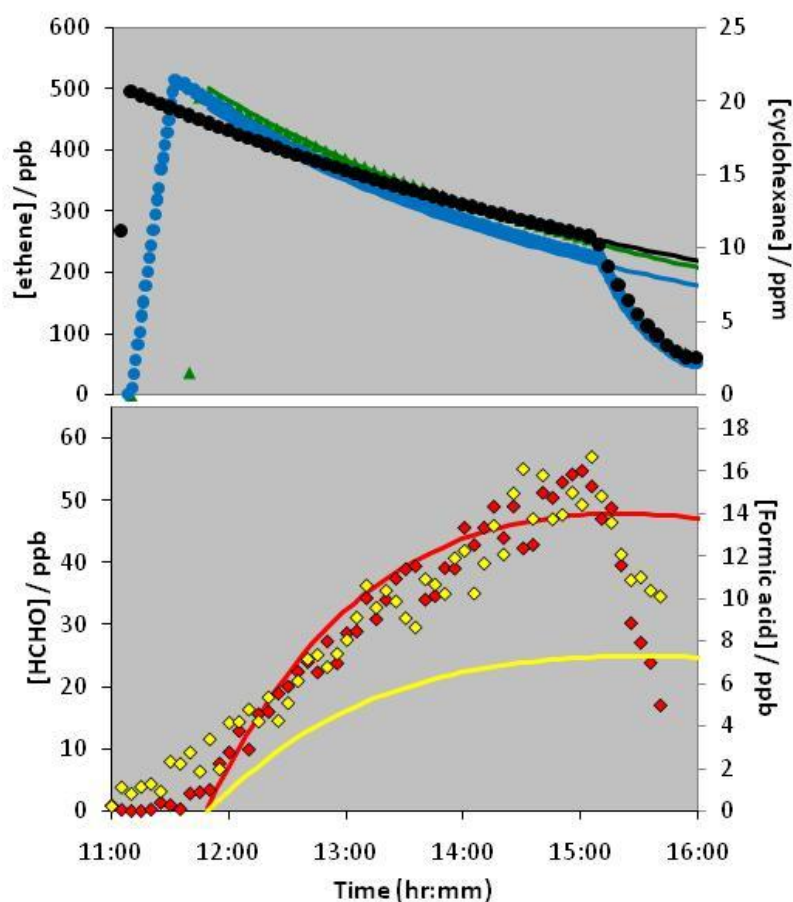


Figure 30. The model output (solid thin lines) compared to experimental measured data (markers or thick solid lines). This experiment utilised cyclohexane (black) as an OH scavenger.

3.2 Isobutene ozonolysis

Isobutene (2-methylpropene, C_4H_8) is a hydrocarbon emitted predominantly in industrial processes. Similar to ethene, ozonolysis reactions of isobutene have been studied with emphasis placed on the production of radical species (particularly OH formation), owing to its small size. Here, this system offers a good comparison of how well different oxidation products (in this case acetone and acetic acid) are modelled compared to chamber studies conducted at the EUPHORE facility. Table 7 shows the experimental conditions run for isobutene ozonolysis experiments while Figure 31 displays the time evolution of key compounds during a cyclohexane scavenged

isobutene ozonolysis experiment. The detection of isobutene concentrations from the FTIR monitor and CIR-ToF-MS show a vast difference from a maximum of 306.5 and 634.3 ppb respectively. A total of 0.251 g was injected into the chamber. Assuming 100% of the VOC was injected, based upon the chamber volume, a standard mole of gas per litre (22.4 L) and the molecular weight of isobutene, a total injection amount of 501 ppb can be calculated which falls outside of the error of the CIR-ToF-MS. Based on this, the measurements by the CIR-ToF-MS seem to exceed the total possible injection capacity of isobutene. The values of isobutene concentrations were based on the surrogate isoprene, chosen based on aspects such as chemical structure, functional groups, polarisability and proton affinity. However, the FTIR also underestimates this value, perhaps indicating influences affecting the injection method such as line sticking. The volatility of isobutene suggests that it should not suffer such loss using this injection method. A comparison of the initial isobutene concentrations are displayed in Figure 32 with measurements taken by FTIR and CIR-ToF-MS along with the calculated concentration of maximum possible injection.

Table 7: Initial experimental conditions of isobutene ozonolysis during TRAPOZ

Exp Date	VOC	Type	Initial Mixing ratios				RH / % ^b	Durat-ion / min	Temp / K ^b
			[VOC] _o / ppbV (nominal)	[Ozon-e] _o / ppb ^a	[CO] _o / ppm	[Cyclohexane] _o / ppm			
02/05/08 (am)	Isobutene	3	500	486.2		142.60	0.2	119	293.5
02/05/08 (pm)	Isobutene	3,4	500	459.9		151.36	21.3	127	294.3
14/05/08 (am)	Isobutene	2	100	217.1	632.09		0.2	143	295.7
14/05/08 (pm)	Isobutene	2,4	100	147.8	630.73		18.4	123	296.9

1, Straight Ozone/alkene, 2 with added CO, 3 with added cyclohexane, 4 with added H₂O, a measurements based on the ozone analyser, b values given as an average values measured over the duration of the experiment c, based on CIR-TOF-MS measurement, d based on FTIR measurement

Additional formation of compounds detected from the ozonolysis are also included in Figure 31 to show the formation of a variety of low mass stable organic species. Despite the large discrepancy of measured isobutene, this scale is not reflected in the two products that were measured both by FTIR and CIR-ToF-MS. Differing to ethene, isobutene has two methyl groups attached to one carbon. Due to these additional functionality groups, more oxidation products are assumed to be produced resulting from the addition of ozone. Figure 31 displays the ozone reaction with isobutene with focus again on the stable organic species.

Like ethene, ozone adds itself to the double bond of isobutene to produce the highly energetic ozonide that decays to produce both HCHO and acetone along with two different Criegee intermediates (CI). These can then collisionally stabilise to form further stable products such as HCHO and acetone. Like ethene, formic acid is again assumed to be produced via a wet channel in the reaction scheme. Additionally, acetone can itself decompose to produce radical intermediates (RI) that may themselves undergo RO_x or HO_x chemistry to form acetic acid and further molecules of HCHO. Due to formation as a primary oxidation product and possible development through other reaction pathways HCHO is again regarded as the dominant product for the ozonolysis of isobutene.

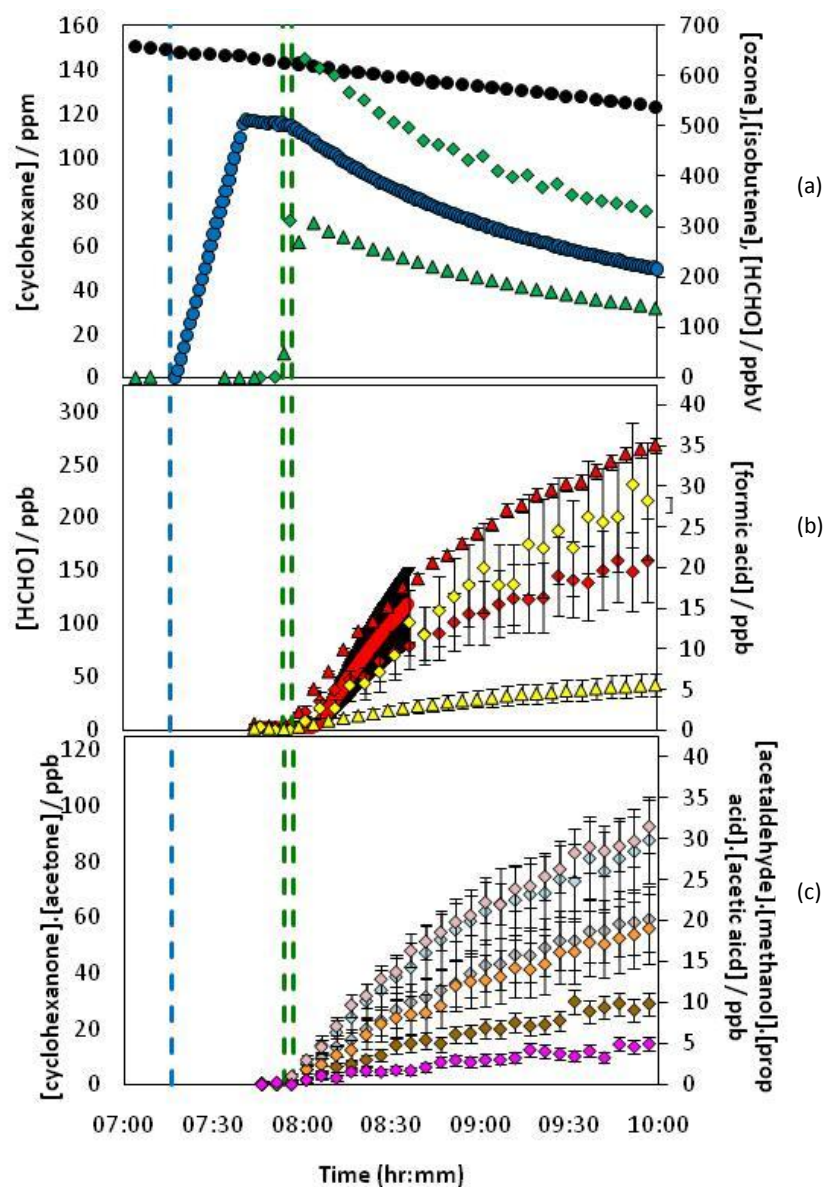


Figure 31. a to c are displayed to show the time evolution of an isobutene ozonolysis reaction conducted on 02/05/08 with the presence of a cyclohexane scavenger. Figure 31a demonstrate major reagents ozone (blue) and isobutene (green) from FTIR (triangles) and CIR-ToF-MS (diamonds) along with the high levels of cyclohexane (black circles). Figure 31b highlights the difference of compounds of formic acid (yellow) and HCHO (red) from the instrumentation available and finally 31c shows the observed mass channels showing growth greater than 3σ of background noise. These include acetic acid (pink), propionic acid (brown), methanol (orange), acetone (grey), cyclohexanone (light blue) and acetaldehyde (light pink). Experimental data from this day is displayed as it highlights the CIR-ToF-MS capability of detecting a range of masses during an experimental run.

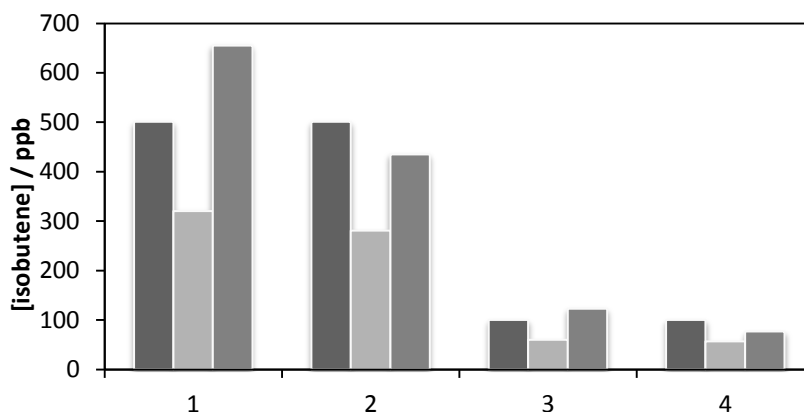


Figure 32. The differing detected maximum concentration values determined from FTIR (light grey) and CIR-ToF-MS (grey) taken from the four different experiments as shown in table 5. In all circumstances the CIR-ToF-MS gives a higher concentration level compared to that of FTIR measurements. These were compared to calculated maximum theoretical concentrations (black).

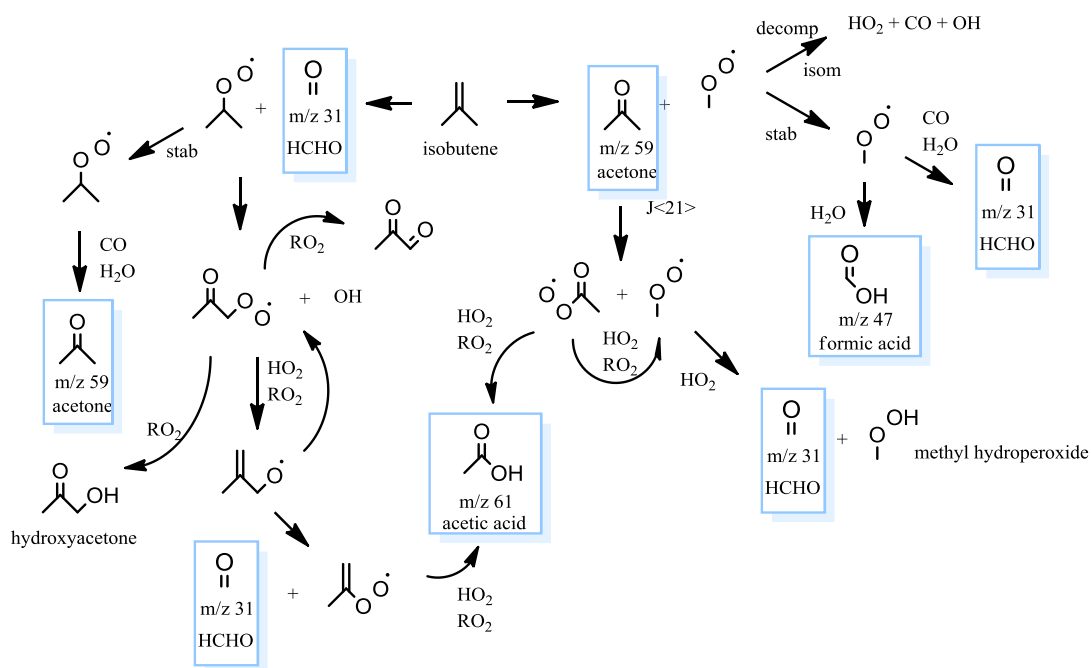


Figure 33. The ozonolysis of isobutene. The formation of formic acid follows that from the C12 intermediate as seen in ethene ozonolysis. The two additional methyl groups enable the formation of acetone, which can further lead to the formation of acetic acid.

3.2.1 Yields of stable organic products from isobutene

Table 8 shows compounds identified based upon m/z values 3σ above the background noise level with yields given as a function of ppb formed per ppb of isobutene reacted. Few product studies of isobutene have been made of atmospheric relevance, Atkinson (1997). The two major oxidation products detected from the ozonolysis of isobutene are acetone and formaldehyde. From the proposed reaction mechanism (Figure 33), this is expected as these two products are formed from the bond cleavage of the primary ozonide following initial ozone addition to the double bond. Acetone yields obtained under CO scavenged conditions compare well to those of 0.30 ± 0.03 established by Neeb., (1999) who also used a CO scavenger. The same can be assumed for studies with a cyclohexane scavenger, where yields ranging from 0.271 to 0.340 were determined by Grosjean et al., (1994); Grosjean and Grosjean (1996), and Tuazon et al., (1997). This high yield also places an emphasis on the production of the radical species CH_2OO^* which is formed from acetone oxidation. These radical species then contribute towards OH production of certain systems. The detection of formic acid can be excluded from potential external sources such as off-gassing from chamber walls because higher concentrations were observed during “wet” conditions. This follows, and further promotes the ideology presented previously within the ethene reactions, where formic acid is formed at larger quantities due to the availability of H_2O to react with the biradical Criegee species also formed from isobutene + ozone reactions. Grosjean et al., (1994) produced a yield of 0.156 ± 0.040 for HCOOH with a relative humidity of 55% and using cyclohexane as a scavenger. Overall the yield is dominated in all experiments by formaldehyde, suggesting there is a greater preference to the formation of the C1 Criegee intermediate compared to the C2.

In addition to the proposed stable products, a heavier m/z ion channel than the precursor was detected at m/z 75. This oxidation product could be propionic acid ($\text{C}_3\text{H}_5\text{OOH}$). Yield determination was made using acetic acid as a surrogate, as both these compounds share similar kinetic properties: the carboxylic acid functional group, the proton affinities of propionic acid and acetic acid (797.2 kJ/mol and 783.7 kJ/mol),

Table 8. Detection of *m/z* ion channels during isobutene experiments

Compound	Identification / Yields
Signals Detected from CIR-TOF-MS	
<i>isobutene + O₃ + CHEX (02/05/08, am)</i>	
58, 57, 42, 41	
99, 81, 75, 73, 71, 61, 59, 55, 47, 45, 33, 31	99 – cyclohexanone / bdl 75 – propionic acid / 0.06 ± 0.01 61 – acetic acid / 0.02 ± 0.01 59 – acetone / 0.33 ± 0.01 47 – formic acid / 0.03 ± 0.01 45 – acetaldehyde / 0.17 ± 0.01 33 – methanol / 0.10 ± 0.01 31 – HCHO / 1.50 ± 0.02 ^b
<i>isobutene + O₃ + CHEX (H₂O) (02/05/08, pm)</i>	
58, 57, 41	
99, 81, 75, 73, 61, 59, 47, 33, 31	99 – cyclohexanone / bdl 75 – propionic acid / 0.22 ± 0.01 61 – acetic acid / 0.06 ± 0.01 59 – acetone / 0.59 ± 0.01 47 – formic acid / 0.28 ± 0.01 ^c 45 – acetaldehyde / 0.21 ± 0.01 ^c 33 – methanol / 0.22 ± 0.01 ^c 31 – HCHO / 1.92 ± 0.08 ^a
<i>isobutene + O₃ + CO (14/05/08, am)</i>	
58, 57, 41	
75, 73, 61, 59, 47, 45, 43, 33, 31	75 – propionic acid / bdl 61 – acetic acid / 0.06 ± 0.01 59 – acetone / 0.31 ± 0.01 47 – formic acid / 0.02 ± 0.01 45 – acetaldehyde / 0.06 ± 0.01 33 – methanol / 0.06 ± 0.01 31 – HCHO / 0.93 ± 0.03
<i>Isobutene + O₃ + CO (H₂O) (14/05/08, pm)</i>	
58, 57, 41	
75, 61, 59, 47, 33, 31	75 – propionic acid / bdl 61 – acetic acid / bdl 59 – acetone / 0.38 ± 0.03 ^c
Table 8. continued	
	47 – formic acid / 0.36 ± 0.01 ^b 33 – methanol / 0.17 ± 0.04 ^c 31 – HCHO / 1.96 ± 0.54 ^c

BOLD = MH⁺ parent ion and related fragments

Measurements taken by: an average of CIR-TOF-MS and FTIR^a; FTIR^b; CIR-TOF-MS^c; HCHO monitor^d

bdl = below detection limit

Precursor concentration based on FTIR values

(H₂O) represents wet experimental conditions, RH > 50%

permanent dipole moment (1.75 D and 1.74 D; where D is Debye) and polarisability ($6.9 \times 10^{-24} \text{ cm}^3$ and $5.1 \times 10^{-24} \text{ cm}^3$). Fractional yields obtained averaged 0.037 under dry conditions and increased with increasing RH to 0.174, also displaying a dependence upon humidity. This also suggests that the degradation pathway from isobutene for propionic acid is similar to that of formic acid.

3.2.2 MCM model comparison of isobutene

The ozonolysis of isobutene with a cyclohexane scavenger is represented in Figure 34. The degradation of isobutene and cyclohexane show good correlation between modelled in the MCM compared to the experimental data. Ozone however appears to be underestimated in the model. This slight difference is also reflected in the oxidation products produced from the ozonolysis experiment. The two major products here imply that HCHO is underestimated by approximately 80 ppb of maximum concentration added. The current MCM model predicts that the branching ratio of formation of HCHO and acetone are 0.5 and 0.5 respectively. To improve the model output for HCHO levels observed, a preferential reaction of pathway Criegee $\text{C}_2\text{H}_6\text{COO}^*$ over CH_2OO^* (Figure 33) is needed. However, this would decrease the acetone output, which also is underestimated in the model by just under half. This would then point towards differing branching ratios further along the reaction scheme as both acetone and HCHO are formed via stabilisation of the Criegee intermediate and further HO_x/RO_x reactions. The formation of formic acid however follows that of ethene, under wet conditions and the stabilisation of the CH_2OO^* radical species. The FTIR trace shows a fairly good match in formic acid, only slightly underestimating by as low as 3 ppb.

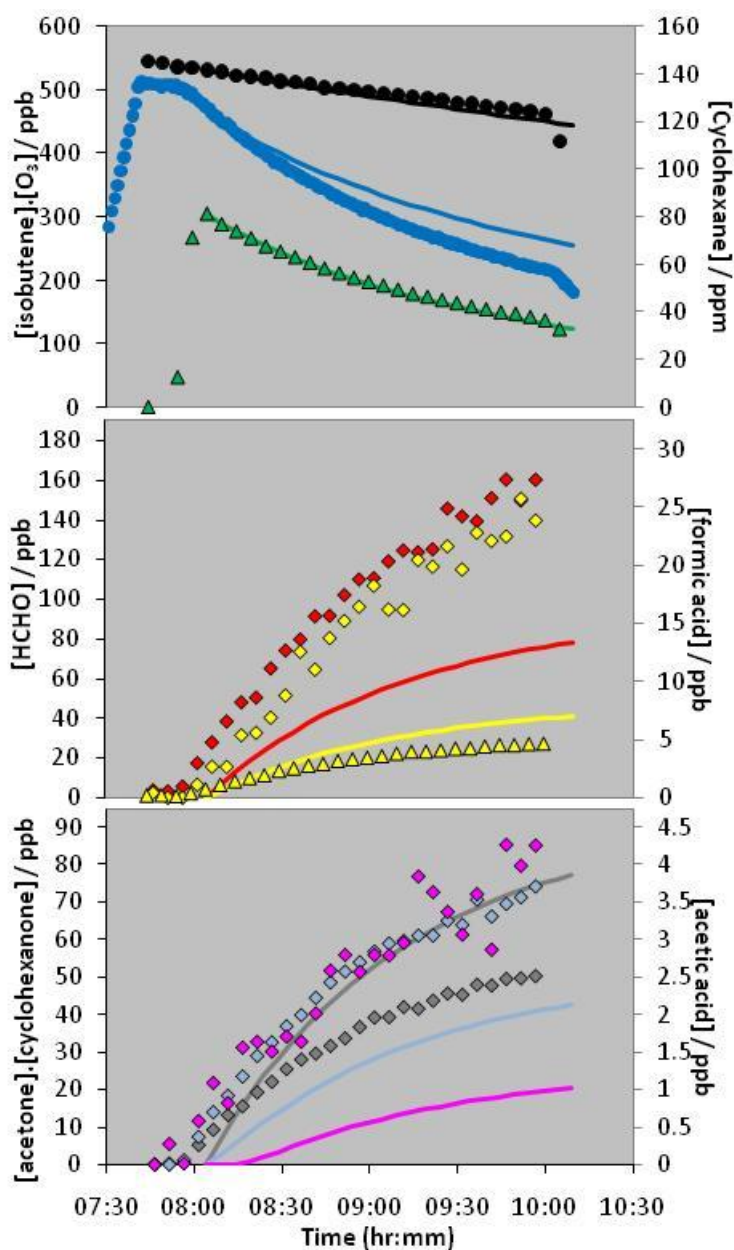


Figure 34. MCM model comparisons to experimentally determined data. Trace profiles are; (Top) Cyclohexane (black), Isobutene (green) and ozone (blue); (Middle) Formic acid (yellow) and HCHO (red); (Bottom) Cyclohexanone (pink), acetone (grey) and acetic acid (light blue). CIR-ToF-MS data (diamonds) is compared to FTIR (triangles) and model predictions (solid lines).

An overestimation of the CIR-ToF-MS is shown for all oxidation products for the exception of cyclohexanone which itself was bordering on the detection limit of the

instrument. However a fairly good representation between observed and simulated data is shown. Compared to the ethene experiments we have shown a general overestimation of this compound due to possible contamination influences such as off-gassing from chamber walls in comparison to the FTIR data. In order to rectify this in the model, either pathway “b” would need to be slightly dominant over “a” or more of the stabilised Criegee needs to be formed rather than the decomposition stages of which a ratio of 0.18 and 0.82 were used. The latter change will also increase more HCHO and acetone as these are formed directly from the stabilised radical and both CO and H₂O. Therefore, it may be assumed that the stabilised Criegee radical is underestimated, which can also influence other important aspects such as OH yields as these are stipulated to be formed from the decomposition of the Criegee intermediate and independent from the concentrations of reagents (Neeb et al., 1999).

3.3 Trans-2-butene ozonolysis

Trans-2-butene (C₄H₈) has a major anthropogenic source produced by the catalytic cracking of crude oil. Here its degradation via ozonolysis was investigated with different scavenger experiments (CO and cyclohexane) in both dry and wet environments. The analysis of oxidation products were conducted in a similar fashion to previous experiments, in which dilution aspects were taken into account for yield calculations. The addition of ozone to the double bond of trans-2-butene produces an ozonide that will decompose to form both an acetaldehyde fragment and an excited Criegee intermediate. Because of the initial formation of acetaldehyde, this forms a good comparison for acetaldehyde as it is the dominantly formed oxidation product. Table 9 shows the initial experimental conditions whilst Figure 35 shows the instrument comparison between the ToF and FTIR data set observed during a cyclohexane scavenged experiment.

Table 9: Initial experimental conditions of trans-2-butene ozonolysis during TRAPOZ

Exp Date	VOC	Type	Initial Mixing ratios				RH / % ^b	Duration / min	Temp/ K ^b
			[VOC] _o / ppbV	[Ozone] _o / ppb ^a	[CO] _o / ppm	[Cyclohexane] _o / ppm			
06/05/08 (am)	Trans-2-butene c	3	184.9	107.6		51.67	0.6	125	292.6
06/05/08 (pm)	Trans-2-butene c	3,4	105.4	106.2		57.43	21.7	120	293.6
15/05/08 (am)	Trans-2-butene c	2	68.6	195.4	723.01		0.3	110	293.7
15/05/08 (pm)	Trans-2-butene d	2,4	82.0	202.5	763.56		20.9	128	294.3

1, Straight Ozone/alkene, 2 with added CO, 3 with added cyclohexane, 4 with added H₂O, a measurements based on the ozone analyser, b values given as an average values measured over the duration of the experiment c, based on CIR-TOF-MS measurement, d based on FTIR measurement

The reaction of ozone with the double bond of butene is given in Figure 36. Initial addition of ozone forms an ozonide which rapidly decomposes to form both acetaldehyde and an excited Criegee intermediate. The acetaldehyde route can then undergo reaction with OH to form a further peroxy radical that follows the reaction steps as seen in the isobutene reaction pathway followed by RO_x and HO_x chemistry (see Section 3.2). Similar to the reaction steps previously shown, the Criegee intermediate can undergo collisional stabilisation which reacts with CO and H₂O to form the stable species of acetic acid and acetaldehyde. The addition of OH of acetic acid can then produce a further peroxy radical that is also produced from decomposition of the peroxy radical as a source of CO and HO₂. Following further RO₂ and HO₂ chemistry smaller stable organic species such as formaldehyde and methanol are formed. Following the reaction steps will produce acetaldehyde in large quantities compared to the other stable species, which was observed during the experiment.

At this stage, it may be worthy of note that two different sources for the production of H₃O⁺ were employed: ²⁴¹Am (during TRAPOZ) and the hollow cathode (HC; during TRAPOZ 2). More hydronium ions were produced with the HC source, however the hollow cathode loses sensitivity with regards to short chain alkenes. The difference in sensitivity is apparent when comparing calibrations from both a standard cylinder comprising a multi-VOC matrix, and experimental results of the butene experiments.

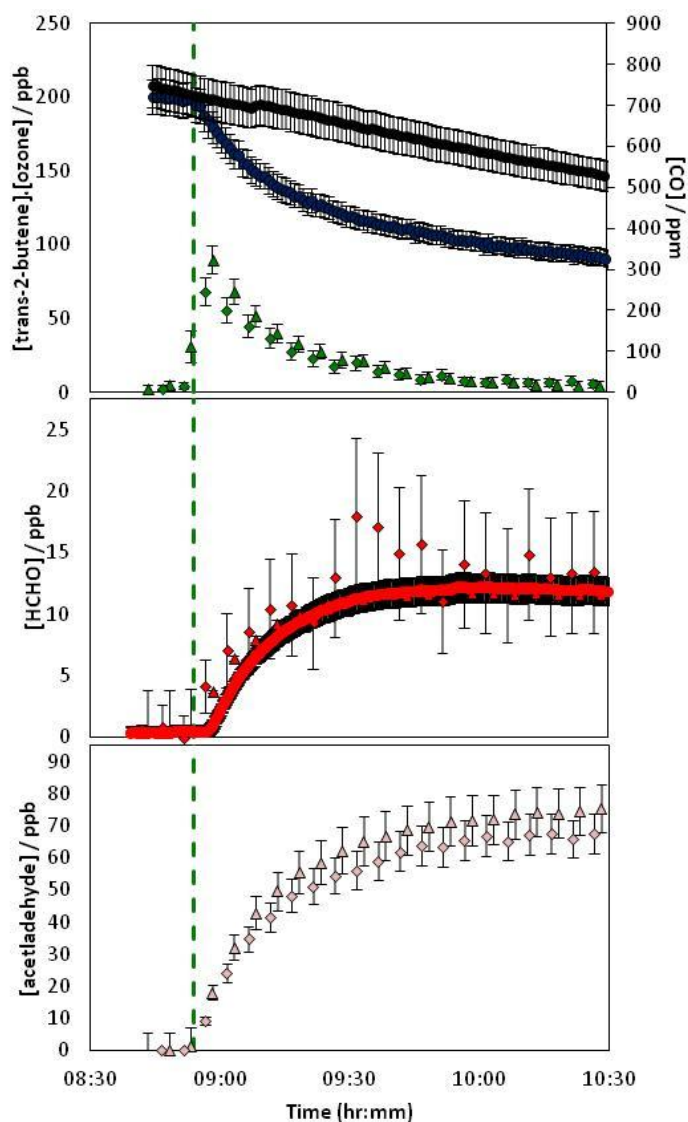


Figure 35. The initial conditions and time traces for the trans-2-butene (green) experiment during a CO (black) scavenged experiment on 15/05/08. The intercomparison between FTIR (triangles), CIR-TOF-MS (diamonds) and monitors (solid lines) detections of trans-2-butene show good correlation, with similar results for major oxidation products acetaldehyde (pink) and HCHO (red).

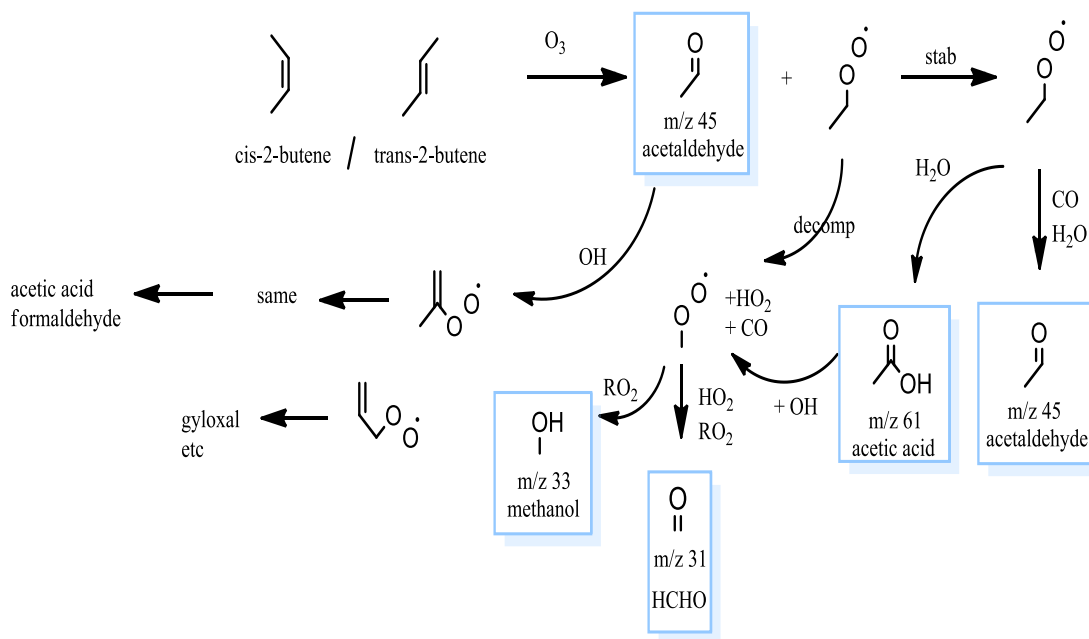


Figure 36. A reaction scheme of trans-2-butene ozonolysis adapted from the MCM mechanism. O₃ attacks the double bond, and owing to the structure of butane species, acetaldehyde and a corresponding Criegee intermediate is formed. Acetaldehyde reacts with OH to produce similar radical species similar to those before and hence promote formation of stable species such as formaldehyde and acetic acid.

No trans-2-butene “wet” calibration runs were conducted, but the ratio of difference between the cis-2-butene value from “dry” and “wet” conditions was used as a guide for the difference in sensitivity of trans-2-butene. Figure 37 shows the difference between sensitivity values of cis-2-butene under wet and dry conditions. The ratio obtained, 0.61 was used to assess the wet calibration value for trans-2-butene. The trans-2-butene sensitivity for the HC source, although already low is much lower for the HC source. This low sensitivity is more clearly displayed with comparison of signal detection between trans-2-butene and cis-2-butene from the two ion sources. However, other compounds increase greatly in sensitivity, such as acetone. Owing to this, the HC source can thereby be selected for analysis of certain systems in which it has an increased sensitivity. This work needs further development but it already has shown potential to be used due to its increase in sensitivity compared to the ²⁴¹Am source.

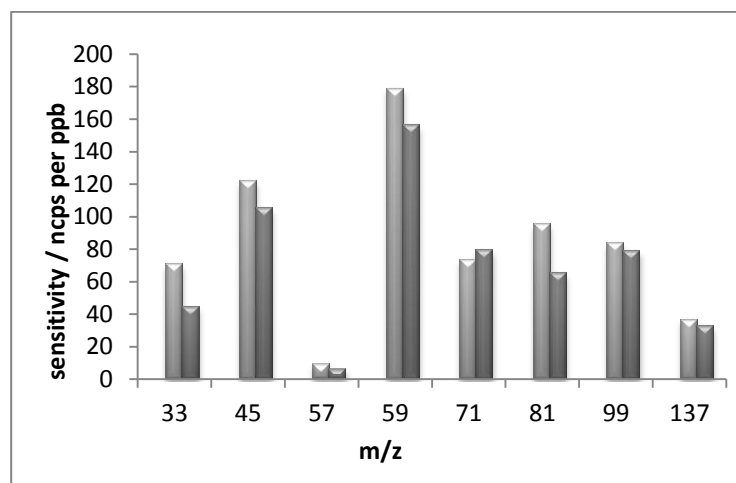


Figure 37. A comparison of the 1 ppm gas standard cylinder (consult Chapter 2 and Table A2 in the appendix) with the ^{241}Am ion source under dry and humid (80% RH) conditions. The overall trend seems to show a decrease in sensitivity with increase in RH.

3.3.1 Yields of stable organic products from trans-2-butene

During the trans-2-butene experiment, all the proposed stable products were identified. The yields obtained for each experiment are presented in Table 10. As predicted, the formation of acetaldehyde dominates the formation of oxidation products. Some detection of formic acid was also observed, but some of this may be ascribed to off-gassing from the chamber walls. Similarly, with the cyclohexane scavenged experiments, cyclohexanone is again detected. Owing to the large dominance of acetaldehyde production, is it a good indicator for acetaldehyde detection with instrumental intercomparison. Figure 38 shows the yield variation obtained from a trans-2-butene + O_3 scavenged experiment.

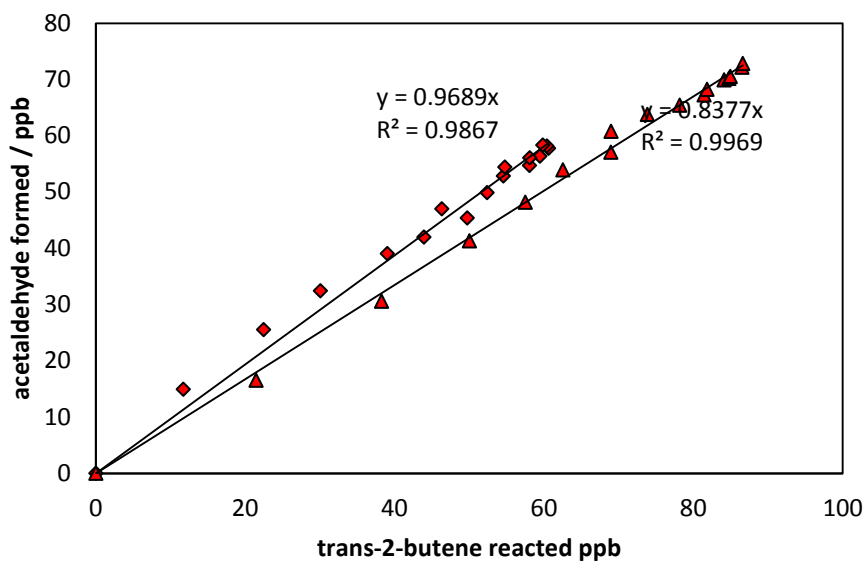


Figure 38. A comparison of yields of acetaldehyde from both FTIR (triangles) and CIR-TOF-MS (diamonds) during a CO scavenged experiment of trans-2-butene + O₃ on 15/05/08. The results show good intercomparison between both instruments.

The major product acetaldehyde was observed in high yields with an average of 0.76 for dry conditions, with an increase again observed for wet conditions averaging 1.03. Compared with past work, these results are consistent (see Table 11). Under cyclohexane scavenged conditions, yields of 0.71 ± 0.03 (Grosjean et al., 1994), 1.150 ± 0.104 (Grosjean et al., 1996) and 1.09 ± 0.09 (Tuazon et al., 1997) were recorded, and unscavenged conditions reported yields of 0.758 (Niki et al., 1977), and 0.899 (Horie and Moortgat 1989). The obtained yields also compare well to previous work with regards to HCHO as previous yields of 0.049 ± 0.016 , 0.126 ± 0.19 , 0.168 ± 0.015 , 0.107, 0.144 were obtained from the aforementioned authors (Table 12). Other oxidation products were not extensively studied, where methanol was only examined under a few experiments, yields ranging from 0.069 to 0.107 (Tuazon et al., 1997 and Horie et al., 1989) accompanied with low yields of 0.05 (Niki et al., 1977) and 0.025 (Horie et al., 1989) for HCOOH, and 0.096 (Grosjean et al., 1994), 0.004 (Horie et al., 1989) for CH₃OOH. Our experiments show consistently low yields of HCOOH with the increase of yield with humidity, which was also shown for the other compounds, including acetic acid.

Table 10. Observed m/z ion channels during trans-2-butene experiments

Compound	Identification / Yield
Signals Detected from CIR-TOF-MS	
<i>Trans-2-butene + O₃ + CHEX (06/05/08, am)</i>	
57, 41	
99, 61, 47, 45, 43, 33, 31	61 – Acetic acid / bdl 47 – Formic acid / bdl 45 – acetaldehyde / 0.63 ± 0.03 ^b 33 – methanol / 0.07 ± 0.01 ^b 31 – HCHO / 0.13 ± 0.02 ^d
<i>Trans-2-butene + O₃ + CHEX (H₂O) (06/05/08, pm)</i>	
57, 41	
99, 61, 47, 45, 43, 33, 31	61 – Acetic acid / 0.22 ± 0.05 ^b 47 – formic acid / 0.02 ± 0.01 ^b 45 – acetaldehyde / 1.03 ± 0.10 ^b 33 – methanol / 0.17 ± 0.02 ^b 31 – HCHO / 0.26 ± 0.07 ^b
<i>Trans-2-butene + O₃ + CO (15/05/08, am)</i>	
57, 41	
61, 46, 45, 43, 33, 31	61 – Acetic acid / 0.02 ± 0.01 ^c 47 – formic acid / bdl 45 – acetaldehyde / 0.90 ± 0.02 ^d 33 – methanol / 0.06 ± 0.01 ^b 31 – HCHO / 0.16 ± 0.01 ^a
<i>Trans-2-butene + O₃ + CO (H₂O) (15/05/08, pm)</i>	
57, 41	
61, 46, 45, 43, 33, 31	61 – Acetic acid / 0.11 ± 0.01 ^b 47 – formic acid / 0.08 ± 0.01 ^a 45 – acetaldehyde 1.02 ± 0.05 ^d 33 – methanol / 0.14 ± 0.01 ^b 31 – HCHO / 0.12 ± 0.01 ^a

BOLD = MH⁺ parent ion and related fragments

Measurements taken by FTIR^a; CIR-TOF-MS^b; HCHO monitor^c; FTIR + CIR-TOF-MS^d
(H₂O) represents wet experimental conditions, RH > 50%

Table 11. Acetaldehyde yields from trans-2-butene ozonolysis under various conditions compared to past literature data

Conditions	Yield (this study)	Past studies	
O ₃	-	0.758 0.889	Niki et al 1977 Horie and Moortgat 1989
O ₃ + CO	0.90 ± 0.02		
O ₃ + CO (H ₂ O)	1.02 ± 0.01		
O ₃ + CHEX	0.63 ± 0.03	0.71 ± 0.03 1.09 ± 0.09	Grosjean et al 1994 Tuazon et al 1997
O ₃ + CHEX (H ₂ O)	1.03 ± 0.10	1.150 ± 0.104	Grosjean et al 1996

(H₂O) is representative of conditions involving RH at levels greater than 50%

Table 12. HCHO yields from trans-2-butene ozonolysis under various conditions compared to past literature data

Conditions	Yield (this study)	Past studies	
O ₃	-	0,107 0.144	Niki et al 1977 Horie and Moorgat 1989
O ₃ + CO	0.13 ± 0.02		
O ₃ + CO (H ₂ O)	0.26 ± 0.07		
O ₃ + CHEX	0.16 ± 0.01	0.049 ± 0.016 0.168 ± 0.015	Grosjean et al 1994 Tuazon et al 1997
O ₃ + CHEX (H ₂ O)	0.12 ± 0.01	0.126 ± 0.019	Grosjean et al 1996

(H₂O) is representative of conditions involving RH at levels greater than 50%

3.3.2 MCM model comparison of trans-2-butene

Figure 39 shows a comparison for the measurements and MCM based-model for CO scavenged experiments under dry conditions. As previously stated, the MCM model agrees well for the degradation of the precursor VOC and scavenger, with an apparent overestimation in ozone as previously observed in the ozone-isobutene model. Unlike the isobutene model however, the two major oxidation products of CH₃CHO and

HCHO show very good matches with the experimentally determined data. This can therefore promote the idea the differing branching ratios needed for the isobutene experiments as both ethene and trans-2-butene experiments have shown good correlation to the MCM model.

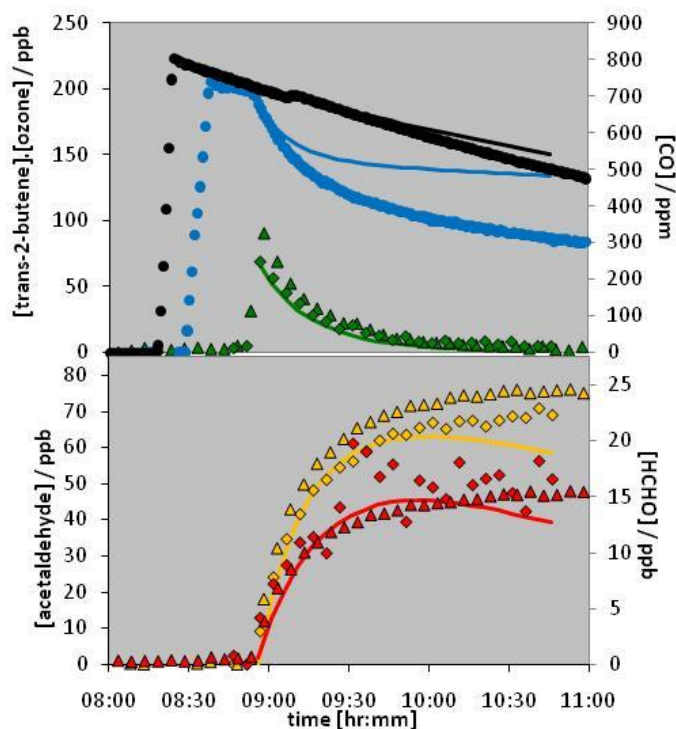


Figure 39. MCM model comparison of the initial reagent conditions, trans-2-butene (green), CO (black) and ozone (blue) above, with a comparison of the two dominant oxidation species formaldehyde (red) and acetaldehyde (gold) below. The model output reflect the experimentally data observed for the exception of ozone decay which it under predicted in the model. Data has been dilution corrected.

3.4 Isoprene oxidation

Isoprene has been extensively studied owing to its role as the premier biogenic volatile organic compound (BVOC), given that the total annual emissions of global VOCs are estimated to be 1150 Tg C (Guenther et al., 1995) with isoprene estimated to comprise between

43% and 48% of this total (Wang 2000; Guenther., 2006; Arneth., 2008), making isoprene one of the most dominant non-methane hydrocarbons in the troposphere (Malkin et al., 2010). Owing to its relatively short atmospheric lifetime during the day, i.e. a lifetime of 1.4 hours corresponding to reactions with OH and a lifetime of 1.3 days with reactions with O₃ (Atkinson., 2003), very little isoprene is transported out of the boundary layer, and therefore its atmospheric chemistry predominantly occurs within the troposphere. Isoprene is a highly volatile C₅ hemiterpene which is emitted in large quantities from the biosphere and concentrations between 1-30 ppb have been reported over forests producing isoprene (Martin., 1991; Kesselmeier., 2002). Although Isoprene has been believed to be of little relevance to aerosol formation (Kamens., 1982), due to the large emission quantity even small yields could have a significant impact on climate and local air quality (Carlton., 2009). The question of isoprene and its potential links to SOA is still one that remains in debate today. There have been contradictory conclusions as to the extent of SOA formation directly from oxidation of isoprene in the atmosphere. Past work has presented arguments for both sides of this conflicted view. Pandis et al (1991) and Kanakidou (2005) conclude that isoprene is not a significant source of secondary aerosol following the photooxidation of the VOC on levels of a few ppb, whilst Kiendler-Scharr et al (2009) go as far as to advise that isoprene can in fact inhibit new particle growth in forest environments, this suppression becoming stronger with higher concentration levels of isoprene. Other work done by Jang et al 2002 and Czoschke et al 2003 conclude that in the presence of acidic seeds the detection of highly volatile isoprene oxidation products in particulate samples (usually expected to remain in the gas phase) can lead to SOA formation. Limbeck et al 2003 found similar results with heterogeneous reactions of isoprene on acid filters but found it difficult to show the importance with regards to SOA formation from isoprene under atmospheric conditions. More recent work regarding isoprene potential for SOA formation lays within its oxidation products, in particular the 2-methyltetrol compounds which have been postulated to contribute to SOA formation under different atmospheric conditions. Ion et al 2005 and Claeys et al (2004) displayed insignificant direct SOA formation from isoprene but highlight the potential from these 2-methyltetrols within a forest environment, whilst Schkolnik et

al (2005) show the presence of these methyl tetrols in biomass burning smoke. Other studies confirm the detection these humic like substances from isoprene oxidation and provide evidence for their involvement in SOA formation (Böge et al 2006, Matsunaga et al 2003). Other studies conducted into the oxidation products of isoprene and their potential for SOA formation include Carlton et al (2006) in which the aqueous phase reactions of water-soluble organics (glyoxal, methylglyoxal and glycolaldehyde) form SOA through the production of carboxylic acids (glyoxylic, glycolic and oxalic acids). In cloud production of oxalic acid from gas-phase precursors have also been identified by Warneck et al (2003) and predictions of cloud processing of water soluble isoprene oxidation products have also been presented that could lead to the formation of low-volatility SOA components (Ervens et al 2004, Lim et al 2005). As such previous work done on isoprene has been extensive under a number of differing environmental conditions, but as to the full extent of isoprene contribution to SOA remains elusive.

The removal of isoprene from the troposphere has been widely attributed to the reaction of the OH radical due to its diurnal cycle, and the importance in the inclusion of isoprene to global models has been illustrated (Henze., 2006). Here we study the oxidation of isoprene under “dark” ozone reactions with and without the presence of scavengers and under “day” conditions with high NO_x levels (nominal ratio VOC:NO_x 2:1) and the presence of a seed. The seeds used were composed of ammonium sulphate and a unique organic seed which was formed from β-caryophyllene photooxidation (see Chapter 5). SOA formation of the isoprene oxidation system in simulation chambers is very much dependent on the chosen experimental conditions. (Ng., 2007) describe the dependence of NO_x concentrations to aerosol yields during photooxidation experiments of terpenes, whilst (Kleindienst., 2007) highlighting the importance of an OH scavenger during ozonolysis reactions, where the OH channel accounted for up to 50% of aerosol formation.

Compared to the previous alkenes, isoprene has two double bonds, making it more reactive as well as having an additional place for ozone addition. A simplified mechanism of isoprene ozonolysis is given in Figure 40. Owing to the diene bonds, isoprene is very reactive

and ozone can either attack the 1,2 carbon double bond, or the 3,4 carbon double bond producing the Cl_1 and Cl_2 Criegee intermediates respectively.

The two major oxidation products of methacrolein (MACR) and methyl-vinyl ketone (MVK) are formed from the stabilisation of the Criegee intermediates through the reaction pathway of CO and H₂O, similar to those expressed previously and so the mechanism has been simplified here. MACR being of importance as this was proposed to contribute to SOA formation compared to MVK (Kroll et al. 2005, 2006). A by-product of Criegee radical formation is HCHO and it can be assumed that based on these mechanistic pathways, the three dominant isoprene oxidation products will consist of HCHO, MACR and MVK.

Under “wet” conditions, methacrylic acid would be expected, however the stabilised product S_1 could also give this signal under “dry” conditions. Due to complications within that m/z channel, as no signal was monitored in m/z 87 throughout any experiments, analysis on the preferred reaction pathway could not be conducted, taking into account any increase in that m/z ion channel under wet conditions that would otherwise be present could not be observed during the experimental runs. The MCD plate detected all other channels, for the exception of m/z 87, the reason for this unclear, it may have been due age of the plate.

The mechanism of OH addition to isoprene is given in Figure 41. Initial OH addition can occur at four different sites, producing four possible hydroxy radicals (Paulson 1992; Carter 1996). Addition to the 2, 3 carbons forms alkyl radicals of which the hydroxy alkyl peroxy radicals can only be formed from O₂ addition to central β carbons to the OH group. OH addition to the terminal carbons leads to the formation of hydroxalkyl peroxy radicals, in this case allowing O₂ addition to either the β or δ carbon centres to the OH group. With NO concentrations greater than 30 ppt (Herrmann 2010) and under polluted conditions (high NO_x conditions) these peroxy radicals (RO₂) can react to form a variety of organic species alongside a potential source of HO₂, NO₂ and ozone in the atmosphere.

Table 13: Initial measured experimental conditions of isoprene ozonolysis during TRAPOZ

Exp Date	VOC	Type	Initial Mixing ratios				RH /% ^b	Duration / min	Temp/ K ^b
			[VOC] _o / ppb ^c	[Ozone] _o / ppb ^a	[CO] _o / ppm	[Cyclohexane] _o / ppm			
29/04/08 (am)	Isoprene	1	174.8	220.8			0.3	130	291.1
29/04/08 (pm)	Isoprene	2	95.6	212.8	1227.4		0.5	110	292.9
05/05/08 (am)	Isoprene	3	248.8	317.8		97	0.4	135	293.1
05/05/08 (pm)	Isoprene	3,4	226.4	281.6		99.6	20.0	120	294.2

1, Straight Ozone/alkene, 2 with added CO, 3 with added cyclohexane, 4 with added H₂O, a measurements based on the ozone analyser, b values given as an average values measured over the duration of the experiment, c based on CIR-TOF-MS measurement

Table 14: Initial measured experimental conditions of isoprene photooxidation during ACES 2

Exp Date / Campaign	VOC	Type	Initial Mixing ratios			Water / % RH	Duration / min
			[VOC] _o / ppbV	[NOx] _o / ppbV	[VOC/NOx] _o / ppbV		
30/06/08	β-caryophyllene	b	33.0	26.0	1.3	70	420
	Isoprene		79.5	14.4	5.5		
03/07/08	β-caryophyllene	b	39.5	54.6	0.7	72	426
	Isoprene		106.0	54.2	2.0		
04/07/08	β-caryophyllene	b	48.4	48.1	1.0	72	423
	Isoprene		297.1	240.7	1.2		
07/07/08	Isoprene	c	172.1	36.8	4.7	67	240

b = β-caryophyllene seed experiment ; c = sulphate (SO₄²⁻) seed experiment

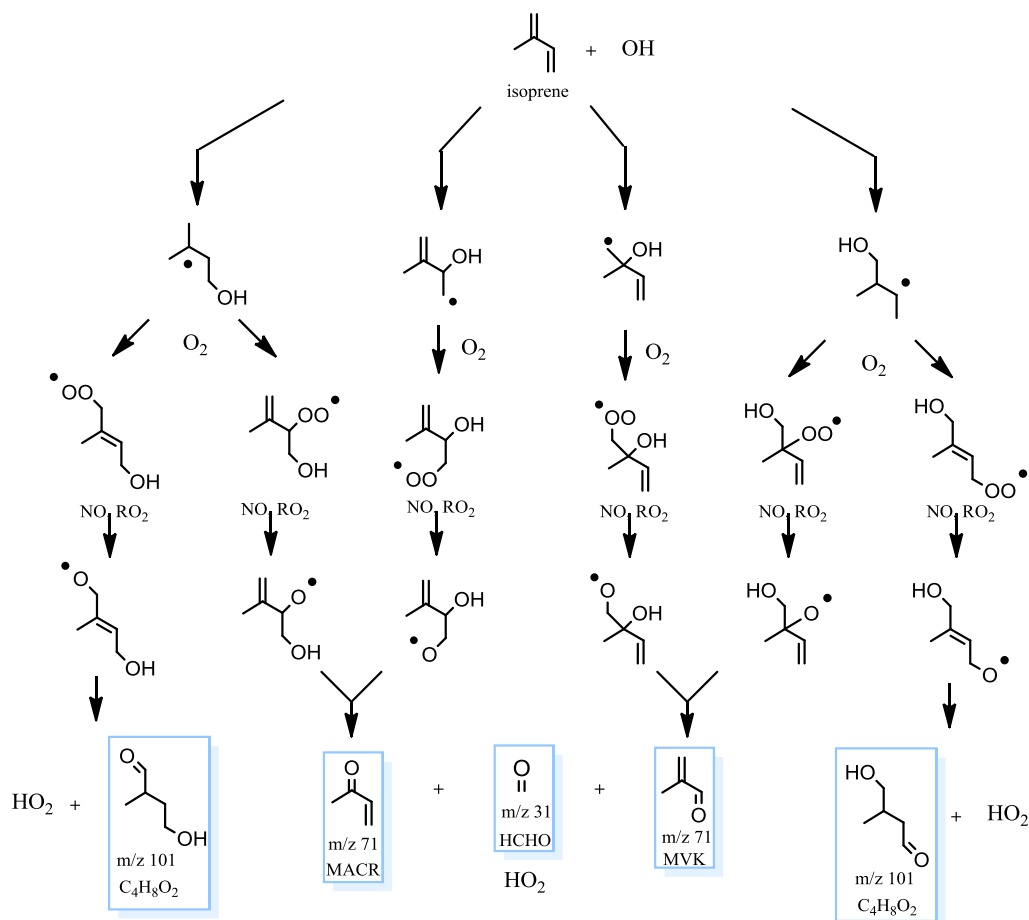


Figure 41. A simplified reaction mechanism of OH addition to isoprene showing the formation of primary stable organic species adapted from the MCM mechanism

Table 13 shows the initial conditions for isoprene ozonolysis experiments and Table 14 gives photooxidation experimental conditions. Figure 42 shows the gas composition comparison between of the initial conditions and the later (2 hours) reacted system of the isoprene + O_3 experiment to simplify the identification of reagent signals compared to product signals. The reacted isoprene signals (m/z 69 and 41) are replaced by stable oxidised species most notably at m/z 71, 59, 47 and 31.

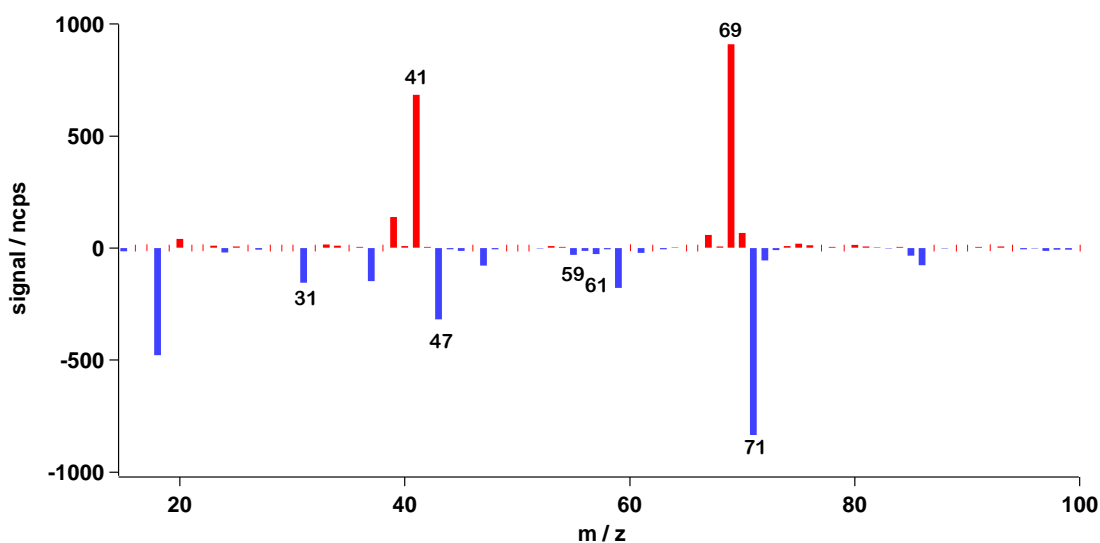


Figure 42. A subtraction of the gas-phase composition from initial conditions (red) from a time 2 hours after reaction start to highlight the differences in gas-phase composition and oxidation products.

Figure 43 shows the temporal profile of the “straight” isoprene-ozone reaction. Following almost immediate isoprene injection, the formation of the three primary gas phase oxidation products of methacrolein (MACR), methyl vinyl ketone (MVK) and formaldehyde (HCHO) are evident. A total of 82 ppb of isoprene is reacted over a time frame of 140 min, with maximum values of the oxidation products observed at the end of the experiment with values of 17 ppb, 10 ppb and 24 ppb respectively. Under photooxidation reactions, isoprene degradation is seen to increase as a total of 100 ppb was reacted over the course of a 180 minute experiment. These products have been established to be the primary oxidation products of isoprene oxidation over varied experimental conditions under both photooxidation and ozonolysis experiments. Further product formation of a previously identified acid, methacrylic acid (Claeys et al., 2004) could not be confirmed within the experiment as problems within m/z channel 87 on the MCP were present throughout the experiment. To note, a slight discrepancy is apparent for the measurement of isoprene between the FTIR and CIR-ToF-MS. To evaluate the accuracy of either instrument, comparisons were made to calculated theoretical concentrations of injection displayed in Figure 44. From these results, the CIR-ToF-MS gives the better accuracy, and accordingly isoprene

degradation data used for calculations were conducted using the data received from the CIR-ToF-MS.

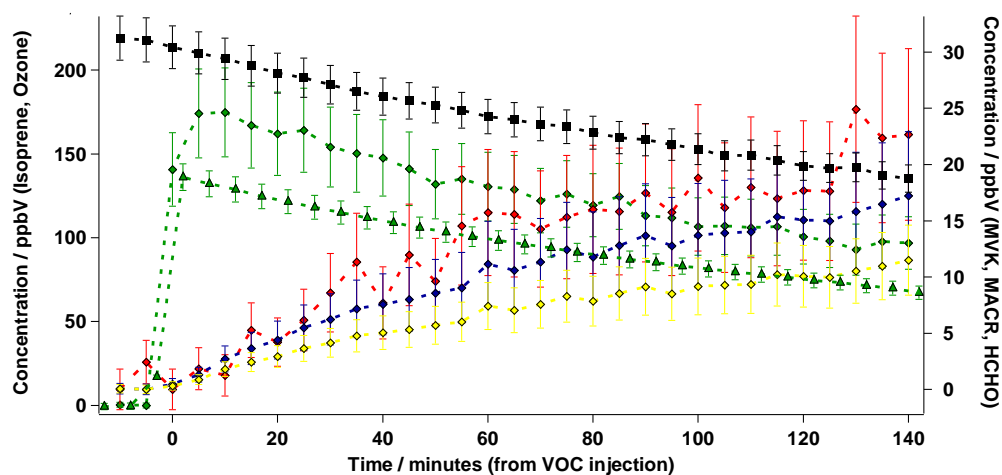


Figure 43. Temporal profiles from Exp 1 (Straight Isoprene + Ozone system). The data has been taken from 10 minutes before injection of the precursor to the time when flushing commences. A steady loss of O_3 (black) is observed during the experiment. The injection of Isoprene (TOF green diamonds, FTIR green triangles) is observed along with the reaction degradation, followed by the formation of the three most dominant gas-phase oxidation products, HCHO (red), MACR (blue) and MVK (yellow) from the CIR-TOF-MS data.

As there is no evidence of isoprene contribution towards aerosol formation via the nucleation route, seeded experiments were conducted. These included experiments with both inorganic and organic seeds.

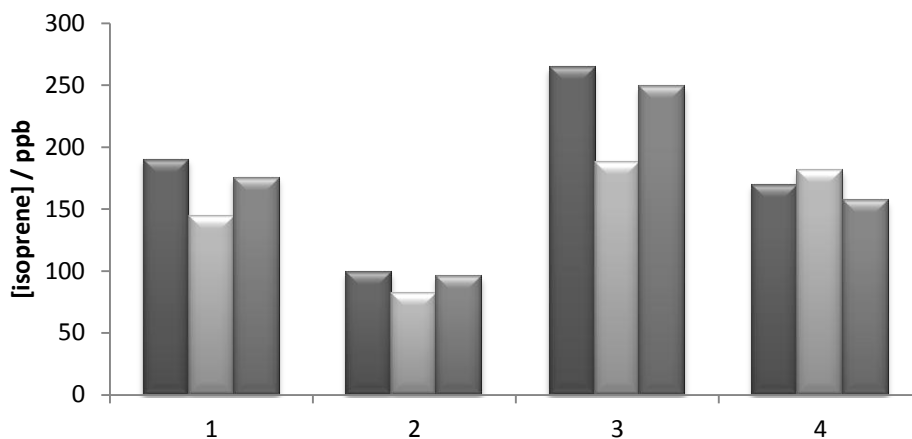


Figure 44. Injection analysis of isoprene for EUPHORE chamber experiments. The CIR-ToF-MS measurements (grey) are very realistic, in all circumstances just below the potential calculated concentration (dark grey). The FTIR reading (light grey) underestimates this value by a greater fraction and so the isoprene data is more reliable with the CIR-ToF-MS data.

3.4.1 Yields of stable organic products from isoprene

An overview of the detected m/z channels for all isoprene experiments is given in Table 15 and 16 along with the gas-phase yields of the identified products. The yields are lower than that obtained from previous studies. The low yields could be attributed to the low-concentration “atmospheric” conditions in which the experiment was run (of a few hundred ppb), whereas past work was conducted in the ppm range of either the precursor or ozone. An increase in yield under humid conditions is also observed in our experiments which follows the observations made by Sauer et al., (1999). The observation of higher yields of methacrolein suggests that the preferred reaction pathway proceeds via the Cl_2 Criegee intermediate, and decomposition of this Criegee intermediate to form the peroxyradical PR_2 is not favoured over the radical PR_1 as signals for the stabilised species S_1 to S_3 were not observed compared to those of formic acid and formaldehyde that form through $\text{CO}/\text{H}_2\text{O}$ reactions of the PR_1 radical species. The “organics” in the reaction mechanism represented include species such as acetaldehyde and methanol. Ultimately it is the site of this addition of ozone that will determine the subsequent products formed and the chemical degradation pathways

undertaken in the isoprene system, and from observed results, this addition is preferred at the 3,4 carbon double bond. Two dominant species MVK and MACR give fractional yields ranging from 0.131 - 0.172 and 0.248 – 0.356 respectively, thereby accounting for approximately 45% of the oxidation products from isoprene oxidation, with HCHO accounting for a further 36%. Previous studies of the two major products of MVK and MACR show divergent results over a number of different studies, although the ratio of MACR to MVK approximating 2:1 is shared with some of these studies shown in table 17. Some results correspond to our observations where higher levels of MACR than MVK present, roughly on yield scales of 30% and 15% respectively.

Table 15. Observed m/z ion channels during isoprene photooxidation experiments

Compound	Identification / fractional yield
Signals Detected from CIR-TOF-MS	
<i>Isoprene (OH) (30/06/08)</i>	
69, 67, 42, 41, 39	Isoprene and fragmentation
87 ^b , 86 ^c , 85 ^d , 73, 71, 61, 59, 57 ^d , 55 ^e , 47, 45,	31 - Formaldehyde 0.37 ± 0.03 ^f
43 ^{a(MVK)} , 37 ^e , 33, 31	33 - Methanol 0.01 ± 0.01 ^f
	45 - Acetaldehyde 0.01 ± 0.01 ^f
	47 - Formic Acid 0.06 ± 0.01 ^f
	59 - Acetone 0.02 ± 0.01 ^f
	61 - Acetic Acid 0.01 ± 0.01 ^f
	71 - MACR 0.30 ± 0.02 ^f
	71 - MVK 0.16 ± 0.01 ^f

MVK is Methyl Vinyl Ketone, MACR is Methacrolein

BOLD = parent compound (MH⁺) and fragments, a = fragment of identified oxidation product

b = Previously identified mass channel, due to technical difficulties these mass channels were not observed

c = isotope (+1 m/z), d = unidentified mass channel

e = water cluster detection (structure can be H₃O⁺.H₂O and further additions of water)

F = CIR-TOF-MS, G = FTIR, h = ToF + FTIR average

Table 16. Observed m/z ion channels during isoprene ozonolysis experiments

Compound	Identification / concentration	
Signals Detected from CIR-TOF-MS		
<i>Isoprene + O₃ (29/04/08, am)</i>		
69, 67, 42, 41, 39	Isoprene and fragmentation	
87 ^b , 86 ^c , 85 ^d , 73, 71, 61, 59, 57 ^d , 55 ^e , 47,	31 - Formaldehyde	0.369 ± 0.034 ^f
45, 43 ^{a(MVK)} , 37 ^e , 33, 31	33 – Methanol	0.014 ± 0.004 ^f
	45 – Acetaldehyde	0.014 ± 0.003 ^f
	47 - Formic Acid	0.058 ± 0.009 ^f
	59 – Acetone	0.022 ± 0.004 ^f
	61 - Acetic Acid	0.014 ± 0.004 ^f
	71 – MACR	0.298 ± 0.015 ^f
	71 – MVK	0.160 ± 0.007 ^f
<i>Isoprene + O₃ + CO (29/04/08, pm)</i>		
69, 67, 42, 41, 39	Isoprene and fragmentation	
87 ^b , 86 ^c , 71, 47, 45, 43 ^{a(MVK)} , 31	31 - Formaldehyde	0.421 ± 0.028 ^h
	45 – acetaldehyde	0.019 ± 0.002 ^f
	47 - Formic Acid	0.012 ± 0.001 ^f
	71 – MACR	0.248 ± 0.015 ^f
	71 – MVK	0.131 ± 0.008 ^f
<i>Isoprene + O₃ + CHEX (05/05/08, am)</i>		
69, 67, 41, 39	Isoprene and fragmentation	
99, 87 ^b , 86 ^c , 81 ^d , 73, 72, 71, 47, 45, 43 ^{a(MVK)}	31 - Formaldehyde	0.298 ± 0.022 ^f
37 ^e , 33, 31	33 – Methanol	0.021 ± 0.002 ^f
	45 – Acetaldehyde	0.019 ± 0.002 ^f
	47 - Formic Acid	0.111 ± 0.011 ^g
	71 – MVK	0.167 ± 0.009 ^f
	71 – MACR	0.316 ± 0.017 ^f
<i>Isoprene + O₃ + CHEX (H₂O) (05/05/08, pm)</i>		
70, 69, 67, 41, 39	Isoprene and fragmentation	
99, 87 ^b , 86 ^c , 81 ^d , 72, 71, 57 ^e , 55 ^e , 47,	47 - Formic Acid	0.150 ± 0.020 ^h
43 ^{a(MVK)} , 41, 37 ^e	71 – MVK	0.172 ± 0.019 ^f
	71 – MACR	0.356 ± 0.040 ^f

MVK is Methyl Vinyl Ketone, MACR is Methacrolein

BOLD = parent compound detection/with fragments, a = fragment of identified oxidation product

b = Previously identified mass channel, due to technical difficulties these mass channels were not observed

c = isotope (+1 m/z), d = unidentified mass channel

e = water cluster detection (structure can be H₃O⁺.H₂O and further additions of water)

F = CIR-TOF-MS, G = FTIR, h = ToF + FTIR average

(H₂O) represents wet experimental conditions, RH > 50%

Table 17. MVK and MACR minimum yields from isoprene oxidation (photooxidation and ozonolysis) under various conditions compared to past literature data.

Compound	This study	Yield of Past Studies	
MACR	0.298 ± 0.015 ^a	0.339 ± 0.026 ^a	Aschmann et al 1994
	0.248 ± 0.015 ^b	0.159 ± 0.387 ^c	Aschmann et al 1994
	0.316 ± 0.017 ^c	0.41 ^a	Kamens et al 1982
	0.298 ± 0.015 ^d	>0.33 ^a	Niki et al 1983
		0.44 ^c	Grosjean et al 1993
		0.37 ^a	Paulson et al 1992
		0.67 ± 0.09 ^c	Paulson et al 1992
		0.21 ^d	Tuazon et al 1990
		0.19 ^f	Peters et al 2010
		0.27 ^d	Karl et al 2006
		0.20 ^d	Ruppert et al 2000
		0.181 ^e	Ruppert et al 2000
		<0.10 ^g	Karl et al 2009
		0.200-0.239 ^d	Gu et al 1985
	0.21 ± 0.05 ^d	Tuazon et al 2004	
0.23 ^d	Kwok et al 1995		
MVK	0.160 ± 0.007 ^a	0.191 ± 0.015 ^a	Aschmann et al 1994
	0.131 ± 0.008 ^b	0.159 ± 0.013 ^c	Aschmann et al 1994
	0.167 ± 0.009 ^c	0.18 ^a	Kamens et al 1982
	0.160 ± 0.007 ^d	>0.13 ^a	Niki et al 1983
		0.17 ^c	Grosjean et al 1993
		0.17 ^a	Paulson et al 1992
		0.26 ± 0.06 ^c	Paulson et al 1992
		0.29 ^d	Tuazon et al 1990
		0.36 ^f	Peters et al 2010
		0.41 ^d	Karl et al 2006
		0.31 ^d	Ruppert et al 2000
		0.152 ^e	Ruppert et al 2000
		<0.10 ^g	Karl et al 2009
		0.136-0.224 ^d	Gu et al 1985
	0.29 ± 0.07 ^d	Tuazon et al 2004	
0.32 ^d	Kwok et al 1995		

a = yield value for O₃ reaction with no scavenger, b = yield value for O₃ reaction with CO scavenger, c = minimum yield value for O₃ reaction with CHEX scavenger, d = yield value for OH-initiated reaction in the presence of NO_x, e = yield value for OH-initiated reaction in NO_x free environment, f = yield from chemistry model predictions, g = observed yield from the Amazon

3.4.2 MCM model comparison of isoprene

The MCM model comparison of isoprene ozonolysis experiments are presented in Figure 45. From these experiments, it seems that the MCM model predictions approximate oxidation formation favourably. The degradation of isoprene and ozone are well presented, from which the traces of the three major oxidation products are also well represented. HCHO may slightly be over predicted in the model, but the MVK and MACR traces correspond well. The current branching ratios of ozone addition to isoprene are therefore accurately represented in the MCM model and so future comparisons with differing experimental conditions should be made to evaluate any differences or dependencies of governing reagents for the formation of carbonyl compounds.

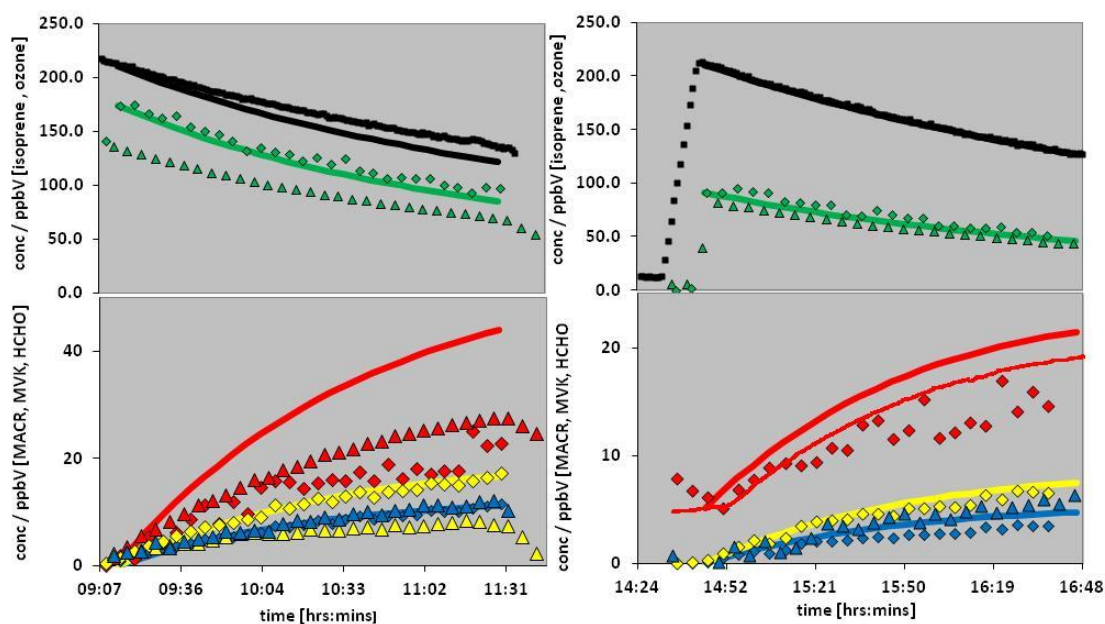


Figure 45. The MCM model comparison to observed data with the initial reactants (top) of isoprene (green) and ozone (black) with the formation of the major products (bottom) of MACR (yellow), MVK (blue) and HCHO (red). Experiments of isoprene ozonolysis experiments from a “straight” ozone reaction (left) and a CO scavenged (right) are compared with CIR-ToF-MS data (diamonds) with FTIR data (diamonds), ozone monitor data (squares) to given model outputs (solid lines).

3.4.3 Carbon balance measurements of isoprene ozonolysis

The organic carbon for ozonolysis during the experiments showed a total of 44% of the carbon involved in the reaction ($208.34 \mu\text{g m}^{-3}$). On average, 34 % of the total carbon consumed in the reaction of isoprene is accounted for by HCHO, MVK and MACR (total of $73.93 \mu\text{g m}^{-3}$). In the case of a photooxidation experiment, a larger mass of isoprene reacted with a time scale of 300 min in which a total of 96% of carbon degraded ($846.89 \mu\text{g m}^{-3}$) with the isoprene trace. The three major products however only account for a total of 26% ($216.61 \mu\text{g m}^{-3}$) of this carbon balance. Figure 46 displays a comparison of the organic carbon total observed throughout a “straight” ozonolysis experiment and a photooxidation “seeded” experiment, with minimal influence on the carbon balance from the other detected products discussed previously. The poor mass balance has been previously reported by other studies, Kwok et al (1995) approximate that 40% of the carbon from isoprene OH-initiated driven reactions has not been identified or quantified. Observed results show that OH-initiated chemistry is dominant over O_3 -initiated for the removal process of isoprene in the atmosphere, which can be reflected by its strong diurnal emission, with NO_3 reactions becoming more dominant at night (Park 2004). In essence this means that isoprene levels follow the pattern of OH concentrations. For example, if OH concentrations are highest at midday, lower isoprene concentrations are observed as it is reacting with the OH. As OH levels drop, approaching night or dark periods, the isoprene levels begin to rise again. This forms the strong argument that OH is the dominant radical that is involved with isoprene reactions in the atmosphere. Past studies however have reported this value to be between 60 and 97% (Arey 1990; Paulson 1992; Kwok 1995; Sprengnether 2002; Zhao 2004) with the remaining carbon accounted for in other products constituting of peroxides, C_5 -diols and C_5 -carbonyls. (Jenkin 1998). Other work done on isoprene oxidation products include products such as glyoxal, methylglyoxal and glycolaldehyde formed through carboxylic acids (Carlton et al 2006), and dicarboxylic acids. Model predictions done by Lim et al (2005) show that oxidised isoprene can lead to the formation of these compounds in the gas phase. The nature of these compounds makes it difficult for the CIR-ToF-MS to detect this scope of products.

Methylglyoxal has been previously hinted at being detected but under the conditions set for optimal detection of the major oxidation products along with the parent VOC can hinder the detection of these other compounds. This can further explain the low accountability for the carbon balance of the gas-phase products from isoprene oxidation. Calibration runs with same set-up used as per experiment was run for calibrations of compounds such as methylglyoxal and dicarboxylic acid structures. The results show that detection of these compounds would have been difficult within the concentration range expected from the oxidation of a few 100 ppb of isoprene. These compounds may have not also been observed in these experiments due to loss of sample to chamber walls. However, with the knowledge of low sensitivity towards certain compounds can provide a theoretical approach as to what compounds make up some of the remaining “missing” carbon, especially if coupled to work done in other isoprene studies, most predictably glyoxal, methylglyoxal and other water-soluble organics. The isoprene experiments do however still show lower accountability for the carbon balance, this could however be a reflection of time restraints if considering the total amount of mass reacted with a continued degradation still visible alongside the continued formation of these oxidation products during the ozonolysis experiment. However previous work displays similar results for carbon balance, e.g. approximately 30% of carbon is accounted by MVK, MACR, 3MF (3-methylfuran) and HCHO based upon a study conducted by Lee et al (2005). In both cases, MACR accounts for most of the carbon, an important oxidation product as Kroll et al (2005) conclude that it is MACR and not MVK that contributes towards SOA formation.

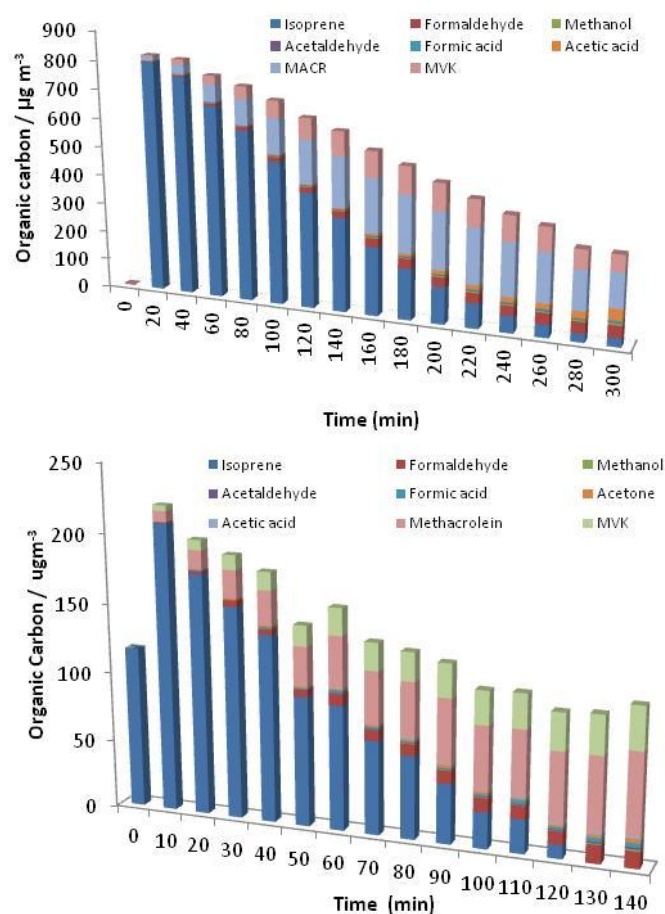


Figure 46. Time profiles for the carbon balance accounted for in the gas-phase of chamber experiments comparable to ozonolysis and photooxidation experiments performed at EUPHORE and MAC respectively.

3.4.4 SOA formation from isoprene

The ozonolysis experiments indicated no growth in either mass or number concentration of particles. It can therefore be concluded that under a variety of “dark” conditions with ozone (e.g. presence of OH scavenger), although expected oxidation products are formed, there is little evidence to show any aerosol formation or growth. These conclusions could be formed during the photooxidation experiments as similar

results were seen, Figure 47 shows the conditions seen in a seeded experiment from photooxidation experiments. For completeness, the formation of the two oxidation products, MVK and MACR have been included. Important to note is the ozone trace, indicating that isoprene is a source of O₃ in the troposphere. Figure 47 shows SOA mass growing following photooxidation of β -caryophyllene. A short dilution period (red dashes) is used to decrease the SOA mass in order to obtain an organic seed at realistic concentrations to stimulate potential SOA growth from isoprene oxidation. This increase in mass growth, or any detectable amounts of SOA mass is not observed following the photooxidation of isoprene, thereby concluding that isoprene does not contribute significantly towards SOA formation under the experimental conditions here described.

The primary oxidation products observed from isoprene were thought to be too volatile to partition into the aerosol phase (Kroll et al., 2006). However evidence from aerosol composition studies have identified compounds with the same carbon skeleton structure as isoprene and one of its primary oxidation products methacrolein: 2-methyltetrol compounds and methylglyceric acid respectively (Edney et al., 2005; Surratt et al., 2006). Even small aerosol yields were established in low NO_x and high NO_x environments (Kroll 2005; Kroll et al., 2006) of 1% and 3%. Henze (2006) discuss the partitioning of semi volatile organic compounds from isoprene oxidation with respect to relevance to higher altitudes, whilst Ng et al (2006) show that aerosol growth continues after the precursor has been consumed, hinting towards either a delayed mass transfer in the partitioning of the gas phase, or a contribution of the secondary oxidation products. This highlights not only the importance of the oxidation of isoprene, but also that of some of the first generation oxidation products potentially contribution towards SOA formation. Isoprene can also undergo homogeneous nucleation to form small particles. These however have been shown not to grow (Kamens et al., 1982) to substantial sizes, but the resulting oxidation products could condense onto pre-existing particles in the natural environment.

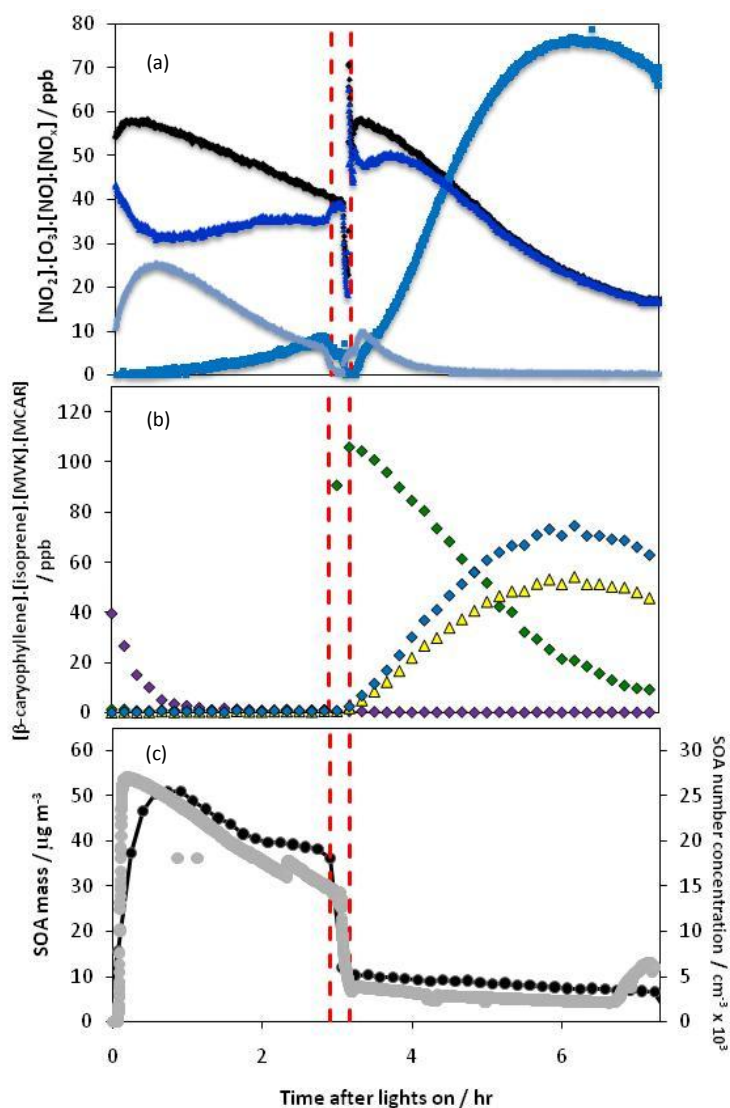


Figure 47. An isoprene (in green) photooxidation experiment conducted in the presence of an organic seed produced from β -caryophyllene (purple) photooxidation. The initial stage (left of the red dashed lines) refers to the oxidation of β -caryophyllene to form the organic seed used for the oxidation of isoprene (right of the red dashed lines). The red dashed lines represent the gap for preparation of the chamber between each experiment. The gas conditions of the chamber are given in Figure 47(a) that include O_3 (blue), NO (light blue), NO_2 (dark blue) and NO_x (black). The VOCs time profiles, β -caryophyllene (purple diamonds) and isoprene (green diamonds) are given with the evolution of the primary oxidation products of MACR (blue diamonds) and MVK (yellow diamonds) in graph 47(b). SOA data is given in graph 47(c) that shows an increase in both SOA mass (black) and SOA number concentration (grey) from the photooxidation of β -caryophyllene, but little is observed from isoprene photooxidation following dilution of the chamber (dashed red lines).

Despite the large global emissions of isoprene, the largest sources of SOA mass are still believed to be due to monoterpenes. Sesquiterpenes and monoterpenes are discussed in the following Chapters. During the seeded experiments, no particle growth was observed from isoprene oxidation. Thus, the chamber work has concluded that over a short time scale, no growth on pre-existing aerosols is apparent, and so must be concluded that the primary oxidation products observed in the chamber studies are too volatile to partition into the aerosol phase with or without the presence of seeds and under differing experimental conditions of ozonolysis and photooxidation, reflecting atmospheric conditions in the troposphere.

3.5 Discussion

The CIR-ToF-MS utilised in the detection of a variety of oxidation products from small alkenes ($< C_4$) ozonolysis experiments overall displayed extremely good instrumental intercomparisons with FTIR and HCHO monitors for the exception of isobutene, isoprene and in some cases HCHO but in particular formic acid under wet conditions giving the biggest contrast. This gives an indication of the suitability of CIR-ToF-MS for use in other experiments, and the accuracy of results in experiments in which no other measuring technique of VOCs were available (e.g. the photooxidation experiments at MAC). The potential improvement for detection of certain oVOCs species were also made possible with the use of a new HC ion source recently investigated on the CIR-ToF-MS instrument. The HC source exhibited improved sensitivity for certain compounds, however, the opposite can be seen for other compounds. In this case trans-2-butene and cis-2-butene, resultantly the new HC ion source can be utilised for improved sensitivity for most compounds, but further investigation regarding potential larger VOCs is still required. The detection of lower masses was evaluated under both dry and wet conditions, although displaying a decrease in sensitivity owing to H₂O influences, the concentrations observed were accurate in comparison to other instruments (e.g., the FTIR monitor).

For all the VOCs investigated, the proposed reaction mechanisms and more specifically, the major primary oxidation products predicted were monitored in real time. For the determination of yields of lower mass compounds <61 m/z was established from the parent ion signal as the assumption that most of that signal is due to the low molecular weight compound, e.g. formaldehyde (m/z 31), methanol (m/z 33), acetaldehyde (m/z 45), formic acid (m/z 47), acetone (m/z 59), acetic acid (m/z 61) and methyl-vinyl ketone/methacrolein (m/z 71). These yields mostly stood in good relation with those conducted in previous studies under a variety of differing experimental conditions.

Overall, the current atmospheric understanding of the species investigated in this Chapter is well represented by the MCM model.

Finally our experiments show that isoprene does not contribute towards SOA formation under either ozonolysis or seeded photooxidation conditions. These findings relate to those found by Claeys et al 2004, Pandis 1991 and Edney 2005. These were run under short time frames (< 4 hours), and so cannot ultimately determine whether the oxidation product of methacrolein is involved in partition into particle phase or growth on existing particles over a longer period. Although some of the major oxidation products such as MVK, MACR and HCHO were observed in these concentrations, only 26% of the organic carbon was accounted for from these three oxidation products. As such, it must be concluded that the missing carbon must be retained in species that were difficult to detect with the CIR-ToF-MS, although past studies have indicated a very poor mass balance. Suspected compounds that are difficult to detect under the conditions set with the CIR-ToF-MS and correspond to other products reported include glyoxal, methylglyoxal, glycolaldehyde and dicarboxylic acid compounds that could account for some of this missing carbon mass. Owing to the malfunction of the m/z channel 87, no investigation on the methacrylic acid could be observed in these chamber studies. Although it has been suggested that some carbon skeleton structures similar to those of isoprene oxidation products are involved in SOA formation, these results conclude that isoprene does not contribute to SOA formation.

CHAPTER 4. Photooxidation and ozonolysis of monoterpenes

The following chapter examines the photooxidation and ozonolysis of the monoterpenes limonene, α -pinene, β -pinene, myrcene, linalool and α -terpinene. Monoterpenes have recently undergone investigation as it is believed that emissions are high in tropical rainforests. These monoterpenes also have high global emissions, highest contributors estimated at 23% for limonene and 35% for α -pinene, with myrcene making up 5% and α -terpinene 1% (Griffin et al 1999a). Using specific yield parameters, Griffin et al 1999(a) also estimated yields of SOA from myrcene, limonene, linalool, α -pinene, β -pinene and α -terpinene as 7.6-12.7%, 6.1-22.8%, 1.9-7.3%, 2.4-7.8%, 4.2-13.0% and 3.4-12.7% respectively. The importance of these monoterpene emissions are common among forest environments as these are primarily emitted from tree species. For example, work done by Staut et al (2000) on *pinus pinea* trees showed major compounds emitted as limonene, linalool and β -ocimene, with other minor compounds of monoterpenes observed including α -pinene, myrcene, β -pinene and α -terpinene. Other work conducted around tropical rainforests, in particular above canopy mixing (Rinne et al 2002) showed isoprene as the dominant emitter (reaching about 4 ppb), with α -pinene the most abundant monoterpene, comprising 50% of the total monoterpene emission (120 ppt), with limonene and β -pinene each comprising 15-20% of total emissions. As such, monoterpenes, as dominant emitter species from trees in combination with their potential to contribute to SOA formation makes these interesting compounds to further analyse to help in advancing knowledge as to their impacts around woodland environments. All of these compounds were analysed during photooxidation experiments at the Manchester Aerosol Chamber (MAC), with “dark” ozonolysis experiments conducted at EUPHORE for myrcene, α -pinene and limonene. A contrast in chemical pathways of these two light and dark systems for the aforementioned monoterpene species, and the impact of relative humidity on ozonolysis reactions, will be explored.

4.1 Monoterpenes in the atmosphere

Monoterpenes react in the troposphere with the OH, NO₃ and O₃ radicals and are reactive VOCs. They are unsaturated hydrocarbons with the chemical formula C₁₀H₁₆ and comprise of primary source of BVOCs (Fuentes., 2007) with total annual emissions estimated at 1150 Tg C⁻¹, 11% of this total has been attributed to monoterpenes (Guenther et al., 1995; Arneth., 2008). The internal double bonds make monoterpenes susceptible to reactions with O₃, making ozonolysis oxidation are dominant compared to OH as seen in isoprene (Pinto., 2007)

The oxidation products of monoterpenes have been considered to be more important in SOA formation compared to that of isoprene as their oxidation products can lead to products with lower volatility (Cahill., 2006).

4.2 Myrcene oxidation

Myrcene is an acyclic monoterpene exhibiting three double bonds, the structure given in Figure 48. The removal processes of myrcene in the atmosphere are similar with respect to both OH and O₃ (concentrations of 2.0 x 10⁶ and 7 x 10¹¹ molecule cm⁻³ respectively), with estimated lifetimes of 39 and 50 minutes respectively (Atkinson 1998). The oxidation processes of myrcene have not been as extensively studied in comparison to other monoterpenes, such as pinenes (discussed in section 4.5). In addition, there is no degradation pathway yet available for myrcene on the MCM. Myrcene has recently received more interest because of its fairly rapid reaction rates in the atmosphere with oxidant species and its concentrations levels emitted from forest environments.

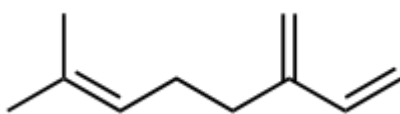


Figure 48. Chemical structure of myrcene

4.2.1 Ozonolysis of myrcene

Table 18 gives the initial experimental conditions for myrcene ozonolysis experiments conducted during TRAPOZ, Table 19 during TRAPOZ2 and Table 20 during the photooxidation experiments conducted during ACES2. Figure 49 shows the different gas-phase composition between the “precursor” system and 2 hours after reaction time. The parent myrcene compound and corresponding fragments (m/z 137 with m/z 95 and m/z 81) are clear (in red), with the formation of oxidation products also evident (in blue). The missing m/z 169 indicates that no primary aldehyde is formed with ozonolysis of myrcene. This is expected given that myrcene is not a cyclic monoterpene. Apparent differences to cyclic monoterpenes are the absence of the larger compounds around m/z 187 (discussed in section 4.5 onwards), and the increase of lower molecular weight signals such as acetone and formaldehyde.

Table 18: Initial experimental conditions of myrcene ozonolysis during TRAPOZ

Exp Date	VOC	Type	Initial Mixing ratios				RH / % ^b	Duration / min	Temp / K ^b
			[VOC] _o / ppbV	[Ozone] _o / ppb ^a	[CO] _o / ppm	[Cyclohexane] _o / ppm			
30/04/08 (am)	Myrcene	1	179.0	103.5			0.3	240	291.7
30/04/08 (pm)	Myrcene	3	141.2	105.3		153.6	0.27	240	295.2

(1) Straight Ozone/alkene, (3) with added cyclohexane, (a) measurements based on the ozone analyser, (b) values given as an average values measured over the duration of the experiment.

Table 19: Initial experimental conditions of myrcene ozonolysis during TRAPOZ 2

Exp Date	VOC	Type	Initial Mixing ratios				RH / % ^b	Duration / min	Temp / K ^b
			[VOC] _o / ppb ^c	[Ozone] _o / ppb ^a	[CO] _o / ppm	[Cyclohexane] _o / ppm			
22/05/09 (am)	Myrcene	2	112.58	82.1			51.03	202	292.6

(2) Straight ozonolysis with H₂O, (a) measurements based on the ozone analyser, (b) values given as an average values measured over the duration of the experiment, (c) based on CIR-TOF-MS measurement.

Table 20: Initial experimental conditions for myrcene photooxidation during ACES 2

Exp Date / Campaign	VOC	Type	Initial Mixing ratios			Water / % RH	Duration / min
			[VOC] _o / ppbV _c	[NOx] _o / ppbV	[VOC/NOx] _o / ppbV		
16/06/08	Myrcene	a	30.73	31.63	0.97	52	363
17/06/08	Myrcene	a	111.94	137.3	0.82	52	360

(a) nucleation experiment, (c) based on CIR-TOF-MS measurement.

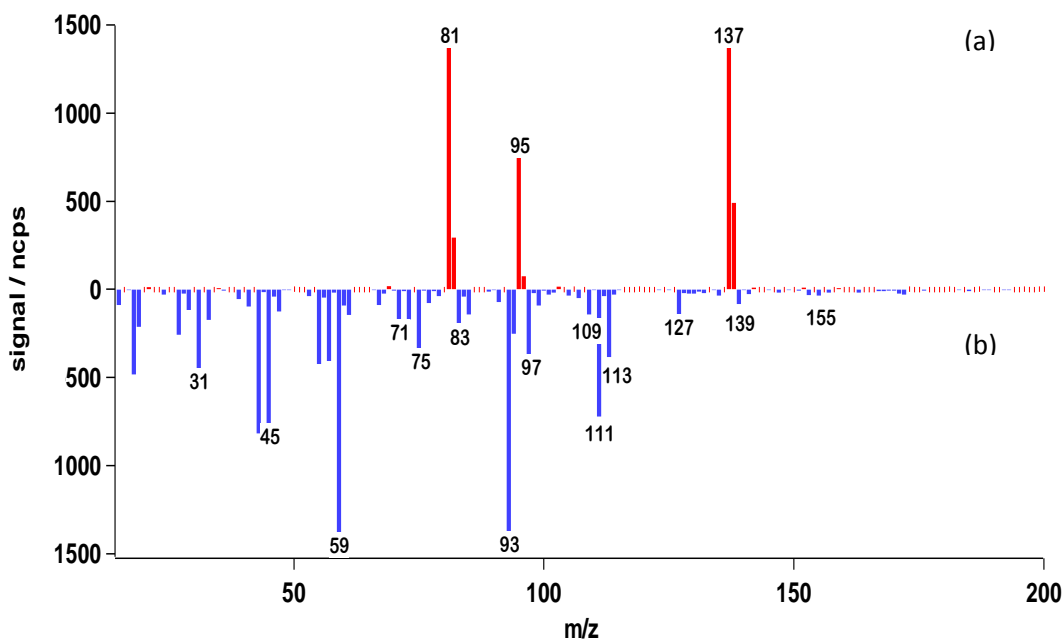


Figure 49. Difference in gas composition of myrcene (m/z 137) ozonolysis experiments from initial composition (a) and oxidation products produced after 2 hours of elapsed experiment time (b)

Table 21 gives an overview of all the detected protonated ions of the myrcene system. Several of these m/z ions are strongly correlated, and having a mass difference of 18, indicative of a dehydrated fragment. The fragment at m/z 93 is a probable water loss fragment of m/z 111, and further water loss can lead to a signal at m/z 75. Potential fragmentations of ions have been included in Table 21. Figure 50 shows the time

evolution of myrcene, ozone and the major oxidation products detected, formaldehyde and acetone. It should be noted that there are high uncertainties associated with the initial myrcene concentration equating to approximately 27% at the highest uncertainty. Only few calibration runs could be made for myrcene and as such a higher error margin than expected was established. Myrcene was injected into the chamber, and the reaction start time (time = 0 minutes) begins with the addition of ozone. As ozone is added to the chamber, it reacts with the myrcene rapidly and the formation of major oxidation products formaldehyde and acetone is observed almost immediately. These products behave in a similar fashion to one another, and after a maximum gas-phase concentration level is reached this level is maintained throughout the experiment. These indicate clear first-generation oxidation products as the concentrations peak and decrease once most of the myrcene has been consumed. This behaviour is exhibited from compounds occurring at m/z 139, 113, 111, 93, 91, and 71. Time evolutions are displayed in Figure 51. These ions have a slight variation in behaviour compared to that of acetone and formaldehyde, in which a slight decline in concentration is observed once the maximum concentration is reached. Apart from exhibiting behaviour of first generation products, these compounds could further react to form other species, or are themselves contributing to aerosol formation or growth. The “fast” formation of these products indicates that they are all first generation products and evolve at a similar time to HCHO and acetone. Different to these first-generation products are compounds relating to m/z 113 that show continuous increase in concentration which are representative of second generation oxidation products as most of the precursor VOC has been consumed.

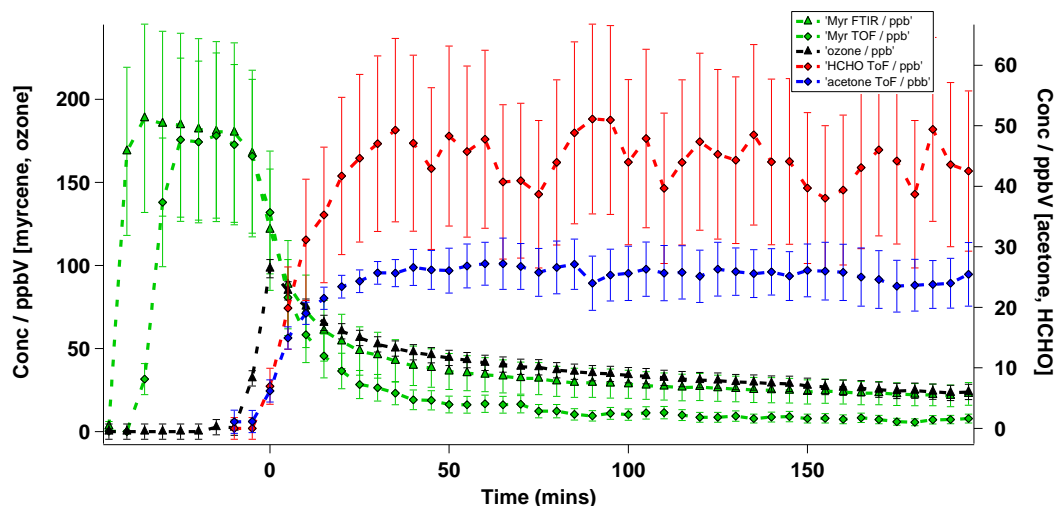


Figure 50 Time evolution profile of the straight myrcene ozonolysis experiment

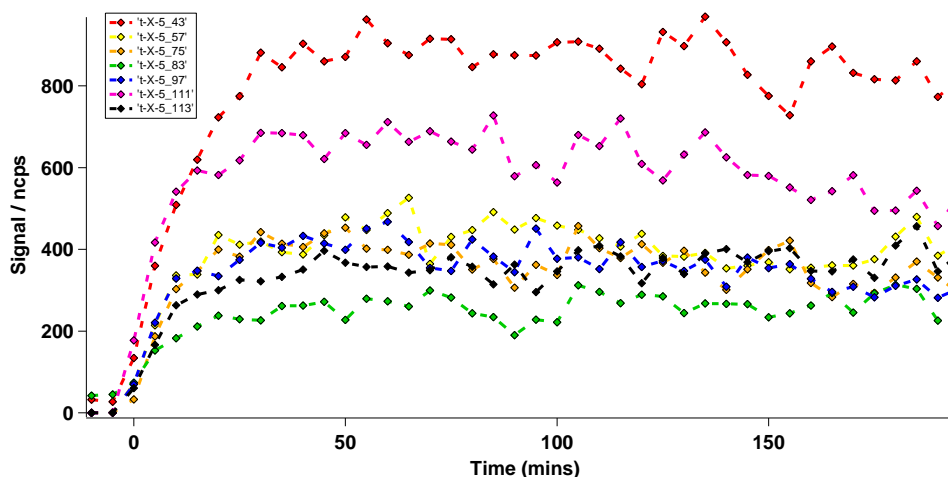


Figure 51 Observed mass channels from myrcene ozonolysis that have been identified from the proposed reaction mechanism of myrcene on (see Figure 52).

A proposed schematic of the ozonolysis reaction of myrcene is presented (Figure 52) based on the current knowledge of ozone addition and the behaviour of reactions in the isoprene, limonene and α -pinene system. Compared to the other monoterpenes studied, complications occur in the myrcene system as there are three possible sites of ozone addition, which could result in a multitude of gas-phase products and fragmentation, and despite the “gentle” ionisation characteristics of the CIR-ToF-MS

(see Chapter 2) the oxidation will lead to many isobaric masses. In mass spectrometry this term is given to ions that contain the same mass. Based on the myrcene system, the first generation products of ozone addition leads to stable species (S1, S2 and S3) (see Figure 51) with an m/z ion signal at 139 (S1 and S3) and 111 (S2). More interestingly is the detection of acetone and HCHO, which is a result of the initial “ozonide bridge” cleavage to give the Criegee radical species. HCHO was found at higher concentrations than that of acetone and could be an indicator towards the preferred pathway taken, but HCHO is formed in more than one pathway, and so this could explain the higher detection of HCHO than acetone. Lee et al (2006) established some observational data using PTR-MS, and found that acetone formed quicker than HCHO coming to the assumption that O_3 addition is preferred at the bi-methyl carbon site (C_6-C_7). This could be a result of a stabilised “induced” effect from both methyl groups. However, our results show simultaneous formation of both products. As such we can conclude that that initial ozone addition to myrcene occurs equally at the bi-methyl carbon site (C_6-C_7). Other masses of interest detected include m/z 113 that correlates to a stable species that is formed after further ozone addition to the second alkene group of myrcene, resulting in a bi-carbonyl species (S4 and S5). Further addition of ozone to the final double bond gives a tri carbonyl species (S6) as proposed in the reaction scheme. Interestingly however is that signals for m/z 115 are absent, and so is indicative that a strong stabilisation of the compound occurs with the addition of two oxygen double bonds which hinders further ozone addition and no formation of the theoretical S6 compound. The time profile of m/z 113 show a first generation product as it forms with acetone and HCHO, but it is only formed in the later stages in the oxidation mechanism. This is reflected in data observed by Lee et al (2006) that recorded a detection of < 1 ppb for mass channel 115, and levels reaching 10 ppb for 111 and 113 m/z ion channels. Other observed m/z channels of interest include that of 155 and 127. These stable species (S8 and S9) are formed after RO_2/HO_2 and H_2O reactions of the Criegee intermediate. Observations of quick detection suggests that these compounds are rapidly formed in the gas-phase. In addition however other compounds of similar mass are formed under further RO_2/RO

conversion and HO₂ reactions that could also contribute to the total of these mass channels.

4.2.2 Photooxidation of myrcene

Similar products to ozonolysis are observed in photooxidation reactions. The time profiles are given in Figure 53. Theoretical reactions of OH, (see Introduction) produces compounds at m/z 169 when following the H-abstraction pathway. There could be some possible formation of this ion in the photooxidation experiment as this is observed; however the strength of signal suggests that this formation is not the dominant chemical processes in myrcene oxidation. For OH-initiated experiments, similar m/z ions were observed to ozonolysis reactions, and early formation of m/z 111 can be produced as a primary oxidation products. This is not unexpected as ozone will also be present in OH-initiated reactions and the result of similar ions indicates that O₃ reactions are also dominant during photooxidation conditions. Other dominant m/z ions of 113 and 93 are observed to be primary products as the time profiles correspond to other primary products. However, when looking at the predicted scheme these products are formed from further oxidation of m/z 111 (Lee et al., 2006), with other routes of formation suggested by internal rearrangement of a peroxy radical species (Vereecken., 2004). This suggests that the theoretical species formed rapidly and that the oxidation process of myrcene and its oxidation products are rapid.

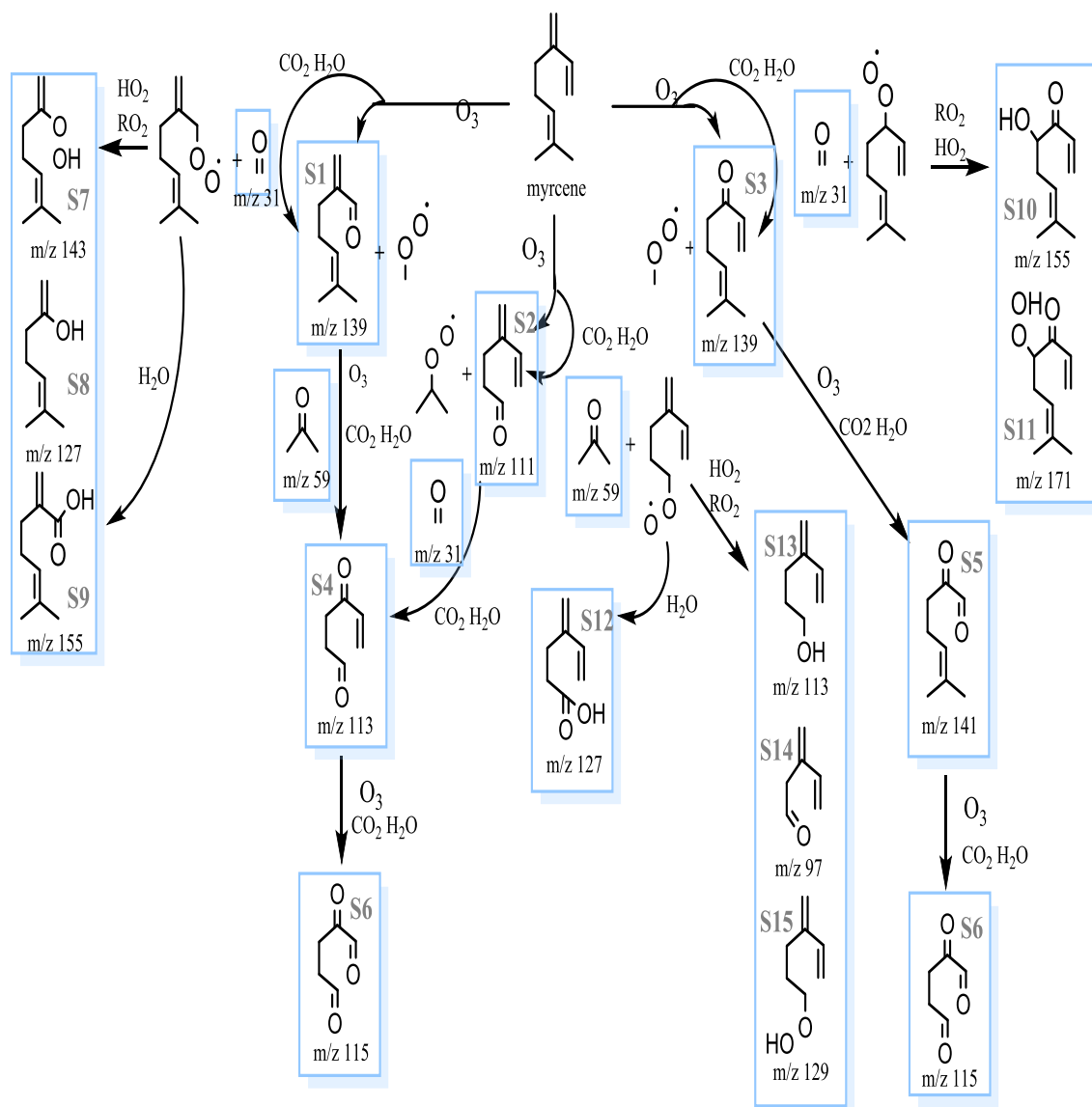


Figure 52 The proposed mechanism of Myrcene ozonolysis based on current knowledge and mechanisms adapted from isoprene reactions (all m/z are MH^+)

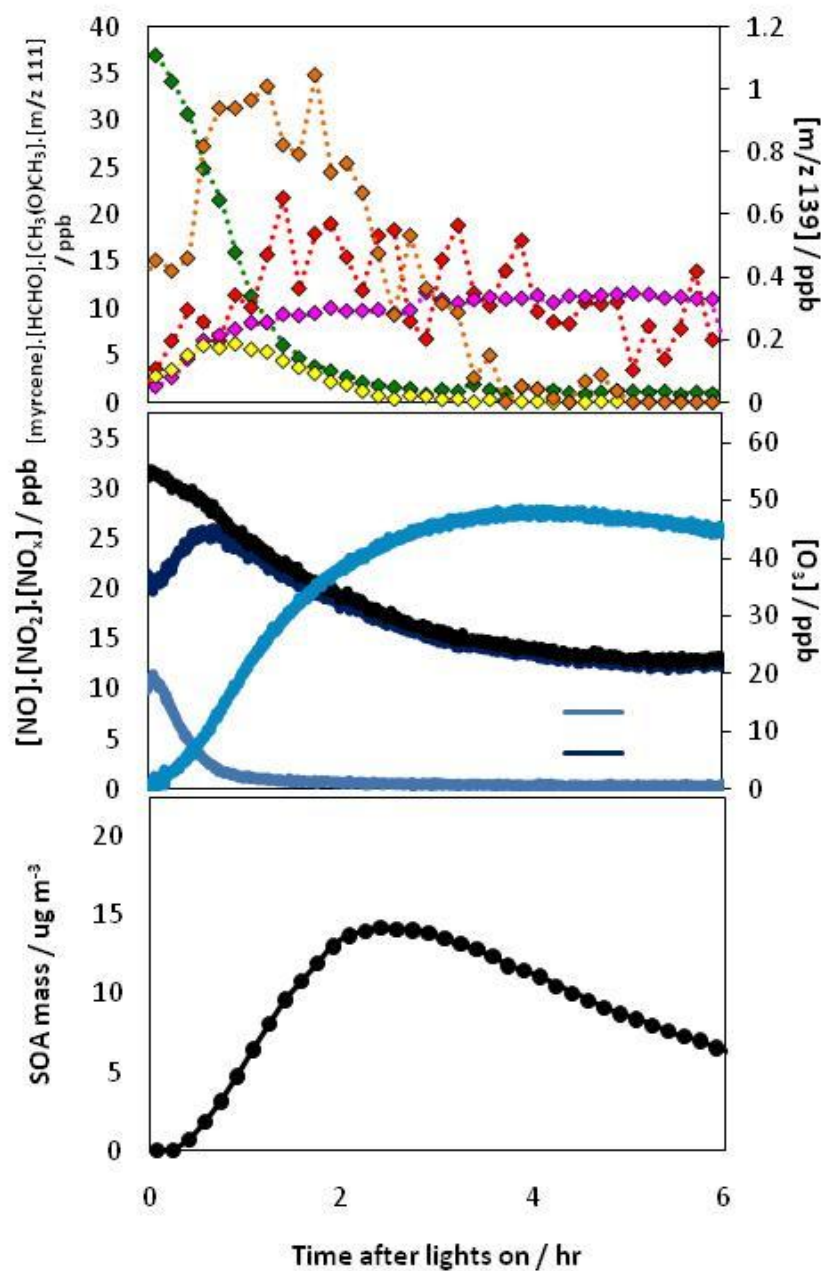


Figure 53. Time profiles of myrcene photooxidation reactions. Top shows the degradation of myrcene (green) with some of the major oxidation products, HCHO (red), m/z ion 111 (orange) and m/z 139 (red). Middle panel describes the chamber conditions with NO (light blue) NO₂ (dark blue), O₃ (blue) and NO_x (black) with the bottom panel showing SOA mass formation (see section 4.1.5).

4.2.3 Yields of stable organic species (myrcene)

Table 21. Detection of m/z ion channels during myrcene ozonolysis experiments (TRAPOZ campaign)

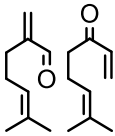
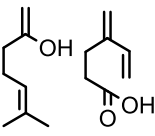
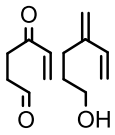
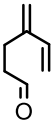
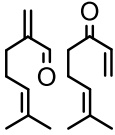
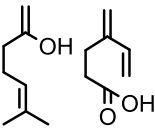
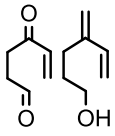
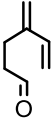
Compound Signals Detected from CIR-TOF-MS	Proposed Compounds	m/z (formula)	Fractional Yield ^{ab}
<i>myrcene + O₃ (30/04/08, am)</i>			
138^c, 137, 95, 82^c, 81		139 (C ₉ H ₁₂ O)	<0.01
155 ^d , 153 ^d , 139 ^d , 127 ^d , 113, 111, 109 ^d , 99 ^d , 97 ⁽¹¹¹⁾ , 94 ^c , 93 ⁽¹¹¹⁾ , 91 ⁽¹¹¹⁾ , 85 ^d , 83 ^d , 77 ^d , 75 ⁽¹¹¹⁾ , 73 ^d , 71 ^d , 67 ^d , 61, 60 ^(c) , 59, 57 ⁽¹¹¹⁾ , 55 ^e , 47, 45, 44 ^c , 43 ^f , 33, 31		127 (C ₇ H ₁₀ O ₂)	0.014 ± 0.003
		113 (C ₆ H ₈ O ₂)	0.052 ± 0.009
		111 + 93 (C ₇ H ₁₀ O)	0.569 ± 0.082
		61 (CH ₃ COOH)	0.017 ± 0.003
		59 (CH ₃ (O)CH ₃)	0.215 ± 0.012
		47 (HCOOH)	<0.01
		45 (CH ₃ CHO)	0.051 ± 0.007
		33 (CH ₃ OH)	0.032 ± 0.007
		31 (HCHO)	0.339 ± 0.061
<i>myrcene + O₃ + CHEX (30/04/08, pm)</i>			
138^c, 137, 95, 82^c, 81		139 (C ₉ H ₁₂ O)	<0.01
155 ^d , 153 ^d , 139 ^d , 127 ^d , 113, 112 ^c , 111, 109 ^d , 100 ^(c) , 99, 98 ^c , 97 ^(111,99) , 94, 93 ^(111,99) , 91 ^(111,99) , 85 ^d , 79 ^d , 77 ^d , 75 ^(111,99) , 73 ⁽⁹⁹⁾ , 71 ^d , 67 ^d , 61, 60 ^c , 59, 57 ⁽¹¹¹⁾ , 55 ^e , 47, 45, 43 ^f , 33, 31		127 (C ₇ H ₁₀ O ₂)	<0.01
		113 (C ₆ H ₈ O ₂)	0.039 ± 0.008
		111 (C ₇ H ₁₀ O)	0.597 ± 0.072

Table 21 continued

61 (CH ₃ COOH)	<0.01
59 (CH ₃ (O)CH ₃)	0.165 ± 0.012
47 (HCOOH)	<0.01
45 (CH ₃ CHO)	0.132 ± 0.011
33 (CH ₃ OH)	0.035 ± 0.009
31 (HCHO)	0.195 ± 0.021

BOLD = parent MH⁺ and fragments

ab = yield obtained from an average taken from FTIR and CIR-ToF-MS

c = isotope (+1 *m/z*)

d = unidentified signal

e = water cluster detection (structure can be H₃O⁺.H₂O and further additions of water)

f = common fragment in CIR-ToF-MS spectra

m/z^(x) = correlation for potential fragment of larger mass x (*R*² > 0.9)

**m/z* ion 99 is product cyclohexanone from cyclohexane oxidation

Table 22. Detection of *m/z* ion channels during myrcene photooxidation experiments (ACES 2)

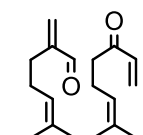
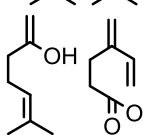
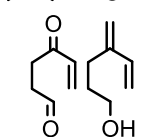
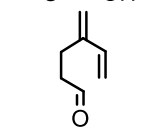
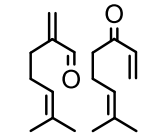
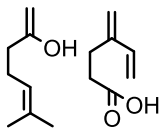
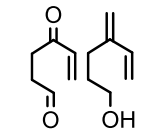
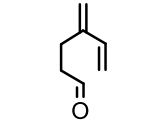
Compound (Date) Signals Detected from CIR-TOF-MS	Proposed compounds	<i>m/z</i> (formula)	Fractional Yield ^b
<i>Myrcene (17/06/08) (nominal 250 ppb)</i>			
138^c, 137^c, 96^c, 95^c, 82^c, 81		139 (C ₉ H ₁₂ O)	0.033 ± 0.005
169, 155 ^d , 153 ^d , 142 ^c , 141 ^d , 140 ^c , 139 ^d , 127 ^d , 125 ^d , 114 ^c , 113, 112 ^c , 111, 110 ^c , 109 ^d , 101, 99 ^d , 97 ⁽¹¹¹⁾ , 94 ^c , 93 ⁽¹¹¹⁾ , 91 ⁽¹¹¹⁾ , 85 ^d , 83 ^d , 77 ^d , 75 ⁽¹¹¹⁾ , 73 ^d , 71 ^d , 69 ^d , 67 ^d , 61, 60 ^(e) , 59, 57 ⁽¹¹¹⁾ , 55 ^e , 53 ^d , 47, 45, 44 ^c , 43 ^f , 31		127 (C ₇ H ₁₀ O ₂)	0.025 ± 0.007
33		113 (C ₆ H ₈ O ₂)	0.079 ± 0.009
		111 (C ₇ H ₁₀ O)	0.380 ± 0.021
		61 (CH ₃ COOH)	0.076 ± 0.012
		59 (CH ₃ (O)CH ₃)	0.219 ± 0.022
		47 (HCOOH)	<0.01
		45 (CH ₃ CHO)	<0.01
		33 (CH ₃ OH)	0.056 ± 0.008
		31 (HCHO)	0.378 ± 0.012

Table 22 continued

myrcene (16/06/08) (nominal 50 ppb)

138, 137, 81		139 (C ₉ H ₁₂ O)	0.020 ± 0.003
141 ^d , 139 ^d , 114 ^c , 113, 111, 99 ^d , 97 ⁽¹¹¹⁾ , 93 ⁽¹¹¹⁾ , 91 ⁽¹¹¹⁾ , 85 ^d , 77 ^d , 73 ^d , 61, 59, 43 ^f , 33		127 (C ₇ H ₁₀ O ₂)	<0.01
155, 115, 101, 83, 75, 47, 31		113 (C ₆ H ₈ O ₂)	0.090 ± 0.012
		111 (C ₇ H ₁₀ O)	0.159 ± 0.025
		61 (CH ₃ COOH)	0.096 ± 0.010
		59 (CH ₃ (O)CH ₃)	0.304 ± 0.022
		47 (HCOOH)	<0.01
		33 (CH ₃ OH)	0.113 ± 0.020
		31 (HCHO)	0.402 ± 0.019

BOLD = parent MH⁺ and fragments

b = yield obtained from CIR-ToF-MS

c = isotope (+1 *m/z*)

d = unidentified signal

e = water cluster detection (structure can be H₃O⁺.H₂O and further additions of water)

f = common fragment in CIR-ToF-MS spectra

m/z^(x) = correlation for potential fragment of larger mass x (*R*² > 0.9)**m/z* ions in *italic* represent compounds showing a growth trend but were 3σ below background levels

Table 20 shows the observed ion channels for ozonolysis experiments during TRAPOZ and Table 21 for those under photooxidation regimes at ACES. Table 23 examines the gas-phase composition with the HC ion source under ozonolysis conditions during TRAPOZ 2. In all cases dominant *m/z* ions of 113 and 111 were detected (assuming an empirical formula of C₇H₁₀O and C₆H₈O₂). During both type of experiments, a similar number of oxidation ions were detected and further interest lies in the larger *m/z*

Table 23. Detection of m/z ion channels during myrcene ozonolysis experiments (TRAPOZ 2 campaign)

Compound Signals Detected from CIR-TOF-MS	Proposed compounds	m/z (formula)	Fractional Yield
<i>myrcene + O₃ (H₂O) (22/05/09)</i>			
138, 137, 95, 82, 81		139 (C ₉ H ₁₂ O)	<0.01
201 ^d , 121 ^d , 113, 111, 109 ^d , 97 ⁽¹¹¹⁾ , 95 ^d , 93 ⁽¹¹¹⁾ , 91 ⁽¹¹¹⁾ , 85 ^d , 83 ^d , 79 ^d , 77 ^d , 75 ⁽¹¹¹⁾ , 73 ^d , 71 ^d , 67 ^d , 61, 60 ^(c) , 59, 57 ⁽¹¹¹⁾ , 53 ^d , 43 ^f , 41 ^f , 33, 31		127 (C ₇ H ₁₀ O ₂)	<0.01
155, 139, 127, 99, 45		113 (C ₆ H ₈ O ₂)	0.021 ± 0.002 ^b
		111 (C ₇ H ₁₀ O)	0.882 ± 0.112 ^b
		61 (CH ₃ COOH)	0.032 ± 0.005 ^{ab}
		59 (CH ₃ (O)CH ₃)	0.237 ± 0.011 ^{ab}
		45 (CH ₃ CHO)	0.430 ± 0.020 ^a
		33 (CH ₃ OH)	<0.01
		31 (HCHO)	0.337 ± 0.040 ^{ab}

BOLD = parent MH⁺ and fragments

a = yield obtained from FTIR

b = yield obtained from CIR-ToF-MS

ab = yield obtained from an average taken from FTIR and CIR-ToF-MS

c = isotope (+1 m/z)

d = unidentified signal

f = common fragment in CIR-ToF-MS spectra

 $m/z^{(x)}$ = correlation for potential fragment of larger mass x ($R^2 > 0.9$)* m/z ion 99 is product cyclohexanone from cyclohexane oxidation* m/z ions in *italic* represent compounds showing a growth trend but were 3σ below background levels (H₂O) represents wet experimental conditions, RH > 50%

channel observed of 155 in both ozonolysis reactions and a 250 ppb VOC photooxidation nucleation experiment. This larger mass could be representative of a carbonyl group with an alcohol functional group (C₉H₁₃O₂). Because both processes in the atmosphere (O₃ and OH) show similar lifetimes with respect to myrcene reaction in the atmosphere, oxidation products produced from both these reactions can be suggested to be important. No calibrations were available for the larger masses for

myrcene oxidation products ($> m/z$ 99) and so suitable surrogates were used. Owing to strong correlation between the signal at m/z 111 and 93 ($R^2 = 0.96$) and the difference of 18 Da, the signal of 93 is most probably a dehydrated fragment of m/z 111. The yield for this compound, owing to the stronger signal at 93 (approximately 5 times in strength) is considered to be more accurate with a sum of both fragments included. For the cyclohexane scavenged experiment, cyclohexanone oxidation follows that of m/z 111 well, and so complicates identification of potential fragments. For example a further increase in the ratio between m/z ion 93 over m/z 111 was observed. Thereby, a ratio of the initial non-scavenged and the scavenged signals was taken to account for any increase in signal strength due to cyclohexanone detection. The yield for $C_7H_{10}O$ averages 0.583 for ozonolysis reactions, ignoring the yield obtained during TRAPOZ 2 as this yield seems to be overestimated. This is most probably due to more calibration work required for the HC ion source and so the surrogate used is most likely overestimating sensitivities for this compound. Lee et al (2006) found similar yields of 0.49 while Reissell (2002) found even higher yields of 0.70, which could suggest that the calibration work done on the HC was sufficient, but as experimental conditions were similar to those run during TRAPOZ, expectant levels would be around 0.50 yields.

Two dominant oxidation products from myrcene include those of $CH_3(O)CH_3$ and HCHO. Orlando (2000) found yields of 0.36 for acetone for OH-initiated oxidation and 0.25 for OH scavenged O_3 reactions. Comparably we observe between 0.22 and 0.30 for OH-initiated reactions with a range between 0.02 and 0.30 for O_3 reactions. It can be noted that the yield of $CH_3(O)CH_3$ formed is less in the latter reaction environment. Other studies have observed acetone yields between 0.21 and 0.29 for O_3 reactions and 0.22 to 0.41 for OH-initiated reactions (Lee et al 2006; Orlando et al 2006; Reissell 1999)

The ozonolysis of myrcene for HCHO have a range of yields reported, from 0.26 and 0.51 (Lee et al 2006; Ruppert 1997) with a large range between 0.30 and 0.74 recorded for OH-initiated reactions (Orlando et al 2000; Lee et al 2006). Comparably we observe an average yield of 0.23 for ozonolysis reactions and 0.39 for OH-initiated, showing

greater formation for OH-initiated over O_3 reactions. Other lower masses observed averaged yields of 0.02 (acetic acid), 0.06 (acetaldehyde) and 0.03 (methanol) for O_3 reactions, whilst yields of were obtained for 0.07 (acetic acid), and 0.05 (methanol) in OH-initiated reactions. Formic acid, while reported in previous studies around 0.05 (Lee et al., 2006; Orlando., 2000) no detection could be made within these studies. This is most likely due to the concentrations approaching those of the instrument detection limits and so no presence could ultimately be confirmed (at levels of low ppbv). As previously described, these yields were able to show mechanistic features which were adapted in the proposed chemical mechanism presented in Figure 51.

4.2.4 SOA formation (myrcene)

Table 24. Aerosol yields of myrcene experiments

Exp date	Campaign	Experiment	Δ VOC [ppb]	Mass peak $\mu\text{g m}^{-3}$	SOA Yield %
30/04/08	TRAPOZ	VOC + O_3	113.99	123.18	17.68
05/05/08	TRAPOZ	VOC + O_3 + CHEX	115.56	13.65	2.12
22/05/09	TRAPOZ2	VOC + O_3 (H_2O)	111.00	80.10	11.87
16/06/08	ACES2	Photooxidation	29.60	14.22	7.90
17/06/08	ACES2	Photooxidation	110.81	103.69	15.39

Table 24 highlights the SOA yield observed from all myrcene experiments conducted. Ozonolysis experiments showed higher yields when compared to scavenged experiments, and the same is observed with VOC concentration dependence in the photooxidation nucleation experiments. An example photooxidation experiment is given in Figure 52 showing important chamber measurements (panel a), with the observed m/z ion channels from the CIR-ToF-MS (panel b) and SOA mass and number concentrations (panel c). The low yield obtained for the cyclohexane scavenged experiment is most likely subject to large errors as an increase in mass by the SMPS was detected before the experiment start time. The yield of cyclohexane scavenged ozonolysis does not compare well with the yield observed by Lee et al (2006) who reported a yield of 12% under scavenged conditions. We see that under scavenged

conditions, the SOA yield is lower and so can assume that the reactions with OH contribute significantly to potential SOA oxidation products. The similarity in oxidation products however show that oxidation products produced both under ozonolysis and photooxidation conditions can contribute to SOA formation. Even higher SOA yields have been determined, 43% (Lee et al 2000), who also identified similar mass oxidation products. This further enhances the idea that primary oxidation products do indeed have the potential to enter in the aerosol phase. Accordingly small molecules identified in the gas phase as primary products are likely to be found in the aerosol phase such as HCHO. Previous work done on HCHO and potential partition have found small concentrations, 0.04-2% and 0.03% (Odabasi et al 2005 and Deandrade et al 1995) from air samples in the aerosol phase. As such HCHO is expected to be in the aerosol phase although HCHO was primarily associated with the gas-phase based on its supercooled liquid vapour pressure ($\log P_L = 0.71$ atm at 25°C). However these studies show that HCHO is present in particulate form, due to partitioning and a fraction maybe forming weak bonds with the suspended particles. These weakly bonded HCHO groups may even act as a shield to HCHO in the finer particles. Temperature affects have also been noted where lower temperatures give higher SOA yields due to the increase in volatility of oVOCs (Saathoff 2009), but because temperature data is unavailable, only a comparison and influences of the presence of seeds could be made.

4.3 α -pinene oxidation (photooxidation & ozonolysis)

The ozonolysis experiments conducted provide a comparison of an α -pinene+O₃ system and a scavenged α -pinene+O₃+CO system under “dry” conditions (RH < 5%).

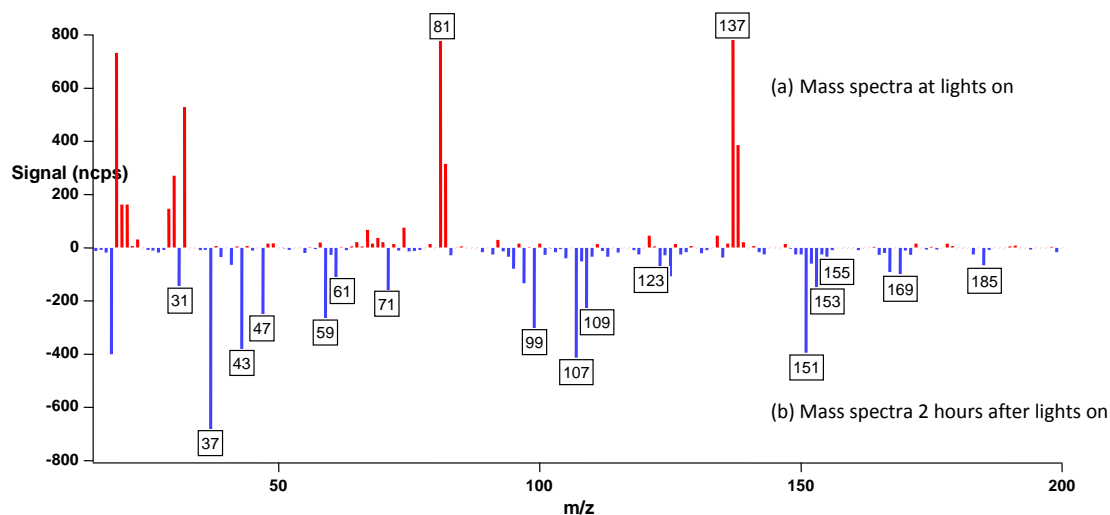


Figure 54. Difference in gas composition of myrcene ozonolysis experiments

Table 25 shows the experimental conditions used during α -pinene ozonolysis is TRAPOZ, Table 26 from ozonolysis from TRAPOZ 2 utilising the HC source, and finally Table 27 for α -pinene photooxidation experiments. Figure 54 shows a typical spectra taken the CIR-ToF-MS from the α -pinene+O₃ system, subtracted at two time intervals at the beginning of the experiment (giving initial conditions at time 0) and 2 hours after the start of reaction to highlight the evolution of the composition of the gas phase products. The identification of higher masses than that of the parent α -pinene are of interest due to the potential of these species contributing towards aerosol formation. Correlation analysis and calibrations of compounds was conducted to aid in deconvoluting the mass spectra from all the observed m/z channels.

Table 25: Initial experimental conditions for α -pinene ozonolysis during TRAPOZ

Exp Date	VOC	Type	Initial Mixing ratios				RH / % ^b	Duration / min	Temp/ K ^b
			[VOC] _o / ppbV ^c	[Ozone] _o / ppb ^a	[CO] _o / ppm	[Cyclohexane] _o / ppm			
13/05/08 (am)	α -pinene	1	129.14	169.9			0.3	295	294.9
13/05/08 (pm)	α -pinene	2	148.62	90.1	656.9	6	0.3	100	297.3

1, Straight Ozone/alkene, 2 with added CO, a - measurements based on the ozone analyser, b - values taken from average readings measured over the duration of the experiment, c - based on CIR-TOF-MS measurement

Table 26: Initial experimental conditions α -pinene ozonolysis during TRAPOZ 2

Exp Date	VOC	Type	Initial Mixing ratios				RH / % ^b	Duration / min	Temp / K ^b
			[VOC] _o / ppb ^c	[Ozone] _o / ppb ^a	[CO] _o / ppm	[Cyclohexane] _o / ppm			
19/05/09 (am)	α -pinene	1	163.59	183.8			0.5	190	297.3
19/05/09	α -pinene	3	87.23	101.8	711.41		22.98	205	297.6

1, Straight Ozone/alkene, 3 with added CO, a - measurements based on the ozone analyser, b - values given as an average values measured over the duration of the experiment, c - based on CIR-TOF-MS measurement

Table 27: Initial experimental conditions for α -pinene photooxidation during ACES 2

Exp Date / Campaign	VOC	Type	Initial Mixing ratios			Water / % RH	Duration / min
			[VOC] _o / ppbV (nominal)	[NOx] _o / ppbV (nominal)	[VOC/NOx] _o / ppbV		
01/11/07	α -pinene	a	250	125	2	52	360
23/11/07	α -pinene	a	50	25	2	52	360

a - "straight" nucleation experiment

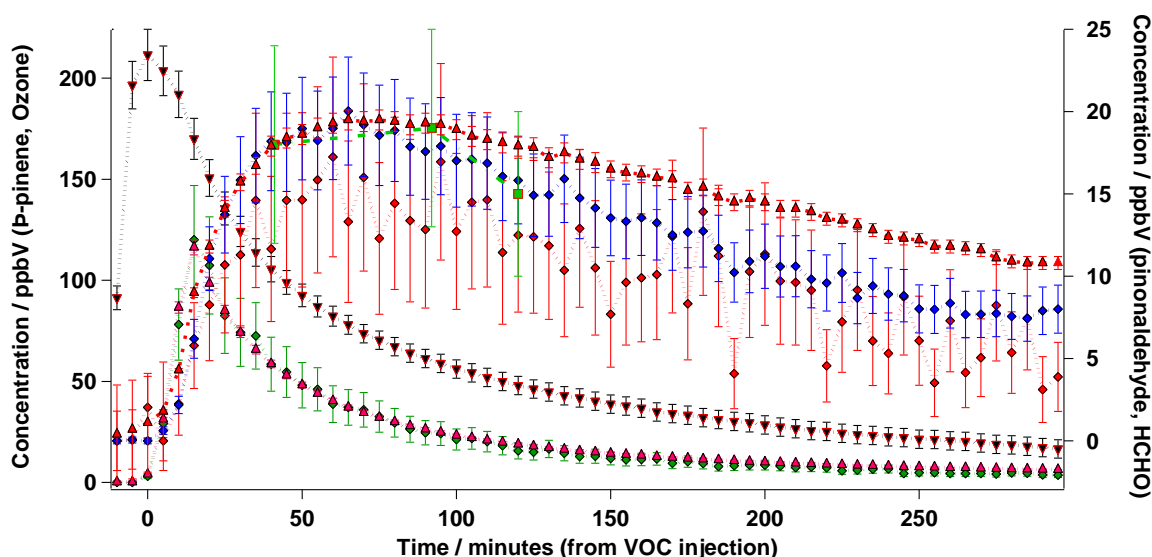


Figure 55. Time evolution of the α -pinene system. Diamond shapes are TOF data, squares are HPLC and triangles is FTIR, Red is HCHO, Black with red line borders (ozone), Green diamonds (ToF), Pink triangle (FTIR) α -pinene, Green is pinonaldehyde (HPLC), blue pinonaldehyde (TOF)

Figure 55 shows the concentration profiles of the α -pinene+O₃ system, with the time evolution of the gas-phase products represented as 5 minute averages of the collected CIR-ToF-MS data for α -pinene, ozone and observed oxidation products. The injection of α -pinene (denoted time 0, or reaction start) and the reaction with ozone is almost immediately followed by the production of stable gas-phase species. A small degradation of ozone is observed before injection of the VOC due to probable loss off the chamber walls. The large uncertainty in α -pinene detection of the CIR-ToF-MS should be noted compared to the FTIR. After a number of calibration runs on α -pinene it is apparent that detection limits is tens of ppb for this compound, which could be indicative of the potential detection levels for other monoterpene species. Following the injection of α -pinene, many gaseous products evolve, most notable that of products pinonaldehyde, HCHO and α -pinene oxide.

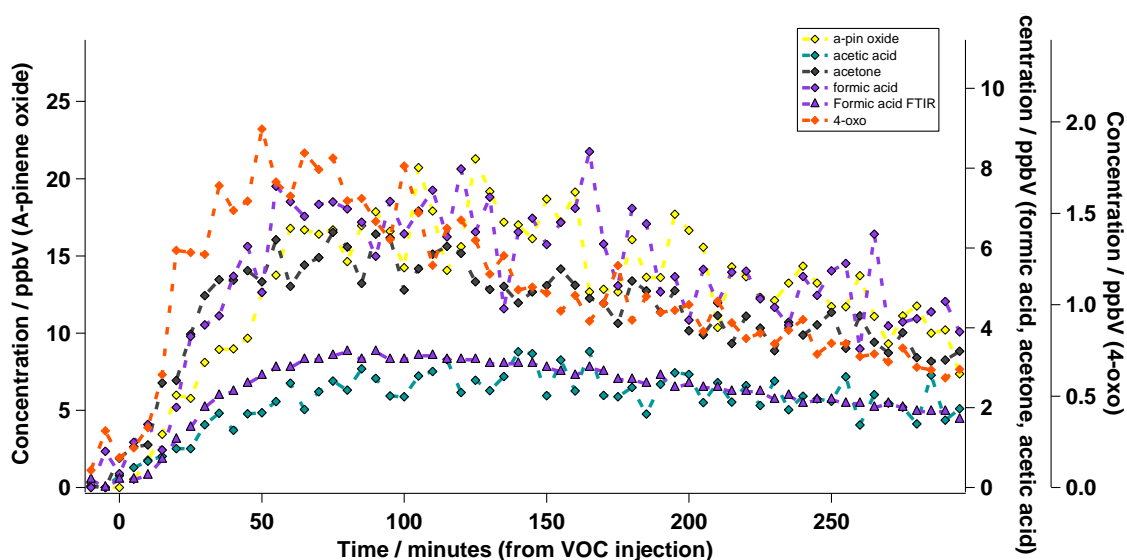


Figure 56. Time profiles of oxidation products, α -pinene oxide (yellow), acetic acid (green), acetone (black), formic acid (purple), 4-oxo (orange). FTIR measurements (triangles) have been included in CIR-ToF-MS (diamonds)

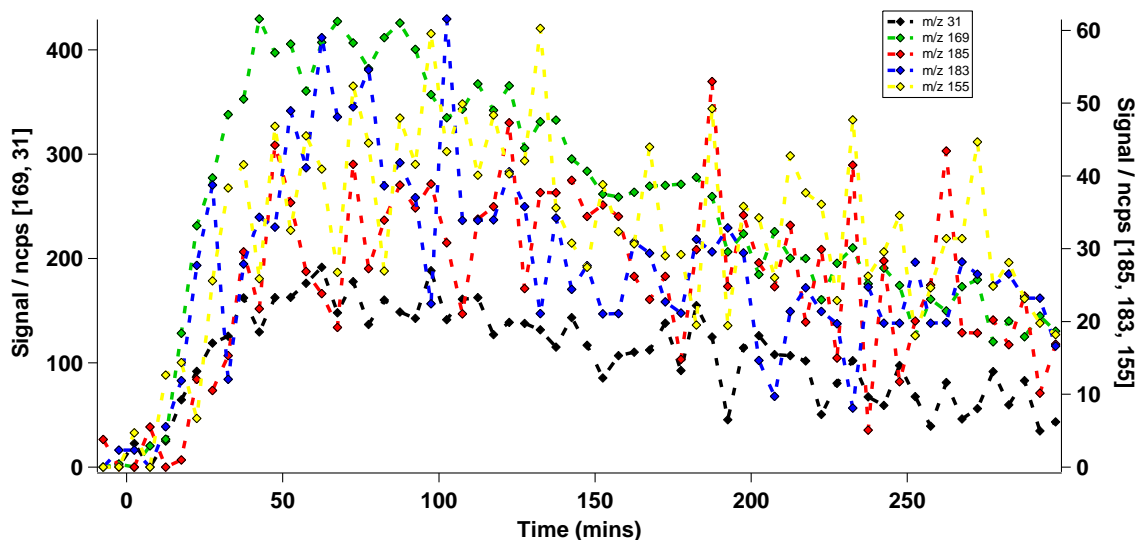


Figure 57. Time profiles of detected mass channels corresponding to the directly produced stable species following the peroxy radical reactions with HO₂ and RO₂ as presented in the reaction mechanism

Table 23 gives an overview of the observed mass channels during both experiments. Almost immediately after a decrease in α -pinene concentrations the gaseous products evolve, namely that of the major oxidation products pinonaldehyde, HCHO and α -pinene oxide. Possible fragmentation and dehydration of the larger molecules can account for a small contribution towards lower mass channels. Common fragments associated with the CIR-ToF-MS consist of acetyl ion and n-propyl ion (m/z 43) (Wyche et al 2005 and Blake et al 2006). The ion at m/z 71 shows a strong correlation (> 90%) in evolution profile to both pinonaldehyde and pinonic acid, indicating that this channel is due to fragmentation of these larger species. Other correlation account for the possible fragmentation of pinonaldehyde in m/z 152, 151, 123, 109, 107, 99, 71 and 43 and isotopes within, with calibration work conducted confirming this fragmentation pattern. However a large number of observed mass channels are still unidentified, where further calibration work looking into fragmentation of specific compounds is required as weaker correlations (<90%) were noted for a number of these mass channels. Other complications occur when fragments appear in the same mass channel as that of the identified products. Dehydration of Pinalic-3-acid (m/z 171 - 18) has been attributed to contribute to the ion m/z 153 (Camredon 2010) that also corresponds to α -pinene oxide. Where possible, calibration values obtained

experimentally were used, but with regards to species that were not characterized, a suitable surrogate was determined taking into consideration the functional groups, proton affinities and their polarisabilities (average numbers adopted from known values of other organic molecules possessing the same number of carbon atoms if unknown, or taken from values of SIFT studies conducted by Španěl et al (1997a, 1997b and 1998). The observation of formic acid (m/z 47) and acetone (m/z 59) indicate several oxidation steps of α -pinene in a fairly rapid time frame (see reaction scheme in figure 58). Acetone is formed after further oxidation of the primary Criegee and the “organics” in the scheme correspond to small mass compounds such as formic acid and HCHO. Figure 56 shows evolution of identified products and Figure 57 shows the observed ions that correspond to directly formed m/z ions greater in mass than the α -pinene as proposed by the MCM, a simplified mechanism given in Figure 58.

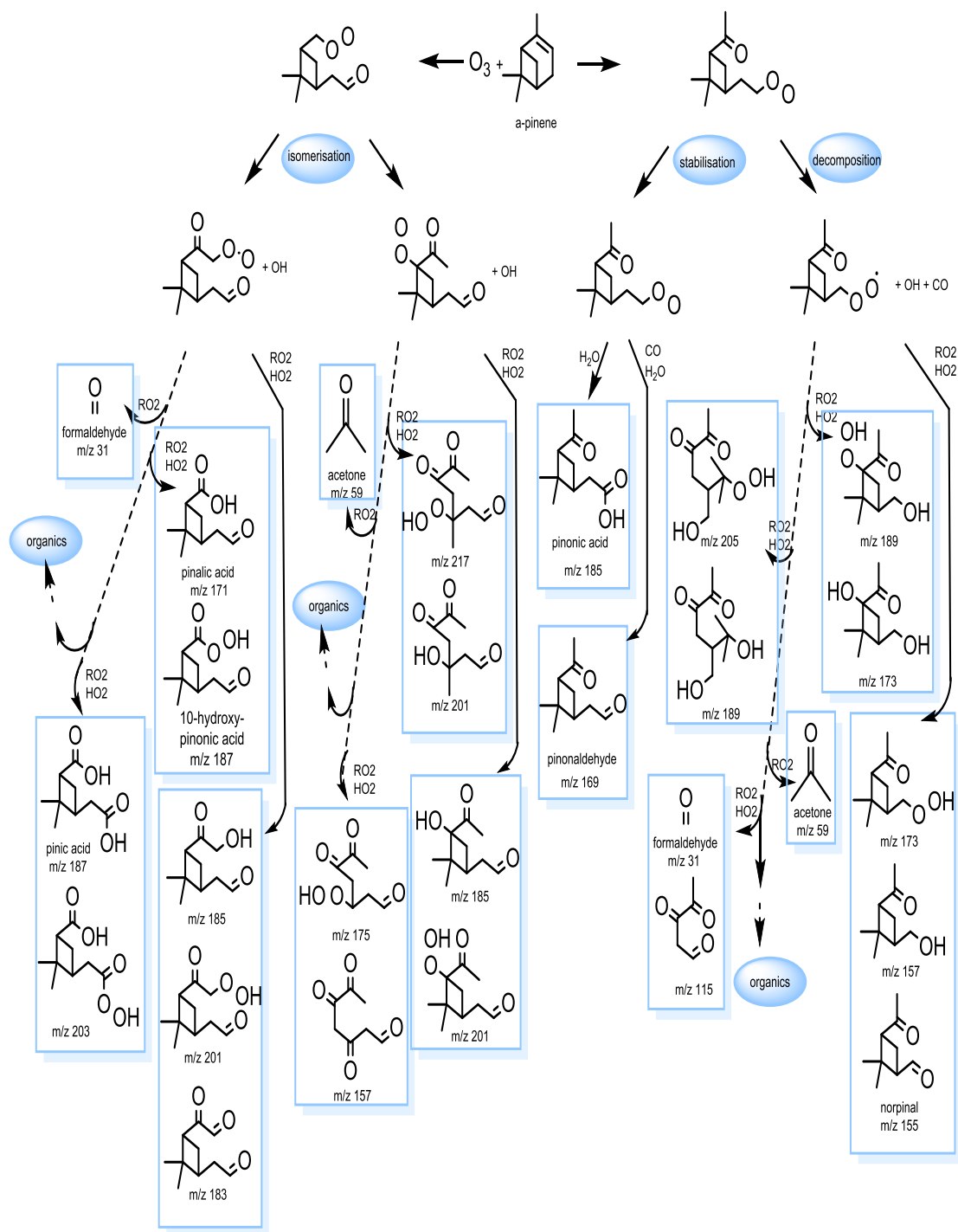


Figure 58. The MCM mechanism route for the ozonolysis of α -pinene, simplified to identify the stable products detected and to show their reaction pathways

The initial ozone addition forms the energy rich ozonide that after ring cleavage forms the two Criegee intermediates with a carbonyl functional group. These Criegees are proposed to then undergo isomerisation, collisional stabilisation or rapid

decomposition. The stabilised Criegee are proposed to react with CO and H₂O to form the products pinonaldehyde and pinonic acid. Under the decomposition and isomerisation regime, the Criegees are a source of OH and produce peroxy radicals that react with HO₂ and RO₂ to produce stable species directly such as formaldehyde, acetone, pinonic acid and norpinal. Further RO₂/RO conversion and isomerisation of these products lead onto the formation of further stable species.

4.3.1 Yields of stable organic species (α -pinene)

Table 28. Detection of m/z ion channels during α -pinene ozonolysis experiments (TRAPOZ)

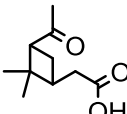
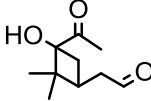
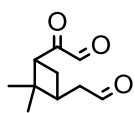
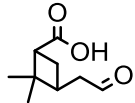
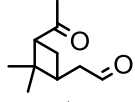
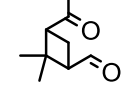
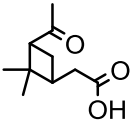
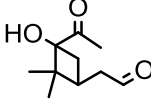
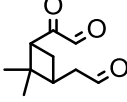
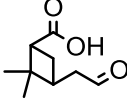
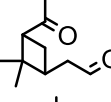
Compound Signals Detected from CIR-TOF-MS	Proposed compound	m/z (formula)	Fractional Yield ^b
<i>α-pinene + O₃</i>			
138^c, 137, 82^c, 81			
185, 183, 171, 169, 167 ^d , 165 ⁽¹⁸³⁾ , 155, 153, 152 ^c , 151 ⁽¹⁶⁹⁾ , 149 ^d , 147 ^d , 141 ^d , 139 ^d , 135 ^d , 133 ^d , 127, 123 ⁽¹⁶⁹⁾ , 111, 109 ⁽¹⁶⁹⁾ ,		185 (C ₁₀ H ₁₆ O ₃)	0.004 ± 0.001
107 ⁽¹⁶⁹⁾ , 99 ⁽¹⁶⁹⁾ , 97 ^d , 95 ^d , 93 ^d , 85 ^d , 83 ^d , 73 ^d , 71 ⁽¹⁶⁹⁾ , 69 ^d , 61, 59, 55 ^e , 47, 45, 43 ^f , 41, 31		183 (C ₁₀ H ₁₄ O ₃)	0.008 ± 0.001
125 ^d		171 (C ₉ H ₁₄ O ₃)	0.002 ± 0.001
		169 (C ₁₀ H ₁₆ O ₂)	0.212 ± 0.016
		155 (C ₉ H ₁₄ O ₂)	0.002 ± 0.001
		153 (C ₁₀ H ₁₆ O)	0.150 ± 0.014
		61 (CH ₃ COOH)	0.021 ± 0.002
		59 (CH ₃ (O)CH ₃)	0.059 ± 0.005
		47 (HCOOH)	0.077 ± 0.007
		45 (CH ₃ CHO)	Bld
		31 (HCHO)	0.139 ± 0.017

Table 28 continued

 α -pinene + O₃ + CO

138, 137, 82, 81		185 (C ₁₀ H ₁₆ O ₃)	0.002 ± 0.001
169, 167 ^d , 165 ^d , 155 ^d , 153, 152 ^c , 151 ⁽¹⁶⁹⁾ , 149 ^d , 147 ^d , 141 ^d , 139 ^d , 135 ^d , 125 ^d , 123 ⁽¹⁶⁹⁾ , 121, 109 ⁽¹⁶⁹⁾ , 108 ^c , 107 ⁽¹⁶⁹⁾ , 105, 100 ^c , 99 ⁽¹⁶⁹⁾ , 97 ^d , 93 ^d , 83 ^d , 72 ^c , 71 ⁽¹⁶⁹⁾ , 69 ^d , 61, 59, 47, 43 ^f , 32 ^c , 31		183 (C ₁₀ H ₁₄ O ₃)	0.014 ± 0.0015
185, 183^d, 85^d, 55^e, 45		171 (C ₉ H ₁₄ O ₃)	Bld
		169 (C ₁₀ H ₁₆ O ₂)	0.131 ± 0.009
		155 (C ₉ H ₁₄ O ₂)	0.002 ± 0.001
		153 (C ₁₀ H ₁₆ O)	0.123 ± 0.012
		61 (CH ₃ COOH)	0.015 ± 0.003
		59 (CH ₃ (O)CH ₃)	0.021 ± 0.002
		47 (HCOOH)	0.053 ± 0.009
		45 (CH ₃ CHO)	0.007 ± 0.002
		31 (HCHO)	0.109 ± 0.015

BOLD is parent compound detection with fragments ions

b = yield obtained from CIR-ToF-MS

c = isotope (+1 *m/z*)

d – unidentified signal

e = water cluster detection (structure can be H₃O⁺.H₂O and further additions of water)

f = common fragment in CIR-ToF-MS spectra

m/z^(x) shows correlation for potential fragment of larger mass x (*R*² > 0.9)**m/z* ion 99 is product cyclohexanone from cyclohexane oxidation**m/z* ions in *italic* represent compounds showing a growth trend but were 3σ below background levels

bdl is below detection limit (3σ above background noise)

Table 29. Detection of *m/z* ion channels during α -pinene photooxidation experiments (ACES)

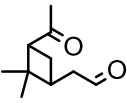
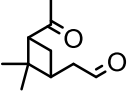
Compound	Proposed Compound	<i>m/z</i> (formula)	Fractional Yield ^b
Signals Detected from CIR-TOF-MS			
<i>α</i> -pinene (01/11/07)			
138, 137, 82, 81		169 (C ₁₀ H ₁₆ O ₂)	0.014 ± 0.002
169, 151, 139 ^d , 125 ^d , 109 ⁽¹⁶⁹⁾ ,		61 (CH ₃ COOH)*	1.086 ± 0.034
107 ⁽¹⁶⁹⁾ , 99 ⁽¹⁶⁹⁾ , 79 ^d , 77 ^d , 71 ⁽¹⁶⁹⁾ , 61,		59 (CH ₃ (O)CH ₃)	0.177 ± 0.009

Table 29 continued

59, 46, 45, 43 ^f , 31		47 (HCOOH)	0.109 ± 0.017
		45 (CH ₃ CHO)	0.017 ± 0.004
<i>153, 141, 135, 123, 97, 93, 85, 83,</i>		33 (CH ₃ OH)	0.054 ± 0.007
<i>47, 31</i>		31 (HCHO)	0.054 ± 0.005
<i>a-pinene (23/11/07)</i>			
138, 137, 82, 81		169 (C ₁₀ H ₁₆ O ₂)	0.237 ± 0.025
169, 151, 143 ^d , 128 ^d , 125 ^d , 109 ⁽¹⁶⁹⁾ ,		61 (CH ₃ COOH)*	0.255 ± 0.014
107 ⁽¹⁶⁹⁾ , 93 ^d ,		59 (CH ₃ (O)CH ₃)	0.156 ± 0.009
85 ^d , 83 ^d , 73 ^d , 71 ⁽¹⁶⁹⁾ , 69 ^d , 59, 45, 43 ^f ,		45 (CH ₃ CHO)	0.106 ± 0.009
33, 31		33 (CH ₃ OH)	0.274 ± 0.014
		31 (HCHO)	0.876 ± 0.024
<i>171, 123, 97</i>			

BOLD is parent compound detection with fragments ions

b = yield obtained from CIR-ToF-MS

d – unidentified signal

f = common fragment in CIR-ToF-MS spectra

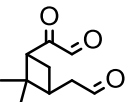
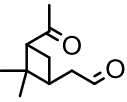
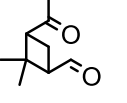
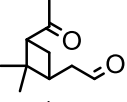
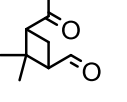
m/z^(x) shows correlation for potential fragment of larger mass x ($R^2 > 0.9$)

*represents late formation potentially due to chamber contamination

m/z ions in *italic* represent compounds showing a growth trend but were 3σ below background levels

Successful detection of gas phase oxidation products compared to those of past studies was made during all experiments. The results of gas phase composition are summarised in tables 28, 29 and 30. All results are fairly consistent with previous yields, but two experiments with yields that differ greatly were seen in the low VOC photooxidation experiment and “wet” run using the HC source. The low yields for the first can be justified by the low concentrations level in which the experiment was run (~24 ppb), as low VOC starting conditions will ultimately lead to lower yields of products as there is less material around to form oxidation products. This is with the assumption that regardless of VOC starting concentrations, the same oxidation (or at least similar) pathways would proceed throughout the oxidising process. The HC source was influenced strongly by an increase in humidity, giving lower detection limits over the range of oxidation products, for the exception of pinonaldehyde. This was seen by spikes in certain *m/z* ion channels alongside the decrease in signal of others. This is believed to be an artefact of the HC source, and so further testing under humid conditions is required to fully understand its behaviour with relative humidity.

Table 30. Detection of m/z ion channels during α -pinene ozonolysis experiments (TRAPOZ 2)

Compound Signals Detected from CIR-TOF-MS	Proposed compounds	m/z (formula)	Fractional yield
<i>a-pinene + O₃</i>			
138, 137, 95, 82, 81, 79, 67		183 (C ₁₀ H ₁₄ O ₃)	0.015 ± 0.005 ^b
169, 167 ^d , 165 ⁽¹⁶⁹⁾ , 155, 153, 152 ^c , 151 ⁽¹⁶⁹⁾ , 141 ^d , 139 ^d , 135 ^d , 133 ^d , 129 ^d , 127 ^d , 125 ^d , 123 ⁽¹⁶⁹⁾ , 121 ^d , 119 ^d , 113 ^d , 111 ^d , 110 ^c , 109 ⁽¹⁶⁹⁾ , 108 ^c , 107 ⁽¹⁶⁹⁾ , 99 ⁽¹⁶⁹⁾ , 97 ^d , 95 ^d , 94 ^c , 93 ^d , 91 ^d ,		169 (C ₁₀ H ₁₆ O ₂)	0.294 ± 0.010 ^{ab}
85 ^d , 83 ^d , 77 ^d , 73 ^d , 71 ⁽¹⁶⁹⁾ , 69 ^d , 61, 60 ^c , 59, 55 ^e , 43 ^{a(pinon)} , 43 ^f , 41, 31		155 (C ₉ H ₁₄ O ₂)	<0.01 ^b
<i>183, 149^d, 147^d, 45,</i>		153 (C ₁₀ H ₁₆ O)	0.053 ± 0.010 ^b
		61 (CH ₃ COOH)	0.024 ± 0.008 ^b
		59 (CH ₃ (O)CH ₃)	0.042 ± 0.008 ^b
		47 (HCOOH)	0.051 ± 0.011 ^b
		45 (CH ₃ CHO)	0.042 ± 0.017 ^b
		33 (CH ₃ OH)	0.007 ± 0.002 ^b
		31 (HCHO)	0.054 ± 0.013 ^b
<i>a-pinene + O₃ + CO (H₂O)</i>			
138, 137, 95, 81, 67			
165 ⁽¹⁶⁹⁾ , 152 ^c , 151 ⁽¹⁶⁹⁾ , 135 ^d , 133 ^d , 123 ⁽¹⁶⁹⁾ , 121 ^d , 109 ⁽¹⁶⁹⁾ , 108 ^c , 107 ⁽¹⁶⁹⁾ , 99 ⁽¹⁶⁹⁾ , 97 ^d , 95 ^d , 93 ^d , 91 ^d , 71 ⁽¹⁶⁹⁾ , 55 ^{e*} , 43 ^f , 41 [*] ,		169 (C ₁₀ H ₁₆ O ₂)	0.476 ± 0.034 ^a
<i>169, 155, 153, 149, 147, 141, 139,</i> <i>129, 127, 125, 119, 111, 85, 83,</i> <i>69, 31**</i>		155 (C ₉ H ₁₄ O ₂)	<0.01 ^b
		153 (C ₁₀ H ₁₆ O)	0.044 ± 0.010 ^b
		31 (HCHO)**	0.821 ± 0.090 ^b

BOLD is parent compound detection with fragments ions

a = yield obtained from FTIR

b = yield obtained from CIR-ToF-MS

ab = yield obtained from an average taken from FTIR and CIR-ToF-MS

c = isotope (+1 m/z)

d – unidentified signal

e = water cluster detection (structure can be H₃O⁺.H₂O and further additions of water)

f = common fragment in CIR-ToF-MS spectra

 $m/z^{(x)}$ shows correlation for potential fragment of larger mass x ($R^2 > 0.9$)*represents m/z channels that spike with H₂O addition (possible ion source characteristic)** signals decrease rapidly with H₂O addition*m/z* ions in *italic* represent compounds showing a growth trend but were 3 σ below background levels (H₂O) represents wet experimental conditions, RH > 50%

The dominant oxidation product seen throughout the experiments was that of pinonaldehyde. The pinonaldehyde yield was established from the m/z ions detected at 169, 151 and 107 that comprise of the majority of the total signal. Relative abundances for observed compounds in α -pinene experiments for which calibration standards were available are given in Table 31. However following extensive work conducted on pinonaldehyde yield shows that there is a variation in final yield dependent upon which m/z ions were used to calculate the yield. For example a different yield would be found if yield analysis was done purely on m/z 169 compared to yield analysis done on m/z ions 169, 151, 107 and 109. Although this range is not vastly different, it has been mentioned before by Lee et al (2006) who reported a small range of yields based on which m/z ions were used for yield calculations as these ultimately gave differing sensitivity values that were to be applied.

Table 31. Relative abundances for fragmentation of large oxidation products detected in the α -pinene system

	<i>m/z (Rel. Abundance)</i>
α-pinene	137 (68 %) 81 (100 %)
pinonic acid	185 (15 %) 167 (47 %) 139 (18 %) 115 (94 %) 71 (100 %) 69 (21 %)
Pinonaldehyhde*	169 (18 %) 151 (76 %) 123 (7 %) 107 (100 %) 109 (15 %) 108 (9 %)
acetic acid	61 (100 %)
Acetone	59 (100 %)
formic acid	47 (100 %)
formaldehyhde	31 (100 %)
acetaldehyde	45 (100 %)
Methanol	33 (100 %)

* m/z ions 139 and 99 also detected in pinonaldehyde calibrations but both show relative abundances of <1 % and so have been excluded.

Table 26 shows the fragmentation and measured m/z ion ratios from calibration runs made from pinonaldehyde. These three m/z ions (169, 151, 107) were chosen as they constitute the major ions. Other work regarding pinonaldehyde yield determination have been made with differing approaches to this, where fragmentation has been confirmed by correlation of time traces. It is ultimately the conditions that determine fragmentation (see chapter 2). Pinonaldehyde yields averaged 0.253 over non-scavenged ozonolysis experiments, with a halving seen in OH scavenged experiments of 0.131. Studies over wide range of experiments also show variation in determined yield products. Lowest yields were obtained by Orlando et al (2000) and Riessel et al (1999) (0.03 and 0.06) ranging to higher yields of 0.19 seen by Lee et al (2006) and Hakola et al (1994). (All yields shown display minimum yields if a range was present). Despite these, other studies also display an increase in gas-phase products with the presence of OH (Fick et al., 2003). In addition to OH dependency, major gas-phase compounds (e.g. pinonaldehyde) also exhibit dependence on humidity, similar to that seen from the production of low mass oVOCs from small alkene species. For ozonolysis reactions the reason for this is apparent when considering the reaction mechanism presented. The formation of pinonaldehyde from α -pinene resembles the pathway for the formation of formic acid from ethene in which CO and H₂O govern the production yield from the Criegee radical presented from initial ozone addition. Yields show strong relative humidity dependence where pinonaldehyde yields of 0.212, 0.131 and 0.294 for dry conditions were observed, whereas higher yields of 0.476 were measured for wet conditions. It should be noted that the latter yields were obtained utilising the HC source that displayed humidity effects (e.g. decreased sensitivities) over a range of m/z ion channels. These effects however were not seen in pinonaldehyde detection, and FTIR yields correlated well with those from the CIR-ToF-MS determined yields and so can be deemed accurate. Work done by Warscheid and Hoffmann (2001) also display this RH dependence for pinonaldehyde as a yield of 0.23 was reported for dry conditions and 0.53 for higher RH (~60%). However Berndt (2003) demonstrated the opposite in which a lower RH produced a 0.42 in contrast to a yield of 0.32 at higher RH. As such, it has been suggested that pinonaldehyde production is

independent of humidity, but our studies show that this is not the case in agreement with the observations made by Warcheid et al (2001).

For photooxidation experiments, similar yield to ozonolysis experiments were observed (0.237). This is fairly consistent with previous work that report yields of 0.30, 0.37, 0.34, 0.31, 0.3, 0.29 (Nozière (1999); Wisthaler (2001); Vinckier (1998); Jaoui (2001); Arey (1990) and Hakola (1994) respectively) to as high as 0.87, 0.56, 0.63 (Nozière (1999), Lee et al (2005) and Hatakeyama (1991) reaching as low as 0.06 (Larsen 2001). From these studies it can be shown that pinonaldehyde production is similar in both ozonolysis and photooxidation conditions. For other higher masses seen in ozonolysis reactions, which could potentially be of importance for aerosol growth as these were detected in filter samples, we observed low yields. For example, norpinal (m/z ion 155) was also observed by Lee et al (2005). Here we only observe low levels of large oxidation products, and as surrogates were used these yields could suffer from larger errors. The low molecular weight products observed are similar to those formed in isoprene experiments. Orlando (2000) observed acetone yields of 0.03 for ozonolysis reactions and 0.04 for photooxidation reactions.

4.3.2 Comparison to atmospheric model (α -pinene)

The reaction of α -pinene with O_3 gave signals of the larger oVOCs of pinonaldehyde and pinonic acid. The model was run using the initial reaction conditions in the chamber. The results indicate that although the degradation of α -pinene is slightly overestimated, with a slight underestimation for the reaction of O_3 , the model represents this data well. Results are given in Figure 59. The major oxidation products in the gas phase, HCHO and pinonaldehyde are also well represented in the model in both concentration and profile aspects. A large overestimation is made for the largest oVOCs observed (m/z 185). This oVOC was modelled as it is present in the particle phase (discussed in the next section). Overestimation of this can cause differing results in potential SOA formation as this was the primary identified product in the aerosol

filter samples, but as a surrogate was used for gas phase concentration determination, this could also lead to slight changes in observed gas-phase concentrations. As the output of this is no greater than 3 ppb, only slight changes in modelling parameters, and as such, calibrations for this compound can evaluate the MCM model more accurately.

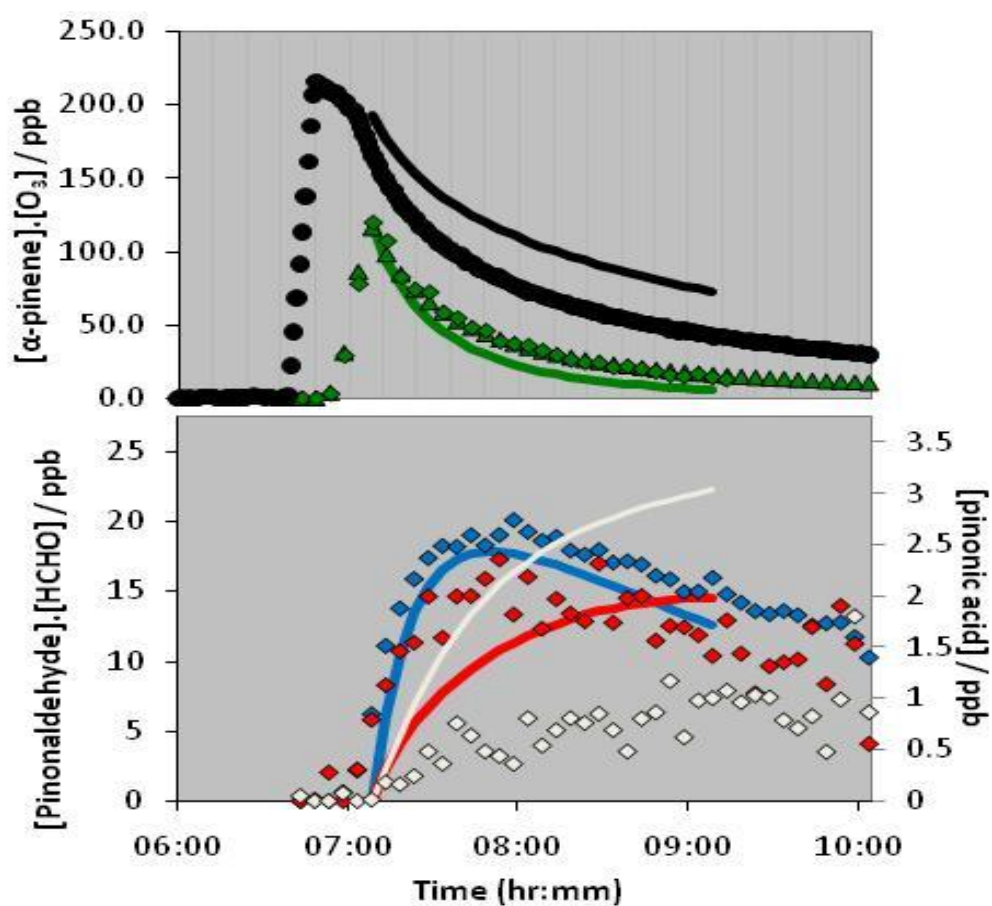


Figure 59. Model comparison (lines) to experimentally determined data by CIR-ToF-MS (diamonds) for reagents α -pinene (green), ozone (black) and oVOCs HCHO (red), pinonaldehyde (blue) and pinonic acid (white) for a $O_3 + \text{VOC}$ reaction in dark conditions.

4.3.3 SOA formation (α -pinene)

Yields obtained for aerosol formation were calculated using an aerosol density of 1.00 g cm^{-3} with the results from α -pinene ozonolysis given in Table 32. Average yield for α -pinene ozonolysis reactions was 42.02% whereas lower yields were observed for OH scavenged reactions (CO) under dry conditions, with even lower yields established for wet conditions, 26.76% and 12.51% respectively. The yields in these investigations were higher compared to those of other studies, with Hoffmann et al., (1997) reporting yields between 13.7 and 23.0% for dark ozonolysis experiments, with a range of 15.5 % and 24.8% reported by Cocker lii et al., (2001)

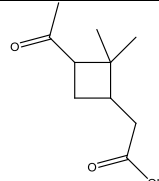
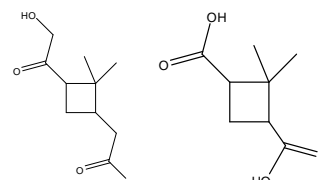
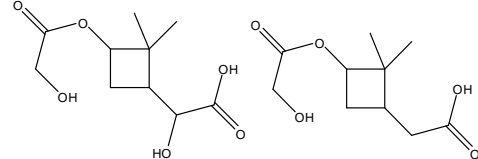
Table 32. Aerosol yields of α -pinene experiments

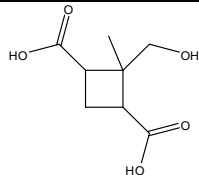
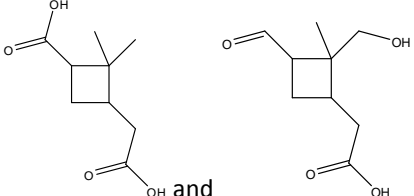
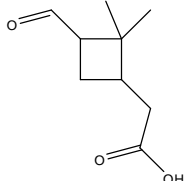
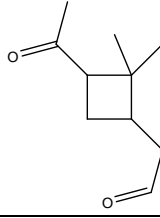
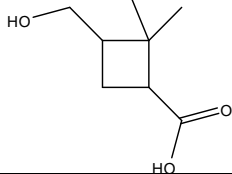
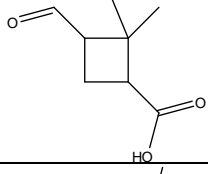
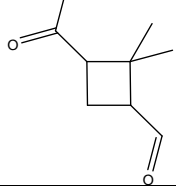
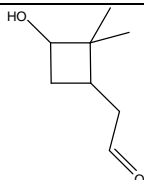
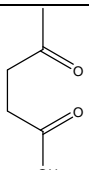
Exp date	Campaign	Experiment	Δ VOC [ppb]	Mass peak $\mu\text{g m}^{-3}$	SOA Yield %
13/05/08 (am)	TRAPOZ	VOC + O ₃	116.35	343.53	48.55
13/05/08 (pm)	TRAPOZ	VOC + O ₃ + CO	66.40	135.60	26.76
19/05/09 (am)	TRAPOZ2	VOC + O ₃	155.12	334.83	35.49
19/05/09 (pm)	TRAPOZ2	VOC + O ₃ + CO (H ₂ O)	70.85	49.48	12.51
01/11/07	ACES	Photooxidation		no data	
23/11/07	ACES	Photooxidation		no data	

Similar to trends seen in yield formation with myrcene ozonolysis the presence of scavengers produce lower yields, hinting towards a relative dependence of OH reactions on aerosol yield. The loss processes of α -pinene with OH and O₃ (2.6 h and 4.6 h) suggest that the dominant removal process encompassed within our experimental conditions is from OH (NO₃ removal lifetimes are quoted as 11 min) (Atkinson., 2003)

Lower mass products were observed similar to those already seen in isoprene and myrcene. The vapour pressure of most of these compounds make these unaccountable for aerosol formation as no nucleation events were observed in

isoprene experiments. It is the larger weight products ($> \alpha$ -pinene parent ion in mass, m/z 153) such as pinonaldehyde which exhibit lower volatility than the low molecular weight compounds, and are important as they ultimately partition and/or condense on new particles formed. Pinonaldehyde has been observed both in ambient air and gas particles both here and other studies (Yu et al., 2008 ; Kavouras et al., 1999). However from these results, pinonaldehyde, although contributing towards aerosol yields, is not the governing compound as pinonaldehyde, both dominant in photooxidation and ozonolysis results. Higher SOA yields obtained in ozonolysis experiments do show that additional compounds are important for SOA mass and particle number for the α -pinene system. Table 33 highlights the products identified from filter samples taken from MAC photooxidation experiments. The major product identified was that of pinonic acid, with two dicarboxylic acids constituting the 2nd and 3rd major products identified in the samples. Higher SOA therefore are due to the formation of these larger less volatile species, and as these compounds are formed from oxidation reactions at the endocyclic double bond, it is this reaction step that can govern the SOA potential of monoterpenes.

Table 33. Detected structures in particle phase from off-line analysis of filter samples of α -pinene conducted by York University. Major product is given at the top, followed by secondary and tertiary products, with the addition of identified structures (right)			
Mass measured / amu	Ion composition (amu)	Molecular Formula	Possible structures
184	$C_{10}H_{16}O_3Na^+$ (207)	$C_{10}H_{16}O_3$	 <p>Pinonic acid</p>
200 172	$C_{10}H_{16}O_4Na^+$ (223) $C_8H_{12}O_4Na^+$ (195)	$C_{10}H_{16}O_4$ $C_8H_{12}O_4$	
232 216	$C_{10}H_{16}O_6Na^+$ (253) $C_{10}H_{16}O_5Na^+$ (239) or $NaC_9H_{12}O_6^+$	$C_{10}H_{16}O_6$ $C_{10}H_{16}O_5$ or $C_9H_{12}O_6$	

188	$C_8H_{12}O_5Na^+$ (211)	$C_8H_{12}O_5$	
186	$C_9H_{14}O_4Na^+$ (209)	$C_9H_{14}O_4$	 Pinic acid
170	$C_9H_{14}O_3Na^+$ (193)	$C_9H_{14}O_3$	
169	$C_{10}H_{16}O_2Na^+$ (191)	$C_{10}H_{16}O_2$	 pinonaldehyde
158	$C_7H_{10}O_4Na^+$ (191)	$C_7H_{10}O_4$	
156	$C_9H_{16}O_2Na^+$ (179)	$C_9H_{16}O_2$	
154	$C_9H_{14}O_2Na^+$ (177)	$C_9H_{14}O_2$	
144	$C_7H_{12}O_3Na^+$ (167)	$C_7H_{12}O_3$	
142	$C_7H_{12}O_3Na^+$ (165)	$C_7H_{12}O_3$	
116	$C_5H_8O_3Na^+$ (139)	$C_5H_8O_3$	

From assumptions made following conclusions of the limonene analysis (see section 4.6.2) predictions of lower SOA yields are expected from photooxidation experiments, making ozone oxidation the dominant process of SOA formation. Filter analysis from ACES experiments shows the major product found in the aerosol phase as pinonic acid. Observations show that this compound was not detected in high enough quantities in the gas phase. As such it can be hypothesised that the low vapour pressure exhibited from larger mass compounds has the potential to rapidly partition and do not accumulate in the gas phase. Work conducted by Capouet et al (2006) predict that the least volatile compounds were pinic acid and pinonic acid, estimated to have vapour pressures around 3×10^{-6} torr and 6×10^{-7} torr respectively. This compares to the primary products, such as pinonaldehyde, which range from vapour pressures as 10^{-5} to 10^{-3} torr. Contradictory to this work, they identified pinic acid and proposed that a pinic acid and pinonic acid adduct is likely to play an important role in observed partitioning of pinonic acid between gas and aerosol phase (Yu et al 1999). Pinic acid was observed in the particle phase but was not present in the gas phase. This suggests that compounds with estimated vapour pressures in the region of 10^{-6} torr or lower (e.g. pinic acid) are likely to partition rapidly into the particle phase. The formation of pinonic acid can be a result of further oxidation of pinonaldehyde as presented in Figure 57. The formation of pinonaldehyde governs the photooxidation reactions as seen in the stable organic yields observed. As a secondary product, possible yield of pinonic acid formation is too small. Due to the observation pinonic acid in the particulate phase, the volatility of this C_{10} compound suggests it prefers to be in the particle phase, making it important in the potential for aerosol formation.

Another important difference to address is the dependence of aerosol formation with relative humidity. Lower yields were obtained from higher RH experiments. The dependence on SOA formation with dependency on water has been surrounded by contradicting results. Jonsson et al., (2005) provide evidence to show that SOA mass, but not necessarily SOA number concentration is dependent upon water vapour. Other studies by Fick et al. (2003) displayed no increase in SOA mass or number concentration, whereas others, Bonn et al., (2002) found the same that increasing water vapour had a decreasing effect on particle number concentration and aerosol

volume in particular for exocyclic compounds, similar to the results obtained in this study. As assumptions can be put forward that SOA yield is governed by the compounds from the stabilised CI instead of dicarboxylic acids as previously assumed. This assumption is based on the evidence that a larger SOA mass is observed with the presence of detectable levels (> 1 ppb) of compounds such as pinonic acid which as shown with ethene reactions, are dominant under “wet” conditions with the stabilised CI. However dicarboxylic acids make-up secondary and tertiary major products in the aerosol, so conditional influences for the formation of these products, and the resulting SOA yields should be studied.

4.4 limonene oxidation

Another monoterpene studied here is limonene, a cyclic monoterpene with an *para*-functional methyl group and alkene (C_1 and C_6). Limonene emissions are high from both biogenic source and household solvents (it is a common addition to cleaning products). In contrast to α -pinene, there are fewer papers describing the mechanism and identification of reaction products from limonene ozonolysis. However due to its high reactivity, and endo and exo-unsaturated bonds of the cyclic carbon structure limonene is regarded as an important monoterpene with regards to potential aerosol formation (Leungsakul., 2005).

A recently developed chemical degradation pathway of limonene has been submitted on the MCM website in 2011. Using this new scheme, amongst the theories based on ozone and photooxidation reactions of limonene, a proposed reaction scheme can be established in aid of establishing oxidation products that are expected from the degradation of the limonene system. The following examines both the ozonolysis and photooxidation pathways.

4.4.1 Limonene ozonolysis

The limonene ozonolysis experiments were conducted under “straight” and scavenged conditions. Tables 34 to 36 summarise the initial experimental conditions conducted from ozonolysis and photooxidation experiments. Figure 60 represents the gas phase composition at reaction start time and the difference in composition after an elapsed time of 2 hours. Important to note are the species of greater mass than that of limonene, as these compounds would be likely to contribute to aerosol formation through partitioning into the particle phase, or further oxidation to produce heavier compounds (with characteristics of low vapour pressures) outside of the maximum m/z range settings via the process of oligomerisation. The spectra are convoluted and fragmentation and water clusters have been identified to deconvolute the mass spectra of the oxidation products.

Table 34: Initial experimental conditions of limonene ozonolysis during TRAPOZ

Exp Date	VOC	Type	Initial Mixing ratios				RH / % ^b	Duration / min	Temp / K ^b
			[VOC] ₀ / ppbV ^c	[Ozone] ₀ / ppb ^a	[CO] ₀ / ppm	[Cyclohexane] ₀ / ppm			
07/05/08 (am)	Limonene	1	192.5	110.2			0.3	240	291.5
07/05/08 (pm)	Limonene	3	197.8	101.7		144.4	0.6	246	292.2

1, Straight Ozone/alkene, 3 with added cyclohexane, (a) measurements based on the ozone analyser, (b) values given as an average values measured over the duration of the experiment, (c) based on CIR-TOF-MS measurement

Table 35: Initial experimental conditions of limonene ozonolysis during TRAPOZ 2

Exp Date	VOC	Type	Initial Mixing ratios				RH / % ^b	Duration / min	Temp / K ^b
			[VOC] _o / ppb ^c	[Ozone] _o / ppb ^a	[CO] _o / ppm	[Cyclohexane] _o / ppm			
21/05/09 (am)	Limonene	1	84.6	117.4			1.1	190	292.8
21/05/09 (pm)	Limonene	3	204.5	113.4		148.4	0.2	210	293.5

1, Straight Ozone/alkene, 3 with added cyclohexane, (a) measurements based on the ozone analyser, (b) values given as an average values measured over the duration of the experiment (c) based on CIR-TOF-MS measurement

Table 36: Initial experimental conditions of limonene photooxidation during ACES and ACES 2

Exp Date	VOC	Type	Initial Mixing ratios			RH / %	Duration / min
			[VOC] _o / ppbV	[NOx] _o / ppbV	[VOC/NOx] _o / ppbV		
26/11/07	Limonene	a	50 (nominal)	25 (nominal)	2	50	380
27/11/07	Limonene	a	250 (nominal)	125 (nominal)	2	50	310
28/11/07	Limonene	a	100 (nominal)	50 (nominal)	2	50	360
25/06/08	β -caryophyllene	b	22.05	33.69	0.65	70	448
26/05/08	Limonene	b	95.42	46.24	2.06	72	447
	β -caryophyllene		64.67	25.4	2.55		
01/07/08	Limonene	c	20.66	20.46	1.01	82	241
	Limonene		118.76	50	2.20		

(a) nucleation experiment ; (b) β -caryophyllene seed experiment ; (c) sulphate (SO₄²⁻) seed experiment

Figure 61 exemplifies the time evolution of m/z ions observed over the limonene + O₃ system represented as 5 minute averages of all data collected from the CIR-TOF-MS. It displays the injection of limonene followed by ozone addition to denote reaction start time (i.e. 0 minutes). Following ozone addition, formation of the primary gas-phase products limonaldehyde and formaldehyde are observed.

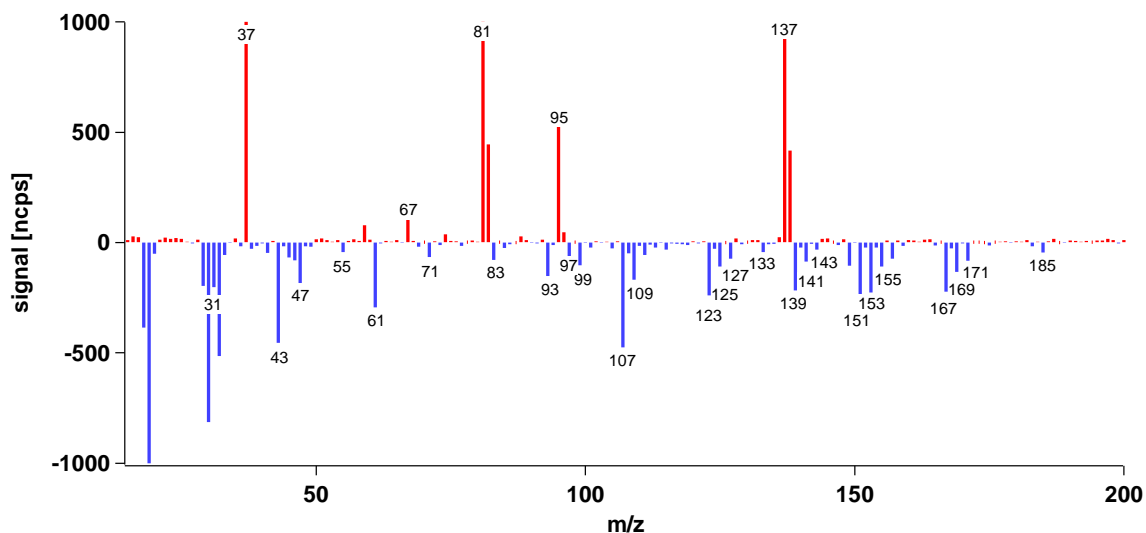


Figure 60. Gas-phase composition of limonene (red) at start of the reaction and the differing composition of the gas-phase after 2 hrs of reaction time (blue). The difference in spectra helps in easily identifying the potential oxidation products, and the fragments from the mass spectra.

Large discrepancies are also noted between instrumentation of FTIR and CIR-ToF-MS for the initial limonene concentration values. Based on the amount injected into the chamber (0.27g) and using the chamber volume, the maximum amount injected is 245 ppb. From this result it can be argued that the FTIR instrument overestimated the limonene concentrations. Examination of the scavenged experiment also highlights an overestimation in FTIR detection. Figure 62 displays the differences of theoretical calculated values compared to detected values of both instruments. FTIR data overestimates the O₃ and cyclohexane experiments 64.35% and 116.79% respectively whilst the CIR-TOF-MS obtains values 21.59% and 1.58% lower if 100% of the mass is assumed to have been into the chamber. Due to this overestimation in initial concentration of limonene, all yield calculations were made using initial concentration data from the CIR-TOF-MS.

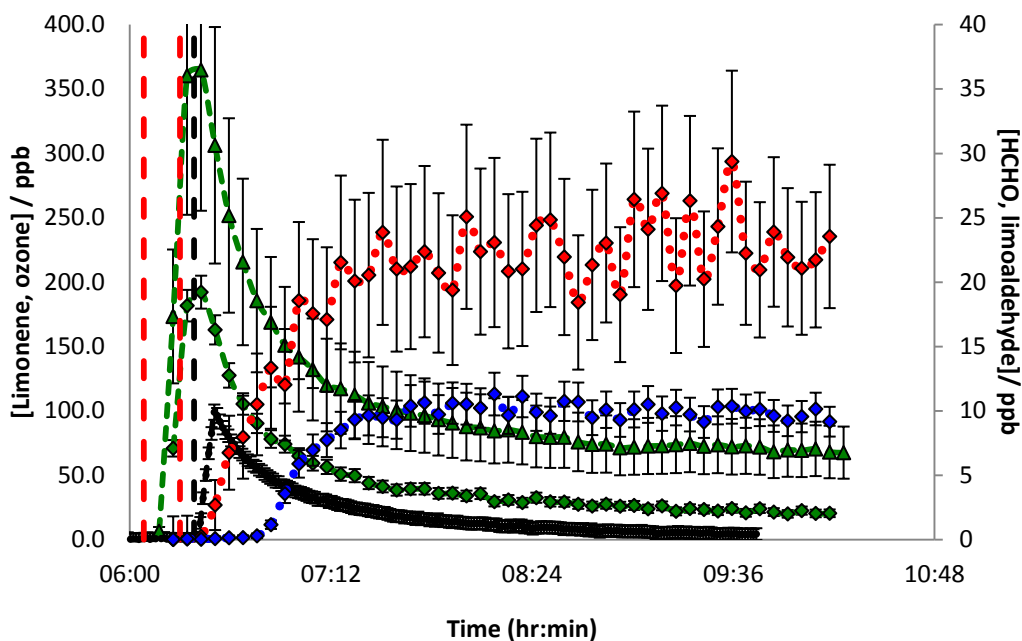


Figure 61. The time profiles of limonene (green) from both CIR-ToF-MS (diamonds) and FTIR (triangles) measurements, ozone (black) and two of the major oxidation products observed during limonene ozonolysis, HCHO (red) and limaldehyde (blue). The injection period of limonene addition (dotted red lines) is closely followed by the reaction start time with ozone addition (black lines). Almost immediate formation of HCHO is detected with fill of ozone into the chamber and after a period of 20 min the primary aldehyde is observed.

Other m/z ion channels of interest are m/z 185, 171, 155, 143 and 139 representing potential acids, ketones and bi-carbonyl species associated with limonene oxidation. These observed compounds are of interest as they all exhibit a mass larger than that of the precursor VOC, and so could have potential in forming larger species after further oxidation, or can themselves have a characteristic of low volatility and can be implicated in gas/particle partition or condensation to facilitate aerosol formation or growth.

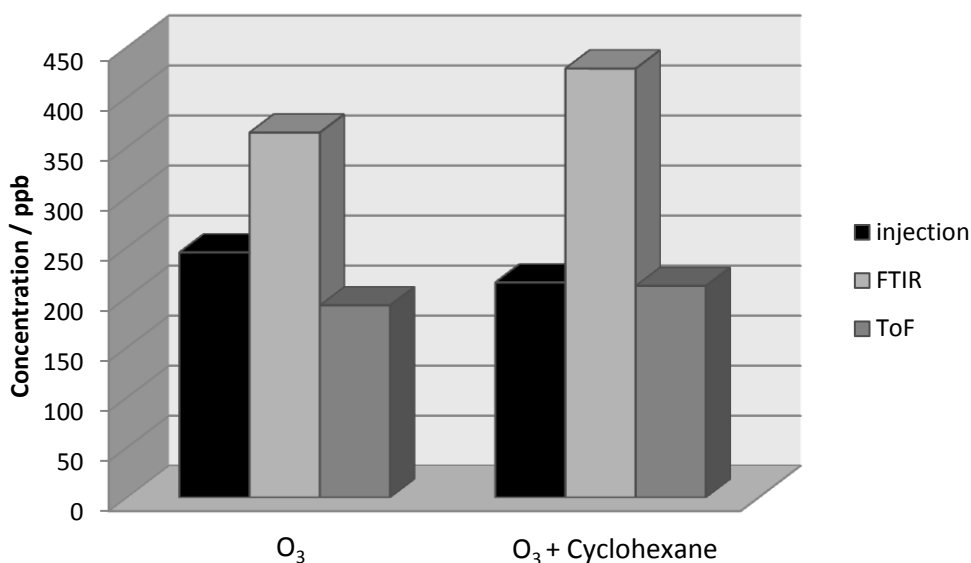


Figure 62. Calculated concentrations based on 100% of mass successfully injected into the chamber (black) and the measured concentration levels observed for both analytical instruments FTIR (light grey) and CIR-TOF-MS (dark grey). Observations conclude an overestimation as high as 116.79% for FTIR measurements and a maximum underestimation of 21.59% for CIR-TOF-MS readings.

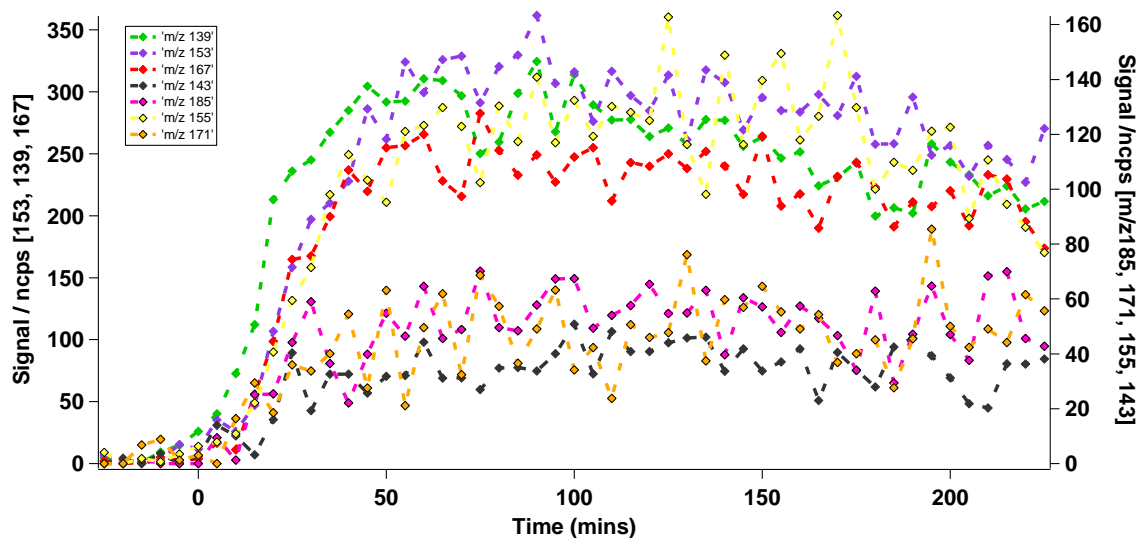


Figure 63. Time evolution of detected ions from the CIR-TOF-MS during the limonene + O₃ system, of those higher in mass than limonene

The proposed mechanism of formation of these compounds is highlighted in Figure 64. Similar to α -pinene, the initial oxidation step consists of the ozone addition to the internal cyclo $>C=C<$ bond, forming an energy-rich ozonide that undergoes rapid bond cleavage to create the Criegee intermediates (CI_1 CI_2). These are proposed to undergo similar RO_2 and HO_2 reactions similar to that postulated for the α -pinene system. The isomerisation and decomposition of the Criegee intermediates (PR_1 , PR_2 , PR_4) produce OH and directly produce stable species (HCHO, norlimal, limalic acid, 10-hydroxy-limononic acid and S_1 to S_9). Further isomerisation, RO_2/RO conversion and HO_2 reactions lead to the formation of further stable species (SI_1 to SI_{12}) and limonic acid. The thermally stabilised peroxy radical (PR_3) reacts with CO and H_2O to form limonaldehyde, and with H_2O to form limonic acid. Further oxidation of the $>C=C<$ bond of limonene produces limoketone, in addition to a formaldehyde along with further Criegee type radical species (CIS_1). This species undergoes further RO_2 and HO_2 reactions to form a new carbonyl, carboxylic acid or alcohol group (SI_{13} to SI_{14}). Of these stable products, only the “tri-carbonyl” was detected. Under dry experimental conditions limononic acid is expected to be formed in low yields due to the absence of H_2O to react with the peroxy radical (PR_3), however small signals were detected in both experiments, indicating possible further mechanistic formations of this acid are possible. Excluded from the mechanism is ozone addition to the external carbon double bond. Assuming similar chemistry with ozonide formation, limonene will retain its cyclo-carbon backbone with a primary product exhibiting a ketone functional group, replacing the external carbon double bond ($>C=CH_2$) with a carbonyl group ($>C=O$). This “keto-limonene” will have a parent ion m/z 139 corresponding to an experimentally observed m/z channel.

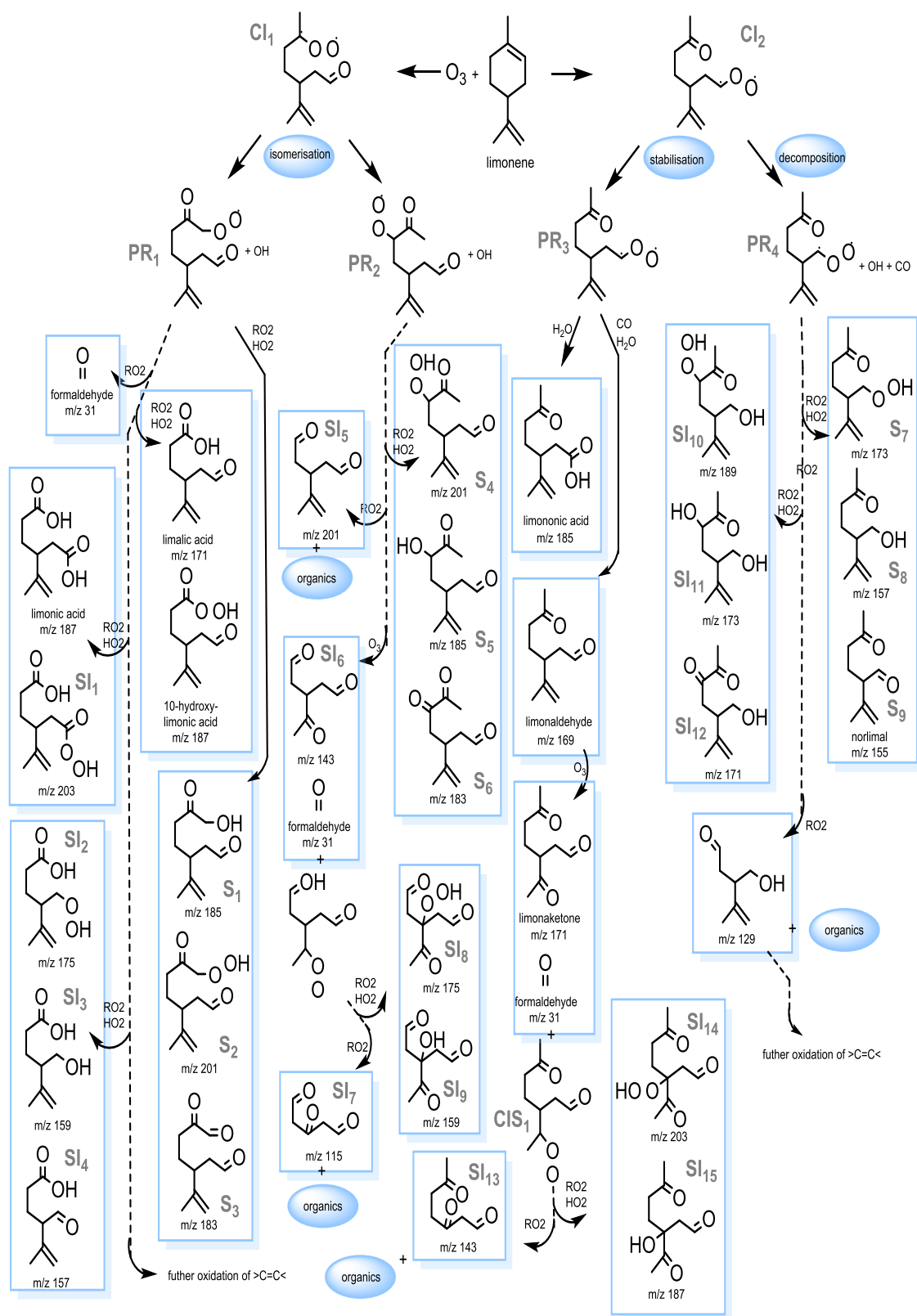


Figure 64. Proposed mechanism of limonene degradation adapted from the newly developed MCM mechanism to evaluate the initial stable oxidation products formed (in boxes). Organics encompass lower mass species HCHO, acetic acid, formic acid, acetone and methanol.

The reaction mechanism described in Figure 64 is a detailed examination of ozone addition to the endocyclic double bond because as previously observed in α -pinene, O_3 addition at this site is responsible for the formation of the larger VOCs formed and observed in both the gas and particle phase. Addition of the ozone to the external double bond will ultimately lead to the formation of a $C_9H_{14}O$ cyclic ketone compound (4-Acetyl-1methylcyclohexene, here referred to as limket as in the MCM mechanism). This would be responsible for the signal seen at m/z 139. The MCM doesn't currently account for this reaction step, but instead exclusively for ozone addition to the ozone double bond. Similar to time traces observed in α -pinene, larger oVOCs compounds were only detected during ozonolysis experiments. For photooxidation experiments, the formation of m/z ion channels were due to both limonaldehyde ($C_{10}H_{16}O_2$) and HCHO. This is expected as H-abstraction and OH addition to the endocyclic limonene will follow similar reaction pathways to α -pinene, where large carboxylic acid and ketone compounds will follow further oxidation of limonaldehyde. OH reaction to the external double bond will however form the limket compound. Nucleation experiments of limonene with three different initial concentration values show this chemistry clearly, as limonaldehyde and limket are primary oxidation products rapidly formed. A decrease in concentration follows due to limonene consumption, with the formation of secondary oxidation products. This increase in secondary oVOCs corresponds to aerosol growth observed in the chamber, discussed in section 4.6.2

4.4.2 Yields of stable organic species (limonene)

Table 32 shows a summary of the detected m/z ion channels of the limonene system under ozonolysis experiments utilising the Am^{241} ion source. The yields obtained were calculated in a similar fashion discussed in the HCHO yield formation in ethene ozonolysis. Different observed mass channels and yields were measured during the ozonolysis of limonene. The major products expected after initial ozone addition to the double-bond are the primary aldehyde (m/z 169, hereafter limonaldehyde), and

the primary ketone (m/z 171, hereafter limoketone). These were observed at the highest levels of any gas-phase product excluding formaldehyde. Dehydration and fragmentation can further complicate the spectrum, and correlation analysis can highlight associated m/z channels with such examples as dehydration (- 18 m/z) as exemplified by m/z channel 149, a dehydrated ion of m/z 167. For completeness of the mass spectra examination, all m/z ion channels have been included in Tables 37 to 39. Correlation data analysis was conducted in an attempt to identify potential fragments of larger mass species where no calibration data was available. The yields for photooxidation experiment were calculated as forementioned.

Little information regarding the kinetics of some of the proposed oxidation products exist. Fractional yields were calculated based on calibrations done based on functional groups. The calibration experiments provided "sensitivity values" for certain compounds. Based on the known sample concentrations calibration runs we are able to assess how many counts per second (cps) were equivalent to that standard sample. From this information we are able to calculate the concentration of a sample based on this sensitivity value. Here, sensitivity values are given in cps that corresponds to one ppb concentration. As seen with terpene calibrations, little variation is seen. Sensitivity values difference only by a maximum of 7.81 (32.56 and 24.75) for 5 separate species limonene, α -pinene, β -pinene, myrcene and α -terpinene. Other specific compounds (e.g. ketones) show similar sensitivity values with a total difference of 13.75 (maximum difference observed between compounds MACR 42.01, and cyclohexanone 55.75). An assumption can be made basing sensitivity values around an average of multiple compounds based on their functionality group. Yield determination of higher mass products (>100) were made on this assumption and averages of sensitivity values applied to the signals experimentally determined. If bi-functional groups were present, averages of both these functional groups were made and applied. A small range of yields would be possible, but as averages were taken the reported fractional yields represent a mid-range value. Example of maximum range of concentration is 2.07 – 3.80 ppb applied to m/z ion 139 taking into account total differences in calibration sensitivities for aldehyde compounds (applied to TRAPOZ dataset on 07/05/08 am). For limonaldehyde, the surrogate of pinonaldehyde was exploited.

Table 37. Detection of *m/z* ion channels during limonene ozonolysis experiments (TRAPOZ) with proposed structures

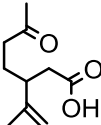
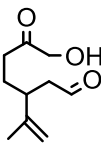
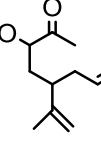
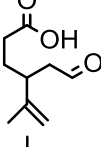
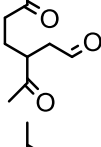
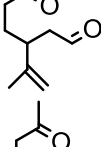
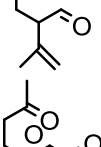
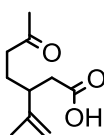
Compound Signals Detected from CIR-ToF-MS	Proposed compounds	<i>m/z</i> (identification)	Fractional yield ^b
<i>limonene + O₃</i>			
138^c, 137, 96^c, 95, 82^c, 81, 67		185 (C ₁₀ H ₁₆ O ₃) limononic acid	0.013 ± 0.004
186 ^c , 185, , 171, 169 ^c , 168, 167 ^d , 165 ^d , 157 ^d , 156 ^c , 155, 154 ^c , 153 ^d , 152, 151 ⁽¹⁶⁹⁾ , 149 ^d , 143, 141 ^d , 140 ^c , 139, 135, 133 ^d , 127 ^d , 125 ^d , 124 ^c , 123 ⁽¹⁶⁹⁾ , 115, 111 ^d , 109 ⁽¹⁶⁹⁾ , 108 ^c , 107 ⁽¹⁶⁹⁾ , 101 ^d , 99 ⁽¹⁶⁹⁾ , 97 ^d , 94, 93 ^d , 85 ^d , 83 ^d , 71 ^(169,99) , 69 ^d , 61, 55 ^e , 47, 45, 43 ^f , 41, 31		169 (C ₁₀ H ₁₆ O ₂) Limonaldehyde	0.193 ± 0.014 g
183 ^d 113 ^d , 33		155 (C ₉ H ₁₄ O ₂) norlimal	0.010 ± 0.003
		171 (C ₉ H ₁₄ O ₃) limalic acid/limonaketone	<0.01
		143 (C ₇ H ₁₀ O ₃)	<0.01
		139 (C ₉ H ₁₄ O) observed by Hakola	0.018 ± 0.002
		115 (C ₅ H ₆ O ₃)	<0.01
		61 (CH ₃ COOH)	0.023 ± 0.002
		47 (HCOOH)	0.035 ± 0.004
		45 (CH ₃ CHO)	0.003 ± 0.001
		33 (CH ₃ OH)	0.006 ± 0.001
		31 (HCHO)	0.134 ± 0.010 ^a

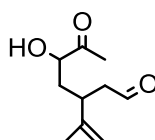
Table 37 continued

*limonene + O₃ + CHEX***138^c, 137, 96^c, 95, 82^c, 81, 67**186^c, 185, 169, 168^c, 167^d, 165,
157, 155, 154^c, 153^d, 151^{a(limon)},
149^d, 142^c, 141^d, 140^c, 139, 133,
127^d, 125^d, 123⁽¹⁶⁹⁾, 121^d, 115,
113^d, 111^d, 109⁽¹⁶⁹⁾, 107⁽¹⁶⁹⁾, 105^d,
101^d, 100^c, 99⁽¹⁶⁹⁾, 97^d, 94^c, 93^d,
86^c, 85^d, 71^(169,99), 69^d, 61, 55^e,
47, 43^f, 31

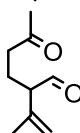
183, 45, 33

185 (C₁₀H₁₆O₃)
limononic acid

<0.01

169 (C₁₀H₁₆O₂)
limonaldehyde

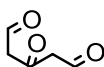
0.037 ± 0.002

155 (C₉H₁₄O₂)
norlimal

0.015 ± 0.003

139 (C₉H₁₄O)

0.026 ± 0.004

115 (C₅H₆O₃)

<0.01

61 (CH₃COOH)

0.018 ± 0.002

47 (HCOOH)

0.035 ± 0.006

45 (CH₃CHO)

0.003 ± 0.001

33 (CH₃OH)

Bdl

31 (HCHO)

0.068 ± 0.010^a**BOLD** is parent compound detection with fragments ions

a = yield obtained from FTIRb = yield obtained from CIR-ToF-MS

c = isotope (+1 *m/z*)*d* – unidentified signale = water cluster detection (structure can be H₃O⁺.H₂O and further additions of water)

f = common fragment in CIR-ToF-MS spectra

m/z^(x) = correlation for potential fragment of larger mass *x* (*R*² > 0.9)*m/z* ions in *italic* represent compounds showing a growth trend but were 3σ below background levels

Table 38. Detection of *m/z* ion channels during limonene photooxidation experiments in ACES (nucleation experiments)

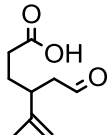
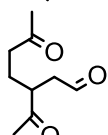
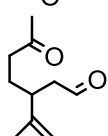
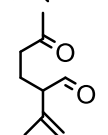
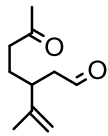
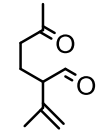
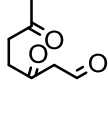
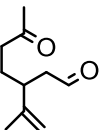
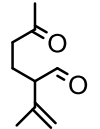
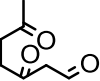
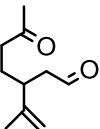
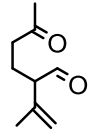
Compound	Proposed compounds	<i>m/z</i> (identification)	Fractional yield ^b
<i>limonene 26/11/07 (50 ppb)</i>			
138^c, 137, 95, 82^c, 81, 67		171 (C ₉ H ₁₄ O ₃) limalic acid/limonaketone	0.080 ± 0.004
169, 153 ^d , 151 ⁽¹⁶⁹⁾ , 139, 124 ^c , 123 ⁽¹⁶⁹⁾ , 107 ⁽¹⁶⁹⁾ , 93 ^d , 61, 45, 31		169 (C ₁₀ H ₁₆ O ₂) limonaldehyde	0.100 ± 0.002
171, 155*, 135 ^d , 127 ^d , 113 ^d , 71 ⁽¹⁶⁹⁾ , 43 ^f		155 (C ₉ H ₁₄ O ₂) norlimal	<0.01
		139 (C ₉ H ₁₄ O) observed by Hakola	0.096 ± 0.008
		61 (CH ₃ COOH)	0.104 ± 0.010
		45 (CH ₃ CHO)	0.030 ± 0.002
		31 – (HCHO)	0.940 ± 0.061
<i>Limonene (250 ppb) 27/11/07</i>			
138^c, 137, 95, 82^c, 81		169 – (C ₁₀ H ₁₆ O ₂) limonaldehyde	0.140 ± 0.020
170 ^c , 169, 168 ^c , 167 ^d , 155*, 153 ^d , 152 ^c , 151 ⁽¹⁶⁹⁾ , 143*, 141 ^d , 139, 135 ^d , 133 ⁽¹⁶⁹⁾ , 127 ^d , 124 ^c , 123 ⁽¹⁶⁹⁾ , 115 ⁽¹⁵⁵⁾ , 109 ⁽¹⁶⁹⁾ , 108 ^c , 107 ⁽¹⁶⁹⁾ ,		155 (C ₉ H ₁₄ O ₂) norlimal	<0.01
101 ^d , 99 ⁽¹⁶⁹⁾ , 97 ^d , 93 ^d , 83 ^d , 77 ^d , 75 ^d , 71 ⁽¹⁶⁹⁾ , 61, 57 ^d , 46 ^c , 45, 43 ^f		143 (C ₇ H ₁₀ O ₃)	<0.01
113, 33, 31		139 (C ₉ H ₁₄ O) observed by Hakola	0.04 ± 0.001
		61 (CH ₃ COOH)	0.157 ± 0.004
		45 (CH ₃ CHO)	0.010 ± 0.003
		31 - f(HCHO)	0.150 ± 0.004

Table 38 continued

Limonene (100 ppb)

137, 95, 81		169 (C ₁₀ H ₁₆ O ₂) limonaldehyde	0.118 ± 0.005
169, 155 [*] , 153 ^d , 151 ⁽¹⁶⁹⁾ , 141 ^d , 139, 127 ^d , 125 ^d , 123 ⁽¹⁶⁹⁾ , 115, 113 ^d , 109 ⁽¹⁶⁹⁾ , 107 ⁽¹⁶⁹⁾ , 99 ⁽¹⁶⁹⁾ , 97 ^d , 83 ^d , 77, 75 ^d , 73 ^d , 71 ⁽¹⁶⁹⁾ , 69 ^d , 61, 59, 43 ^f		155 (C ₉ H ₁₄ O ₂) norlimal	0.011 ± 0.002
167 ^d , 143 ^d , 135, 133 ⁽¹⁶⁹⁾ , 93 ^d , 33, 31		143 (C ₇ H ₁₀ O ₃)	<0.01
		139 (C ₉ H ₁₄ O) observed by Hakola	0.092 ± 0.004
		61 (CH ₃ COOH)	0.140 ± 0.005
		59 (CH ₃ (O)CH ₃)	0.032 ± 0.006
		33 (CH ₃ OH)	0.033 ± 0.008

Limonene b car seed 25/06/08

138, 137, 95, 82, 81, 67		169 (C ₁₀ H ₁₆ O ₂) limonaldehyde	0.072 ± 0.004
169, 167 ^d , 155 [*] , 153 ^d , 151 ⁽¹⁶⁹⁾ , 139, 135 ^d , 133 ⁽¹⁶⁹⁾ , 123 ⁽¹⁶⁹⁾ , 109 ⁽¹⁶⁹⁾ , 108, 107 ⁽¹⁶⁹⁾ , 101 ^d , 77, 61, 55 ^e , 47 ^{**} , 43 ^f , 33		155 (C ₉ H ₁₄ O ₂) norlimal	<0.01
143, 141, 127, 125, 115, 113, 99, 93, 83, 75, 73, 71, 69, 59, 31		139 (C ₉ H ₁₄ O) observed by Hakola	0.033 ± 0.008
		61 (CH ₃ COOH)	0.087 ± 0.010
		59 (CH ₃ (O)CH ₃)	0.013 ± 0.004
		45 (CH ₃ CHO)	<0.01
		33 (CH ₃ OH)	0.045 ± 0.005
		31 - (HCHO)	0.151 ± 0.010

Limonene b car seed 26/06/08

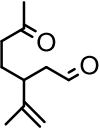
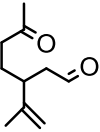
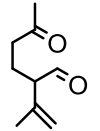
138, 137, 82, 81		169 (C ₁₀ H ₁₆ O ₂) limonaldehyde	0.079 ± 0.004
151 ⁽¹⁶⁹⁾ , 107 ⁽¹⁶⁹⁾ , 73 ^d , 61, 45, 43 ^f , 33		61 (CH ₃ COOH)	0.896 ± 0.091
		59 (CH ₃ (O)CH ₃)	0.046 ± 0.006
169, 139, 101, 75, 59		45 (CH ₃ CHO)	Bdl
		33 - (CH ₃ OH)	0.158 ± 0.010

Table 38 continued

Limonene SO4 seed

138, 137, 82, 81		169 (C ₁₀ H ₁₆ O ₂) limonaldehyde	0.056 ± 0.004
169, 155*, 153, 151, 123, 109, 107, 75, 71, 61, 59, 47, 45, 43, 33,		155 (C ₉ H ₁₄ O ₂) norlimal	<0.01
135, 127, 115, 113, 101, 99, 83, 77, 73, 31		61 (CH ₃ COOH) 59 (CH ₃ (O)CH ₃) 47 (HCOOH) 45 (CH ₃ CHO) 33 (CH ₃ OH)	0.053 ± 0.004 0.009 ± 0.001 0.047 ± 0.006 0.016 ± 0.001 0.030 ± 0.006 0.134 ± 0.010

BOLD is parent compound detection with fragments ions

b = yield obtained from CIR-ToF-MS

c = isotope (+1 *m/z*)

d – unidentified signal

e = water cluster detection (structure can be H₃O⁺.H₂O and further additions of water)

f = common fragment in CIR-ToF-MS spectra

m/z^(x) = correlation for potential fragment of larger mass x (*R*² > 0.9)*m/z* ions in *italic* represent compounds showing a growth trend but were 3σ below background levels

*Shows late formation of detected ion (~ 1 hr after lights on)

**rapid increase in detection nearing end of experiment, therefore signal due to contaminant in chamber

Table 39. Detection of *m/z* ion channels during limonene ozonolysis experiments (TRAPOZ 2)

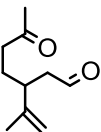
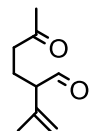
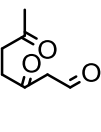
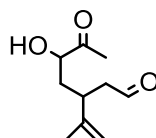
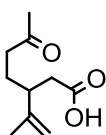
Compound	Proposed compounds	<i>m/z</i> (identification)	Fractional Yield ^b
Signals Detected from CIR-TOF-MS			
<i>limonene + O₃ (21/05/09)</i>			
137, 81, 67		169 (C ₁₀ H ₁₆ O ₂) limonaldehyde	0.076 ± 0.003
169, 167 ^d , 153 ^d , 151 ⁽¹⁶⁹⁾ , 149 ^d , 139, 133 ⁽¹⁶⁹⁾ , 125 ^d , 123 ⁽¹⁶⁹⁾ , 111 ^d , 109 ⁽¹⁶⁹⁾ , 108 ^c , 107 ⁽¹⁶⁹⁾ , 97 ^d , 93 ^d , 83 ^d , 71 ⁽¹⁶⁹⁾ , 61, 44 ^c , 43 ^f		155 (C ₉ H ₁₄ O ₂) norlimal	<0.01
155, 143, 141, 127, 113, 99, 85, 33		143 - 139 - (C ₉ H ₁₄ O) observed by Hakola 61 - (CH ₃ COOH) 47 - (HCOOH) 33 - (CH ₃ OH) 31 - (HCHO)	<0.01 0.036 ± 0.001 0.041 ± 0.002 0.043 ± 0.014 Bdl 0.230 ± 0.021 ^a

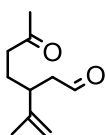
Table 39 continued

*limonene + O₃ + CHEX***138^c, 137, 95, 82^c, 81, 67**185, 169, 168^c, 167^d, 165^d, 155, 153^d,
151⁽¹⁶⁹⁾, 149^d, 140^c, 139, 133⁽¹⁶⁹⁾, 127^d,
125^d, 124^c, 123⁽¹⁶⁹⁾, 121^d, 111^d, 109⁽¹⁶⁹⁾,
108^c, 107^(169,99), 100^c, 99, 97^d, 87^d,
71^(169,99), 69^d, 61, 59, 53^d, 45, 43^f, 31

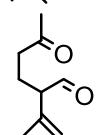
143, 141, 113, 33

185 - limononic acid

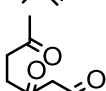
<0.01

169 (C₁₀H₁₆O₂)
limonaldehyde

0.029 ± 0.004

155 -(C₉H₁₄O₂)
norlimal

<0.01



143

<0.01

139 - (C₉H₁₄O)
observed by Hakola

0.029 ± 0.003

61 - (CH₃COOH)

0.010 ± 0.001

47 - (HCOOH)

0.032 ± 0.004

45 - (CH₃CHO)

0.004 ± 0.001

33 - (CH₃OH)

Bdl

31 - (HCHO)

0.156 ± 0.009^a**BOLD** is parent compound detection with fragments ions

a = yield obtained from FTIR and HCHO monitor b = yield obtained from CIR-ToF-MS

c = isotope (+1 *m/z*)*d* – unidentified signal

f = common fragment in CIR-ToF-MS spectra

m/z^(x) = correlation for potential fragment of larger mass *x* (*R*² > 0.9)*m/z* ions in *italic* represent compounds showing a growth trend but were 3σ below background levels

The detection of the limonoinc acid species (C₁₀H₁₆O₃, *m/z* 185) is only observed during ozonolysis experiments which is expected as this compound is predicted to be formed as a primary oxidation product from ozone addition to the internal double bond, resulting in ring cleavage after the Criegee radical (PR₃) reacts with water. As no “wet” conditions for ozonolysis reactions with limonene were made, no dependence

on RH can be made, but the presence of a scavenger reduces this fractional yield from 0.013 to less than 0.01.

Overall the presence of a scavenger reduced yields in all detected mass channels. This observation can suggest a dependence on OH reactions of limonene to produce primary aldehydes, (eg limonaldehyde ($C_{10}H_{16}O_2$)) similar to that seen in α -pinene formation of pinonaldehyde. Hakola et al., (1994) and Arey et al., (1990) have proposed the observation of limona-ketone ($C_9H_{14}O$) with yields of 0.20 and 0.174 respectively. Correlation analysis of m/z ion 139 shows it to be similar in formation of pinonaldehyde and its fragmentation ions. As previous described, these ions account for less than 1% of relative abundance of m/z ions detected for pinonaldehyde fragmentation, so the assumption can be made that the signal is responsible for the limona-ketone compound. Other compounds were only detected during ozonolysis experiments, highlighting unique oxidation products that are formed from an ozonide following immediate addition of ozone to a double bond. Grosjean et al., 1993 did not see any products formed from solely addition of ozone to the internal double bond. Here we have seen higher masses that represent potential compounds in which addition of ozone purely to the double bond can occur at this internal site. For lower mass species in nearly all cases, the oxidation product dominant was HCHO. During experiments with high RH this feature can be explained by the lowered sensitivity of the CIR-ToF-MS as previously mentioned. There seems to be relationship between sensitivity and increases in RH. As a result a small signal will produce high yields, as a lower sensitivity value (from wet calibrations) were applied to the observed "cps" signal.

4.4.3 Comparison to atmospheric model (limonene)

The MCM degradation model of limonene has only recently been updated to the website in 2011. As such, little comparison work has yet been accomplished with it. The model was run by using the current reaction rates of limonene used within the current model design, in which some of the reaction steps have not been fully

characterised. Instead construction is based on work by Saunders (2003) and Jenkin (2003). Initial set-up of the experiment conditions for an $O_3 + VOC$ reaction scheme were used to initialise the model. The results are given in Figure 65. The modelled data of the degradation of limonene fits well with the observed data obtained from CIR-ToF-MS data. Ozone degradation however is more in the model than monitored in the chamber. This could lead to potential differences in concentrations of oxidation products formed as O_3 was the major oxidant in the reaction. Both major compounds limonaldehyde and HCHO in the gas-phase are well presented with the time evolution profiles computed from the model, with the HCHO monitor and FTIR data showing a better fit than that of the CIR-ToF-MS data. As such, yield data for this compound was taken from the HCHO monitor and FTIR data. HCHO can be a difficult compound to detect under differing conditions as mentioned before (see Chapter 3). In comparison to the α -pinene model, the concentration of the limonaldehyde is overestimated. Two plausible reasons can explain this occurrence, firstly, the surrogate of pinonaldehyde used for concentration calculations are not accurate with the use of limonaldehyde as a calibrant, and secondly, the degradation pathways of the model for the formation of this compound is in its infancy and needs more experimental data to determine accurate branching ratios and reactions rates of steps leading up to this compound. The model does present good understanding of the formation of these compounds based on the shapes of the profiles given, and so further experimental work is needed to ascertain the aforementioned parameters in order to supply more accurate chemical pathways. Similar to limonaldehyde, HCHO traces are slightly overestimated in the model, suggesting a potential preference in the formation of PR_2 over PR_1 and a greater affinity to decompose the Cl_2 rather than stabilisation, as this would lower both concentrations of HCHO and limonaldehyde concentrations over the model.

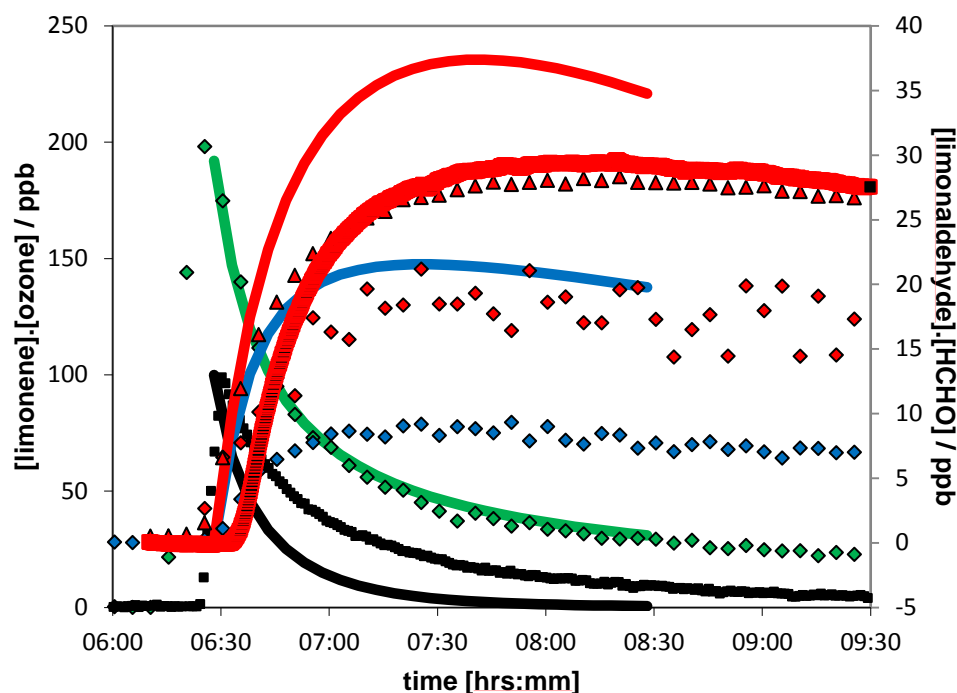


Figure 65. Comparison of experimentally determined gas-phase data (triangles FTIR, diamonds CIR-ToF-MS) to MCM outputs (lines) for a O_3 + limonene reaction depicting the degradation of limonene (green) and ozone (black) accompanied by the formation of limonaldehyde (blue) and HCHO (red)

4.4.4 SOA formation from limonene

The SOA yields obtained from limonene oxidation are given in Table 40. Here larger m/z ions are observed from ozonolysis reactions compared to photooxidation, with both relative humidity and the presence of OH scavenger having little influence on the SOA yield. An apparent difference can be seen in the SOA yield between the photooxidation and ozonolysis reactions, with the greater yield measured for the latter. As already shown, different gas-phase products are observed in the gas-phase from ozone reaction to limonene compared to photooxidation reactions. It is the formation of these larger less volatile organics that can contribute to greater extents to SOA formation compared to oVOCs found in the gas-phase under both reaction schemes (namely limonaldehyde). The presence of NO_x can also be contributing to lower yields observed in the photooxidation experiments. The formation of larger

organics is a product of oxidation to the endocyclic double bond (limononic acid [m/z 185] limonaketone [m/z 171]). Other products are present in both photooxidation and ozonolysis conditions (limonaldehyde [m/z 169], norlimal [m/z 155] and limonoketone [m/z 139] implying that SOA formation is increased from oVOCs formed as a result of endocyclic oxidation. Zhang et al., (2006) studied the effect of NO_x during ozonolysis experiments and concluded that under high NO_x conditions heterogeneous processes (oxidation of the endocyclic double bond is followed rapidly by oxidation of the exocyclic double bond) are inhibited, and oxidation of the terminal double bond dominates. Under low NO_x conditions this heterogeneous reaction is not restricted, providing further evidence that the capacity for limonene to form SOA, is governed by oxidation of the endocyclic double bond as oVOCs resultant from this are dominant in the aerosol phase. Lower SOA mass was also observed for the seeded experiments in comparison to ozonolysis conditions. This can result from the larger masses not condensing onto existing aerosols (instead oxidising to form lower mass compounds), or the absence of the larger, more oxidised species found in ozonolysis reactions, and in the presence of high NO_x .

Table 40. Aerosol yields of limonene experiments

Exp date	Campaign	Experiment	ΔVOC [ppb]	Mass peak $\mu\text{g m}^{-3}$	SOA Yield %
07/05/08(am)	TRAPOZ	VOC + O_3	171.76	401.57*	38.44
07/05/08 (pm)	TRAPOZ	VOC + O_3 + CHEX	158.28	378.14	39.28
21/05/09 (am)	TRAPOZ2	VOC + O_3	81.10	493.22	57.74
21/05/09 (pm)	TRAPOZ2	VOC + O_3 + CO (H_2O)	176.01	385.01	35.97
26/11/07	ACES	Photooxidation (low ppb)	35.31	2.78	1.29*
27/11/07	ACES	Photooxidation (high ppb)		no data	
29/11/07	ACES	Photooxidation (mid ppb)		no data	
25/05/08	ACES2	Seeded (β - caryophyllene)	94.10	572.33	9.35
26/05/08	ACES2	Seeded (β - caryophyllene)	19.76	10.35	8.61
01/07/08	ACES2	Seeded ammonium sulphate		No data	

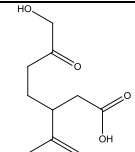
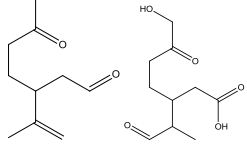
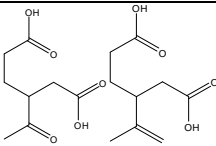
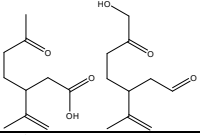
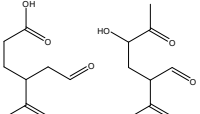
*data has not been wall loss corrected

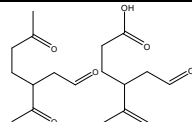
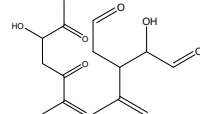
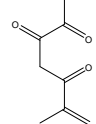
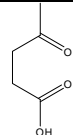
However analysis of filter samples analysed at the University of York during the photooxidation experiments have shown the presence of some of these large C₉ and C₁₀ species. It can therefore be said that these organic compounds can contribute greatly towards SOA formation. The major compounds in the particle phase identified correspond to limonic acid (m/z 201), limonaldehyde (m/z 169) and a diol carbonyl species C₁₀H₁₆O₅ (m/z 217). From these it is only limonaldehyde that has been detected in both gas and particle-phase, showing that these larger compounds exhibiting lower volatilities have a preference towards partitioning into the aerosol phase as no detection in the gas-phase of these species was made during photooxidation experiments. This corresponds to the work done by Leungsakul et al (2005) in which they observe immediate “bursts” of aerosol concentrations. These are believed to provide surfaces for more compounds to partition onto, increasing aerosol size growth. Primarily it is aldehydes in the particle phase that are capable of undergoing polymerization, forming dimers and trimers (C₃₀ to C₂₀ compounds) that have vapour pressures in the range of 10⁻⁶ to 10⁻⁹ torr. These pressures are lower than the estimated vapour pressure of the parent C₁₀ aldehydes formed from initial oxidation of limonene, predicted 2.3-7.5 at 10⁻² torr. Leugsakul et al (2005) predicted these vapour pressures using the standard method provided by MacKay et al (1982). In contrast to α -pinene oxidation products, in which it is predicted that partition of gas phase species happens readily around vapour pressures at 10⁻⁶ torr or lower, it suggests that the presence of seeds will form higher SOA yields, which was observed during the ACES experiments. The reason for this can be explained by looking at the forementioned reaction scheme where these compounds are formed from further oxidation of the aldehyde species in a OH environment. Under ozonolysis reactions, these compounds can be formed as first generation oxidation products that demonstrate dependence on relative humidity. These are governed by reactions of water vapour with the stabilised Cl to form these compounds. As such it can be suggested that the presence of water can have an influence on not only the concentrations of oVOCs formed, but also the final aerosol yield dependent upon the contribution that these species have on SOA formation.

Regarding relative humidity impacts, similar to the results observed in α -pinene show that for ozonolysis experiments, there was no dependence of water on SOA formation. Jonsson et al., (2005) investigated the humidity impacts on different terpenes and found limonene was the most efficient at forming aerosol, while least efficient was α -pinene, with an increase found with increased relative humidity. Both mass and number concentrations were observed to increase and water up-take can be explained for increase in mass, but not increase in number.

Other larger mass species identified in both gas-phase and aerosol phase were those of limonic acid. Consulting the reaction mechanism proposed earlier, limonene reactions are expected to produce a number of C_9 and C_{10} compounds, displaying low vapour pressures to accumulate into the aerosol phase. Our photooxidation yields are far below that observed by Hoffmann et al where, under

Table 41. Detected structures in particle phase from off-line analysis of filter samples from limonene. Major product is given at the top, followed by secondary and tertiary products, with the addition of identified structures (bottom)

Mass measured / amu	Ion composition (amu)	Molecular Formula	Possible structures
200	$C_{10}H_{16}O_4Na^+$ (223)	$C_{10}H_{16}O_4$	 Limonic Acid
216 168	$C_{10}H_{16}O_5Na^+$ (239) or $C_9H_{12}O_6Na^+$ $C_{10}H_{16}O_2Na^+$ (191)	$C_{10}H_{16}O_5$ $C_9H_{12}O_6$ $C_{10}H_{16}O_2$	 Limonaldehyde (<i>m/z</i> 217)
188 186	$C_8H_{12}O_5Na^+$ (211) $C_9H_{14}O_4Na^+$ (209)	$C_8H_{12}O_5$ $C_9H_{14}O_4$	
184	$C_{10}H_{16}O_3Na^+$ (207)	$C_{10}H_{16}O_3$	
172	$C_8H_{12}O_4Na^+$ (195)	$C_8H_{12}O_4$	

170	$C_9H_{14}O_3Na^+$ (193)	$C_9H_{14}O_3$	
156	$C_9H_{16}O_2Na^+$ (179) $C_8H_{12}O_3Na^+$ (193)	$C_9H_{16}O_2$ $C_8H_{12}O_3$	
154	$C_9H_{14}O_2Na^+$ (177)	$C_9H_{14}O_2$	
144	$C_7H_{12}O_3Na^+$ (167)	$C_7H_{12}O_3$	
142	$C_7H_{12}O_3Na^+$ (165)	$C_7H_{12}O_3$	
130	$C_7H_{14}O_2Na^+$ (153)	$C_7H_{14}O_2$	
116	$C_5H_8O_3Na^+$ (139) $C_6H_{12}O_2Na^+$ (139)	$C_5H_8O_3$ $C_6H_{12}O_2$	

daylight + NO_x conditions, SOA yields between 35.68% and 40.50 % for limonene were reported. These resemble more closely the yields we obtained from our ozonolysis experiments.

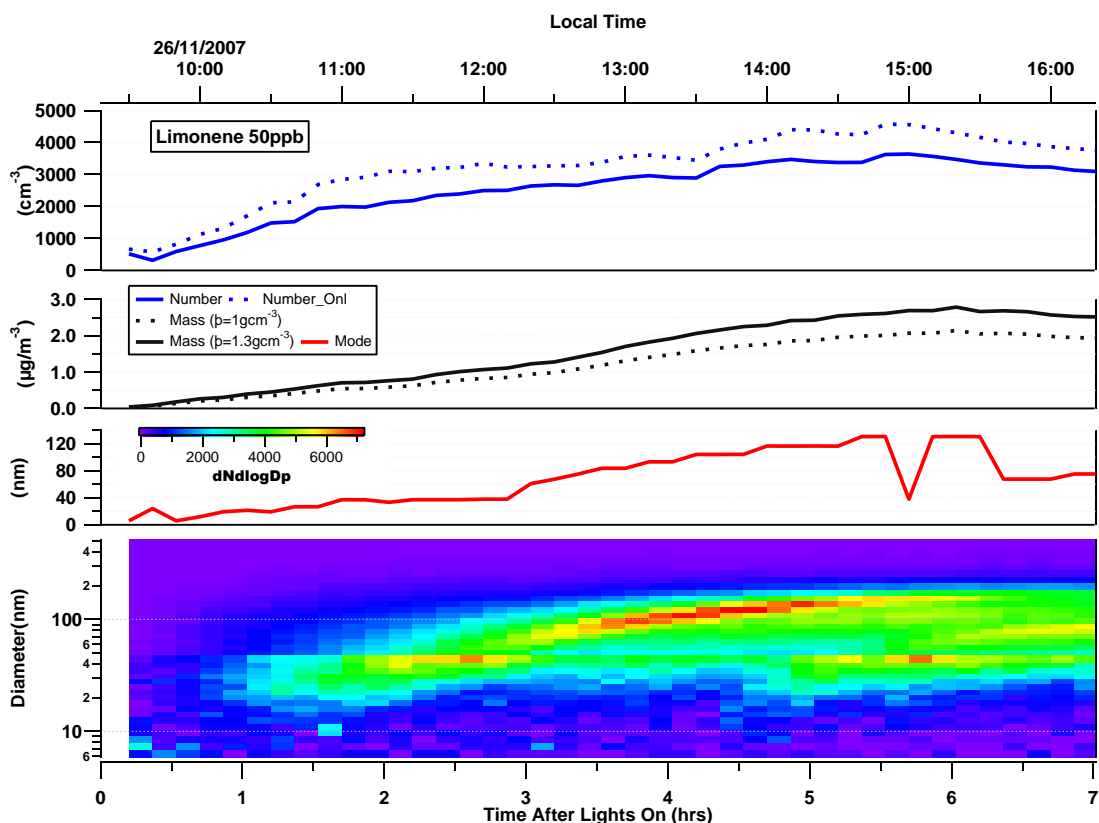


Figure 66. SOA mass analysis of limonene for low ppb concentrations, showing nucleation events and growth of aerosol.

Figure 66 displays aerosol properties of a low concentration nucleation experiment. The mass has been calculated for both a density of 1 and 1.3 to highlight the difference between the SOA mass obtained from the density used as a standard for most of the simple alkenes ozonolysis work during TRAPOZ, and the latter value, applied to those of the monoterpene experiments at MAC based on recent literature values (Bahreini., 2005; Varutbangkul., 2006).

SOA formation is not observed until after approximately 1 hour after lights on. This time interval relates to the detection of the afore mentioned compounds, namely the $C_9H_{14}O_2$ (amu 154) and $C_7H_{10}O_3$ (amu 142). Therefore these species can be principle compounds for initial partitioning of gaseous species into aerosol for further compounds to condense onto. When considering these species, the time profiles indicate that they start to form after 10 minutes in the gas phase (see Fig 63). It is after 60 minutes that the concentration stabilise to constant concentration. This event also

correlates to the formation of SOA and implies that it is at this time frame that these species (e.g. $C_7H_{10}O_3$) reach supersaturation. Further analysis done on filter samples at the University of York have identified products of similar mass in the aerosol and chemical make-up to those observed in the gas-phase at the point of nucleation in the experiment. A complete summary of analysis for limonene samples during photooxidation experiments are given in Table 36. The primary products observed in these samples belong to the primary aldehyde (limonaldehyde) and large carboxylic acid compound (m/z 185). Owing to this, plateau of limonaldehyde levels in the gas phase can be due to two reasons. The first is the partition of limonaldehyde into the particle phase, whilst itself can also be oxidised to form the other compounds as predicted in the reaction mechanism (see figure 64), including HCHO. Resultingly, limonaldehyde is a primary source for SOA formation, either directly, or indirectly and so further investigations into the fate of limonaldehyde needs to be carried out.

4.5 Discussion

Here we have presented work to show the SOA potential for 2 separate monoterpenes, α -pinene and limonene. Highlighted are the proposed dominant reaction pathways for gas-phase reactions in the chamber based on the composition and evolution of real time measurements from the chemical make-up of the chamber.

Although high mass oVOCs were responsible for SOA formed in the chamber studies, low mass oVOCs identification and yield calculations were established. The yields of HCHO observed were fairly consistent among the monoterpene species, with an increase noted under wet conditions and for myrcene. This increase in yield was detected in nearly all mass channels, showing a dependence of relative humidity on the formation of these species. The yields for acetaldehyde, formic acid, acetic acid and methanol were found to be < 15% for all monoterpenes, which corresponds to the finding found by Lee et al., (2006) and Orlando et al., (2000).

The acrylic Myrcene oxidation provided increased yields of acetone in comparison to other cyclic monoterpenes. This increase in formation can be attributed to the multiple double bonds, where primary or secondary oxidation of these double bonds is accompanied by loss of HCHO or CH₃(O)CH₃ as a result of scission.

The majority of comparisons made are focused on the higher mass oVOCs as these are likely candidate compounds that partake in SOA. Here cyclic limonene and α -pinene formed detectable levels of oVOCs with masses as large as 185, representing C₁₀ carboxylic acids. These compounds were only observed from ozonolysis experiments, as formation of these as primary sources are from O₃ addition to the endocyclic bond. This bond then cleaved following the ozonide formed and the resulting carboxylic acid and ketone functional groups. Interestingly, this keto-carboxylic acid compound is also the major product identified in filter aerosol samples during photooxidation experiments, but not detected in the gas phase. Greater SOA yields are obtained with oxidation to this endocyclic bond with precursors of the same carbon number backbone. The formation of this compound is second generation following the OH-initiated oxidation of primary aldehyde and so can account for the lower levels. Higher SOA was formed under ozonolysis conditions, indicating that the keto-carboxylic acid compound is important for SOA formation as higher levels of this compound were also observed in the gas-phase with O₃ reactions, indicating that loss of carbons with oxidation will produce compounds with higher volatile characteristics.

For cyclic monoterpenes, the primary oxidation pathways lead to a primary aldehyde under both photooxidation and ozonolysis reactions. This primary aldehyde from filter samples analysed leads to the conclusion it is also a major contributor to SOA formation, especially if it is considered that further oxidation results in the formation of these larger, less volatile compounds. These larger compounds are estimated to have vapour pressures as low as 10⁻⁶ and lower, indicating that compounds with these vapour pressures prefer to partition into the particle phase. The aldehyde compound also displayed dependence of humidity, greater quantities formed with elevated RH's, but independent of OH scavenger effects. Overall, less SOA was observed under a photooxidation regime, which supports this evaluation. SOA yields are generally the

same for the different monoterpenes with the same reaction conditions. This is in contrast to work by Leungsakul et al., (2005) that show that limonene showed higher SOA potential compared to α -pinene. Overall high SOA yields were found in dark ozonolysis reactions without the presence of an OH scavenger. These yields then declined with the presence of a scavenger, or the increase of relative humidity in all cases.

The initial MCM model comparisons to the experimental data generally show good correlation in both concentration and profile relationships. Ultimately for important detected oVOC species, calibrations of specific compounds are required to definitely compare the model output as surrogates used could slightly alter the “actual” concentrations. Despite this, the modelled results, in particular for the precursor VOCs and compounds for which calibrants were available result in good results, indicating that the MCM current modelling methods are appropriate to be applied to the gas-phase chemistry of specific compounds. However, for the trace oVOCs detected at low concentrations, further work is required as this potentially governs the SOA potential of the BVOCs investigated.

CHAPTER 5. Sesquiterpene (β -caryophyllene) Photooxidation

This chapter investigates the photooxidation of a sesquiterpene species, β -caryophyllene. The gas phase composition identified low mass ($< 100 m/z$) volatile compounds similar to those in the previous chapters for monoterpenes such as formaldehyde, acetone and acetic acid etc. Higher mass compounds were also detected that relate to oVOCs obtained from a proposed reaction mechanism developed in this work. Nucleation experiments were conducted in which SOA was produced at levels between 7 and 14 %. Rapid nucleation was observed in all experiments and this was used to produce an organic seed that is likely to be found in the atmosphere. Two BVOCs, isoprene and limonene underwent photooxidation in the presence of this seed. This chapter concentrates on the gas phase composition of β -caryophyllene oxidation, and a brief discussion mention of how the organic seed was formed and utilised.

5.1 β -caryophyllene in the atmosphere

β -caryophyllene ($C_{15}H_{24}$) is a sesquiterpene. Sesquiterpenes have not been as extensively studied as the monoterpenes and can be emitted from vegetation in large quantities (Arey., 1991; Winer., 1992; König., 1995; Helmig., 2006) and account for approximately 9% of non-methane hydrocarbons (Helmig 1999). The lifetime of β -caryophyllene is 53 min with respect to OH-radical chemistry, but as low as 2 min for reaction with ozone. As such it is postulated that the dominant removal process of β -caryophyllene is from ozonolysis and recent work has focused around that reaction scheme (Jaoui., 2003; Kanawati., 2008; Nguyen., 2009; Winterhalter., 2009; Li., 2011). Here, we examine the OH-initiated reaction of β -caryophyllene oxidation.

5.2 β -caryophyllene photooxidation

The fast aerosol growth resulting from rapid degradation of β -caryophyllene observed during these experiments prompted the development of a novel technique using a β -caryophyllene formed organic seed (Hamilton, 2011). β -caryophyllene was to produce SOA in the chamber, and this SOA was then used as a seed for the corresponding photooxidation experiment. Here, we are interested in the initial oxidation of β -caryophyllene to form the organic seed. β -caryophyllene was used as a precursor of the organic seed for photooxidation experiments of two VOCs, isoprene and limonene as part of the ACES campaign in 2008. The rapid reaction with the OH radical is almost immediately followed by a nucleation event (a few minutes). These characteristics make it a good seed for current chamber studies due to its fast seed production. Similarly Dommen et al., (2009) used α -pinene as an SOA seed for isoprene oxidation experiment. To obtain low concentrations of particles, the resulting seed underwent dilution from the chamber by extraction of air. "Clean" air was then filled to re-establish a filled bag before the VOC was introduced. The dilution of the seed resulted in amounts approximating 4 to 13 $\mu\text{g m}^{-3}$. From the results of CIR-ToF-MS almost all the β -caryophyllene reacted after 3 hours of elapsed reaction time. The bulk composition of β -caryophyllene was studied using c-TOF-AMS. The work focused on the ion m/z 44 channel as an indicator towards oxygenation level of organic aerosols (expressed as a fraction of total organic signal (Zhang 2007)). Results can be found in Hamilton et al., (2011) where the percentage of m/z 44 in the ams signal was obtained to be 4.6% showing that the first generation products are contributing to nucleation and so have low oxidation potential.

Photooxidation of β -caryophyllene was studied at the MAC facility. Initial "nucleation" experiments were conducted to run at "high" (~ 250 ppb) and "low" (~ 50 ppb) concentrations at a VOC and NO_x ratio of 2:1, resembling the conditions set for isoprene and monoterpene experiments discussed in previous chapters. The initial conditions as measured by the CIR-ToF-MS can be found in the appendix.

Following OH radical chemistry on β -caryophyllene, a reaction mechanism can be postulated. Figure 67 shows the initial degradation if the theory of OH addition to carbon-carbon double bond in the ring structure is applied.

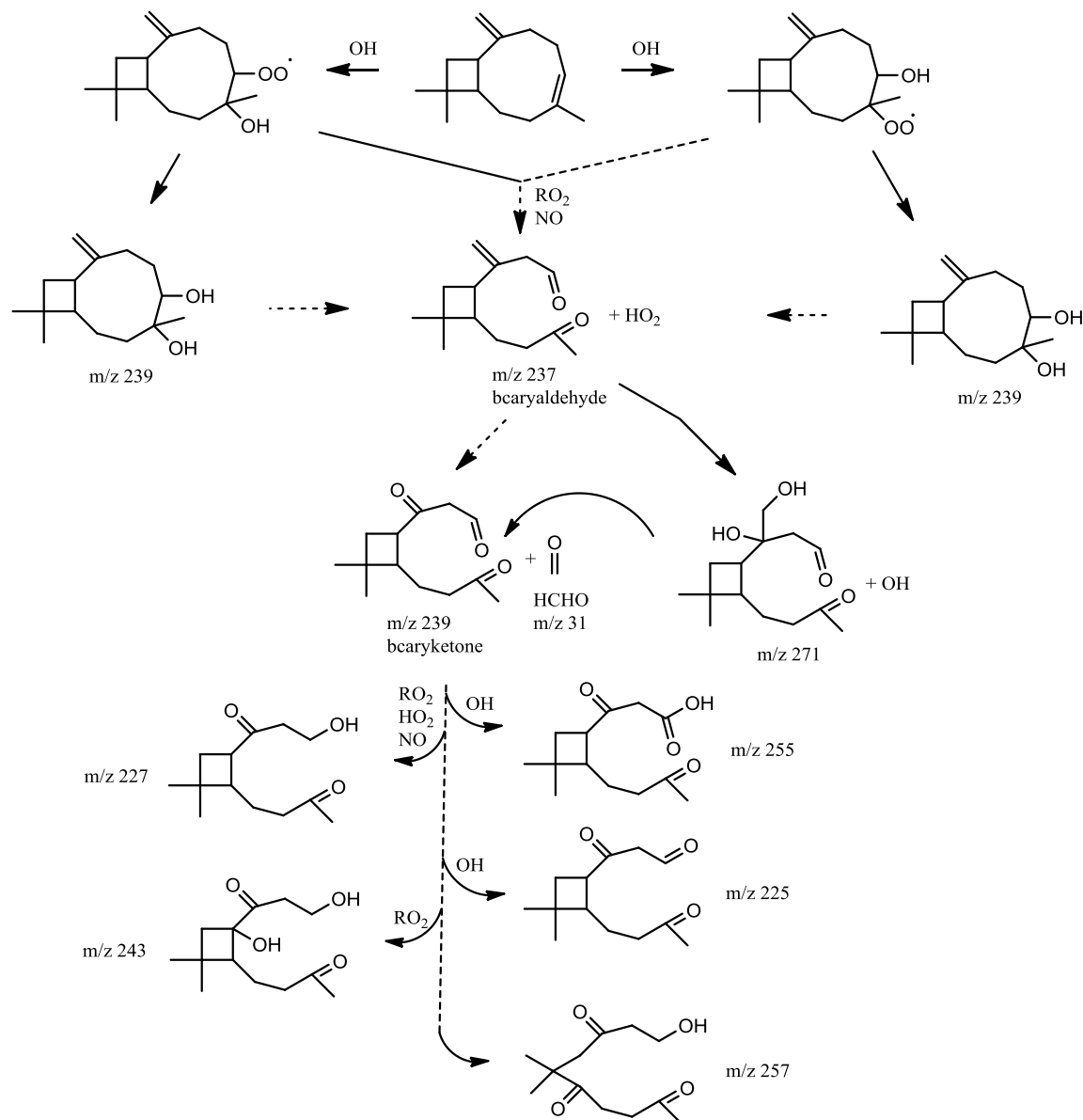


Figure 67. Degradation pathway of initial OH addition to the internal carbon-carbon double bond. This mechanism is adapted from the mechanism produced by the MCM version 2.1. The dotted lines represent several intermediate radical species formed throughout the reaction pathway. Adapted from Jenkin et al (2012).

The OH electron forms a bond with one of the electrons involved in the π -bond of the internal double bond. This leaves a localised electron around the carbon bond

adjacent to the OH addition and in an oxygen rich environment will form the excited intermediates depending on the geography of initial OH addition. Despite the two different radical species formed, the following RO_x and NO_x chemistry will form primary oxidation products (m/z 239), which in turn will also form the primary ketoaldehyde (m/z 237, here named bcaryketoaldehyde). Further degradation can form diketo-aldehyde species (m/z 239, here named bcarydiketoalde) along with formaldehyde owing to the formation of the ketone group of the external double bond. A potentially short-lived product (m/z 271) is produced from the degradation of the primary ketoaldehyde which also acts as a source of OH, before itself oxidising into the secondary diketo-aldehyde. Undergoing several oxidation steps, this diketo-aldehyde can then form further products.

Owing to the multiple bonds present in β -caryophyllene, OH addition can also occur at the external site. Figure 67 represents the mechanism where this addition can occur. With OH addition to the external double bond, following formation of the radical species, with NO and RO₂ chemistry, a primary ketone with a single carbonyl group is expected (m/z 207), unlike the heavier ketone (m/z 239) expected from addition of OH to the internal double bond formed following bond cleavage. Further RO_x, OH and NO oxidation will ultimately result in the formation of this heavier species once the internal double bond becomes oxidised. With addition of ozone to the internal double bond, following ring cleavage, the primary aldehyde is expected to be formed, and as such will follow a degradation scheme similar to that displayed in Figure 68.

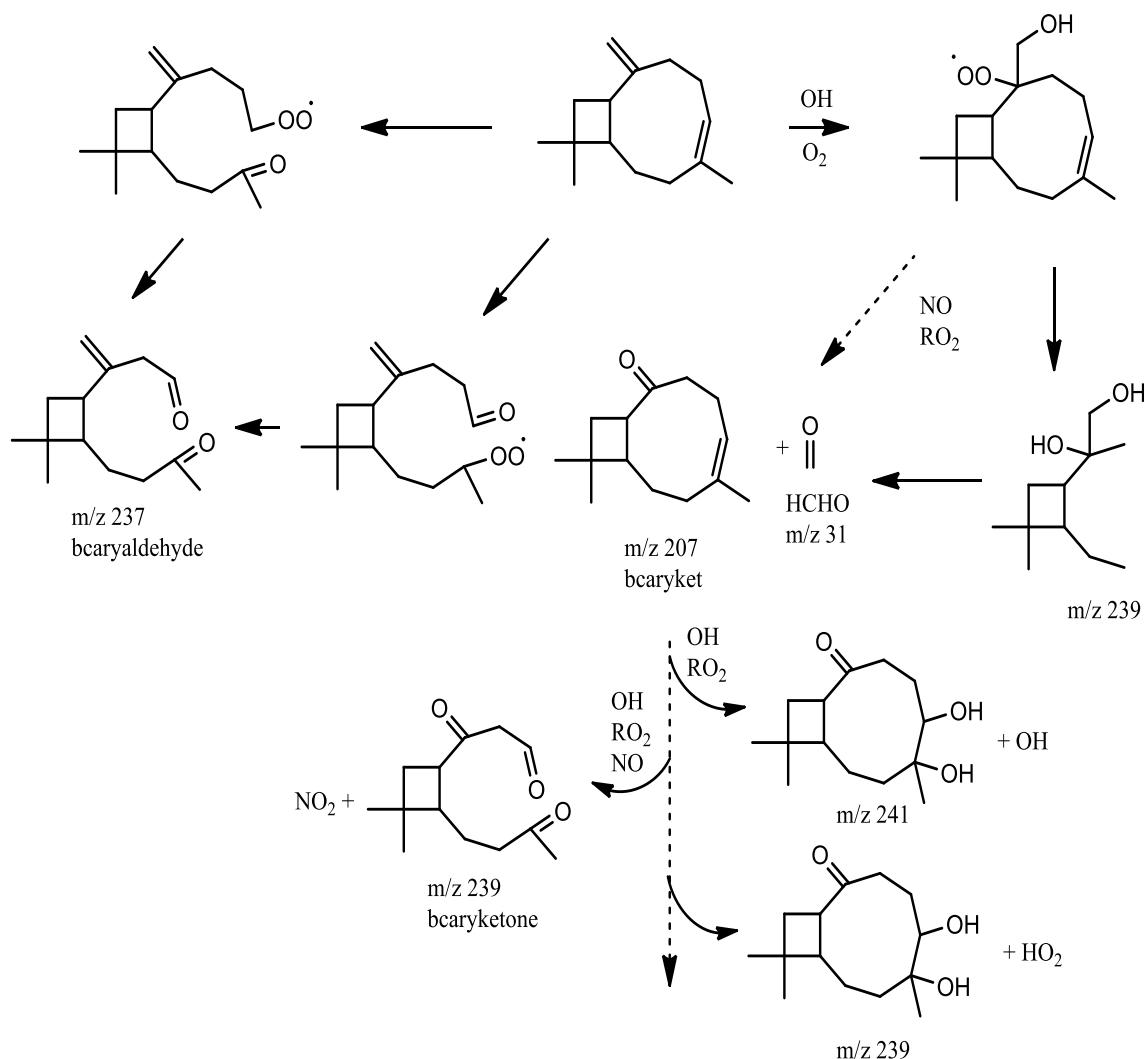


Figure 68. Chemical reaction mechanism to represent the addition of OH to the external double bond and ozone addition to the internal double bond. Following oxidation similar products are expected to be formed to those with OH addition to the internal double bond. Represented here are the expected primary oxidation products.

HCHO is expected to be produced as a result of the bond cleavage in forming the ketone species. Owing to the similarity of the oxygenated products from β -caryophyllene reactions with both OH and O_3 , the dominant species expected are the primary aldehyde and ketone species at m/z 207, 237 and 239. The detected ions detected throughout the β -caryophyllene experiments are reported in the following section.

5.2.1 Gas phase composition (β -caryophyllene)

Table 42 and 43 display the initial experimental conditions for photooxidation of β -caryophyllene during both “straight” nucleation and seeded experiments. From lights on, a rapid degradation of β -caryophyllene is observed (see Figure 69). This degradation is accompanied by production of the larger mass species followed by a slow decline in signal after steady state levels have been reached (between 1 and 2 hours). This loss is most likely due to the partition of these species into the aerosol phase giving their mass and probable lower volatilities. Analysis of filter samples (taken 2 hours and 6 hours after experiment start) identified two major oxidation compounds β -caryophyllonic acid and β -caryophyllinic acid (m/z 253 and 255). Observed lower masses such as HCHO increase steadily throughout the experiment over time.

Table 42: Initial experimental conditions of β -caryophyllene nucleation experiments during ACES

Exp Date	VOC	Type	Initial Mixing ratios			Water / % RH	Duration / min
			[VOC] _o / ppbV (nominal)	[NOx] _o / ppbV (nominal)	[VOC/NOx] _o / ppbV		
05/11/07	β -caryophyllene	a	50	25	2	52	345
06/11/07	β -caryophyllene	a	250	125	2	52	332
20/11/07	β -caryophyllene	a	50	25	2	52	340
23/11/07	β -caryophyllene	a	250	125	2	52	333

a = nucleation experiment ; b = β -caryophyllene seed experiment ; c = sulphate (SO_4^{2-}) seed experiment

As reaction of β -caryophyllene is favoured with O_3 over OH (owing to lifetimes associated with the radical species), the slow ozone formation observed during β -caryophyllene nucleation experiment can be surmised to be approximately equal to the rate of formation of ozone under conventional chamber photooxidation chemistry.

Table 43: Initial experimental conditions of β -caryophyllene seeded experiments during ACES 2

Exp Date	VOC	Type	Initial Mixing ratios			Water / % RH	Duration / min
			[VOC] ₀ / ppbV	[NOx] ₀ / ppbV	[VOC/NOx] ₀ / ppbV		
30/06/08	β -caryophyllene	b	32.97	26.04	1.27	70	420
	Isoprene		79.52	14.37	5.53		
03/07/08	β -caryophyllene	B	39.47	54.56	0.72	72	426
	Isoprene		106.01	54.17	1.96		
04/07/08	β -caryophyllene	b	48.43	48.13	1.01	72	423
	Isoprene		297.06	240.70	1.23		
25/06/08	β -caryophyllene	B	22.05	33.69	0.65	70	448
	Limonene		95.42	46.24	2.06		
26/05/08	β -caryophyllene	B	64.67	25.4	2.55	72	447
	Limonene		20.66	20.46	1.01		

a = nucleation experiment ; b = β -caryophyllene seed experiment ; c = sulphate (SO_4^{2-}) seed experiment

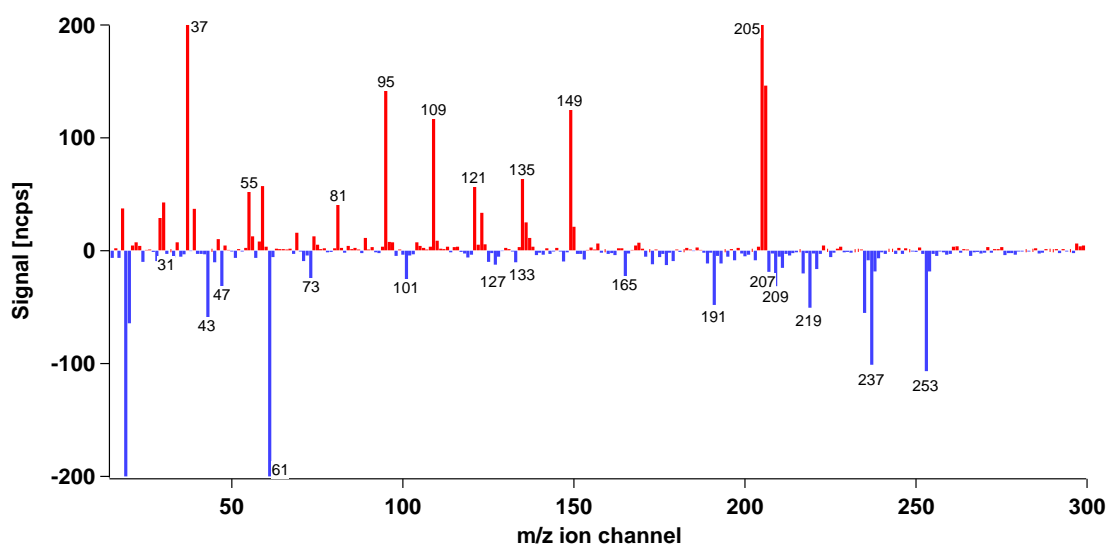


Figure 69 represents the gas phase composition of the chamber at lights on (red) and 1.5 hour after reaction time (blue) to highlight the difference in mass spectra obtained to clearly evaluate the mass channels representative of the reacted precursor and resulting oxidation products. Obvious higher mass channels of interest are visible, those at m/z ion channels 253, 237, 219, 209 and 207. Experimental results were taken from 3rd July 2008.

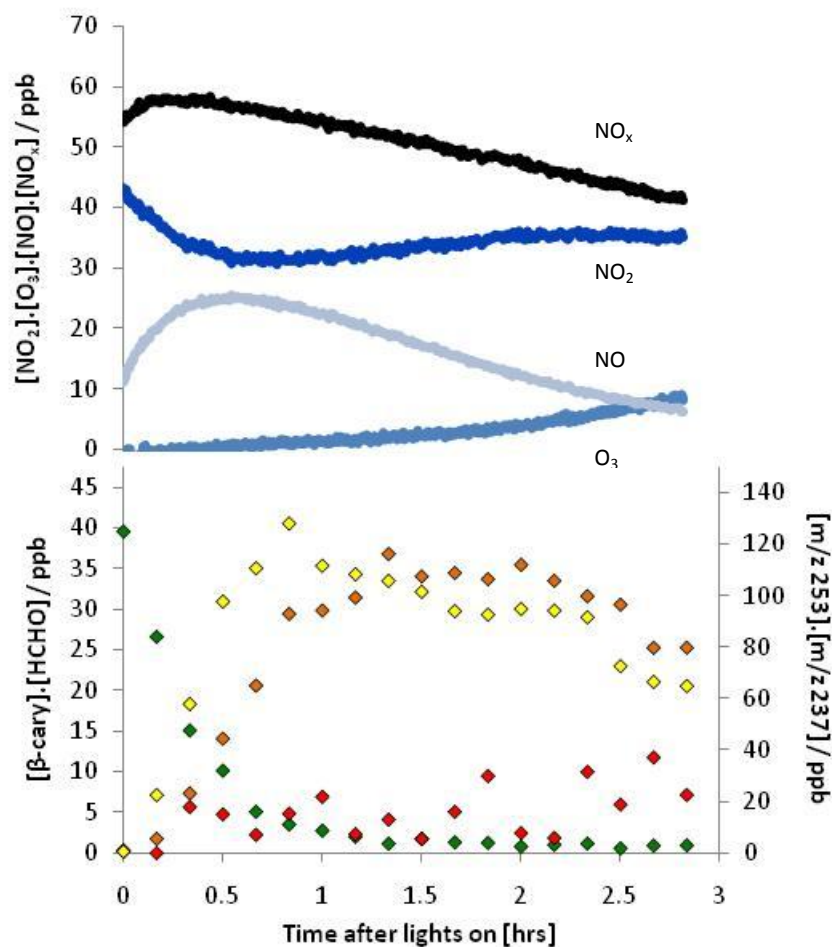


Figure 70. Initial chamber conditions (top panel) observed from the initial β -caryophyllene nucleation experiment to form an organic seed for isoprene on 3rd July 2008 for ozone (blue), NO (light blue), NO_2 (dark blue) and NO_x (black). The ozone profile differs from the other experiments observed (see monoterpene experiments in Chapter 4) where ozone formation seems to be suppressed. Uncharacteristic NO_x chemistry is also observed as NO_2 seems to stabilise during the experiment compared to a decrease accompanied by an increase in NO from other photooxidation experiments. The bottom panel shows the gas phase compositions of important species identified. CIR-ToF-MS results show rapid decreases in β -caryophyllene (green) and the evolution of high mass species, m/z 253 (orange) and m/z 237 (yellow). Formaldehyde (red) also forms gradually over the experiment time at low concentration levels.

As a result, suppressed ozone levels are measured compared to observations made in isoprene and monoterpene reactions, where a larger net increase in ozone is

monitored. This can also explain the NO_x chemistry observed during the experiment. In other chamber experiments at the same facility for different species, the reactions are “kicked-started” by the photooxidation of NO_2 , especially under the nominal conditions of 2:1 NO_x to VOC. This leads to the formation of both NO and ozone. Reactions of ozone with light and VOCs then formulate further radical species such as OH. During β -caryophyllene photooxidation experiments, initially the temporal profile of the gas chamber conditions (Figure 70) show unusual NO_x chemistry in which ozone seems to be suppressed from forming. As such the sesquiterpene acts like an ozone sink without influencing on the radical chemistry owing to the observation of the stabilised trends regarding NO and NO_2 profiles. The lack of response on the NO_x chemistry of the chamber indicates lack of radical production resultant from decomposition pathways. Similar observations were made by Hoffmann et al., (1997). After sufficient oxidation products have been formed from β -caryophyllene photooxidation, more radical species become available making the ozone less suppressed in the system. This is shown from the gradual increase in ozone levels after approximately 1.5 hours, in which more typical chamber characteristics begin to form as ozone formation is observed alongside NO to NO_2 conversion (similar to those seen in previous chapters).

Calogirou (1997) identified several oxidation products including large aldehyde oxidation products among carboxylic acids and other oxygenated products under reactions of caryophyllene with ozone. The fast reactivity in the chamber study (2 hours for almost complete reaction of β -caryophyllene) can explain the observations found by Ciccioli (1999) where detection of the sesquiterpene was discovered within the canopy but not above orange groves. β -caryophyllene was also observed as high as $0.15 \mu\text{g m}^{-3}$ in ambient air in this environment (Calogirou et al., (1997) and references within).

5.2.2 Yields of stable organics

Table 44 and 45 gives the m/z ion channels observed from all the “straight” nucleation experiments. Straight nucleation is the term given to the experiments where β -caryophyllene is photooxidised from synthesised light. The seeded experiments consisted of β -caryophyllene organic seeds were produced following straight nucleation. For purposes of β -caryophyllene analysis, only the initial stage of photooxidation during the seeded experiments is described here. The results of the final stage with isoprene and limonene introduction are described elsewhere in Chapter 4. It should also be noted that the first nucleation experiments of “high” and “low” concentrations were conducted during initial set-up of both the chamber and CIR-ToF-MS instrumentation resulting in fewer observed channels compared to the later nucleation experiments or seeded experiments. They have been included here for completeness of the experimental campaign. The intended concentrations of the “high” concentration experiments were aimed to be around 250 ppb and 50 ppb for the “low” concentrations whilst keeping a constant VOC to NO_x ratio of 2:1.

Table 44. Detection of m/z ion channels during β -caryophyllene nucleation experiments

Compound	m/z - Identification	Fractional yield
Signals Detected from CIR-TOF-MS		
β -caryophyllene (50 ppb) (05/11/07)		
205 149, 135, 123, 109, 95, 81	61** (CH_3COOH)	0.682 ± 0.271
101, 61, 43	59** ($\text{CH}_3(\text{O})\text{CH}_3$)	0.122 ± 0.039
59,	47 (HCOOH)	Not observed
	45 (CH_3CHO)	Not observed
	31 (HCHO)	< 0.01
β -caryophyllene (250 ppb) (06/11/07)		
206, 205, 149, 135, 123, 109, 95, 81		
237*, 221 ^{(239)^} , 207, 107, 97, 61, 59, 55, 45, 43	253 ($\text{C}_{15}\text{H}_{24}\text{O}_3$)	0.014 ± 0.002
	237** ($\text{C}_{14}\text{H}_{23}\text{O}_4$)	0.035 ± 0.004
	61** (CH_3COOH)	0.711 ± 0.329
253*, 101,	59** ($\text{CH}_3(\text{O})\text{CH}_3$)	0.060 ± 0.009
	47 (HCOOH)	<0.01
	45 * (CH_3CHO)	0.030 ± 0.006
	31 (HCHO)	<0.01

Table 44 continued β -caryophyllene (250 ppb) (23/11/07)

206, 205, 149, 135, 123, 109, 95, 81,		
254, 253, 237, 236, 235, 221 ^{(239)^} , 219, 217,	253 (C ₁₅ H ₂₄ O ₃)	0.070 ± 0.008
209, 208, 207, 204, 203, 197, 195, 193,	237 (C ₁₄ H ₂₃ O ₄)	0.023 ± 0.005
191, 189, 179, 177, 175, 167, 165, 161, 153, 151, 147,	61 (CH ₃ COOH)	0.120 ± 0.010
127, 125, 115, 113, 101, 93, 85, 83, 71, 61, 59, 45, 43,	59 (CH ₃ (O)CH ₃)	0.015 ± 0.003
33, 31	45 (CH ₃ CHO)	0.013 ± 0.002

 β -caryophyllene (50 ppb) (20/11/07)

205, 149, 135, 123, 109, 95, 81		
253, 237, 171, 129, 119, 107, 101, 89, 85, 83, 77, 75,	253* (C ₁₅ H ₂₄ O ₃)	0.289 ± 0.015
73, 61, 59, 45, 43, 33,	237 (C ₁₄ H ₂₃ O ₄)	0.013 ± 0.002
235, 207, 221, 219, 207, 193, 191, 189, 177, 165, 33, 31	61 (CH ₃ COOH)	0.421 ± 0.198
	59* (CH ₃ (O)CH ₃)	0.183 ± 0.052
	45** (CH ₃ CHO)	0.476 ± 0.212
	33 (CH ₃ OH)	bdl
	31 (HCHO)	bdl

BOLD = parent MH⁺ and fragments

*Detection of increase only observed 1.75 hrs after lights on and yield calculation based accordingly

** Detection of increase observed after 3 hrs after lights on. Yield is based on low concentration of VOC reacted from this time

^ Lee et al observe an *m/z* ratio ion at 239. 221 is most probably a dehydrated fragment of this.Italic *m/z* ion represent channels in which growth is detected, but is less than 3 σ of background detection.**Table 45.** Detection of *m/z* ion channels during β -caryophyllene seeded experiments

Compound	<i>m/z</i> - Identification	Fractional Yield
Signals Detected from CIR-TOF-MS		
β -caryophyllene (seed limonene) (25/06/08)		
205 149, 135, 109, 95, 81,		
254, 253, 238, 237, 235, 221, 217, 209, 193, 192, 191,	253 (C ₁₅ H ₂₄ O ₃)	0.121 ± 0.028
165, 61, 55, 43	237 (C ₁₄ H ₂₃ O ₄)	0.065 ± 0.013
	207	<0.01 ±
*Lower masses do not increase substantially	61 (CH ₃ COOH)	0.112 ± 0.024
β -caryophyllene (seed limonene) (26/06/08)		
206, 205, 149, 135, 109, 95, 81		
254, 253, 238, 237, 235, 221, 219, 217, 209, 208, 207,	61 (CH ₃ COOH)	0.259 ± 0.098
203, 191, 189, 179, 165, 147, 87, 61, 55, 45, 43,		

Table 45 continued

β -caryophyllene (seed isoprene) (30/06/08)		
205 149, 135, 109, 95, 81,	253 (C ₁₅ H ₂₄ O ₃)	0.144 \pm 0.021
254, 253, 237, 235, 209, 191, 61, 55	237 (C ₁₄ H ₂₃ O ₄)	0.054 \pm 0.009
	207	0.018 \pm 0.003
	61 (CH ₃ COOH)	0.269 \pm 0.034
	33 (CH ₃ OH)	0.036 \pm 0.002
β -caryophyllene (seed isoprene) (03/07/08)		
205 149, 135, 109, 95, 81,	253 (C ₁₅ H ₂₄ O ₃)	0.248 \pm 0.047
253, 237, 235, 219, 209, 207, 203, 191, 179, 177, 165,	237 (C ₁₄ H ₂₃ O ₄)	0.053 \pm 0.007
133, 87, 73, 71, 61, 59, 55, 47, 45, 43, 33	207	0.014 \pm 0.001
	61 (CH ₃ COOH)	0.194 \pm 0.027
	47 (HCOOH)	0.039 \pm 0.010
	33 (CH ₃ OH)	0.054 \pm 0.010
β -caryophyllene seed isoprene) (04/07/08)		
206, 205 149, 135, 109, 95, 81,	253 (C ₁₅ H ₂₄ O ₃)	0.154 \pm 0.023
254, 253, 237, 235, 219, 217, 209, 208, 207, 191, 189,	237 (C ₁₄ H ₂₃ O ₄)	0.070 \pm 0.009
165, 153, 147, 139, 101, 99, 61, 59, 45,	207	0.024 \pm 0.007
	61 (CH ₃ COOH)	0.161 \pm 0.021
	59 (CH ₃ (O)CH ₃)	0.025 \pm 0.007
	47 (HCOOH)	Bdl
	33 (CH ₃ OH)	Bdl

BOLD = parent MH⁺ and fragments

The β -caryophyllene experiments produce several oxidation products. Previous experiments on monoterpenes show the presence of species with higher masses than the parent VOC. These are likely to be characteristic of lower volatilities and are candidates for aerosol formation. The primary oxidation products observed in the experiment corresponded to m/z ion channels 253 and 237. Other smaller oxidation products were also observed in the form of acetone, formic acid, acetic acid and acetaldehyde. The larger mass compounds detected could be representative of the primary aldehyde and ketone established from the reaction mechanism described in Figure 67 and 68. Using the proposed mechanistic steps based on theoretical reaction steps, primary aldehyde and primary keto-compounds are expected with corresponding m/z ion channels 239 (β -nocaryophyllene aldehyde) and 237 (β -caryophyllene aldehyde) respectively. These two masses were reported by Jaoui et al 2003 as observed condensed products of β -caryophyllene ozonolysis as they exhibit

low volatilities. Experiments detected the β -caryophyllene aldehyde (m/z 237) at substantial concentrations in the gas phase when compared to other detected products. The time profile of this mass channel indicates rapid formation after lights on followed by a decrease in concentration after 0.83 hours. Unlike the atmospheric chamber in Spain, the flexible collapsible bag of the Manchester aerosol chamber forms a dynamic environment in which the dilution aspect is minimal. As such, this loss observed is most likely due to the primary aldehyde oxidising further to form the primary ketone, and partitioning into the particle phase as well as wall loss to the chamber. Owing to the small amount of potential primary ketone detected at m/z ion channel 239, it can be theorised that the loss of primary aldehyde is due to partitioning into the particle phase. Examination of the filter samples taken analysed at the University of York will ultimately confirm or deny this hypothesis. The absence of the primary ketone cannot be ignored however, as filter samples from monoterpene experiments demonstrated the presence of species predicted to be formed in the gas-phase identified in only the aerosol phase. Similar results could transpire here with direct partitioning into particle phase of some of the large gas phase species with low volatility.

Even higher m/z ions were detected at 253. Given the time evolution it corresponds to the characteristics displayed by the primary ketoaldehyde, and so can be deemed a primary oxidation product. Further, the proposed mechanism described in Figure 66 shows the formation of the primary ketone following OH addition to the external bond. Here, we have detected the formation of a ketone species (named bcaryket), corresponding to the m/z ion channel 207. Past work on the gas-phase examination of the β -caryophyllene system with ozone by Colagiriou et al., (1997) did not detect the C_{14} unsaturated ketone compared to the work done by Grosjean et al., (1993). Here we have tentatively identified a suspected ketone species at the corresponding mass. Obvious reasons for Colagiriou et al., (1997) not detecting this ketone is owing to the ozone focused experiment, whereas this ketone is formed from OH addition to the external C-C double bond. However, Colagiriou et al., (1997) do identify three dominant oxidation products, one ketoaldehyde (m/z 237) detected in our experiments with high concentration and seeded experiments. A second dominant

oxidation species proposed is the diketoaldehyde species that we assume in the mechanism with a mass of 238. Colagirou et al., (1997) identify this compound, however within our experimental results we do not identify this mass channel. We also do not observe m/z ion at 239.

Low mass compounds detected are similar to those seen in isoprene and monoterpene oxidation. Colagirou et al., (1997) identify formaldehyde as another major product from β -caryophyllene ozonolysis. We do not substantially detect formaldehyde is quantities above 3σ of the background noise, used as an indicator for any species observed above background levels. Although formaldehyde is suspected to accompany the formation of some of the primary oxidation products, we cannot quantitatively say we detect its formation.

The yields of low mass species are dominated by acetic acid given a fractional yield from as low as 11% to a high of 77%. The temporal profiles of acetic acid formation during different experiments also produced differing results, with late detection of acetic acid observed for several experiments (these observations have been highlighted in the summary Tables 23 and 24). Unknown characteristics of the newly developed hollow cathode ion source could provide an explanation for these unexpected results as similar observations were also seen amongst other low mass compounds. Thereby an obvious conclusion is that these results come from artefacts of the ion source or external interferences from the laboratory environment. Lee et al (2005) reported on yields of lower mass compounds from formaldehyde (mass 30) to acetic acid (mass 60) under ozonolysis experimental regimes. Here the yields obtained differ substantially. Owing to the low concentrations and wet conditions this observation is not unexpected owing to the difficulty in detection of formaldehyde as explained previously in Chapter 3.

Yields of lower mass species were difficult to determine as observations displayed uncharacteristic time profiles of oxygenated species. For example Figure 71 displays the time profiles of acetic acid from two different experiments. The red trace displays "normal" profiles as acetic acid is formed following reaction start over time. The blue trace displays aberrant profiles, where acetic acid is observed at the start of some

experiments, with a delayed formation of acetic displayed after 100 min where 77% of β -caryophyllene has been reacted. These results were observed under the direct nucleation experiments from first ACES campaign. However, during the photooxidation of β -caryophyllene in the seeded experiments (conducted during the second intensive ACES field campaign) higher levels were detected for lower mass compounds (Figure 72). Resultant yields of the smaller weight species were taken predominately from the seeded experimental work.

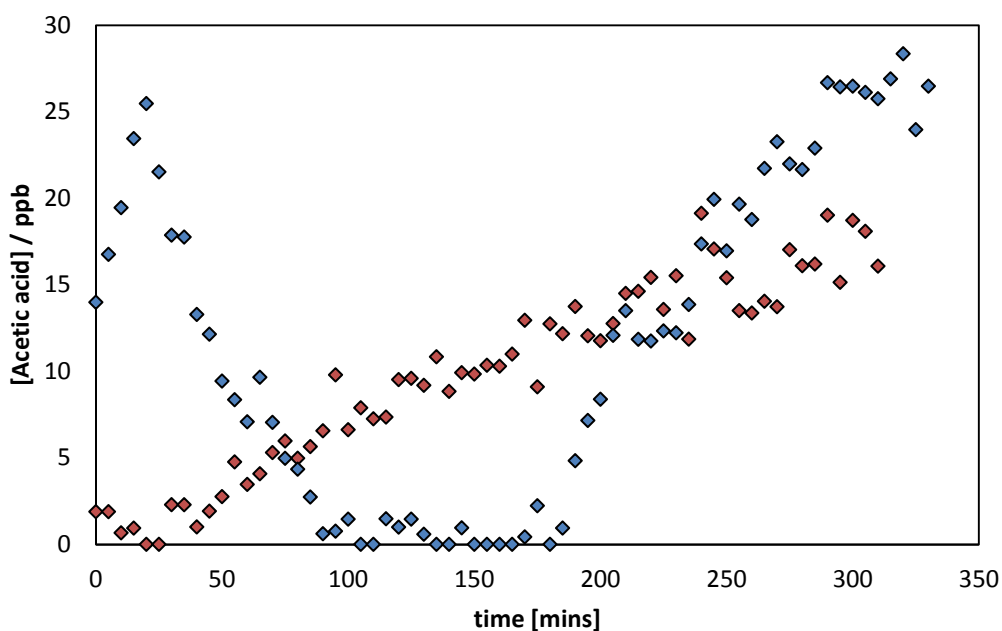


Figure 71. Acetic acid time profiles obtained from “straight” β -caryophyllene nucleation experiments. Differing profiles made yield determination difficult to assess for specific experiments. 250 ppb experiment (red), 250 ppb experiment original (blue)

Lee et al., (2006) found that formaldehyde was the major oxidation product of the lower mass species ($m/z < 100$). Our results show that acetic acid was the dominant oxidation product at 20% yield of the lower range masses. Several reasons could explain this observation, firstly the high levels of acetic acid could be due to external sources, potential injection problems within the chamber set-up, and the low concentrations of β -caryophyllene examined, coupled with the difficulty of humid concentrations on ion exchange within the drift cell would bring detection close to

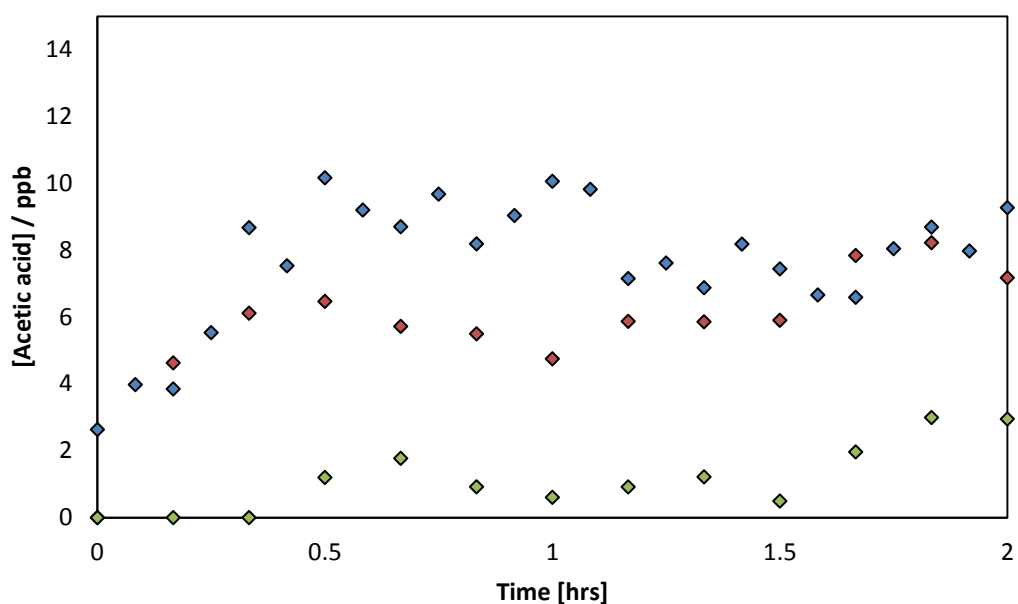


Figure 72. Acetic acid time profiles during phase 1 of the seeded isoprene experiments. Compared to the nucleation experiments in figure 68, the shape of evolution of acetic acid are consistent among all three experiments conducted on 30th June (green), 3rd July (red) and 4th July (blue)

minimum sensitivity levels of the CIR-ToF-MS instrument utilised. With formaldehyde previous work established yields at high as 80% (Grosjean et al (1993) and 76% (Lee., 2006), and as low as 14% (Calogirou., 1997). Our work reports yields below this owing to the sensitivity problem associated with our instrument in humid conditions. Other lower mass compounds such as acetone were only detected for a few experiments, and along with methanol, formic acid and acetaldehyde. Our average yields show 0.081, 0.036, 0.039 and 0.173 respectively (when observed above background signal). Fractional yields reported from Lee et al., (2005) show acetone (0.011 ± 0.003), formic acid (0.039 ± 0.001) and acetaldehyde (0.009 ± 0.003) indicating that low mass species for β -caryophyllene are not as prevalent compared to other species discussed in previous chapters. Despite this, the more interesting larger mass compounds in terms of SOA formation potential were clearly detected, the most intriguing at m/z ion 253 which, to our knowledge, has yet to be reported elsewhere in yields in the gas phase. Reported yields here must be regarded as tentative analysis for these larger species, as

sensitivity values were employed based around the functional groups, and no direct calibration was possible.

5.3 SOA yield (β -caryophyllene)

The aerosol yield obtained from the DMPS was calculated based on the approximation of a mass density of 1.3 taken from the work conducted by Bahreini., (2005) and Varutbangkul., (2006) following the same theory as previously described (see Chapter 2). Figure 73 displays the SOA mass and SOA number concentrations obtained from DMPS measurements.

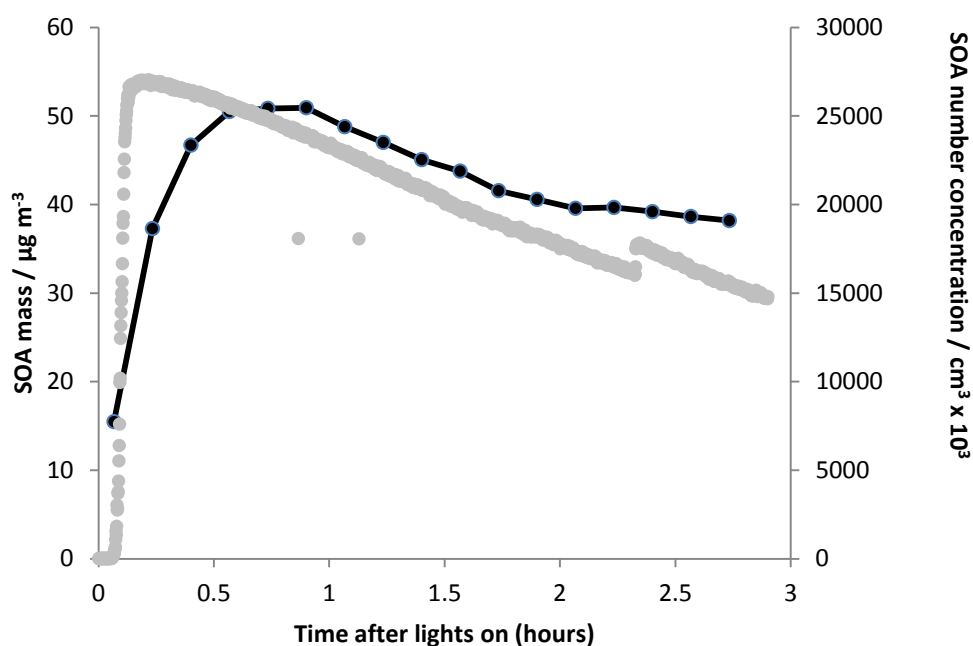


Figure 73. DMPS data for the SOA mass (black) and SOA number concentration (grey) for photooxidation of β -caryophyllene for the initial stage of a seeded experiment from an isoprene photooxidation experiment on 3rd July 2008

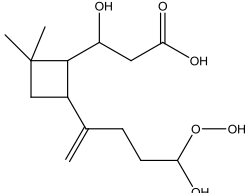
Table 46 Aerosol yield of β -caryophyllene seeded experiments during 2008

Exp date	Type	AVOC [ppb]	Mass peak $\mu\text{g m}^{-3}$	SOA Yield %
25 th June	Seed for limonene	21.21	27.37	14.14
26 th June	Seed for limonene	63.95	40.93	7.01
30 th June	Seed for isoprene	31.81	34.38	11.85
3 rd July	Seed for isoprene	38.92	50.92	14.34
4 th July	Seed for isoprene	47.55	46.70	10.77

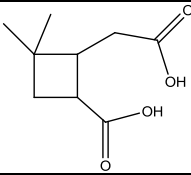
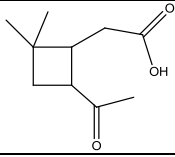
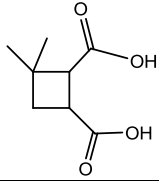
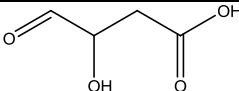
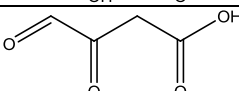
Mass data from the DMPS has not been wall loss corrected.

During the experiments in which β -caryophyllene was used as an organic seed DMPS observed SOA mass peaks of $27.12 \mu\text{g m}^{-3}$ and $40.60 \mu\text{g m}^{-3}$ for the limonene experiments and a range between $34.38 \mu\text{g m}^{-3}$ and $50.92 \mu\text{g m}^{-3}$ for the isoprene experiments, all within 1 hour of reaction time. The results are given in Table 46. The overall aerosol yield of the initial nucleation experiment over a 3 hour period was found to be in the region of 7-15%, lower than that of previously reported yields of 45% and 39% respectively (Lee et al (2006) and Jaoui et al (2003)). Aerosol yields observed are marginally higher for β -caryophyllene compared to limonene for photooxidation experiments from the same chamber studies (by 9 %). This suggests that β -caryophyllene is a greater contributor to SOA formation than limonene, and so sesquiterpenes should be considered important for SOA formation despite their lower global emission estimations.

Table 47. Detected structures in particle phase from off-line analysis of filter samples from β -caryophyllene. Major product is given at the top, followed by secondary and tertiary products, with the addition of identified structures (bottom)

Mass / amu	Ion composition (AMU)	Molecular Formula	Possible structures
288	$\text{C}_{14}\text{H}_{24}\text{O}_6\text{Na}^+$ (311)	$\text{C}_{14}\text{H}_{24}\text{O}_6$	

272	$C_{13}H_{20}O_6Na^+$ (295)	$C_{13}H_{20}O_6$	
268	$C_{15}H_{24}O_4Na^+$ (291)	$C_{15}H_{24}O_4$	
256	$C_{13}H_{20}O_5Na^+$ (279)	$C_{13}H_{20}O_5$	
254 (caryophyllinic acid)	$C_{14}H_{22}O_4Na^+$ (277)	$C_{14}H_{22}O_4$	
252 (caryophyllonic acid)	$C_{15}H_{24}O_3Na^+$ (275)	$C_{15}H_{24}O_3$	
242	$C_{13}H_{22}O_4Na^+$ (265)	$C_{13}H_{22}O_4$	
238	$C_{14}H_{22}O_3Na^+$ (251)	$C_{14}H_{22}O_3$	
226	$C_{12}H_{18}O_4Na^+$ (249)	$C_{12}H_{18}O_4$	
200	$C_{10}H_{16}O_4Na^+$ (223)	$C_{10}H_{16}O_4$	
198	$C_{11}H_{19}O_3Na^+$ (221)	$C_{11}H_{19}O_3$	

186	$C_9H_{14}O_4Na^+$ (199)	$C_9H_{14}O_4$	
184	$C_{10}H_{16}O_3Na^+$ (197)	$C_{10}H_{16}O_3$	
172 (nor-caryophyllenic acid)	$C_9H_{16}O_3Na^+$ (195)	$C_9H_{16}O_3$	
118	$C_4H_6O_4Na^+$ (141)	$C_4H_6O_4$	
116	$C_4H_4O_4Na^+$ (139)	$C_4H_4O_4$	

Dekermenjian et al., (1999) identified ketones and aldehydes as the dominant functional groups in the aerosol-phase reaction products. In addition, carbonyl groups were also observed with hydroxyl groups present in both carboxylic acid and alcohol structures. Aerosol phase composition from β -caryophyllene oxidation are analysed from LC-MS (Hamilton et al., 2008), the results of 19 identified compounds given in Table 47. The most abundant compounds were identified as β -caryophyllonic acid (m/z 253) and β -caryophyllinic acid (m/z 255). Oxidation of the external double bond will result in loss of 1 carbon and the resulting oVOC will be a prime example for SOA formation owing to the low volatility of the C_{14} compound. The presence of lower volatility species can explain the higher aerosol mass obtained. Past studies have found even higher aerosol yields in photooxidation experiments. Griffin (1999) recorded yields up to 80% whilst Hoffman et al., (1997) established yields of greater than 100% under daylight experiments in the presence of NO_x . Despite these high numbers, lower SOA yields have also been reported by Winterhalter et al., (2009) giving a range between 6% and 41% under varied ozonolysis experiments. Our yield results fall within the lower range of those reported, indicating that ozone reaction with β -caryophyllene is an important atmospheric process with regards to SOA

formation. Here we demonstrate that, although the sesquiterpene SOA yield is still greater than those compared to monoterpenes under similar experimental conditions, the levels are lower than those expected under an ozonolysis regime owing to the fast reactivity of the compound, and the SVOC that are formed under these differing conditions. It should be noted also that the yields represented here are of lower limit values, as data for SOA yield from the chamber is not wall loss corrected as full characterisation of the newly developed MAC facility is ongoing. The ageing of β -caryophyllene SOA is currently in analysis and more detailed descriptions of this work can be found in the upcoming paper by Alfarra et al., (2012). Here only the results are highlighted. Off line-sampling of SOA filter samples were made at two time intervals of 2 and 6 hours during the experiments. A total of 19 compounds were identified in the SOA (see table 42). The composition of initial SOA was simpler than compared to monoterpene SOA and indeed to that of the aged β -caryophyllene SOA. This change in complexity can be due the larger contribution of lower weight compounds. No change in hygroscopic properties of SOA was determined.

5.4 Discussion

The degradation of β -caryophyllene was examined under photooxidation conditions at the MAC facility. We have identified the gas phase composition, with an average total of 36 ions detected, and provide an organic seed similar to expected atmospheric seeds formed from potential sesquiterpene oxidation for use in other experiments. For this chapter, only the initial stage of these seeded experiments (β -caryophyllene oxidation) are described. The formations of these seeds were conducted following the rapid reaction of β -caryophyllene under “straight” nucleation experiments, in which after 2 hours complete degradation of β -caryophyllene is observed. These experiments were subject to faulty readings owing to external factors and initial set-up of the instrument. Resultantly, the experiments in which seeds were formed provide good comparisons to “real” data expected from the initial experiments. From these

experiments, from the total number of ions were detected in the gas phase is included 10 ions of greater mass than the precursor. Of these, the most important for SOA formation were 253 and 239, as these were detected both as major oxidation gas phase products of β -caryophyllene oxidation, and in the particle phase. Another abundant large mass in the gas phase, ion m/z ratio 237 was not observed in the particle phase. During this work we show observations of ions not observed in other studies, for example the C_{14} unsaturated ketone. Owing to the large structure and low volatility of this compound, low concentration detections of this compound in the past may not have been possible as it was in the particle phase. The same seems to be plausible for other large mass compounds as rapid formation of larger compounds were seen to decay after initial detection, showing signs of condensable species. Ultimately it is the conditions of the experiment that govern formation of certain species. Hoffmann et al 1996 found greater aerosol yields were established during ozone reactions under high NO_x for species of sesquiterpenes making daytime chemistry potentially the lower limit to these biogenic contributions to aerosol yield in the atmosphere. Under these conditions, peroxy radicals formed will react with VOCs present. Here we have no direct comparison to “dark” ozone experiments, but do comment on the uncharacteristic chamber chemistry observed. The yield of OH with reactions of ozone has been shown to be low (Atkinson 2003) and so the initial chemistry is governed by NO_2 conversion to NO undergoing photooxidation, as suppression of ozone formation is observed during all β -caryophyllene experiments. After sufficient oxidation of β -caryophyllene, oxidation products are formed that can act as additional sources of radicals (e.g. photooxidation of HCHO). β -caryophyllene photooxidation experiments show almost immediate nucleation owing to the high reactivity of the VOC and low volatility of oxidation products formed. Ageing of β -caryophyllene SOA was also studied showing an increase in complexity of SOA, but no change in hygroscopic properties.

CHAPTER 6. Mesocosm Experiment

The previous chapters have all examined the oxidation systems of specific compounds under a variety of controlled experimental conditions. This chapter applies these findings to “real life” simulations of a forest environment during a mesocosm campaign conducted at the Manchester aerosol chamber. The tree species, *Ficus cyathistipula*, *Ficus benjamina* and *Caryota millis*, were designed to simulate or resemble Asian tropical conditions based on the environment of the Borneo rainforest. The experiments conducted in Borneo were a subsection of the APPRAISE project of which the ACES campaign was also part of, including the mesocosm experiment. The purpose of the mesocosm experiment was to compare common European silver birch species *Betula Pendula* with more tropical fig species to aid in study of emission species of these trees and identify any resulting potential SOA formation from these species.

6.1 Experimental methodology

The mesocosm campaign was designed to look at contrasting emission species from these highly emitting of isoprene to those dominantly emitting monoterpene compounds, from the *Ficus* and *caryota* species to the *betula* family respectively. High emissions of isoprene will portray natural environments dominated by broad-leave tree species (Harley., 1999). The chamber set-up was used to simulate typical concentrations of isoprene found above these isoprene dominant ecosystems, measurements ranging from 1-30 ppbV (Martin, 1991; Kesselmeier, 2002; Fuentes, 2007). As monoterpene emissions are substantially less than isoprene lower concentrations of specific ecosystems have been measured in the range of 50-100 ppt (Hakola., 2003; Rinne., 2005). The conditions were also set to encompass a tropical environment similar to that of the southeast Asian environment, where monoterpene

emissions dominant ecosystems exist (Kuhn 2004). Work as part of the ACES project was to monitor the Southeast Asian environment in the Borneo rainforest. Work conducted at the Borneo rainforest as part of ACES played a role in the determination of the tree species selected for the mesocosm experiment. Accordingly two fig species, *Ficus Benjamina* and *Ficus Cyathistipula* and a palm species, *Caryota Millis*, were selected for the study. No known emission data is available for the two species of *Ficus Cyathistipula* and *Caryota Millis* but *Ficus Benjamina* has been previously studied and emit predominantly isoprene at levels ranging from 0.03 to 8.7 $\mu\text{g C g}^{-1} \text{h}^{-1}$, with lower emissions of other VOCs, monoterpenes limonene and β -ocimene (0.02 $\mu\text{g C g}^{-1} \text{h}^{-1}$ and 1.8 – 2.5 $\mu\text{g C g}^{-1} \text{h}^{-1}$ respectively) and sesquiterpenes β -caryophyllene and α -copaene. Other species, aldehydes and benzaldehyde were also determined (69 $\mu\text{g C g}^{-1} \text{h}^{-1}$ and 0.53 $\mu\text{g C g}^{-1} \text{h}^{-1}$) to be emitted from this species in a potted environment (Carvalho 2005; Geron 2006). Further to the tropical tree species, analysis of a common silver birch tree was also conducted, *Betula Pendula*. This birch tree species has been studied in chamber studies in the past (Mentel 2009), while Kiendler-Scharr (2009) found it to produce high emissions of monoterpenes and low isoprene emissions.

Experiments were run to examine nucleation and condensation aspects of SOA formation from emission of BVOCs from the trees with and without the presence of seed (ammonium sulphate) particles.

6.2 Experimental set-up

The plant chamber consisted of a cubic chamber with dimensions (1.3m x 1.9m x 1.9m) and consisted of two rectangular sections made from Teflon bags (0.05 mm FEP, Adtech Polymer Engineering, UK) supported by aluminium frames (Speed Frame, RS Components, UK). The top section was designed to be removed to allow access to substitute the tree species which were kept under environmental conditions using lamps to create light and heat to simulate tropical environments for the plants. The base plywood base section was mounted on foil while air-tight seals were

accomplished from PVC foam strips (RS Components, UK). The Teflon bag was affixed to the frames with double sided tape (RS components, UK) and only the Teflon surface comprised the interior of the chamber.

Air was filled into the plant chamber through a mass flow controller and regulator (ALICAT MCR-500 SLPM-D, Premier Control Technologies Ltd, UK) at a controlled flow 250 to 300 L min⁻¹. This air was humidified in a pre-chamber by passage through a 2L Teflon barrel filled with warmed distilled water. Potential particle and VOC contaminants in the air were removed by filters prior to the humidification stage. The introduction into the plant chamber was completed through a perforated 12.7 mm OD PTFE tube circling the bottom of the chamber. Table 48 displays the conditions of the plant chamber during the campaign, measurements taken by an EGM probe (EGM-4, PP Systems, UK).

Table 48. Conditions measured during the mesocosm experiments.

Measured parameter	Daytime concentration	Night concentration
CO ₂	335 – 385 ppm	390 – 404 ppm
Relative Humidity	29 – 40%	33 – 44%
Temperature	304.15 – 306.55 K	295.15 – 297.15 K

The reaction chamber was the Manchester Aerosol Chamber, described in detail in Chapter 2. The reaction chamber was linked to the plant chamber via 50 mm OD stainless steel pipe, equipped with a valve to enable venting of the plant chamber into the laboratory outside of experimental runs.

The CIR-ToF-MS was connected for sampling of the reaction chamber in a similar fashion to the experiments run investigating individual BVOC systems described in prior chapters, utilising the same stainless steel line sampling directly from the centre of the Teflon bag of the reaction chamber. In addition to this standard set-up, a three-way Swagelok connector was included before the mass flow controller of the sample inlet line. Here, two further Teflon tubes were fixed via Swagelok fittings to sampling lines connected from the plant chamber and the air fill system prior to the plant chamber. This provided gas-phase analysis of the three aspects of the experiment, the “clean” air flow into the plant chamber, direct emissions of species from the trees in

the plant chamber and finally the photooxidation of these species in the reaction chamber. Making direct measurements of the clean air and chamber air allowed the determination of any possible contaminants within the “clean” air. Sampling parameters of all these locations were constant with a flow through 3.2 mm PTFE tubing, and switching between each site was conducted manually via manual movement of Teflon valves attached to each inlet line.

Prior to the experiment, the plants were placed into the plant chamber and allowed to acclimatise for a period of 48 hrs. To reduce possible contamination emissions from the soil and the plastic pots housing the trees were covered with PTFE sheets. Investigation of selected tree species, 3 in total were conducted over a weekly basis with removal of the trees made at the end of the week accompanied by replacement of the new tree species. SOA growth was measured in the reaction chamber utilising the on-site instrumentation (ToF-AMS).

6.3 Results (BVOC emissions and gas phase products)

BVOC emissions and gas phase products were measured and identified using CIR-ToF-MS and GC-MS. Compared to experiments previously discussed (see Chapter 2), little gas composition data was ascertained during the mesocosm experiment. The dominant products detected were monoterpene traces and isoprene along with its primary oxidation products MVK and MACR. Figure 74 displays an experimental run of the tropical fig species. These were found to emit predominantly isoprene measured at levels between 30 and 40 ppb in the reaction chamber and plant chamber respectively. These results not only indicate the expected isoprene species but also show good transfer of material from the plant chamber into the reaction chamber.

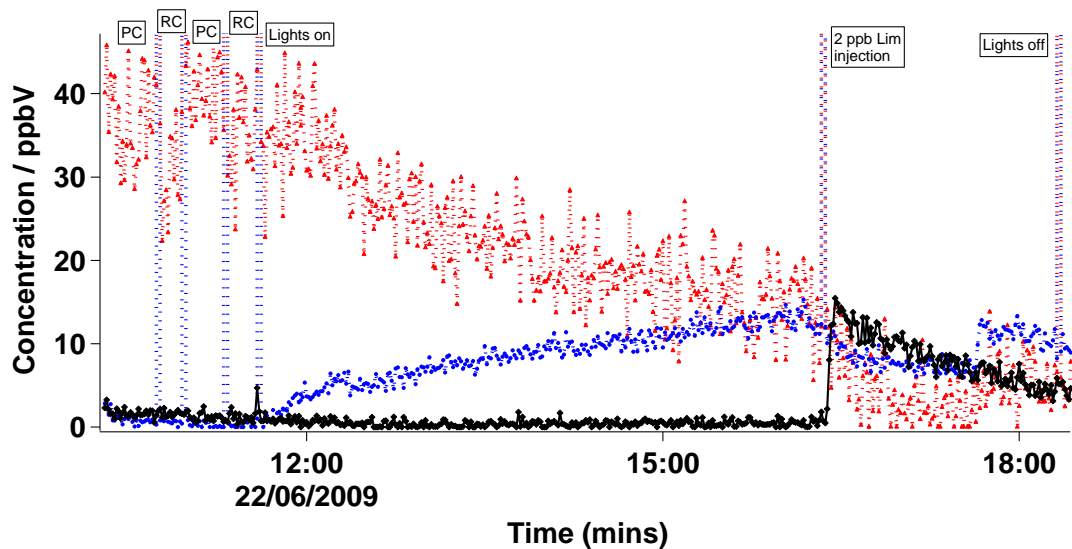


Figure 74. Fig tree species time evolution of the major oxidation product of isoprene (red) from both the plant chamber and reaction chamber. Included here is the formation of the major oxidation products MVK and MACR (blue). The increase in monoterpene detection (black) after lights on is due to the injection of 15 ppb of limonene into the reaction chamber following lights off to ensure capable detection of monoterpenes with the hollow cathode source. PC is plant chamber measurements and RC is reaction chamber observations.

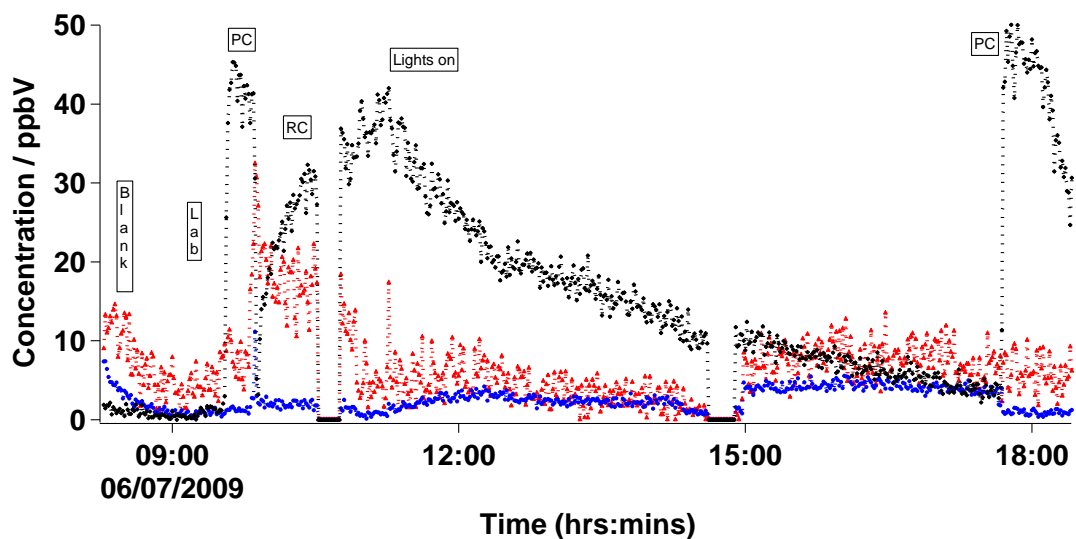


Figure 75. Time evolution of dominant BVOCs of silver birch during a nucleation experiment. The monoterpene (black) emission concentrations are larger than that of isoprene (red), the opposite observation compared to the tropical fig species in figure 71. Sudden decreases in signal represent pressure problems with the MCP plate and no data was collected during this time. PC is the plant chamber, RC the reaction chamber with blank and lab air measurements at the beginning of the experiment.

An experimental run conducted with the silver birch is shown in Figure 75. The beginning of the experiment measures the blank air. The dominant BVOC measured occupies the monoterpene channel. Isoprene levels were also detected but of lower magnitude than that of the figs.

The major gas-phase oxidation product detected from all experiments conducted is that of MACR and MVK, especially from the fig tree species (*Ficus benjamina* and *Ficus cyathistipula*) where the dominant BVOC was that of isoprene. It was expected from the silver birch species that some of the primary oxidation product from monoterpene oxidation would be detected. These include species such as primary aldehydes. However, detection of these were not confirmed, and only the species MVK and MACR, methyl furan, formaldehyde and hydroxyl hydroperoxides (tentatively) were accountable from these studies. Although pinonaldehyde does hold a fragment (m/z 71), this is a minor fragment compared to the dominant fragmentation channels (m/z 151 and 107) and due to the lack of detection of either of these two channels it can be concluded that the detection of the m/z channel is almost exclusively due to isoprene oxidation products, MVK and MACR. Other potential signals observed belong to hydroxyacetone (m/z 75) and formic acid (m/z 47).

Sampling for GC-MS analysis was taken from the same reaction chamber as the gas-phase data at the same time. GC-MS analysis was able to differentiate from the different monoterpenes during this experiment, showing that both α - and β -pinene were the dominant monoterpene (C_{10} species) for the silver birch, whilst α -pinene and limonene governed the fig tree emissions. Interestingly, although no sesquiterpene species were detected in the gas-phase, they were reported as two dominant compounds in the aerosol phase by GC-MS. These were identified as β -caryophyllene and α -cubebene.

Table 49. The yields of observed gas-phase oxidation products based on the amount BVOC reacted and oxidation product formed. Table adapted from publication currently in progress from Ryan et al., (“Mesocosm studies of secondary organic aerosol formed from real tropical plant emissions”)

Hydroperoxides	MVK + MACR	Hydroxyacetone	Formaldehyde	Past studies
0.33	0.26	0.07		(Williams 2001)
0.05	0.36	0.05		Williams et al 2001
	0.33		0.67	(Zhang 2002)
	0.46- 0.60		0.86-0.96	(Niki 1983)
	0.45			Kamens et al 1982
				(Rickard 1999)
0.01 – 0.03	0.17 – 0.36	0 – 0.02	0.02 – 0.07	This study

This is not unexpected when regarding the results seen in Chapter 5, where β -caryophyllene is seen to react very quickly in the gas-phase. Owing to these results it can be stated that the GC-MS application was better suited for analysis of samples with a mixture of compounds, particularly with regards to a mixture of compounds with the same mass. Although being able to differentiate between these compounds, it cannot be definitively said that this technique is more sensitive, as the CIR-ToF-MS was looking at the gas phase. As mentioned in the previous chapters, compounds with low vapour pressures partition readily into the particle phase and would make detection of these in the gas phase extremely hard. Other identified species include monoterpenes (sabinene, linalool, ocimene, γ -terpinene, camphene), sesquiterpenes (α -cedrene, α -farnesene and α -copaene) and other products including acetaldehyde (*F. Benjamina* and *B. Pendula*), acetic acid (*F. Cyathistipula*), Caryophyllene epoxide (*B. Pendula*), Benzoquinone, pyridine, methyl salicate and decanal (*F. Benjamina*). Overall GC-MS identified more products in filter masses than direct gas-phase measurements. Obvious reasons for this were the low levels of emissions from tree species that not surprisingly have levels close to detection limits, where differential between measured species and “noise” levels become hard to distinguish (see chapter 2). The yields of

detected oxidation products are given in Table 44. The only comparable yields obtained are for those of the major oxidation species detected, MVK and MACR, where the others all are lower compared to previous work. The yields obtained also correlate well with the direct isoprene studies performed and reported in Chapter 3 and references within.

6.4 SOA formation

Aerosol growth and nucleation was only observed from the European silver birch tree species during both seeded and non-seeded experiments, which contradicts past studies of direct experimental measurements that have reported fresh nucleation particle suppression from experiments involving existing seed particles, but fresh nucleation particles formed in the absence of seeds. Under tropical tree conditions, although a slight increase in particle number is detected, these did not grow to significant numbers to initiate a nucleation event (Figure 76). In other cases levels did not even reach above background levels. Correspondingly, the European birch trees only demonstrated growth of pre-existing seeds alongside newly formed particles in seeded experiments. This observation may not be too surprising as we have already indicated that isoprene does not form SOA. The monoterpene dominant emitting Birch tree species do show SOA formation potential, consistent with the results reported in previous chapters.

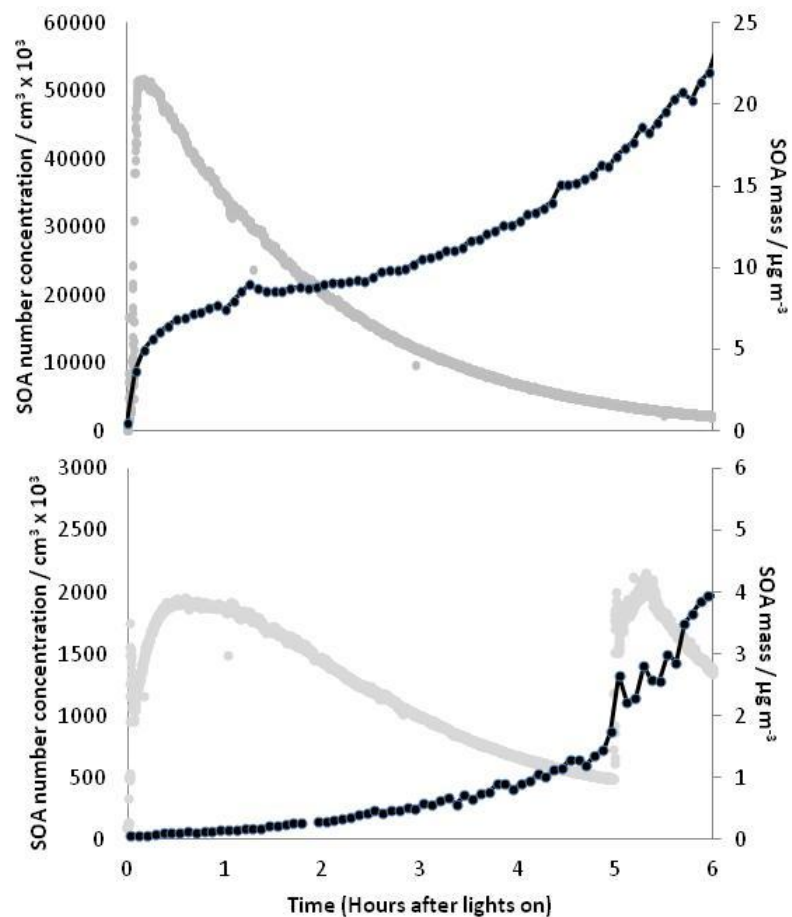


Figure 76. SOA mass formation for two different tree species. The top panel displays the SOA mass (black) and number concentrations (grey) for a birch tree experiment conducted on 6th July 2009. The bottom panel displays the SOA data for a fig tree experiment conducted on 23rd June 2009.

6.6 Discussion

Detailed discussion of isoprene oxidation can be found in chapter 3. Here we concluded that isoprene forms little to no SOA formation under both photooxidation and ozonolysis conditions under a variety of NO_x conditions and presence of seeded particles. However, in addition to this the tree chamber studies indicated evidence to support that isoprene may in fact suppress SOA formation, that would otherwise be

formed from other VOC precursors (Kiendler-Scharr et al., 2009), namely that from monoterpenes. This result is in line with the conclusions put forward by Kiendler-Scharr et al (2009).

During the experiment the analysis of fig tree species and silver birch tree species were successfully conducted to examine the differing of influences of pre-dominantly isoprene and monoterpene emitting species. In addition to this a mixed plant study was also conducted. Only few gas-phase products were identified in the experiment, displaying the difficulty in sensitivity when applied to “real” atmospheric concentrations. Despite this, BVOCs were measured to accurate levels, along with yields of the major oxidation products (MVK and MACR) that correlate well to yields obtained here previously, and to past work included. The fig tree species of isoprene dominant emissions displayed oxidation products formed in the reaction chamber coupled with no evidence of SOA formation. Under high NO_x conditions isoprene does not contribute to aerosol formation. The silver birch consisting of high monoterpene emissions showed significant SOA formation. These results were consistent with other over all experiments conducted, regardless of the presence of a pre-existing seed in the chamber. The mesocosm experiments thereby confirm the findings on the results reported in chapters 3 and 4, although the question of isoprene SOA potential is still a big question in the atmosphere, as oxidation products measured here, may have been at concentrations levels too low to partake in SOA as has been reported elsewhere (see chapter 3). The yields of oxidation products here are reported to be lower than that of previous studies (for the exception of MVK and MACR). Products identified here, hydroperoxides, hydroxyacetone are all believed to participate in SOA formation (Claeys et al., 2004; Kroll et al., 2006; Surratt et al., 2006; Kleindiest et al., 2007). The work here regarding these species will be covered in detail from an upcoming publication from Ryan et al (see Table). The lower yields obtained in the experiments could give some explanation towards the lack of SOA formation, but considering the other isoprene experiments all displayed similar results, it must be concluded that isoprene, or its oxidation products do not form SOA for the conditions outlined here, and in chapter 3.

This work can potentially show regional implications based upon the vegetation present, e.g. the dominant tree species in an ecosystem. Biogenic SOA formation would be expected to a lower degree with tree species emitting more dominantly isoprene (European) compared to monoterpene dominant emitters (Tropical). Further modelling work will have to be conducted in order to determine the accuracy of the proposed statement.

CHAPTER 7. Conclusion

Numerous chamber studies have been investigated in detail reflecting boundary layer conditions under two strict experimental regimes, ozonolysis and photolysis. These two “types” of experiments were conducted at differing aerosol chamber facilities, EUPHORE (ozonolysis) and MAC (photolysis). A variety of instruments were employed to analyse different parameters of the chamber studies, including SMPS/DMPS, FTIR, LC-MS, TOF-AMS and HPLC. Work reported here is heavily focused upon the real-time gas phase measurements made by CIR-ToF-MS for a number of different VOCs. Ozonolysis reactions of ethene, isobutene, trans-2-butene, isoprene, α -pinene and limonene have been studied, on top of the photolysis reactions of α -pinene, limonene and β -caryophyllene. Work here provides a direct comparison to each experimental environment. The ozonolysis experiments were completed with the absence and in the presence of an OH scavenger with cyclohexane and CO (concentrations used to scavenge > 95% of OH produced in side reactions) under both dry and humid conditions. For the photolysis experiments, all were run with humid conditions in the presence or absence of pre-existing seeds. In the case of limonene and isoprene, a novel technique of producing an atmospherically relevant organic seed from β -caryophyllene nucleation. Finally a mesocosm experiment was conducted to try and study BVOCs and SOA potential at atmospheric concentrations from biogenic emissions. Analyse of data was focused upon the gas-composition fingerprint to provide in-depth results for formation of oxidation products in real time. From these, overall yields were determined where possible for all detected gas-phase species. Some of the determined yields are subject to error owing to the unavailability of standards. Complicated yield determinations have been reported where necessary. SOA yields were also reported for available data and finally, for ozonolysis experiments, comparisons to current models from the MCM were made to evaluate current knowledge, especially for the newly constructed model for limonene degradation.

Further future development of the CIR-ToF-MS for a new ion source, hollow cathode discharge (HCD), is also examined. This resulted in the first time a HCD source was fitted onto the University of Leicester CIR-ToF-MS. Sensitivity values reported here are not only based on ions formed in the drift cell (H_3O^+) but also with direct comparisons of detected small mass compounds between the two sources, providing an idea of the potential enhancements of using the HCD over ^{241}Am source, other than the operational benefits of the HCD (e.g. no radiation applications). Examination of small alkene species provided good comparisons for the two different ion sources owing not only to their small masses, but also due to simplified oxidative systems expected.

The ozonolysis of ethene identified two oxidation products HCHO and HCOOH. Yields of HCHO were recorded as 1.547 ± 0.053 for dry conditions and 3.083 ± 0.151 under wet conditions. These observations provided evidence of increased difficulty of HCHO detection under humid conditions. The back reaction of H_3O^+ to H_2O with wet conditions reduces the sensitivity greatly for ^{241}Am source, falling from a calibration value of 12 down to 1. This large decrease is not seen with the HCD source. Increases in yield were also observed for HCOOH yields, determining yields of 0.033 ± 0.002 and 0.555 ± 0.027 for dry and wet conditions. However these results were expected as H_2O reactions with the Criegee intermediate from ethene + O_3 reactions favour formation of HCOOH. The yields determined here were of good correlation compared to previous work. Further examination with comparison of the experimentally determined data to model outputs of the MCM show good fits to each to provide evidence for good experimental data as ethene models are well understood. Further comparisons to on-site instrumentation during ozonolysis experiments by FT-IR further enhances the ability of the CIR-ToF-MS for certain compounds, especially for compounds that were extensively calibrated for. For the majority of compounds that were available as standards, the CIR-ToF-MS produced more reliable results than the FTIR. However, results became more eradicate with the use of surrogates displaying the need for accurate calibrations to be conducted for measurements to be done on the CIR-ToF-MS, as this proves not to be an absolute technique.

Further investigations of simple alkenes provided yields resembling those of previous studies. Isobutene ozonolysis resulted in the detection and identification of 8 oxidation products, three of which of higher mass than the parent VOC (propionic acid, acetic acid and acetone). Reported average yields for dry conditions of 0.037 ± 0.004 (propionic acid), 0.312 ± 0.006 (acetone), 0.039 ± 0.005 (acetic acid), 0.026 ± 0.001 (formic acid), 0.188 ± 0.004 (acetaldehyde), 0.080 ± 0.004 (methanol) and 1.215 ± 0.027 (HCHO) making acetone and HCHO two dominant species for isobutene ozonolysis. This is backed up by a theoretical reaction mechanism produced from ozone addition to double bonds to form ozonides as first postulated by Criegee et al. Finally for trans-2-butene a total of 5 oxidation products were observed and detected from ozonolysis experiments, only one higher in mass than the parent VOC (acetic acid). Two dominant oxidation products, HCHO and CH₃CHO had average yields determined of 0.145 ± 0.005 and 0.766 ± 0.018 respectively for dry conditions, and 0.188 ± 0.035 and 1.025 ± 0.077 for wet conditions. During the small alkene ozonolysis, a general theme of increased yield with increased RH is observed. The small alkene compounds were a good method of scrutinising the ability of the CIR-ToF-MS to monitor, accurately, yields of small mass compounds in simple gas-phase systems. Owing to the small compounds (better resolution is expected) and the good correlation to previous studies, the results here are accurate and precise.

Larger compounds with more complex mechanisms resulted in the detection of a larger number of oxidation products. During isoprene ozonolysis reactions a maximum total number of 8 different products were detected and identified, two of which higher in mass than the parent precursor, MVK and MACR. It should be noted that substantially less products were detected during photolysis experiments of isoprene than the ozonolysis experiments. A slight decrease in products detected is also observed with the introduction of an OH scavenger to the ozone reaction system. This highlights a potential importance of OH radicals in the production of diverse gas-phase products. In all experiments, HCHO, MVK and MACR dominated the gas phase composition obtained, giving average yields for ozonolysis reactions of 0.363 ± 0.025 , 0.153 ± 0.011 and 0.287 ± 0.012 respectively, and 0.369 ± 0.034 , 0.160 ± 0.007 and

0.298 ± 0.015 for photolysis reactions. These again are in good agreement with past work.

Monoterpene species (C₁₀) provided even more gas phase ions. Under ozonolysis conditions 10 products were identified from for myrcene oxidation, 11 oxidation products for α-pinene and a maximum of 10 products as a result of limonene oxidation. For photolysis experiments only 7 oxidation products were confirmed. Of these products 4 to 5 were higher in mass than the parent monoterpenes. The most dominant in all cases were the primary aldehyde. The primary aldehyde and other larger species potentially show characteristics allowing them to partake in SOA formation either through nucleation or condensation onto pre-existing particles. Compounds predicted in the reaction schemes are detected within the gas phase and particle phases. The vapour pressures estimated for these larger compounds, pinonic acid in α-pinene oxidation are in the region of 10⁻⁷ torr and preferably partition into the particle phase. Primary aldehydes are also observed in the particle phases that have estimated vapour pressures of 10⁻³ to 10⁻⁵ torr. However a larger yield of these aldehydes are detected in the gas phase indicating that as these vapour pressures other factors play a role in the partitioning of these compounds into the aerosol phase. For example aldehydes undergo acid-catalysed heterogeneous reactions in the particle phase and can lead to enhanced particle formation (Jang et al., 2002 and Toloka et al., 2004). Indeed increased SOA formation was observed with the presence of a seed coupled with a decrease in gas-phase aldehyde yield. As such these aldehydes can reside in both gas and particulate phases, with the preference falling in the latter in the presence of seed particles as higher SOA yields (8.98%) of limonene were observed compared to unseeded experiments (1.29%), suggesting evidence for dimer and oligomer reactions to occur on surfaces on aerosols. However lower mass yields were still identified, reporting <15% yield for all monoterpene species for oVOCs acetaldehyde, formic acid, acetic acid and methanol in accordance with past studies done by Orlando et al 2000 and Lee et al 2006. Limonene and α-pinene also record *m/z* ion at 185 Daltons in contrast to myrcene, whose highest detection was *m/z* 155 over all experiments. Interestingly the high masses from limonene and α-pinene were only observed during ozonolysis experiments. These large compounds thereby must

be created with the addition of ozone to the endocyclic double bond, creating multi-functional species containing both ketone and carboxylic functional groups. Primary aldehyde species were also detected at m/z 169 for cyclic monoterpenes, which could prove of importance these species themselves partake in SOA formation but with further oxidation can lead to even larger, less volatile compounds. The MCM models comparisons for α -pinene and limonene displayed accurate degradation representation, along with fairly good oxidation product formation.

The sesquiterpene species β -caryophyllene was also studied under photolysis experiments. Most of the previous work is focused around the ozone reaction on account of the high reactivity β -caryophyllene has with O_3 , a lifetime approximating only a few minutes. The high reactivity of β -caryophyllene is observed during our experiments, as almost complete degradation is noted after 2 hours of reaction. As a result, an organic seed created from a nucleation experiment was used to make as a seed, and chemical ageing of this seed is the focal point of a paper in progress by Alfarrá et al., (2012). A total of 7 oxidation products were tentatively identified during the photooxidation of β -caryophyllene, although it should be noted that a large number of ions were detected. Only 2 of these products were in higher mass than the parent VOC, these compounds likely to contribute to SOA formation.

For all monoterpene species and sesquiterpenes, fresh particle growth was observed via nucleation events. Previous studies have postulated that the chemical make-up of the VOC is important is determining its potential contribution to SOA formation. Past studies have postulated that species without a cyclic structure (e.g. myrcene) result in the lowest SOA yields, and species with one external bond from a cyclic structure produce intermediate SOA yields. The following study presented data with SOA yields for myrcene ranging from 7.9 % – 15.39 % for photolysis reactions and 2.12 % – 17.68 % for ozonolysis reactions. Other determined SOA yields are; limonene 8.61 – 9.35 % (photolysis) and 35.97 % – 57.74 % (ozonolysis); α -pinene 12.51 % - 48.55 % (ozonolysis) and β -caryophyllene 7.01 % – 14.34 % (seeded experiments). No real trend can be ascertained from the current results, for the exception that ozone reactions seem to form higher SOA yields compared to OH-initiated reactions. When

considering the gas-compositions make-up, large compounds are only seen within these reactions, particularly the m/z ion 185, representing a C_{10} carboxylic acid. This product could be an important precursor for SOA formation or a precursor to further, heavier oxidation products. Filter samples analysed of aerosol species conveys products that are also identified in the gas-phase. The primary aldehyde (m/z 169, pinonaldehyde, limonaldehyde etc) formed from cyclic monoterpene oxidation has been detected in both gas-phase and particle-phase showing its importance in SOA. Limonaldehyde ($C_{10}H_{16}O_2$) is both dominant in the gas-phase and particle-phase, although accurate concentrations of limonaldehyde could not be determined (no standard available for calibration). Other species observed in as dominant products in both phases include pinonaldehyde (m/z 169) and pinonic acid (m/z 185) for α -pinene and β -caryophyllonic acid (m/z 253) for β -caryophyllene. So this identifies important species for SOA in the atmosphere.

Monoterpenes and β -caryophyllene demonstrate the ability to form SOA. Isoprene however in our studies does not. Also during the mesocosm experiment, although isoprene was detected, no aerosol growth was detected upon any reasonable level. As such it must be concluded that despite other work identifying isoprene oxidation products, for experiments based on our time length and conditions, isoprene does not contribute towards SOA. Under European Silver Birch experiments (dominant monoterpene emitters) SOA was detected which further enhances the conclusion that monoterpene and sesquiterpene species are more important in the atmosphere for contribution of SOA formation.

Future Work

The work conducted here has shown results that detect and identify important oVOC species in the atmosphere. Critical to the success of accurate measurements is the calibration of standards compounds in question. Some yield based work here is based on appropriate selection of surrogates. As such, to obtain more accurate results, it is

recommended that standards are run for the larger mass compounds detected during this campaign as yield quotations will become more accurate.

The hollow cathode discharge source showed real potential to increase sensitivity of a range of compounds, gathered from the direct comparisons of standards currently available. Characterisation of this source is crucial if further experiments involving this source are to be made. The construction of the new source began during intensive field campaigns, and so I believe the source has not yet been one fully characterised, or two, the true potential of the source has yet to be discovered. Sensitivity towards a greater scope of compounds over that of the regular ^{241}Am source has already been established, but along with this is the problem with NO^+ contamination signals. If more R & D time is spend on this in the lab, the potential for this source can be achieved.

Further experiments, under the same experimental conditions, for a broader range of compounds, particularly for monoterpenes and sesquiterpenes could shed more light on the importance of the genetic make-up of VOCs in the atmosphere. Is it important to contain multiple double bonds, if so, how many would give optimal SOA formation? We have so far proven this may not be the case, and if so why not for our experimental conditions. Several questions still remain, but this work has shown the potential of a new source of CIR-ToF-MS, the identification of gas-phase products that contribute to SOA, as well as the groups of BVOCs that have potential to form SOA. More chamber study work can also benefit the evaluation of the computerised models as experimental data is usually associated with larger error bars. Modelling itself of the mesocosm experiment can aid to ultimately determine the regional impacts of certain types of VOC emitting tree species. Of interest would be the formulation of on-line analysis of aerosol (or single particles) rather than off-line analysis. Optical tweezers could be used to separate aerosol particles and identification methods already common, e.g. GC, used to identify the species in the aerosol. The effect of ageing on aerosols should also be considered over a prolonged period of time rather than 4 – 6 hours of the experimental time that we currently employed. It is a clear challenge to try and bridge the gap in scientific knowledge between the gas-phase processes and particle matter in the atmosphere, but with current developments on instruments

making progress, fast-highly reactive VOCs or oVOCs could be studied to further enhance our understanding.

- Akimoto, H. (2003). "Global Air Quality and Pollution." Science AAAS **302**(5651): 1716-1719.
- Alam, M. S., M. Camredon, et al. (2011) "Total radical yields from tropospheric ethene ozonolysis." Physical Chemistry Chemical Physics **13**(23): 11002-11015.
- Alfarra, M. R. (2006). "A mass spectrometric study of secondary organic aerosols formed from the photooxidation of anthropogenic and biogenic precursors in a reaction chamber." Atmospheric Chemistry and Physics **6**: 5279-5293.
- Arey, J. (1990). "Product Study of the Gas-Phase Reactions of Monoterpenes With the OH Radical in the Presence of NO." Journal of Geophysical Research **95**(d11): 18539-18546.
- Arey, J. (1991). "Terpenes Emitted From Agricultural Species Found in California's Central Valley." Journal of Geophysical Research **96**(d5): 9329-9336.
- Arnth, A. (2008). "Why are estimates of global terrestrial isoprene emissions so similar (and why is this not so for monoterpenes)?" Atmospheric Chemistry and Physics **8**(16): 4605.
- Aschmann, S.M. and Atkinson, R. (1994). "Formation Yields of Methyl Vinyl Ketone and Methacrolein from the Gas-Phase Reaction of O₃ with Isoprene." Environmental Science & Technology **28**(8): 1539-1542.
- Atkinson, R. (2000). "Atmospheric chemistry of VOCs and NO_x." Atmospheric Environment **34**(12-14): 2063-2101.
- Atkinson, R. (2003). "Gas-phase tropospheric chemistry of biogenic volatile organic compounds: a review." Atmospheric Environment **37**: 197.
- Atkinson, R., Arey, J. (2003). "Atmospheric degradation of volatile organic compounds." Chemical Reviews **103**: 4605-4638.
- Bahreini, R. (2005). "Measurements of Secondary Organic Aerosol from Oxidation of Cycloalkenes, Terpenes, and -Xylene Using an Aerodyne Aerosol Mass Spectrometer." Environmental Science & Technology **39**(15): 5674-5688.
- Baltensperger, U., M. Kalberer, et al. (2005). "Secondary organic aerosols from anthropogenic and biogenic precursors." Faraday Discussions **130**: 265-278.

- Bartels, M., K. Hoyer mann, et al. (1982). "Elementary reactions in the oxidation of ethylene: The reaction of OH radicals with ethylene and the reaction of C₂H₄OH radicals with H atoms." Symposium (International) on Combustion **19**(1): 61-72.
- Berndt, T. (2003). "Gas-phase ozonolysis of [alpha]-pinene: gaseous products and particle formation." Atmospheric Environment **37**(28): 3933.
- Becker, K. H. (1996) EUPHORE: Final Report to the European Commission, Contract EV5V-CT92-0059. Final Report of the EC-Project. Bergische Universität Wuppertal, Germany.
- Blake, R. S., C. Whyte, et al. (2004). "Demonstration of Proton-Transfer Reaction Time-of-Flight Mass Spectrometry for Real-Time Analysis of Trace Volatile Organic Compounds." Analytical Chemistry **76**(13): 3841-3845.
- Blake, R.S. (2005). "Monitoring Tropospheric Composition using Time of Flight Chemical Ionisation Mass Spectrometric Techniques." PhD Thesis, University of Leicester
- Böge, O., Miao, Y., et al (2006). "Formation of secondary organic particle phase compounds from isoprene gas-phase oxidation products: An aerosol chamber and field study." Atmospheric Environment **40**(14): 2501-2509.
- Bonn, B., G. Schuster, et al. (2002). "Influence of Water Vapor on the Process of New Particle Formation during Monoterpene Ozonolysis." The Journal of Physical Chemistry A **106**(12): 2869-2881.
- Buseck, P. R., Pósfai, M. (1999). "Airbourne minerals and related aerosol particles: Effects on climate and the environmnet." PNAS **96**(7): 3372-3379.
- Cahill, T. M. (2006). "Secondary organic aerosols formed from oxidation of biogenic volatile organic compounds in the Sierra Nevada Mountains of California." Journal of Geophysical Research. Biogeosciences **111**: D16312
- Calogirou, A. (1997). "Product analysis of the gas-phase reaction of [beta]-caryophyllene with ozone." Atmospheric Environment **31**(2): 283.
- Calvert, J.G. (2000). "The mechanisms of atmospheric oxidation of the alkenes." New York, US: Oxford University Press.
- Camredon, M. (2010). "Distribution of gaseous and particulate organic composition during dark alpha-pinene ozonolysis." Atmospheric Chemistry and Physics **10**(6): 2893.
- Carlton, A. G., Turpin, B. J., et al. (2006). "Link between isoprene and secondary organic

- aerosol (SOA): Pyruvic acid oxidation yields low volatility organic acids in clouds." Geophysical Research Letters **33**: L06822.
- Carlton, A. G. (2009). "A review of Secondary Organic Aerosol (SOA) formation from isoprene." Atmospheric Chemistry and Physics **9**: 4987.
- Carter, W. P. L. (1996). "Condensed atmospheric photooxidation mechanisms for isoprene." Atmospheric Environment (1994) **30**(24): 4275.
- Carvalho, L. R. F. (2005). "Measurements of biogenic hydrocarbons and carbonyl compounds emitted by trees from temperate warm Atlantic rainforest, Brazil." Journal of Environmental Monitoring **7**(5): 493.
- Charlson, R. J. (1992). "Climate Forcing by Anthropogenic Aerosols." Science **255**(5043): 423-430.
- Chameides, W.L., Lindsay, R.W., et al (1988). "The role of biogenic hydrocarbons in urban photochemical smog: atlanta as a case study." Science **241**(4872): 1473-1475
- Chameides, W. L., Yu, H., et al (1999). "Case study of the effects of atmospheric aerosols and regional haze on agriculture: An opportunity to enhance crop yields in China through emission controls?" PNAS **96**(24): 13626-13633.
- Ciccioli, P. (1999). "Emission of reactive terpene compounds from orange orchards and their removal by within-canopy processes." Journal of Geophysical Research. **104**(d7): 8077-8094.
- Claeys, M., Graham, B., et al (2004). "Formation of Secondary Organic Aerosols Through Photooxidation of Isoprene." Science AAAS **303**(5661): 1173-1176.
- Claeys, M., W. Wang, et al. (2004). "Formation of secondary organic aerosols from isoprene and its gas-phase oxidation products through reaction with hydrogen peroxide." Atmospheric Environment **38**(25): 4093-4098.
- Clyne, M. A. A. (1964). "Kinetics of the chemiluminescent reaction between nitric oxide and ozone." Transactions of the Faraday Society **60**(0): 359.
- Cocker III, D. R., S. L. Clegg, et al. (2001). "The effect of water on gas-particle partitioning of secondary organic aerosol. Part I: α -pinene/ozone system." Atmospheric Environment **35**(35): 6049-6072.

- Criegee, R. (1975). "Mechanism of Ozonolysis." Angewandte Chemie International Edition in English **14**(11): 745-752.
- Czoschke, M. N., Jang, M, et al. (2003). "Effect of acidic seed on biogenic secondary organic aerosol growth." Atmospheric Environment **37**(30): 4287-4299.
- de Gouw, J. (2007). "Measurements of volatile organic compounds in the earth's atmosphere using proton-transfer-reaction mass spectrometry." Mass Spectrometry Reviews **26**(2): 223-257.
- Dekermenjian, M. (1999). "FTIR analysis of aerosol formed in the ozone oxidation of sesquiterpenes." Aerosol Science and Technology **30**(4): 349.
- Deandrade, J.B., Pinheiro, H.L.C., et al (1995). "The formaldehyde and acetaldehyde content of atmospheric aerosol." Journal of the Brazilian Chemical Society **6**:287-290.
- Dommen, J. (2009). "Determination of the Aerosol Yield of Isoprene in the Presence of an Organic Seed with Carbon Isotope Analysis." Environmental Science & Technology **43**(17): 6697-6702.
- Donahue, N. M., Kroll J. H., et al. (1998). "Direct observation of OH production from the ozonolysis of olefins." Geophysical Research Letters **25**(1): 59-62
- Donahue, N. M., Robinson, A. L., et al (2006). "The coupled partitioning, dilution, and chemical aging of semivolatile organics." Environmental Science Technology **40**, 2635.
- Drewnick, F. (2005). "A New Time-of-Flight Aerosol Mass Spectrometer (TOF-AMS)—Instrument Description and First Field Deployment." Aerosol Science and Technology **39**(7): 637-658.
- Edney, E. O., T. E. Kleindienst, et al. (2005). "Formation of 2-methyl tetrols and 2-methylglyceric acid in secondary organic aerosol from laboratory irradiated isoprene/NO_x/SO₂/air mixtures and their detection in ambient PM_{2.5} samples collected in the eastern United States." Atmospheric Environment **39**(29): 5281-5289.
- Ervens, B., Feingold. G., et al. (2004). "A modelling study of aqueous production of dicarboxylic acids: 1. Chemical pathways and speciated organic mass production." Journal of Geophysical Research **109**: D15205.

- Fick, J., L. Pommer, et al. (2003). "Effect of OH radicals, relative humidity, and time on the composition of the products formed in the ozonolysis of α -pinene." Atmospheric Environment **37**(29): 4087-4096.
- Finlayson-Pitts, B. J. and J. Pitts, James N. (2000). "Chemistry of the Upper and Lower Atmosphere: Theory, Experiments and Applications." London, UK: Elsevier Science & Technology.
- Fuentes, J. D. (2007). "Biogenic Hydrocarbon Chemistry within and Above a Mixed Deciduous Forest." Journal of Atmospheric Chemistry **56**(2): 165-185.
- Geron, C. (2006). "Volatile organic compounds from vegetation in southern Yunnan Province, China: Emission rates and some potential regional implications." Atmospheric Environment (1994) **40**(10): 1759.
- Griffin, R.J., Cocker III, D.R., et al (1999a). "Estimate of global atmospheric organic aerosol from oxidation of biogenic hydrocarbons." Geophysical Research Letters **26**(17): 2721-2724.
- Griffin, R. J. (1999b). "Organic aerosol formation from the oxidation of biogenic hydrocarbons." Journal of Geophysical Research **104**(d3): 3555.
- Grosjean, D., E. Grosjean, et al. (1994). "Atmospheric chemistry of olefins: a product study of the ozone-alkene reaction with cyclohexane added to scavenge hydroxyl radical." Environmental Science & Technology **28**(1): 186-196.
- Grosjean, D., E. L. Williams, et al. (1993). "Atmospheric oxidation of biogenic hydrocarbons: reaction of ozone with β -pinene, D-limonene and trans-caryophyllene." Environmental Science & Technology **27**(13): 2754-2758.
- Grosjean, E., J. B. de Andrade, et al. (1996). "Carbonyl Products of the Gas-Phase Reaction of Ozone with Simple Alkenes." Environmental Science & Technology **30**(3): 975-983.
- Grosjean, E. and D. Grosjean (1996). "Carbonyl Collection Efficiency of the DNPH-Coated C₁₈ Cartridge in Dry Air and in Humid Air." Environmental Science & Technology **30**(3): 859-863.
- Grosjean, E. and D. Grosjean (1996). "Carbonyl products of the gas-phase reaction of ozone with 1-alkenes." Atmospheric Environment **30**(24): 4107-4113.

- Gu, C. L., Rynard, C. M, et al. (1985). "Hydroxide radical oxidation of isoprene." Environmental Science & Technology **19**(2): 151-155.
- Guenther, A. (2007). "Estimates of global terrestrial isoprene emissions using MEGAN (Model of Emissions of Gases and Aerosols from Nature)." Atmospheric Chemistry and Physics **7**: 4327.
- Guenther, A., C. N. Hewitt, et al. (1995). "A global model of natural volatile organic compound emissions." Journal of Geophysical Research **100**(D5): 8873-8892.
- Gutbrod, R., Ralph, N, et al. (1996). "Formation of OH radicals in the gas phase ozonolysis of alkenes: the unexpected role of carbonyl oxides." Chemical Physics Letters. **252**(2-3): 221-229.
- Gutbrod, R., E. Kraka, et al. (1997). "Kinetic and Theoretical Investigation of the Gas-Phase Ozonolysis of Isoprene: Carbonyl Oxides as an Important Source for OH Radicals in the Atmosphere." Journal of the American Chemical Society **119**(31): 7330-7342.
- Hakola, H. (1994). "Product formation from the gas-phase reactions of OH radicals and O₃ with a series of monoterpenes." Journal of Atmospheric Chemistry **18**(1): 75-102.
- Hakola, H. (2003). "Seasonal variation of VOC concentrations above a boreal coniferous forest." Atmospheric Environment **37**(12): 1623.
- Hallquist, M., Wenger, J.C, et al. (2009). "The formation, properties and impact of secondary organic aerosol: current and emerging issues." Atmospheric Chemistry and Physics **9**: 5155-5236.
- Hamilton, J. F. (2007). "Comprehensive Two-Dimensional Gas Chromatography Coupled to Time-of-Flight Mass Spectrometry of Coal Liquids Produced During a Coal Liquefaction Process." Energy & fuels **21**(1): 286-294.
- Hamilton, J. F. (2008). "Characterization of Polar Compounds and Oligomers in Secondary Organic Aerosol Using Liquid Chromatography Coupled to Mass Spectrometry." Analytical Chemistry **80**(2): 474-480.
- Hamilton, J. F. (2011). "Investigating the use of secondary organic aerosol as seed particles in simulation chamber experiments." Atmospheric Chemistry and Physics **11**(12): 5917-5929.

- Hansel, A., A. Jordan, et al. (1995). "Proton transfer reaction mass spectrometry: on-line trace gas analysis at the ppb level." International Journal of Mass Spectrometry and Ion Processes **149-150**(0): 609-619.
- Hansel, A., W. Singer, et al. (1997). "Energy dependencies of the proton transfer reactions $\text{H}_3\text{O}^+ + \text{CH}_2\text{O} \leftrightarrow \text{CH}_2\text{OH}^+ + \text{H}_2\text{O}$." International Journal of Mass Spectrometry and Ion Processes **167-168**(0): 697-703.
- Hanson, D. R., J. Greenberg, et al. (2003). "Proton transfer reaction mass spectrometry at high drift tube pressure." International Journal of Mass Spectrometry **223-224**: 507-518.
- Hanson, D. R., M. Koppes, et al. (2009). "Proton transfer mass spectrometry at 11 hPa with a circular glow discharge: Sensitivities and applications." International Journal of Mass Spectrometry **282**(1-2): 28-37.
- Harley, P. C. (1999). "Ecological and evolutionary aspects of isoprene emission from plants." Oecologia **118**(2): 109-123.
- Harrison, R. M., Yin, J (2000). "Particulate matter in the atmosphere: which particle properties are important for its effects on health?" Science of The Total Environment **249** (1-3): 85-101.
- Heald, C. L., Henze, D. K., et al (2008). "Predicted change in global secondary organic aerosol concentrations in response to future climate, emissions and land use change." Journal of Geophysical Research **113**: D05211
- Hegg, D. A. (2008). "Measurements of size-resolved hygroscopicity in the California coastal zone." Atmospheric chemistry and physics **8**: 7193-7203
- Helmig, D. (1999). "Biogenic volatile organic compound emissions (BVOCs) I. Identifications from three continental sites in the US." Chemosphere **38**(9): 2163.
- Helmig, D. (2006). "Sesquiterpene emissions from loblolly pine and their potential contribution to biogenic aerosol formation in the Southeastern US." Atmospheric Environment **40**(22): 4150.
- Henze, D. K. (2006). "Global secondary organic aerosol from isoprene oxidation." Geophysical research letters **33**(9): 4.

- Herrmann, A. (2010). "The chemistry and biology of volatiles." Chichester, UK: John Wiley & Sons.
- Herron, J. T. and R. E. Huie (1977). "Stopped-flow studies of the mechanisms of ozone-alkene reactions in the gas phase. Ethylene." Journal of the American Chemical Society **99**(16): 5430-5435.
- Hewitt, C. N., S. Hayward, et al. (2003). "The application of proton transfer reaction-mass spectrometry (PTR-MS) to the monitoring and analysis of volatile organic compounds in the atmosphere." Journal of Environmental Monitoring **5**(1): 1-7.
- Hoffmann, T., J. R. Odum, et al. (1997). "Formation of Organic Aerosols from the Oxidation of Biogenic Hydrocarbons." Journal of Atmospheric Chemistry **26**(2): 189-222.
- Holmes, N. S (2006). "A review of particle formation events and growth in the atmosphere in the various environments and discussion of mechanistic implications." Atmospheric Environment **41**: 2183-2201
- Horie, O. and G. K. Moortgat (1989). "A new transitory product in the ozonolysis of trans-2-butene at atmospheric pressure." Chemical Physics Letters **156**(1): 39-46.
- Horie, O. and G. K. Moortgat (1991). "Decomposition pathways of the excited Criegee intermediates in the ozonolysis of simple alkenes." Atmospheric Environment, Part A. General Topics **25**(9): 1881-1896.
- Howard, C. J. (1976). "Rate constants for the gas-phase reactions of OH radicals with ethylene and halogenated ethylene compounds." The Journal of Chemical Physics **65**(11): 4771.
- Hunter, E. P. L., S. G. Lias, et al. (1998). "Evaluated gas phase basicities and proton affinities of molecules : an update." [New York], American Chemical Society : Washington, D.C. : American Chemical society.
- Isidorov, V. A., V. T. Vinogorova, et al. (2003). "HS-SPME analysis of volatile organic compounds of coniferous needle litter." Atmospheric Environment **37**(33): 4645-4650.

- Jang, M., Czoschke, M, N, et al. (2002). "Heterogeneous Atmospheric Aerosol Production by Acid-Catalyzed Particle-Phase Reactions." Science AAAS **298** (5594): 814-817.
- Jaoui, M. (2001). "Mass balance of gaseous and particulate products analysis from α -pinene/NO /air in the presence of natural sunlight." Journal of Geophysical Research **106**(d12): 12541-12558.
- Jaoui, M. (2003). "Gas and particle products distribution from the reaction of β -caryophyllene with ozone." Journal of Atmospheric Chemistry **45**(3): 261-287.
- Jenkin, M. E. (1998). "Peroxy radical kinetics resulting from the OH-initiated oxidation of 1, 3-butadiene, 2, 3-dimethyl-1, 3-butadiene and isoprene." Journal of Atmospheric Chemistry **29**(3): 267-298.
- Jenkin, M. E, Saunders, S. M, et al (2003). "Protocol for the development of the Master Chemical Mechanism, MCM v3 (Part B): tropospheric degradation of aromatic volatile organic compounds." Atmospheric Chemistry and Physics **3**(1): 181.
- Jonsson, Å. M., M. Hallquist, et al. (2005). "Impact of Humidity on the Ozone Initiated Oxidation of Limonene, Δ^3 -Carene, and α -Pinene." Environmental Science & Technology **40**(1): 188-194.
- Kamens, R. M., M. W. Gery, et al. (1982). "Ozone–isoprene reactions: Product formation and aerosol potential." International Journal of Chemical Kinetics **14**(9): 955-975.
- Kanakidou, M., Seinfeld, J, H., et al. (2005). "Organic aerosol and global climate modelling: a review." Atmospheric Chemistry and Physics **5**(4): 1053-1123.
- Kanawati, B. (2008). "Mass spectrometric characterization of β -caryophyllene ozonolysis products in the aerosol studied using an electrospray triple quadrupole and time-of-flight analyzer hybrid system and density functional theory." Rapid Communications in Mass Spectrometry **22**(2): 165-186.
- Kavouras, I. G. (1999). "Formation and gas/particle partitioning of monoterpenes photo-oxidation products over forests." Geophysical Research Letters **26**(1): 55.
- Keady, P.B., F.R. Quant and G.J. Sem (1986). "A Condensation Nucleus Counter for

- Clean Rooms" Proc. Institute of Environmental Sci., Annual Technical Mtg: 445-451
- Kesselmeier, J. (2002). "Concentrations and species composition of atmospheric volatile organic compounds (VOCs) as observed during the wet and dry season in Rondonia (Amazonia)." Journal of Geophysical Research **107**: 8053.
- Kiendler-Scharr, A., Wildt, J., et al. (2009). "New particle formation in forests inhibited by isoprene emissions." Nature **461**, 381-384
- Kiendler-Scharr, A. (2009). "Aerosol Mass Spectrometric Features of Biogenic SOA: Observations from a Plant Chamber and in Rural Atmospheric Environments." Environmental Science & Technology **43**(21): 8166-8172.
- Kleindienst, T. E. (2007). "Ozone-isoprene reaction: Re-examination of the formation of secondary organic aerosol." Geophysical Research Letters **34**(1): L01805.
- Koch, D., Bond, T. C., et al (2007). "Global impacts of aerosols from particular source regions and sectors." Journal of Geophysical Research **112**: D02205.
- König, G. (1995). "Relative contribution of oxygenated hydrocarbons to the total biogenic VOC emissions of selected mid-European agricultural and natural plant species." Atmospheric Environment (1994) **29**(8): 861.
- Kroll, J. H. (2001). "Mechanism of HO Formation in the Gas-Phase Ozone-Alkene Reaction. 2. Prompt versus Thermal Dissociation of Carbonyl Oxides to Form OH." The Journal of Physical Chemistry **105**(18): 4446-4457.
- Kroll, J. H. (2005). "Secondary organic aerosol formation from isoprene photooxidation under high-NO conditions." Geophysical Research Letters **32**(18): L18808.
- Kroll, J. H., N. L. Ng, et al. (2006). "Secondary Organic Aerosol Formation from Isoprene Photooxidation." Environmental Science & Technology **40**(6): 1869-1877.
- Kuhn, U. (2004). "Seasonal differences in isoprene and light-dependent monoterpene emission by Amazonian tree species." Global Change Biology **10**(5): 663-682.
- Kwok, E. S. C. (1995). "Observation of Hydroxycarbonyls from the OH Radical-Initiated Reaction of Isoprene." Environmental Science & Technology **29**(9): 2467-2469.
- Lathiere, J. (2005). "Past and future changes in biogenic volatile organic compound emissions simulated with a global dynamic vegetation model." Geophysical Research Letters **32**(20): 1.

- Leather, K. E. (2012) "Acid-yield measurements of the gas-phase ozonolysis of ethene as a function of humidity using Chemical Ionisation Mass Spectrometry (CIMS)." Atmospheric Chemistry and Physics **12**: 469-479.
- Lee, A. (2006). "Gas-phase products and secondary aerosol yields from the ozonolysis of ten different terpenes." Journal of Geophysical Research. Biogeosciences **111**: D07302.
- Leungsakul, S. (2005). "Kinetic Mechanism for Predicting Secondary Organic Aerosol Formation from the Reaction of α -Limonene with Ozone." Environmental Science & Technology **39**(24): 9583-9594.
- Li, Y. J. (2011). "Second-generation products contribute substantially to the particle-phase organic material produced by β -caryophyllene ozonolysis." Atmospheric Chemistry and Physics **11**(1): 121-132.
- Lim, H., Carlton, A.G., et al. (2005). "Isoprene forms secondary organic aerosol through cloud processing: Model simulations." Environmental Science & Technology **39**(12): 4441-4446.
- Limbeck, A., Kulmala M, et al. (2003). "Secondary organic aerosol formation in the atmosphere via heterogeneous reaction of gaseous isoprene on acidic particles." Geophysical Research Letters **30**(19):6.
- Lindinger, W. and A. Jordan (1998). "Proton-transfer-reaction mass spectrometry (PTR-MS): on-line monitoring of volatile organic compounds at pptv levels." Chemical Society Reviews **27**(5): 347-375.
- Lohmann, U., Feichter, J (2005). "Global indirect aerosol effects: a review." Atmospheric Chemistry and Physics **5**: 715-737.
- Mackay, D., Bobra, et al. (1982). "Vapor-pressure correlations for low-volatility environmental chemicals." Environmental Science & Technology **16**(10): 645-649.
- Malkin, T. L., A. Goddard, et al. (2010). "Measurements of OH and HO(2) yields from the gas phase ozonolysis of isoprene." Atmospheric Chemistry and Physics **10**(3): 1441-1459.

- Mamyrin, B. A. (1973). "The mass-reflectron, a new nonmagnetic time-of-flight mass spectrometer with high resolution." Journal of Experimental and Theoretical Physics **37**: 45.
- Martin, R. S. (1991). "Measurement of isoprene and its atmospheric oxidation products in a central Pennsylvania deciduous forest." Journal of Atmospheric Chemistry **13**(1): 1-32.
- Matsunaga, S., Mochida, M., et al. (2003). "Growth of organic aerosols by biogenic semi-volatile carbonyls in the forestal atmosphere." Atmospheric Environment **37**(15): 2045-2050.
- Mentel, T. F. (2009). "Photochemical production of aerosols from real plant emissions." Atmospheric Chemistry and Physics **9**(13): 4387.
- Monks, P. S., Grainer, C., et al (2009). "Atmospheric composition change – global and regional air quality." Atmospheric Environment **43**: 5268-5350.
- Neeb, P. (1999). "Formation of OH Radicals in the Gas-Phase Reaction of Propene, Isobutene, and Isoprene with O₂: Yields and Mechanistic Implications." The Journal of Physical Chemistry **103**(45): 9003-9012.
- Neeb, P., O. Horie, et al. (1998). "The Ethene-Ozone Reaction in the Gas Phase." The Journal of Physical Chemistry A **102**(34): 6778-6785.
- Neeb, P., F. Sauer, et al. (1997). "Formation of hydroxymethyl hydroperoxide and formic acid in alkene ozonolysis in the presence of water vapour." Atmospheric Environment **31**(10): 1417-1423.
- Ng, N. L. (2007). "Effect of NO_x level on secondary organic aerosol (SOA) formation from the photooxidation of terpenes." Atmospheric Chemistry and Physics **7**: 5159-5174.
- Ng, N. L., J. H. Kroll, et al. (2006). "Contribution of First- versus Second-Generation Products to Secondary Organic Aerosols Formed in the Oxidation of Biogenic Hydrocarbons." Environmental Science & Technology **40**(7): 2283-2297.
- Nguyen, T. L. (2009). "The gas-phase ozonolysis of β -caryophyllene (C₁₅H₂₄). Part II: A theoretical study." Physical Chemistry Chemical Physics : PCCP **11**(21): 4173.
- Niki, H. (1983). "Atmospheric ozone-olefin reactions." Environmental Science & Technology **17**(7): 312A-322A.

- Niki, H., P. D. Maker, et al. (1977). "Fourier transform IR spectroscopic observation of propylene ozonide in the gas phase reaction of ozone-cis-2-butene-formaldehyde." Chemical Physics Letters **46**(2): 327-330.
- Novakov, T., Penner J.E. (1993). "Large contribution of organic aerosols to cloud-condensation-nuclei concentrations." Nature **365**: 823-826.
- Nozière, B. (1999). "Kinetics of the reactions of pinonaldehyde with OH radicals and with Cl atoms." International Journal of Chemical Kinetics **31**(4): 291-301.
- Olzmann, M. (1997). "Energetics, Kinetics, and Product Distributions of the Reactions of Ozone with Ethene and 2,3-Dimethyl-2-butene." The Journal of Physical Chemistry **101**(49): 9421-9429.
- Orlando, J. J. (2000). "Product studies of the OH- and ozone-initiated oxidation of some monoterpenes." Journal of Geophysical Research **105**(d9): 11561-11572.
- Orzechowska, G. E. and S. E. Paulson (2005). "Photochemical Sources of Organic Acids. 1. Reaction of Ozone with Isoprene, Propene, and 2-Butenes under Dry and Humid Conditions Using SPME." The Journal of Physical Chemistry A **109**(24): 5358-5365.
- Odabasi, M. and Seyfioglu, R (2005). "Phase partitioning of atmospheric formaldehyde in a suburban atmosphere." Atmospheric Environment **39**: 5149-5156.
- Pandis, S.N., Paulson, S.E., Seinfeld, J.H. and Flagan, R.C (1991). "Aerosol formation in the photooxidation of isoprene and β -pinene." Atmospheric Environment. Part A. General Topics **25**(5-6) 997-1008.
- Pankow, J.F. (1994). "An absorption model of the gas/aerosol partitioning involved in the formation of secondary organic aerosol." Atmospheric Environment **28**(2): 189-193.
- Park, J. (2004). "OH/OD Initiated Oxidation of Isoprene in the Presence of O and NO." The Journal of Physical Chemistry **108**(48): 10688-10697.
- Paulsen, D., J. Dommen, et al. (2005). "Secondary organic aerosol formation by irradiation of 1,3,5-trimethylbenzene-NO_x-H₂O in a new reaction chamber for atmospheric chemistry and physics." Environmental Science & Technology **39**(8): 2668-2678.

- Paulson, S. E. (1992). "Atmospheric photooxidation of isoprene part I: The hydroxyl radical and ground state atomic oxygen reactions." International Journal of Chemical Kinetics **24**(1): 79-101.
- Pérez, N., Pey, J., et al (2008). "Partitioning of major and trace components in PM₁₀-PM_{2.5}-PM₁ at an urban site in Southern Europe." Atmospheric Environment **42**: 1677-1691.
- Pfeiffer, T. (2001). "The contribution of the ozonolysis of terpenes to tropospheric OH concentrations." Canadian Journal of Physics **79**(2-3): 131-142.
- Piccot, S. D. (1992). "A global inventory of volatile organic compound emissions from anthropogenic sources." Journal of Geophysical Research **97**(d9): 9897.
- Pinto, D. M. (2007). "The effects of increasing atmospheric ozone on biogenic monoterpene profiles and the formation of secondary aerosols." Atmospheric Environment (1994) **41**(23): 4877.
- Pöschl, U. (2005). "Atmospheric Aerosols: Composition, Transformation, Climate and Health Effect." Angewandte Chemie International Edition **44**(46): 7520-7540
- Pöschl, U., Rudich, Y., et al (2007). "Kinetic model framework for aerosol and cloud surface chemistry and gas-particle interactions – part 1: general equations, parameters, and terminology." Atmospheric Chemistry and Physics **7**: 5989-6023.
- Reissell, A. (1999). "Formation of acetone from the OH radical- and O -initiated reactions of a series of monoterpenes." Journal of Geophysical Research **104**(d11): 13869-13879.
- Reissell, A. (2002). "Products of the OH radical- and O -initiated reactions of myrcene and ocimene." Journal of Geophysical Research **107**(d12): 4138.
- Rickard, A. R. (1999). "OH Yields in the Gas-Phase Reactions of Ozone with Alkenes." The journal of physical chemistry. A, Molecules, spectroscopy, kinetics, environment, & general theory **103**(38): 7656-7664.
- Rinne, J. (2005). "On-line PTR-MS measurements of atmospheric concentrations of volatile organic compounds in a European boreal forest ecosystem." Boreal Environment Research **10**(5): 425.

- Saathoff, H. (2009). "Temperature dependence of yields of secondary organic aerosols from the ozonolysis of α -pinene and limonene." Atmospheric Chemistry and Physics **9**(5): 1551.
- Sauer, F., C. Schäfer, et al. (1999). "Formation of hydrogen peroxide in the ozonolysis of isoprene and simple alkenes under humid conditions." Atmospheric Environment **33**(2): 229-241.
- Saunders, S. M. (2003). "Protocol for the development of the Master Chemical Mechanism, MCM v3 (Part A): tropospheric degradation of non-aromatic volatile organic compounds." Atmospheric Chemistry and Physics **3**(1): 161.
- Schkolnik G., Falkovich, A. H., et al. (2005). "New Analytical Method for the Determination of Levoglucosan, Polyhydroxy Compounds, and 2-Methylerythritol and Its Application to Smoke and Rainwater Samples." Environmental Science & Technology **39**(8): 2744-2752.
- Seinfeld, J. H., Pandis, S. N., et al (1998). "Atmospheric Chemistry and Physics: From Air Pollution to Climate Change." New York, US: American Institute of Physics ISSN:0031-9228.
- Španěl, P., Ji, Y., et al (1997a). "SIFT studies of the reactions of H_3O^+ , NO^+ , O_2^+ with a series of aldehydes and ketones." International Journal of Mass Spectrometry and Ion Processes **165-166**: 25-37.
- Španěl, P and Smith, D. (1997b). "SIFT studies of the reactions of H_3O^+ , NO^+ , O_2^+ with a series of alcohols." International Journal of Mass Spectrometry and Ion Processes **167-168**: 375-388.
- Španěl, P and Smith, D. (1998). "SIFT studies of the reactions of H_3O^+ , NO^+ , O_2^+ with a series of volatile carboxylic acids and esters." International Journal of Mass Spectrometry and Ion Processes **172**(1-2): 137-147.
- Sprengnether, M. (2002). "Product analysis of the OH oxidation of isoprene and 1, 3-butadiene in the presence of NO." Journal of Geophysical Research **107**(8): 8.
- Staudt, M., Bertin, N., et al (2000). "Seasonal Variation in Amount and Composition of monoterpenes emitted by young Pinus pinea trees – Implications for Emission Modeling." Journal of Atmospheric Chemistry **35**(1): 77-99.

- Steeghs, M., H. P. Bais, et al. (2004). "Proton-Transfer-Reaction Mass Spectrometry as a New Tool for Real Time Analysis of Root-Secreted Volatile Organic Compounds in Arabidopsis." Plant Physiology **135**(1): 47-58.
- Su, F., J. G. Calvert, et al. (1980). "A FT IR spectroscopic study of the ozone-ethene reaction mechanism in oxygen-rich mixtures." The Journal of Physical Chemistry **84**(3): 239-246.
- Sullivan, R.C., Guazzotti, S.A., et al (2007). "Direct observations of the atmospheric processing of Asian mineral dust." Atmospheric Chemistry and Physics **7**(1): 1213-1236.
- Sun, J., Ariya, P.A. (2006). "Review: Atmospheric organic and bio-aerosols as cloud condensation nuclei (CCN): A review." Atmospheric Environment **40**: 795-820.
- Surratt, J. D., S. M. Murphy, et al. (2006). "Chemical Composition of Secondary Organic Aerosol Formed from the Photooxidation of Isoprene." The Journal of Physical Chemistry A **110**(31): 9665-9690.
- Tang, Y. H., Carmichael, G. R., et al. (2004). "Impacts of dust on regional tropospheric chemistry during the ACE-Asia experiment: A model study with observations." Journal of Geophysical Research **109**(19): D19S21.
- Tang, M. J., Thieser, G., et al. (2010). "Uptake of NO₃ and N₂O₅ to Saharan dust, ambient urban aerosol and soot: a relative rate study." Atmospheric Chemistry and Physics **10**: (2965-2974).
- Thompson, A. M. (1992). "The Oxidizing Capacity of the Earth's Atmosphere: Probable Past and Future Changes." Science **256**(5060): 1157-1165.
- Tolocka, M.P., Jang, M, et al (2004). "Formation of Oligomers in Secondary Organic Aerosol." Environmental Science & Technology **38**(5): 1428-1434.
- Trainer, M., Williams, E. J., et al (1987). "Models and observations of the impact of natural hydrocarbons on rural ozone." Nature **329**: 705-707.
- Tsigaridis, K., Kanakidou, M. (2007). "Secondary organic aerosol importance in the future atmosphere." Atmospheric Environment **41**(22): 4682-4692.
- Tuazon, E.C. and Atkinson, R. (1990). "A product study of the gas-phase reaction of Methacrolein with the OH radical in the presence of NO_x." International Journal of Chemical Kinetics **22**(6): 591-602.

- Tuazon, E. C., S. M. Aschmann, et al. (1997). "Products of the Gas-Phase Reactions of O₃ with a Series of Methyl-Substituted Ethenes." Environmental Science & Technology **31**(10): 3004-3009.
- Tuazon, E.C. and Atkinson, R. (2004). "A product study of the gas-phase reaction of Isoprene with the OH radical in the presence of NO_x." International Journal of Chemical Kinetics **22**(12): 1221-1236.
- Varutbangkul, V. (2006). "Hygroscopicity of secondary organic aerosols formed by oxidation of cycloalkenes, monoterpenes, sesquiterpenes, and related compounds." Atmospheric Chemistry and Physics **6**: 2367-2388.
- Vereecken, L. (2004). "Nontraditional (Per)oxy Ring-Closure Paths in the Atmospheric Oxidation of Isoprene and Monoterpenes." The Journal of Physical Chemistry **108**(24): 5197-5204.
- Volkamer, R. (2010). "Oxidative capacity of the Mexico City atmosphere? Part 1: A radical source perspective." Atmospheric Chemistry and Physics **10**: 6969-6991.
- Wang, K. Y. (2000). "Modelling terrestrial biogenic isoprene fluxes and their potential impact on global chemical species using a coupled LSM-CTM model." Atmospheric Environment **34**(18): 2909.
- Warneck, P. (2003). "In-cloud chemistry opens pathway to the formation of oxalic acid in the marine atmosphere." Atmospheric Environment **37**(17): 2423-2427.
- Warneke, C. Veres, P. (2011). "Airborne formaldehyde measurements using PTR-MS: calibration, humidity dependence, inter-comparison and initial results." Atmospheric Measurement Techniques **4**: 2345-2358.
- Warscheid, B. and T. Hoffmann (2001). "On-line measurements of α -pinene ozonolysis products using an atmospheric pressure chemical ionisation ion-trap mass spectrometer." Atmospheric Environment **35**(16): 2927-2940.
- Wayne, R. P. (1993). Chemistry of Atmospheres, 2nd edition.
- Weber, R.J., McMurray, P.H., et al. (1998). "A study of new particle formation and growth involving biogenic and trace gas species measured during ACE 1." Journal of Geophysical Research. Atmospheres **103**(D13): 16385-16396.

- Wegener, R. (2007). "Simulation chamber investigation of the reactions of ozone with short-chained alkenes." Journal of Geophysical Research. Biogeosciences **112**(d13): D13301.
- Went, F., (1960). "Blue haze in the atmosphere." Nature **187**: 641-643
- Williams, J. (2001). "An atmospheric chemistry interpretation of mass scans obtained from a proton transfer mass spectrometer flown over the tropical rainforest of Surinam." Journal of Atmospheric Chemistry **38**(2): 133-166.
- Winer, A. M. (1992). "Emission rates of organics from vegetation in California's Central Valley." Atmospheric Environment (1994) **26**(14): 2647.
- Winterhalter, R. (2009). "The gas-phase ozonolysis of β -caryophyllene (C₁₅H₂₄). Part I: an experimental study." Physical Chemistry Chemical Physics : PCCP **11**(21): 4152.
- Wisthaler, A. (2001). "Measurements of acetone and other gas phase product yields from the OH-initiated oxidation of terpenes by proton-transfer-reaction mass spectrometry (PTR-MS)." Atmospheric Environment (1994) **35**(35): 6181.
- Wolff, M. M. (1953). "A Pulsed Mass Spectrometer with Time Dispersion." Review of Scientific Instruments **24**(8): 616.
- Wolff, S., A. Boddenberg, et al. (1997). "Gas-phase ozonolysis of ethene in the presence of carbonyl-oxide scavengers." Atmospheric Environment **31**(18): 2965-2969.
- Wyche, K. P. (2007). "Technical Note: Performance of Chemical Ionization Reaction Time-of-Flight Mass Spectrometry (CIR-TOF-MS) for the measurement of atmospherically significant oxygenated volatile organic compounds." Atmospheric Chemistry and Physics **7**: 609.
- Wyche, K. P., C. Whyte, et al. (2008). "Atmospheric Monitoring With Chemical Ionisation Reaction Time-of-Flight Mass Spectrometry (CIR-TOF-MS) and Future Developments: Hadamard Transform Mass Spectrometry". Advanced Environmental Monitoring, Springer Netherlands: 64-76.
- Xu, X. (2003). "Comprehensive two-dimensional gas chromatography (GC x GC) measurements of volatile organic compounds in the atmosphere." Atmospheric Chemistry and Physics **3**(3): 665.

- Yu, S. (2000). "Role of organic acids formic, acetic, pyruvic and." Atmospheric research **53**: 185.
- Yu, Y., M. J. Ezell, et al. (2008). "Photooxidation of α -pinene at high relative humidity in the presence of increasing concentrations of NO_x." Atmospheric Environment **42**(20): 5044-5060.
- Zhang, Y., Sunwoo, Y., et al (1994). "Photochemical oxidant processes in the presence of dust: An evaluation of the impact of dust on particulate nitrate and ozone formation." J. Appl. Meteor **33**: 813-824.
- Zhang, D. (2002). "Mechanism of OH formation from ozonolysis of isoprene: kinetics and product yields." Chemical Physics Letters. **358**(3-4): 171.
- Zhang, J., K. E. Huff Hartz, et al. (2006). "Secondary Organic Aerosol Formation from Limonene Ozonolysis: Homogeneous and Heterogeneous Influences as a Function of NO_x." The Journal of Physical Chemistry A **110**(38): 11053-11063.
- Zhang, Q. (2007). "Ubiquity and dominance of oxygenated species in organic aerosols in anthropogenically-influenced Northern Hemisphere midlatitudes." Geophysical Research Letters **34**(13): L13801.
- Zhao, J. (2004). "Quantification of Hydroxycarbonyls from OH–Isoprene Reactions." Journal of the American Chemical Society **126**(9): 2686-2687.

Appendix

All chemicals available for calibrations runs available are given in Table A1.

Table A1. Compounds used for the bag calibrations					
Compound	Purity	FW (g mol ⁻¹)	Density (g cm ⁻³)	CAS	Supplier
limonene	98%	136.24	0.843	57989-27-5	Sigma-Aldrich
pinonaldehyde	>95%	168.23	0.958	-	Inhouse ^a
β-caryophyllene	≥80%	204.36	0.902	87-44-5	SAFC
acetaldehyde	≥99.5 %	44.05	0.788	75-07-0	Sigma-Aldrich
acetone	≥99.9 %	58.08	0.791	666-52-4	Sigma-Aldrich
benzaldehyde	≥99.0 %	106.12	1.042	100-52-7	Sigma-Aldrich
2-butanone	≥99.0 %	72.11	0.805	78-93-3	Sigma-Aldrich
3-carene	90.0%	136.24	0.867	14466-78-9	Sigma-Aldrich
2(5H)furanone	98.0%	84.07	1.185	497-23-4	Sigma-Aldrich
hexanal	≥90.0 %	100.16	0.814	66-25-1	Sigma-Aldrich
2-hexanone	98.0%	100.16	0.811	591-78-6	Sigma-Aldrich
3-hexanone	>95%	100.16	0.811	589-38-8	Sigma-Aldrich
Hydroxyacetone	90.0%	74.08	1.082	116-09-6	Fluka
Isoprene	≥99.0 %	68.12	0.681	78-79-5	Sigma-Aldrich
(-)-linalool	≥95.0 %	154.25	0.858	126-91-0	Fluka
Methacrolein	95.0%	70.09	0.847	78-85-3	Sigma-Aldrich
2-methyl-3-buten-2-ol	≥98.0 %	86.13	0.820	115-18-4	Sigma-Aldrich
Methyl vinyl ketone	95.0%	70.09	0.841	78-94-4	Alfa aesar
(-)-α-pinene	≥99.0 %	136.23	0.858	7785-26-4	Sigma-Aldrich
(1S)-(-)-β-pinene	≥99.0 %	136.23	0.872	18172-67-3	Sigma-Aldrich
1-propanol	≥99.5 %	60.10	0.803	71-23-8	Sigma-Aldrich
Toluene (anhydrous)	99.8 %	92.14	0.870	108-88-3	Sigma-Aldrich
Cyclohexanone	≥95.0 %	98.15	0.948	108-94-1	Sigma-Aldrich

Note: other calibrations were made at the EUPHORE facility using on-site chemicals.

Additional chemicals were available in permeation tubes for calibrations (acetaldehyde, acetone, pentene, formic acid, acetic acid, isoprene, methanol, methyl vinyl ketone, methacrolein, α-pinene and formaldehyde)

Accurate concentrations of compounds in the 1ppm standard gas cylinder (BOC, UK) are given in table A2

Table A2. List of compounds used for calibrations and their concentrations from the 1 ppm gas standard

Compound	FW (g mol ⁻¹)	Density (g cm ⁻³)	Accurate certified concentration (ppb)
Methanol	32.04	0.792	970
Acetaldehyde	44.05	0.788	990
Trans-2-butene	56.11	-	1030
Acetone	58.08	0.791	1020
Methacrolein	70.09	0.847	980
Cyclohexanone	98.15	0.948	1290
β-pinene	136.23	0.872	1050

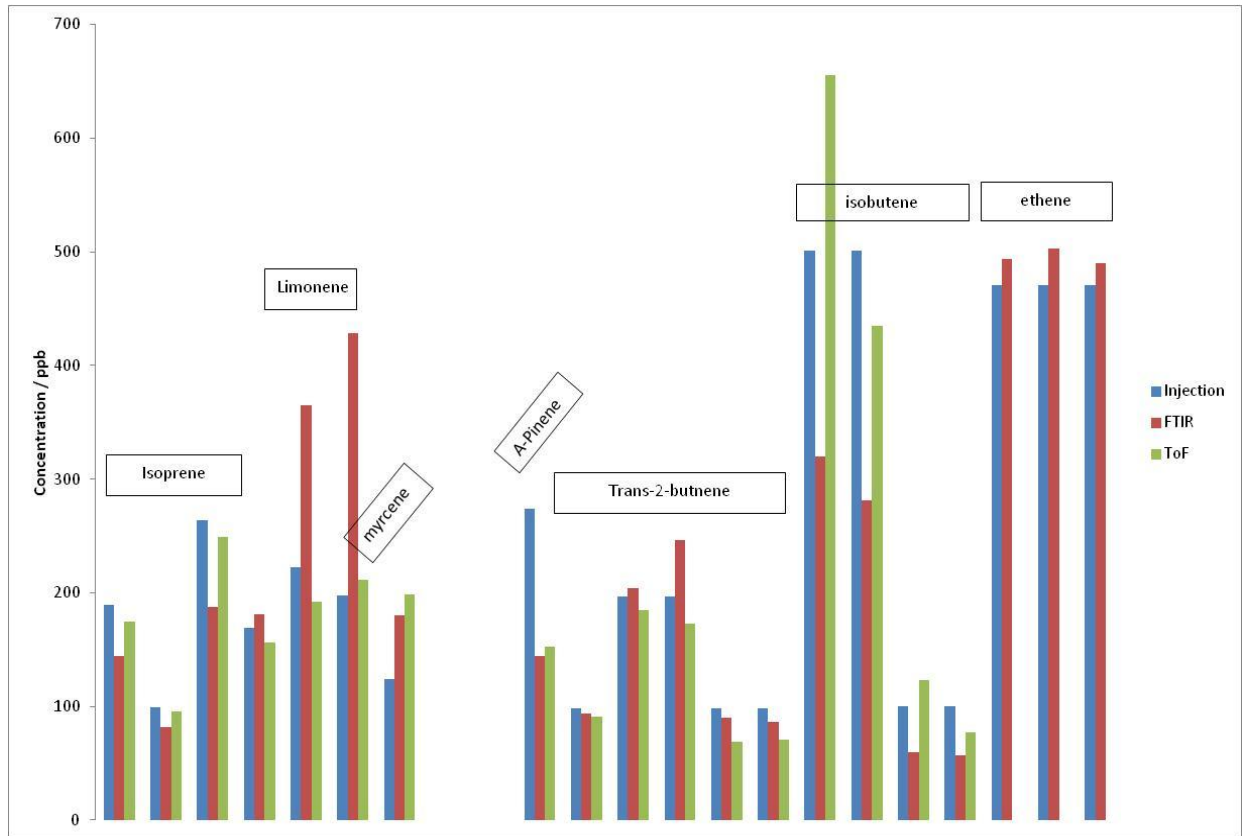


Figure A1: Comparisons of injection concentration from both measured parameters, CIR-ToF-MS (Green) and FTIR (Red) to calculated concentrations based on possible 100% theoretical injections possible governed by volume or masses injected.